

**EVALUATION OF THE ANTI-APOPTOTIC PROPERTY OF
CELLULAR PRION PROTEIN IN KIDNEY, ORAL AND COLON
CANCER CELL LINES**

By

YEANNIE YAP HUI YENG

A thesis submitted to the Faculty of Engineering and Science,
Universiti Tunku Abdul Rahman,
in partial fulfillment of the requirements for the degree of
Master of Science

March 2011

ABSTRACT

EVALUATION OF THE ANTI-APOPTOTIC PROPERTY OF CELLULAR PRION PROTEIN IN KIDNEY, ORAL AND COLON CANCER CELL LINES

Yeannie Yap Hui Yeng

Since the discovery of PrP^C, most studies have focused on its role in neurodegenerative diseases, whereas its function outside the nervous system remains obscure. This study was intended to evaluate the anti-apoptotic property of PrP^C in renal adenocarcinoma (ACHN), oral squamous cell carcinoma (HSC-2), and colon adenocarcinoma (LS 174T). Transiently transfected PrP^C-expressing ACHN and LS 174T which underwent tumour necrosis factor- α treatment at 100ng/ml and basal cell cycle analysis, had significantly higher cell viability (81.2% vs. 65.2%; 54.2% vs. 45.3%) and proliferative index (0.46 vs. 0.40; 0.47 vs. 0.44) compared to the vector-transfected control cells, respectively. High endogenous PrP^C level in HSC-2 cells were knock-downed using short hairpin RNA (shRNA), and together with the stably transfected PrP^C-overexpressing LS 174T were treated with tunicamycin (TUN) and hydrogen peroxide (H₂O₂) to elicit N-linked glycosylation inhibition and oxidative stress-induced cell death, respectively. MTT analysis showed that PrP^C in HSC-2 and LS 174T exhibited an anti-apoptotic role upon H₂O₂ treatment at IC₅₀ with significantly higher cell viability (78.6% vs. 48.7%; 80.7% vs. 55.3%) but an opposing role was found

after N-glycosylation inhibition (59.1% vs. 83.0%; 61.1% vs. 83.9%); in comparison to the non-PrP^C expressing control cells, respectively. The ability of PrP^C to scavenge ROS following H₂O₂ treatment at 3mM were reduced with suppression of N-linked glycosylation where the 2',7'-dichlorofluorescein fluorescence intensity which is in proportion to the total ROS levels were increased from 171.06 to 320.44 and 345.72 to 598.84 in HSC-2 and LS 174T, respectively. Cell cycle synchronization using TUN had demonstrated the ability of PrP^C to promote proliferation and G₁/S-phase transition in HSC-2 and LS 174T cells. Taken together, PrP^C confers resistance against TNF- α and oxidative stress apoptosis and promotes proliferation in oral and colon cancer cell lines, but these properties are abolished by glycosylation inhibition. Further elucidation of the anti-cytotoxic and pro-proliferative effects of PrP^C in cancer cell lines might shed new light in finding the role of PrP^C and its glycosylation in cancer biology.

ACKNOWLEDGEMENT

This work was supported by the Malaysian Ministry of Science, Technology & Innovation (MOSTI) e-Science Grant 02-02-11-SF0068. I would like to acknowledge my supervisor, Dr. Say Yee How for his vital encouragement, understanding and support. I also thank Dr. Lim Yang Mooi (Faculty of Medicine and Health Sciences, Universiti Tunku Abdul Rahman) for providing us with the ACHN, HSC-2 and LS 174T cancer cell lines. I am very thankful to my fellow lab mates for the help and inspirations they extended. Last but not least, I would like to extend my heartfelt gratitude most especially to my family and friends for their constant reminders and much needed motivation.

APPROVAL SHEET

This thesis entitled **“EVALUATION OF THE ANTI-APOPTOTIC PROPERTY OF CELLULAR PRION PROTEIN IN KIDNEY, ORAL AND COLON CANCER CELL LINES”** was prepared by YEANNIE YAP HUI YENG and submitted as partial fulfillment of the requirements for the degree of Master of Science at Universiti Tunku Abdul Rahman.

Approved by:

(Dr. SAY YEE HOW)
Assistant Professor/Supervisor
Department of Biomedical Science
Faculty of Science
Universiti Tunku Abdul Rahman

Date:.....

FACULTY OF ENGINEERING AND SCIENCE
UNIVERSITI TUNKU ABDUL RAHMAN

Date: _____

PERMISSION SHEET

It is hereby certified that **YEANNIE YAP HUI YENG** (ID No: **09UEM02358**) has completed this thesis entitled “EVALUATION OF THE ANTI-APOPTOTIC PROPERTY OF CELLULAR PRION PROTEIN IN KIDNEY, ORAL AND COLON CANCER CELL LINES” under the supervision of Dr. Say Yee How (Supervisor) from the Department of Biomedical Science, Faculty of Science.

I hereby give permission to the University to upload softcopy of my thesis in pdf format into UTAR Institutional Repository, which will be made accessible to UTAR community and public.

Yours truly,

(YEANNIE YAP HUI YENG)

DECLARATION

I hereby declare that the dissertation is based on my original work except for quotations and citations which have been duly acknowledged. I also declare that it has not been previously or concurrently submitted for any other degree at UTAR or other institutions.

Yeannie Yap Hui Yeng

Date _____

TABLE OF CONTENTS

	Page
ABSTRACT	ii
ACKNOWLEDGEMENT	iv
APPROVAL SHEET	v
PERMISSION SHEET	vi
DECLARATION	vii
TABLE OF CONTENTS	viii
LIST OF TABLES	xii
LIST OF FIGURES	xiii
LIST OF ABBREVIATIONS	xvi
LIST OF PUBLICATIONS	xix
CHAPTER	
1.0 INTRODUCTION	1
2.0 LITERATURE REVIEW	7
2.1 Prion Diseases and the Prion Hypothesis	7
2.2 Functional Characteristics of PrP ^C	10
2.2.1 Molecular Structure of PrP ^C	11
2.2.2 Biogenesis and Cellular Localization of PrP ^C	13
2.2.3 PrP ^C Glycosylation	17
2.2.4 Physiological Functions of PrP ^C	19
2.2.4.1 PrP ^C and Signal Transduction	19
2.2.4.2 Functional Role of PrP ^C in Synapses	20
2.2.4.3 Cell Adhesion Regulation by PrP ^C	21
2.3 An Overview of Cancer Biology	21
2.3.1 Introduction to Cancer	21
2.3.2 Hallmarks of Cancer	23
2.3.3 Apoptosis: A Cell Suicide Mechanism	25
2.3.3.1 Death Receptor (DR) Pathway: TNF- α -mediated Apoptosis	26
2.3.3.2 Intrinsic Pathway: Mitochondria-mediated Cell Death	27
2.3.3.3 Cross-talk between Extrinsic and Intrinsic Pathways	28
2.3.4 Cell Cycle Arrest and Apoptosis	29
2.3.4.1 Cell Cycle Regulation	31
2.3.5 Oxidative Stress and Apoptosis	31
2.3.6 Unfolded Protein Response, ER Stress and Apoptosis	33
2.4 The Role of PrP ^C in Cancer Biology	34
2.4.1 The Anti-apoptotic Property of PrP ^C	35

	2.4.1.1 <i>In Vivo</i> Neuroprotection Evidences	35
	2.4.1.2 <i>In Vitro</i> Neuroprotection Evidences	36
	2.4.1.3 Controversy of PrP ^C Anti-apoptotic Property	38
	2.4.2 PrP ^C , Copper Binding and Oxidative Stress	38
	2.4.3 PrP ^C and Tumour Resistance	40
	2.4.4 PrP ^C and Tumour Progression	41
2.5	RNA Interference	42
3.0	MATERIALS AND METHODS	46
3.1	Chemicals and Reagents	46
3.2	List of Formula	47
3.3	Molecular Biology	48
3.3.1	The pcDNA TM 3.1 Vector	48
	3.3.1.1 Cloning of Human PrP ^C cDNA into pcDNA TM Vector	49
3.3.2	The pCMV-SPORT6 Vector	53
	3.3.2.1 Creating pCMV-SPORT6 Empty Vector	54
3.3.3	The pLKO.1 TRC Cloning Vector	55
	3.3.3.1 Construction of shRNA for the Knockdown of <i>PRNP</i> Gene	56
3.3.4	Preparation of Competent <i>E.coli</i> Cells using Calcium Chloride	62
	3.3.4.1 Transformation of DNA into Competent <i>E.coli</i> Cells	63
3.4	Cell Culture	64
3.4.1	The Cell Lines	64
	3.4.1.1 Oral Squamous Carcinoma, HSC-2 (JCRB0622)	64
	3.4.1.2 Renal Cell Adenocarcinoma, ACHN (CRL-1611)	65
	3.4.1.3 Colorectal Adenocarcinoma, LS 174T (CL-188)	66
3.4.2	Cell Lines Maintenance	67
	3.4.2.1 Preparation of Complete Culture MEM Medium	67
	3.4.2.2 Preparation of OPTI-MEM	68
3.4.3	Sub-culturing of Adherent Cell Lines	68
3.4.4	Freezing and Thawing of Cells	69
3.4.5	Cell Counting	69
3.5	Cells Transfection	70
	3.5.1 Linearization of Plasmid DNA for Transfection Purposes	71
	3.5.2 Electroporation Method for the Transfection of Cells	71
	3.5.3 Cells Transfection using Cationic Lipids	73
3.6	Immunofluorescence Microscopy	74
3.7	Sodium dodecyl sulphate polyacrylamide gel electrophoresis (SDS-PAGE) and Western Blot Analysis	75

3.7.1	Preparation of Cell Lysate	75
3.7.1.1	Quantitation of Total Protein	75
3.7.2	Sodium dodecyl sulphate polyacrylamide gel electrophoresis	76
3.7.3	Western Blotting	76
3.7.3.1	Stripping of PVDF Membrane for Repeated Hybridization	78
3.7.3.2	Amido Black Staining of PVDF Membrane	78
3.8	Treatment Paradigm	79
3.9	Cell Viability Assessment using MTT Assay	80
3.10	Apoptotic Markers Detection by Western Blot Analysis	81
3.10.1	Bax/Bcl-xL Ratio Quantification	81
3.11	Cell Cycle Analysis by Flow Cytometry	82
3.11.1	Cell Cycle Synchronization	83
3.12	FITC Annexin V-PI Dual Staining	83
3.13	Determination of Antioxidant Activity Using DCFH-DA	84
3.14	Statistical Analysis	85
4.0	RESULTS	86
4.1	Molecular Biology	86
4.1.1	The pCMV-SPORT6 Empty Vector Construction	86
4.1.2	Cloning of Human PrP ^C cDNA into pcDNA TM 3.1 Construct	87
4.1.3	Short Hairpin RNA (shRNA) Cloning into pLKO.1 TRC Cloning Vector	89
4.2	Assessment of PrP ^C Expression in Cancer Cells	91
4.2.1	PrP ^C Expression in Transiently Transfected Cancer Cells	91
4.2.2	Stably-transfected LS 174T Cells Overexpress PrP ^C	94
4.2.3	Depletion of Endogenous PrP ^C in <i>PRNP</i> Gene Knockdown HSC-2	97
4.3	PrP ^C Expression in Cells Suppresses TNF- α -induced Cell Death	99
4.3.1	PrP ^C Exerts Its Protective Effect in TNF- α -induced Cell Death through Bax Regulation	103
4.3.2	LS 174T Cells are Bax-deficient	106
4.4	Glycosylation Inhibition of PrP ^C Promotes Endoplasmic Reticulum stress-induced Cell Death in Cells	107
4.5	PrP ^C is Anti-apoptotic During Oxidative Stress-induced Cancer Cell Death	116
4.6	Blocking of PrP ^C Glycosylation Impedes its ROS Scavenging Activity	125
4.7	PrP ^C Regulates Cell Cycle Progression and Cell Proliferation in Cultured Cancer Cells	131

5.0	DISCUSSION	143
5.1	Inefficient Co-transfection using Electroporation Method	143
5.2	Protective Effect of PrP ^C towards TNF- α -induced Cell Death	145
5.2.1	Protective Effect of PrP ^C in TNF- α -mediated Apoptosis Involves the Suppression of Bax	146
5.2.2	A Plausible Protective Role of Cytosolic PrP Which Involves Bax	148
5.3	Stable Knockdown of PrP ^C Expression Using HuPrPshRNA 1	150
5.4	PrP ^C is Protective during Oxidative Stress-induced Apoptosis	151
5.4.1	Association of PrP ^C with Copper Metabolism and SOD Activity	153
5.4.2	PrP ^C Deregulation, Copper Elevation, and Oxidative Stress: A Targeted Cancer Therapy	155
5.5	Glycosylation Inhibition in PrP ^C Provokes ER Stress-induced Apoptosis in Cancer Cells	157
5.5.1	Accumulation of Unglycosylated PrP ^C Triggers Oxidative Stress-related Unfolded Protein Response	160
5.5.2	Glycosylation Inhibition of PrP ^C via TUN: A Promising Anticancer Strategy	162
5.6	A Role of PrP ^C in Cell Cycle Progression	164
5.7	Concluding Remarks and Future Directions	167
6.0	CONCLUSIONS	170
	REFERENCES	173
	APPENDIX	195

LIST OF TABLES

Table		Page
2.1	The prion diseases	8
3.1	Formulations of buffers and solutions	47
3.2	Preparation of PCR reaction mixture	50
3.3	Cycling conditions for PCR	50
3.4	shRNA oligos corresponding to siRNA sequences known to knockdown PrP ^C	58
3.5	shRNA oligos against human PrP ^C mRNA sequence (BC012844)	58
3.6	Attempted electroporation parameters for human HSC-2, ACHN, and LS 174T cancer cell lines	72
3.7	Effective working concentrations of selective antibiotics towards human cancer cell lines	72
3.8	Protocol for 15% polyacrylamide gel	76
3.9	Antibodies for western blotting analysis	78
3.10	Seeding density for cell lines in various types of culture vessels	79
4.1	Quantification of the Bax/Bcl-xL ratio in TNF- α -treated cells	104
4.2	Effects of PrP ^C on cell proliferation in cancer cell lines	132

LIST OF FIGURES

Figures		Page
2.1	Biochemical and biophysical properties of PrP ^C and PrP ^{Sc}	11
2.2	Scheme illustrating post-translational modifications of PrP ^C and PrP ^{Sc}	12
2.3	Biogenesis of PrP ^C	14
2.4	Cross-talk between extrinsic and intrinsic pathways	30
2.5	Mechanism of gene silencing by RNAi	44
3.1	Map of pcDNA TM 3.1 vector	49
3.2	Map of pCMV-SPORT6 vector	54
3.3	Map of pLKO.1 TRC cloning vector	56
3.4	Selection of siRNA targets in <i>PRNP</i> gene	60
3.5	Cell morphology of HSC-2	64
3.6	Cell morphology of ACHN	65
3.7	Cell morphology of LS 174T	66
4.1	The construction of pCMV-SPORT6 empty vector	87
4.2	Human PrP ^C cDNA cloning into pcDNA TM 3.1 vector	88
4.3	shRNA cloning into pLKO.1 TRC cloning vector	90
4.4	Western blot analysis on transiently pcDNA 3.1-PrP transfected cancer cell lines	93
4.5	PrP ^C overexpression in LS 174T cells	96
4.6	Inhibition of PrP ^C expression using shRNA oligonucleotide	98
4.7	PrP ^C in transiently transfected cells suppresses TNF- α -induced cell death	101
4.8	PrP ^C resists cytotoxicity of TNF- α in cancer cells	102

4.9	Western blot analysis of Bax and Bcl-xL in TNF- α -treated cells	105
4.10	Analysis of Bax status in HSC-2, ACHN and LS 174T	106
4.11	Effects of TUN on PrP ^C expressing HSC-2 and LS 174T cells	107
4.12	Induction of cell death following treatment with TUN	109
4.13	Blocking of PrP ^C glycosylation by TUN promotes cell death	110
4.14	Apoptosis induction in PrP ^C expressing HSC-2 cells treated with TUN	112
4.15	Apoptosis induction in PrP ^C expressing LS 174T cells treated with TUN	113
4.16	Inhibition of glycosylation of PrP ^C induces apoptosis in cancer cells	115
4.17	Induction of cell death following treatment with H ₂ O ₂	117
4.18	PrP ^C exerts its protective effect towards oxidative stress-induced cell death in cultured cancer cells	119
4.19	Protective effects of PrP ^C in HSC-2 cells treated with H ₂ O ₂	121
4.20	Protective effects of PrP ^C in LS 174T cells treated with H ₂ O ₂	122
4.21	PrP ^C exerts its anti-apoptotic effects in H ₂ O ₂ -induced cell death	124
4.22	Inhibition of glycosylation in PrP ^C provokes cell death in H ₂ O ₂ -induced oxidative stress in cultured cells	126
4.23	PrP ^C modulates H ₂ O ₂ -induced burst of ROS in HSC-2 cells	128
4.24	PrP ^C modulates H ₂ O ₂ -induced burst of ROS in LS 174T cells	129
4.25	PrP ^C expression increases the growth rate of cancer cells	133
4.26	Effects of PrP ^C on cell cycle distribution in HSC-2 cells upon synchronization	137

4.27	Effects of PrP ^C on cell cycle distribution in LS 174T cells upon synchronization	140
------	--	-----

LIST OF ABBREVIATIONS

APS	Ammonium persulfate
BCA	Bicinchoninic acid
BGH	Bovine growth hormone
$C_2H_3NaO_2$	Sodium acetate
$CaCl_2$	Calcium chloride
CDK	Cyclin-dependent kinase
CMV	Cytomegalovirus
DCF	2',7'-dichlorofluorescein
DCFH	2',7'-dichlorofluorescein
DCFH-DA	2',7'-dichlorofluorescein diacetate
ddH ₂ O	Sterile distilled water
DMSO	Dimethyl sulfoxide
dsRNA	Double stranded RNA
ECL	Enhanced chemiluminescence
EDTA	Ethylenediaminetetraacetic acid
ER	Endoplasmic reticulum

FI	Fluorescence intensity
FITC	Fluorescein isothiocyanate
GPI	Glycosylphosphatidylinositol
H ₂ O ₂	Hydrogen peroxide
IC ₅₀	Half maximal inhibitory concentration
IFM	Immunofluorescence microscopy
MDR	Multidrug-resistant
MgCl ₂	Magnesium chloride
MgSO ₄	Magnesium sulphate
MPO	Myeloperoxidase
mRNA	Messenger RNA
MTT	3-(4,5-dimethylthiazol-2-yl)-2,5-diphenyltetrazolium bromide
NaCl	Sodium chloride
NaHCO ₃	Sodium bicarbonate
NaOH	Sodium hydroxide
PBS	Phosphate buffered saline
PCR	Polymerase chain reaction

PI	Propidium iodide
PIC	Protease inhibitor cocktail
PMSF	Phenylmethanesulfonylfluoride
PrIn	Proliferative index
PrP ^C	Cellular prion protein
PrP ^{Sc}	Scrapie prion
ROS	Reactive oxygen species
RT	Room temperature
SDS-PAGE	Sodium dodecyl sulphate polyacrylamide gel electrophoresis
SEM	Standard error of the mean
shRNA	Short hairpin RNA
siRNA	Small interfering RNA
TBS	Tris buffered saline
TNF- α	Tumour necrosis factor α
TPD1TR	TransPass D1 Transfection Reagent
TUN	Tunicamycin
UPR	Unfolded protein response

LIST OF PUBLICATIONS

Several aspects of the thesis have already been included in a peer-reviewed publication as per below:

1. Yap, Y. H., & Say, Y. H. (2011). Resistance against apoptosis by the cellular prion protein is dependent on its glycosylation status in oral HSC-2 and colon LS 174T cancer cells. *Cancer Letters*, 306(1), 111-119.
(appended at the back of the thesis)
2. Yeannie Hui-Yeng Yap & Yee-How Say (2011). Over-expression of the cellular prion protein confers resistance to tumour necrosis factor-alpha apoptosis in oral, colon and kidney cancer cell lines. *Cell Biology International* (Submitted; in review).

CHAPTER 1

INTRODUCTION

The cellular prion protein (PrP^{C}) is a highly conserved, 254 amino acids (for humans) sialoglycoprotein found abundantly in neuronal and glial cells of the central nervous system (CNS) with glycosylphosphatidylinositol (GPI)-anchored to the plasma membrane (Stahl, Borchelt, Hsiao, & Prusiner, 1987). It consists of a highly-conserved hydrophobic region (106–126), a disordered N-terminal region (23-124), a C-terminal region (125-228) composed of three α -helices, which is monomeric and two short β -strands flanking the first α -helix and a single unique disulphide bridge between the two Cysteines in the most structured C-terminus domain. An octarepeat region of PHGGGWGQ encompassing the codon 51 through 91 of the N-terminus is responsible for copper binding (Aronoff-Spencer et al., 2000; Riek et al., 1996; Wang, Chuang, Soong, Shan, & Kao, 2009; Zahn et al., 2000).

Upon post-translational conversion, PrP^{C} is converted into its pathogenic isoform, the scrapie prion (PrP^{Sc}) which is responsible for the transmission of prion diseases, also known as transmissible spongiform encephalopathies (TSEs) (Sy, 2003). TSEs are a group of rare neurodegenerative diseases which includes kuru, fatal familial insomnia (FFI), sheep scrapie, bovine spongiform encephalopathy (BSE), Creutzfeldt-Jakob disease (CJD), Gerstmann-Sträussler-Scheinker syndrome in humans, as well as chronic wasting disease in elk and deer (McNally, Ward, & Priola, 2009). In comparison to PrP^{Sc} , PrP^{C}

is rich in α -helical secondary structure, soluble in mild detergents, proteinase K-sensitive, and exists in a stable monomeric state (Stöhr et al., 2008).

PrP^C consists of two N-linked glycosylation sites at Asn₁₈₁ and Asn₁₉₇ of human PrP which may be present as di-, mono-, or unglycosylated species upon glycosylation (Harris, 1999; Lehmann, Milhavet, & Mangé, 1999). The N-linked glycans play an important role during glycoprotein trafficking, structure maintenance, and may contribute to the functional properties of the membrane-associated PrP^C as well as during the early steps of secretory pathway by enhancing folding efficiency of the newly synthesized proteins (Fiedler & Simons, 1995; Parodi, 2000; Varki, 1993). The association between PrP glycosylation alterations and transmissible spongiform encephalopathies (TSE) diseases is well established. For instance, the expression of PrP mutant, E200K (substitution of Glutamic acid with Lysine at codon 200) containing an aberrant glycan at residue 197 was found in 50% of inherited CJD. E200K increased the production of truncated fragments and impaired transport of the unglycosylated isoform to the cell surface (Capellari et al., 2000).

The catalogue of the physiological functions of PrP^C is beginning to be elucidated through the wide-ranging research in the last decade. Indeed, some of the major proposed functions for PrP^C which have been documented include the protection against apoptotic and oxidative stress, cellular uptake or binding of copper ions, transmembrane signaling, formation and maintenance of synapses, and adhesion to the extracellular matrix (Westergard, Christensen, & Harris, 2007). Most studies have focused on the role of PrP^C in

neurodegenerative prion diseases since its discovery, whereas its function outside the nervous system remains unclear. Nevertheless, several captivating lines of evidence have emerged signifying that it plays an essential role not only in the nervous system, but also throughout the human body. PrP^C is expressed most abundantly in the brain, but has also been detected in other non-neuronal tissues such as lymphoid cells, lung, heart, kidney, gastrointestinal tract, muscle, and mammary glands (Mehrpour & Codogno, 2010).

One of the promising functions of PrP^C is its protective role in cell survival with regards to the protection against oxidative stress, serum deprivation, and TNF- α induced apoptosis (Christensen & Harris, 2008). The neuroprotective activity of PrP^C has also been demonstrated by *in vivo* study using N-terminally deleted forms of PrP in transgenic mice. Severe ataxia and progressive neurodegeneration limited to the granular layer of the cerebellum was observed in mice with two larger PrP deletions (Δ 32–121 or Δ 32–134) as early as 1-3 months after birth while introduction of single copy wild-type PrP gene completely abolishes the defect (Shmerling et al., 1998). Using human primary neurons *in vitro*, PrP in the presence of the octarepeat region has been shown to potently inhibit Bax-mediated neuronal apoptosis in spite of the GPI anchor signal peptide truncation (Bounhar, Zhang, Goodyer, & LeBlanc, 2001). It has also been shown that overexpression of PrP^C causes the conversion TNF- α -sensitive MCF7 cells into TNF- α -resistant cells, at least in part, by a mechanism involving alteration of cytochrome *c* release from mitochondria and nuclear condensation (Diarra-Mehrpour et al., 2004).

Since PrP has been associated with cellular survival, proliferation, and differentiation, aberrant PrP function may also contribute to carcinogenesis. Pan et al. (2006) demonstrated that PrP^C is highly expressed in metastatic gastric cancer tissues, and the protein exhibits an invasion-promoting effect on gastric cancer cells at least in part by a mechanism involving the activation of MEK/ERK pathway and transactivation of matrix metalloproteinase-11 (MMP11). In accordance, Li et al. (2009) also proposed that the binding of pro-PrP to filament A (FLNa) perturbs FLNa function, thus contributing to the aggressiveness of pancreatic ductal adenocarcinoma. Some of these collections of data indicate that PrP^C may be implicated in biology of glioblastoma, breast cancer, prostate and gastric cancer (Mehrpour & Codogno, 2010).

Cancer or malignant neoplasm is a type of genetic diseases in which a group of cells display uncontrolled growth, invasion, and sometimes metastasis (Smart, 2010). The six hallmarks of cancer include self-sufficiency in growth signals, insensitivity to growth-inhibitory signals, evasion of programmed cell death (apoptosis), limitless replicative potential, sustained angiogenesis, and tissue invasion and metastasis (Hanahan & Weinberg, 2000). It has been a fact that cancer is the leading cause of death worldwide where it is accounted for 7.4 million deaths (around 13% of all deaths) in 2004 and deaths from cancer worldwide are projected to continue rising, with an estimated 12 million deaths in 2030 (World Health Organization [WHO], 2009). Colorectal cancer is the third most common cancer in both men and women where an estimated 639,000 deaths are expected to occur each year (WHO, 2009). In Peninsular Malaysia alone, colorectal cancer was the second most common cancer with a

total of 2,866 cases in 2006 while kidney and oral cancer have total of 383 and 22 cases registered, respectively (National Cancer Registry [NCR], 2006). With regards to the high prevalence of digestive system cancers, lacking of marker for early diagnosis might even worsen the prognosis as early cancer detection is important, when cancer is highly curable. Hence, the elucidation of the role of PrP^C in cancer biology might have significant implications on not only providing an early tumour marker, but also a striking target for therapeutic intervention in human digestive system cancers.

Moreover, understanding of apoptosis has been shown to be important for carcinogenesis; due the expansion of a population of neoplastic cells upon apoptosis defect, and as a basis for novel targeted therapies that are able to cause cell death or to establish cytotoxic agents and radiation therapy sensitization in cancer cells. Such novel agents include those which target the extrinsic and intrinsic pathways such as tumour necrosis factor-related apoptosis-inducing ligand receptor 1, antisense bcl-2 oligonucleotides, p53, NF- κ B, PI3K pathway, and ubiquitin/proteosome pathway (Ghobrial, Witzig, & Adjei, 2005; Giménez-Bonafé, Tortosa, & Pérez-Tomás, 2009). PrP^C has also been shown to be highly associated with the apoptosis pathways (Liang et al., 2006). Thus, investigation on PrP^C serves to be a spot-on direction as a candidate cancer protein owing to its previous neuroprotective properties and high levels of expression in certain cancers.

Given the insinuation of PrP^C in cancer biology, three cancer cell lines namely, oral squamous carcinoma (HSC-2), renal cell adenocarcinoma (ACHN), and

colorectal adenocarcinoma (LS174T) were chosen to study the role of PrP^C plays in carcinogenesis. Therefore, the objectives of this study are:

- (a) To investigate the levels of endogenous PrP^C expression in HSC-2, ACHN and LS174T cancer cell lines, and thereby to transiently or stably overexpress or knockdown PrP^C.
- (b) To evaluate the anti-apoptotic and anti-oxidative properties of PrP^C in cancer cell lines overexpressing or have knocked-down PrP^C, against tumour necrosis factor- α (TNF- α)-mediated cell death, hydrogen peroxide (H₂O₂)-induced oxidative stress and tunicamycin (TUN)-induced endoplasmic reticulum (ER) stress. The anti-apoptotic and anti-oxidative properties were established by 3-(4,5-dimethylthiazol-2-yl)-2,5-diphenyltetrazolium bromide (MTT) cell viability assay, flow cytometry analysis of Annexin V and Propidium iodide (PI) dual staining or 2',7'-dichlorofluorescein diacetate (DCFH-DA) staining and Western blot analysis to measure the expression levels of Bax and Bcl-xL proteins.
- (c) To study the role of PrP^C in cancer cell cycle progression via cell cycle synchronization using tunicamycin (TUN), a chemical which is able to trigger suppression of S-phase and arrest cell cycle in late G₁-phase.

CHAPTER 2

LITERATURE REVIEW

2.1 Prion Diseases and the Prion Hypothesis

The word prion which refers to proteinaceous infectious particles was first coined by Dr. Stanley B. Prusiner in the year 1982 (Prusiner, 1982). The abnormal isoform of this protein, scrapie prion (PrP^{Sc}) is the causative agent of prion diseases, which are also known as transmissible spongiform encephalopathies (TSEs). TSEs are a group of rare neurodegenerative diseases which includes kuru, fatal familial insomnia (FFI), sheep scrapie, bovine spongiform encephalopathy (BSE), Creutzfeldt-Jakob disease (CJD), Gerstmann-Sträussler-Scheinker syndrome in humans, as well as chronic wasting disease in elk and deer (McNally et al., 2009). These diseases are characterized by spongiform change, progressive vacuolation of neutrophil, neuronal degeneration, protein aggregation which lead to further amyloid plaque formation along with gliosis (Prusiner, 1998). TSEs or prion diseases can be infectious, sporadic, or genetic, or a combination of these factors in nature (Table 2.1). Prion diseases affect approximately 1.5 person per million worldwide annually, a rate that has remained stagnant over the last few decades. Fifteen percent of the human cases of TSEs are familial CJD which are inherited as autosomal dominant mutation of the PrP gene (*PRNP*) while the majority of human prion diseases are sporadic (Brown & Mastrianni, 2010).

Table 2.1: The prion diseases

Disease	Host	Mechanism of Pathogenesis
Kuru	Fore people	Infection through ritualistic cannibalism
iCJD	Humans	Infection from prion-contaminated HGH, dura mater grafts, etc
vCJD	Humans	Infection from bovine prions?
fCJD	Humans	Germ-line mutations in PrP gene
GSS	Humans	Germ-line mutations in PrP gene
FFI	Humans	Germ-line mutations in PrP gene (D178N, M129)
sCJD	Humans	Somatic mutation or spontaneous conversion of PrP ^C into PrP ^{Sc} ?
FSI	Humans	Somatic mutation or spontaneous conversion of PrP ^C into PrP ^{Sc} ?
Scrapie	Sheep	Infection in genetically susceptible sheep
BSE	Cattle	Infection with prion-contaminated MBM
TME	Mink	Infection with prions from sheep or cattle
CWD	Mule deer, elk	Unknown
FSE	Cats	Infection with prion-contaminated bovine tissues or MBM
Exotic ungulate encephalopathy	Greater kudu, nyala, oryx	Infection with prion-contaminated MBM

Note: iCJD, iatrogenic CJD; vCJD, variant CJD; fCJD, familial CJD; sCJD, sporadic CJD; GSS, Gerstmann–Sträussler–Sheinker disease; FFI, fatal familial insomnia; FSI, fatal sporadic insomnia; BSE, bovine spongiform encephalopathy; TME, transmissible mink encephalopathy; CWD, chronic wasting disease; FSE, feline spongiform encephalopathy; HGH, human growth hormone; MBM, meat and bone meal. Adapted from Prusiner, 1998.

Sporadic prion diseases are thought to be triggered by a rare and stochastic change of the normal cellular prion protein (PrP^C) conformation, which leads to the formation of PrP^{Sc}. However, the mechanisms that cause these changes are not known. Metabolic disturbances in the brain such as metal imbalance, oxidative damage, or impairment in proteasome activity may promote this conversion process (Sy, 2003).

A major pathological trait of prion diseases includes cerebral deposition of the PrP^{Sc}. The infectious scrapie prion is abnormally folded, mostly comprises of β -sheet monomers. They form insoluble aggregates such as amyloid plaques within the CNS and is partially resistant to proteinase K, which is only able to remove an estimate of 67 amino acid residues (6-7kDa) from the amino terminus of each residual molecule in the aggregates (Caughey, Kocisko, Raymond, & Lansbury, 1995).

Another unique feature of prion diseases is that they are self-propagating and transmissible. The pathogenic agent, PrP^{Sc} is self-propagating by an autocatalytic mechanism causing it to bind to the PrP^C and directing its post-translational conformational conversion to the PrP^{Sc} state. In other words, scrapie prion is able to alter the normal conformation of PrP^C, converting them into the infectious isoform. This mechanism is infectious in the fact that they are transmissible, hence is threatening to both humans and animals (Caughey, Baron, Chesebro, & Jeffrey, 2009; Cobb & Surewicz, 2009).

The protein-only hypothesis remains controversial and is still debated by a minority of researchers who favour the virion hypothesis. Generation of scrapie prions *in vitro* by several studies strongly suggest against virion hypothesis of prion transmission (Castilla, Saá, Hetz, & Soto, 2005; Deleault, Harris, Rees, & Supattapone, 2007). A recent study by Ma's team generated infectious prions featuring traits of the pathogenic PrP isoform such as aggregation, protease-resistance, and self-perpetuating, using recombinant murine PrP expressed from *E.coli*. Subsequent to recombinant prion intracerebral injection, mice

succumbed to prion disease and were able to serially transmit the disease (F. Wang, X. Wang, Yuan, & Ma, 2010). Thus, this is in accordance with the prion hypothesis which states that altered PrP conformation is responsible for the infectivity of prion disease in mammals. Conversely, Manuelidis (2007) proposed the virion hypothesis and reported that TSEs might be caused by a replicable informational molecule (which is likely to be a nucleic acid) bound to PrP, possibly a unique class of unidentified "slow" viruses; a virion of 25nm in diameter, which is found in estimated 10% of their scrapie-infected cells in culture. Furthermore, the specific and distinct biological properties of many TSEs such as strain variations, long incubation period, and rapid onset of symptoms which could not be explained by prions provide added advantages to further support the virion hypothesis (Manuelidis, Yu, Barquero, & Mullins, 2007).

2.2 Functional Characteristics of PrP^C

PrP^C is encoded by the highly conserved *PRNP* gene which consists of three exons with the entire open reading frame located in exon 3 and localized in the p12/p13 region of human chromosome 20 (Basler et al., 1986). This normal cellular protein is anchored to the plasma membrane and mainly expressed in the CNS (Stahl et al., 1987). While PrP^C and PrP^{Sc} possess the same primary structure, as opposed to PrP^{Sc}, the non-infectious PrP^C is rich in α -helical secondary structure, soluble in mild detergents, and exists in a stable monomeric state. The membrane bound PrP^C is proteinase K-sensitive and can be released from the cell surface *in vitro* by the enzyme phosphatidylinositol

phospholipase C, which cleaves the GPI moiety (Stöhr et al., 2008). Figure 2.1 shows the biochemical and biophysical properties differences between PrP^C and PrP^{Sc}.

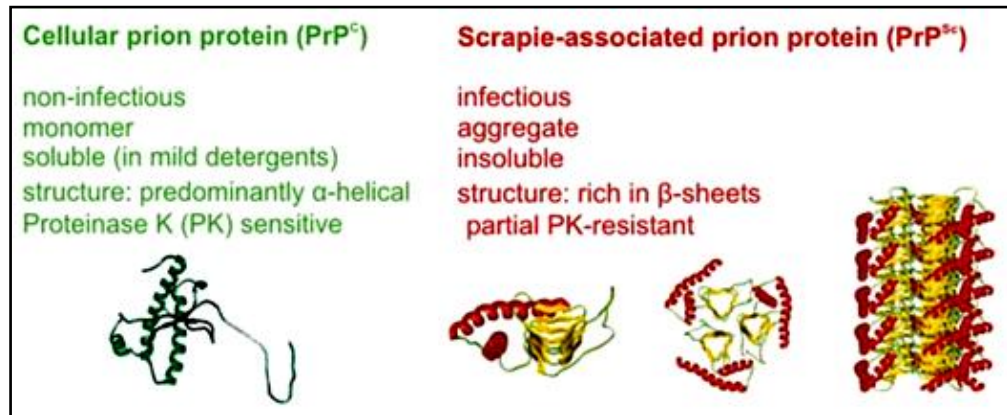


Figure 2.1: Biochemical and biophysical properties of PrP^C and PrP^{Sc}. Structure of PrP^{Sc}-like oligomers in comparison with PrP^C. Figure taken from Govaerts, Wille, Prusiner, and Cohen, 2004.

2.2.1 Molecular Structure of PrP^C

Mature PrP^C is a highly conserved GPI-anchored sialoglycoprotein consisting of 209 amino acid residues which is normally attached to the cell surface. PrP^C contains a hydrophobic N-terminal signal peptide (N-ter¹⁻²³) sequence of 22 amino acids. The pre-assembled GPI anchor is attached to the PrP after cleavage of the second hydrophobic C-terminal GPI signal peptide (C-ter²³¹⁻²⁵⁴) (Shyng, Heuser, & Harris, 1994; Sunyach et al., 2003). NMR spectroscopy and X-ray crystallography indicate that the 3-D structure of PrP^C consists of a highly-conserved hydrophobic region (106–126), a disordered N-terminal region (23-124) and a C-terminal region (125-228) composed of three α -

helices, which is monomeric and two short β -strands flanking the first α -helix (Riek et al., 1996; Zahn et al., 2000).

The PrP^C has two N-linked glycosylation sites at Asn₁₈₁ and Asn₁₉₇ of human PrP and a single unique disulphide bridge between the two Cysteines (Cys¹⁷⁹–Cys²¹⁴) in the most structured C-terminus domain. An octarepeat region of PHGGGWGQ encompassing the codon 51 through 91 of the N-terminus is responsible for copper binding. Two additional copper binding sites at Histidine 95 and 110 are termed the “5th Site” as four copper ions can bind to the octarepeat region (Aronoff-Spencer et al., 2000; Wang et al., 2009). Figure 2.2 illustrates the post-translational modifications of PrP^C and its isoforms.

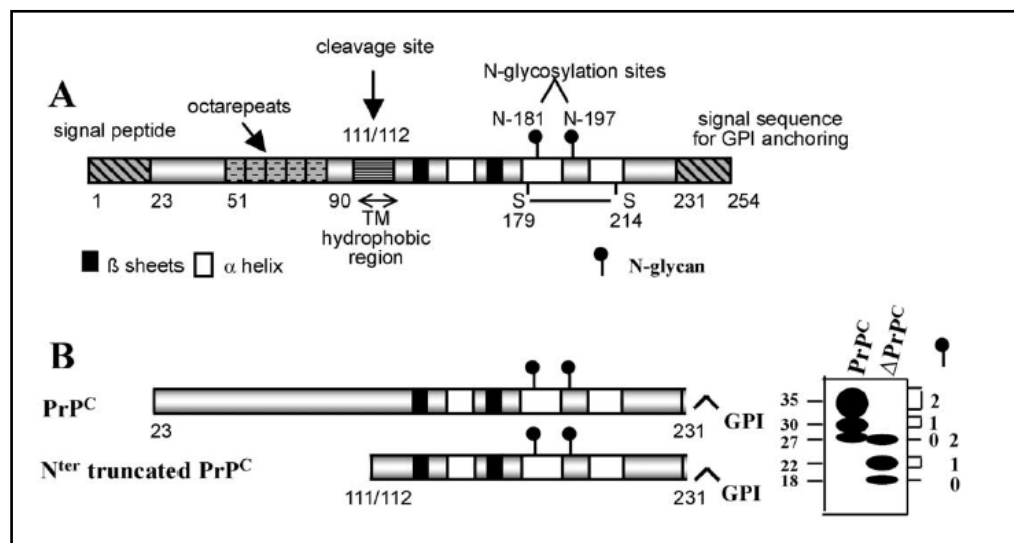


Figure 2.2: Scheme illustrating post-translational modifications of PrP^C and PrP^{Sc}. (A) Primary structure of PrP^C. (B) Different isoforms (native and truncated) and glycoforms of PrP^C. By western blotting (right scheme), full length as well as N-terminally truncated PrP^C (Δ PrP^C) are found as di-, mono- and non-glycosylated species. Figure taken from Ermonval, Mouillet-Richard, Codogno, Kellermann, and Botti, 2003.

2.2.2 Biogenesis and Cellular Localization of PrP^C

The biogenesis of PrP^C appears routine at the onset just like any other secretory protein as shown in Figure 2.3. The newly synthesized PrP^C of 254 amino acid residues is translocated to the endoplasmic reticulum (ER), which is the first compartment of the secretory pathway, due to the presence of an N-terminal that is then cleaved co-translationally. PrP^C undergoes further processing and is subjected to several post-translational modifications in the ER concurrently or in a subsequent reaction such as the addition of immature high mannose-type oligosaccharide (Glc₃–Man₉–GlcNAc₂) at the two N-linked glycosylation sites, formation of disulphide bond as well as the attachment of a GPI moiety after the removal of the C-terminal GPI signal peptide via transamidation reaction (Singh et al., 2006).

The modified PrP is transported from the ER to the cell surface along the secretory pathway where it is predominantly localized to lipid rafts via the GPI anchor. Further processing of the N-linked oligosaccharides in the different stacks of the Golgi apparatus and in the trans-Golgi network during PrP trafficking results in modified glycosylation to achieve their mature highly sialylated form (Vey et al., 1996). At the cell surface, PrP^C may be shed via cleavage of the GPI anchor by specific phospholipases or as a part of its normal life cycle, undergoes endocytosis and recycles between endocytic compartment and the cell surface (Chen et al., 1995; Perini et al., 1996).

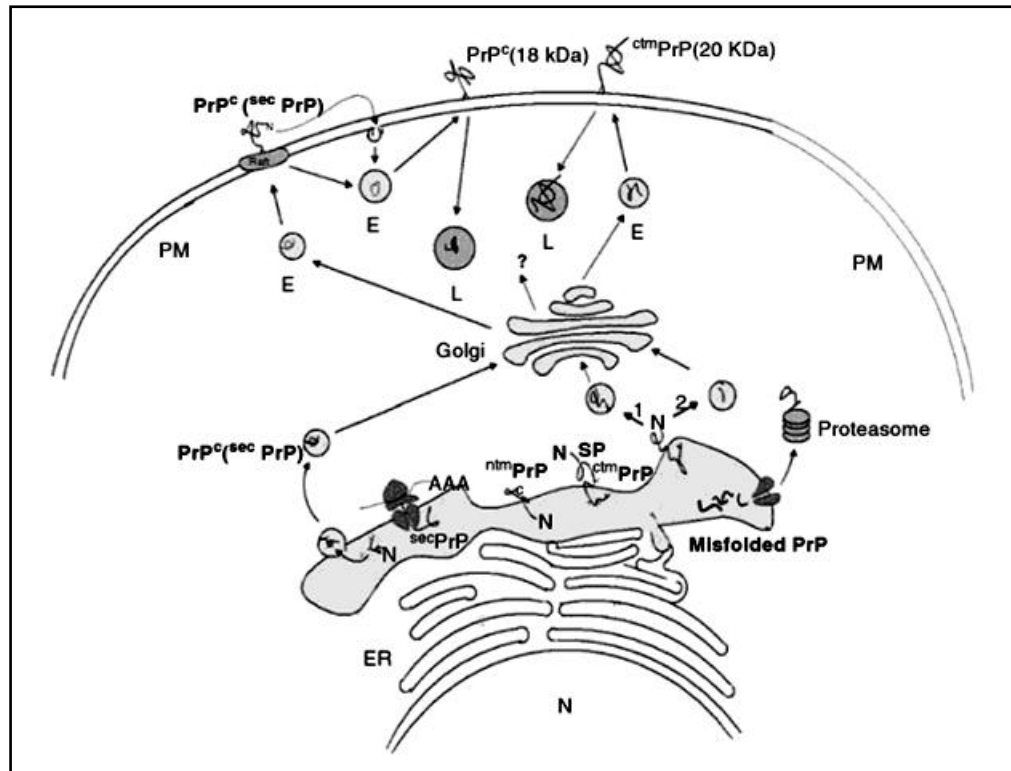


Figure 2.3: Biogenesis of PrP^C. PrP is synthesized in three distinct topological forms at the ER membrane. ^{Sec}PrP or PrP^C is translocated fully into the ER lumen and is transported along the secretory pathway. During constitutive rounds of recycling through lipid rafts or clathrin-coated pits, PrP^C is truncated, and the C-terminal 18kDa fragment is transported back to the plasma membrane. ^{Ctm}PrP is either retained in the ER (1), truncated at ~residue 90 and the C-terminal fragment is transported to the plasma membrane (2), or is transported to the Golgi apparatus, beyond which its fate is uncertain. The fate of ^{Ntm}PrP is unclear. PM: plasma membrane; E: endosome; L: lysosome; ER: endoplasmic reticulum; N: nucleus. Figure taken from Singh et al., 2006.

During endocytosis, full length PrP^C undergoes α -cleavage at position 111/112 within the conserved hydrophobic region by a disintegrin and metalloprotease (ADAMs) 10 and 17 (also known as TACE) resulting in a truncated C-terminal 18kDa fragment PrP^{Cter113–235}, namely C1, that is transported back to the plasma membrane while the N-terminal fragment PrP^{Nter23–111}, N1, is released in the extracellular space (Chen et al., 1995; Perini et al., 1996). Moreover, recent data indicate that α -cleavage may also occur in the late secretory pathway rather than, or in addition to, the endocytic pathway (Walmsley, Watt, Taylor,

Perera, & Hooper, 2009). Noteworthy, the 18kDa fragment is different from the ROS-mediated β -cleavage products; 21kDa C-terminal fragment, C2 and the corresponding N-terminal fragment, N2 which is at or near residue 90, in association with the amyloidogenic 106-126 region of PrP (Singh et al., 2006). Mammalian PrP^C normally has a half-life of 6hr where the regulation of lysosomal degradation is responsible for its turnover. A minor but significant population of PrP^C is believed to be degraded by the proteasomal pathway (Parodi, 2000).

Besides the secretory form ^{sec}PrP which is translocated across the ER membrane and is the precursor of the GPI-anchored PrP^C, a few topological forms corresponding to distinct transmembrane forms of PrP^C have also been described. Transmembrane PrP exists as either ^{Ctm}PrP, with its C-terminus located in the ER lumen or ^{Ntm}PrP, in the opposite orientation where the C-terminus is in the cytosol (Hegde et al., 1998). Both transmembrane forms are integrated into the lipid bilayer through the hydrophobic transmembrane domain (residues 112–136), referred to as TM1 via mechanism that may involve modulation of the ER targeting step (Holscher, Bach, & Dobberstein, 2001; Kim, Rahbar, & Hegde, 2001; Stewart, Drisaldi, & Harris, 2001) and/or partitioning of populations at the translocation channel (Kim & Hegde, 2002).

As opposed to ^{Ntm}PrP, ^{Ctm}PrP is GPI-anchored, contains an uncleaved N-terminal signal peptide in the cytosol, and can be glycosylated (Singh et al., 2006). The expression of ^{Ctm}PrP in post-ER compartments during neurodegeneration is attributed to mutations in PrP or even in the trans-acting

factors regulating topology at the ER. These might eventually cause disease as in certain cases of Gerstmann-Sträussler-Scheinker (GSS) syndrome, the PrP mutation Ala117Val led to increased ^{Ctm}PrP expression in frozen brain samples of two Ala117Val GSS patients but not in a control patient (Hegde et al., 1998). No ^{Ntm}PrP has been reported in association to any prion diseases and has only been demonstrated in cultured cell and transgenic animal systems. However, ^{Ntm}PrP was expressed intracellularly and up-regulated on the activated platelet membrane of patients with paroxysmal nocturnal haemoglobinuria (Holada et al., 2002). Transmembrane forms of PrP are exclusively degraded by the proteasome under steady state conditions (Helenius, 1994).

In addition to the topological isoforms as mentioned earlier, cytosolic soluble forms of PrP have been described. The cytosolic appearance of PrP arises from either retrotranslocation of misfolded or mutant PrP forms lacking the N-terminal signal peptide from the ER into the cytosol, defensive quality control in the ER or failed translocation into the ER due to intact weak signal peptide (Drisaldi et al., 2003; Rane, Yonkovich, & Hegde, 2004). CyPrP has been shown to possess both protective and toxic functions since the protein protects against Bax-mediated cell death in human neurons but is toxic to mouse neuroblastoma N2a cells and cerebellar neurons. Under certain circumstances, CyPrP is cytotoxic and becomes infectious if spared by the proteosomal degradation machinery (Lin, Jodoin, Baril, Goodyer, & Leblanc, 2008).

2.2.3 PrP^C Glycosylation

The biogenesis of PrP yields a final protein of 209 amino acid residues which may be present as di-, mono-, or unglycosylated species upon glycosylation, depending on the number of glycosylation sites (Asn181IleThr and Asn197PheThr in humans) occupied with N-linked oligosaccharide (Harris, 1999; Lehmann et al., 1999). By means of biochemical and mass spectrometry, more than 50 different glycans have been reported in PrP^C purified from Syrian hamster brains (Endo, Groth, Prusiner, & Kobata, 1989; Rudd et al., 1999).

Carbohydrates, particularly the N-linked glycans play an important role during glycoprotein trafficking, as well as at early steps of the secretory pathway by enhancing folding efficiency of the newly synthesized proteins. N-glycans initiate proper protein folding by promoting interference of classical chaperones and other folding-assisting proteins. *In vitro* studies using exogenously expressed forms of PrP^C has established the significance of glycosylation in its structure maintenance. The complex N-linked glycans are regularly interacting with the environment due to their physical characteristics, particularly their high hydrophathy and may contribute to the function of membrane proteins (Fiedler & Simons, 1995; Parodi, 2000).

N-glycans also play structural role by conferring stability on the proteins to which they are attached where upon N-linked glycosylation inhibition, conversion of PrP^C to PrP^{Sc} occurs more readily (Joao & Dwek, 1993; Taraboulos et al., 1990). The N-linked glycans might shield a large part of PrP^C

surface owing to their relative size compared to the protein structure. Eventually, diglycosylated PrP^C carrying two N-linked glycans is expected to increase the free energy barrier to the transition state and further delays the conversion (Korth, Kaneko, & Prusiner, 2000). Lehmann and Harris (1997) reported that PrP molecules with properties similar to PrP^{Sc} such as non-ionic detergent insolubility and partially resistant to digestion by proteinase K have been generated upon mutation of glycosylation consensus sites (AsnXaaThr) or tunicamycin treatment in cells expressing recombinant PrP^C. This suggests that absence of N-linked glycosylation favours the likeliness of PrP^C sequence to adopt a β -sheet conformation (Lawson, Collins, Masters, & Hill, 2005).

The association between PrP glycosylation alterations and TSE diseases is well established. PrP instability either directly or indirectly through trafficking perturbation in N-linked glycosylation impaired mutants, D178N, can be partially corrected by N-glycosylation in transfected cells reproducing the FFI and CJD178 genotypes (Petersen, Parchi, Richardson, Urig, & Gambetti, 1996). The expression of PrP mutant E200K containing an aberrant glycan at residue 197 was found in 50% of inherited CJD. E200K increased the production of truncated fragments and impaired transport of the unglycosylated isoform to the cell surface (Capellari et al., 2000). In due course, a comparison sugar analysis revealed that both PrP^{Sc} and PrP^C contains different but overlapping sets of glycan structures where a higher proportion of the tri- and tetra-antennary complex type glycans were found in PrP^{Sc}. This suggests that the former is more accessible to the glycan-processing enzymes, N-acetylglucosaminyltransferase III (Rudd et al., 1999).

2.2.4 Physiological Functions of PrP^C

PrP^C is expressed in a wide range of tissues throughout the body although it is predominantly expressed in the CNS region. Yet, the complete catalogue of its functions has not been fully determined. Most studies have focused on its role in neurodegenerative diseases, whereas its function outside the nervous system remains obscure. Some of the proposed foremost functions of PrP include protection against apoptosis and oxidative stress, cellular survival, proliferation, and differentiation, cellular uptake or binding of copper ions, transmembrane signaling, formation and maintenance of synapses, and adhesion to the extracellular matrix (Nicolas, Gavín, & del Río, 2009; Westergard et al., 2007). Protective function of PrP^C against apoptosis and oxidative stress as well as its role as a copper-binding protein will be discussed further in Section 2.4.

2.2.4.1 PrP^C and Signal Transduction

Localization of PrP^C in the lipid raft domains on the plasma membrane enriched in sphingolipids and cholesterol indicates the participation of PrP in cell signalling pathways (Petrakis & Sklaviadis, 2006). Studies of signal transduction patterns suggest that PrP^C can activate various transmembrane signaling pathways responsible for neurite outgrowth, neuronal survival or differentiation and neurotoxicity (Westergard et al., 2007).

Deletion of PrP^C in Prnp^(0/0) mice has been shown to impair the PI3K/Akt signalling pathway upon down-regulation of post-ischaemic phospho-Akt expression, subsequent to post-ischaemic Caspase-3 activation, and neuronal injury aggravation after focal cerebral ischaemia. This finding suggests a neuroprotective role of PrP^C by regulation of the PI3K/Akt pathway (Weise et al., 2006). Conversely, PrP^C conveys its neurotoxic effects via specific signaling cascade activation. The synthetic peptide PrP106–126, which displays certain biochemical properties of PrP^{Sc} has been reported to trigger PrP^C signaling pathways probably the JNK-c-Jun pathway. JNK-c-Jun pathway activation is responsible for the PrP^C-mediated neurotoxicity (Carimalo et al., 2005; Pietri et al., 2006).

2.2.4.2 Functional Role of PrP^C in Synapses

The up-regulation of PrP^C expression at synapses suggests a prominent role of the protein in synaptic structure, function, and maintenance. Regulation of synapse formation by PrP^C has been demonstrated in Kanaani's study where upon exposure of cultured rat fetal hippocampal neurons to purified recombinant PrP, rapid elaboration of axons and dendrites, and synaptic contacts elevation was observed (Kanaani, Prusiner, Diacovo, Baekkeskov, & Legname, 2005). Likewise, PrP^C have been shown to facilitate synaptic transmission by inducing acetylcholine release potentiation at the neuromuscular junction (Re et al., 2006). Other evidences relating to the participation of PrP^C in synapse formation and function include reorganization of mossy fibre, circadian activity alterations, and cognitive deficits in mice

devoid of PrP (Colling, Khana, Collinge, & Jefferys, 1997; Criado et al., 2005; Tobler et al., 1996).

2.2.4.3 Cell Adhesion Regulation by PrP^C

PrP^C has been found to play a role in cell adhesion modulation by interacting with cell adhesion molecule such as neural cell adhesion molecule (N-CAM). This direct interaction promotes the redistribution of N-CAM to lipid rafts followed by activation of fyn kinase, an enzyme involved in NCAM-mediated signalling, and further enhancement of neurite outgrowth in cultured hippocampal neurons (Santuccione, Sytnyk, Leshchyns'ka, & Schachner, 2005). Using PC12 cells and hippocampal neurons, PrP^C has also been shown to be a saturable, specific and high-affinity receptor to laminin which is responsible for cell proliferation, neurite outgrowth, and cellular migration (Graner et al., 2000).

2.3 An Overview of Cancer Biology

2.3.1 Introduction to Cancer

Malignant neoplasm, which is more well-liked with the name cancer, is a type of genetic disease in which a group of cells display uncontrolled growth (division beyond the normal limits), invasion (intrusion on and destruction of adjacent tissues), and sometimes metastasis (spread to other locations in the body via lymph or blood) (Smart, 2010).

Cancer is the leading factor of death globally where it accounted for 7.4 million deaths, which is around 13% of all deaths in 2004. The top cancer killers include lung, stomach, liver, colon, and breast cancer. Deaths from cancer worldwide are expected to continue rising, with an estimated 12 million deaths in 2030 (WHO, 2009). In Malaysia alone, nearly 22,000 new cancer cases were diagnosed among Malaysians in Peninsular Malaysia in 2006. The most frequent cancer among Malaysians during that period was breast followed by colorectal, lung, cervix, and nasopharynx (NCR, 2006).

Digestive system cancers refer to a malignancy that affects the gastrointestinal system, which involves the alimentary canal or gastrointestinal (GI) tract that open at both ends from the mouth to the rectum (mouth, pharynx, esophagus, stomach, intestines) as well as other various organs that are connected to the GI tract such as the salivary glands, teeth, liver, gall bladder, pancreas and vermiform appendix. The types of digestive system cancers include stomach cancer, esophagus cancer, small intestine cancer, colon cancer, colorectal cancer, and others (Sargh & Gross, 2007).

Colorectal cancer is the third leading cause to overall cancer mortality of estimated 639,000 deaths reported each year (WHO, 2009) while in Peninsular Malaysia, colorectal cancer was the second most common cancer with a total of 2,866 cases registered with NCR in 2006. The colorectal cancer was the most frequent cancer among men and Chinese. On the other hand, kidney and oral cancer have total of 383 and 22 cases registered, respectively (NCR, 2006).

2.3.2 Hallmarks of Cancer

Most if not all cancers have acquired the same set of features during their development as they become cancerous. The six hallmarks of cancer include self-sufficiency in growth signals, insensitivity to growth-inhibitory (antigrowth) signals, evasion of programmed cell death (apoptosis), limitless replicative potential, sustained angiogenesis, and tissue invasion and metastasis (Hanahan & Weinberg, 2000).

Dependence on exogenous growth stimulation is greatly reduced in cancer cells. Instead, they possess autonomy during heterotypic signaling, involving alteration of either extracellular growth signals, transcellular transducers of those signals, or intracellular circuits that translate those signals into action (Hanahan & Weinberg, 2000). Cancer cells synthesize their own growth signals such as PDGF (platelet-derived growth factor) and TGF α (tumor growth factor α) in glioblastomas and sarcomas, respectively, or behave as if a growth stimulus were present even in the absence of growth hormone, thus creating a positive feedback loop, termed as autocrine stimulation (Fedi, Tronick, & Aaronson, 1997). Nevertheless, cancer cells have the ability to evade the antigrowth signals, possibly by modulating the components governing the transit of the cell through the G₁-phase of its proliferative cycle, thus maintaining their replicative capacities and fueling their uncontrolled growth and division (Hanahan & Weinberg, 2000). Apoptosis is vital for normal developmental processes as well as providing a means to remove DNA damaged cells in adults. Unlike normal cells, cancer cells have the ability to

evade apoptosis and thus they grow and divide uncontrollably even as they accumulate mutations (Hanahan & Weinberg, 2000). At least 50% of human cancers show mutations involving the p53 tumour suppressor gene, which in turn resulting in functional inactivation of its product, the p53 protein and subsequent removal of a key component of the DNA damage sensor that can induce the apoptotic effector cascade (Harris, 1996).

Progressive shortening of telomeres by about 50-100bp loss of telomeric DNA during each successive cell division eventually halt cell division as these telomeres become too short, thus leading to replicative cell senescence (Counter et al., 1992). Cancer cells achieve immortalization and infinite replicative potential by lengthening their telomeres via telomerase enzyme, which adds hexanucleotide repeats onto the ends of telomeric DNA (Bryan & Cech, 1999). Besides, cancer cells induce angiogenesis (new blood vessel formation) and sustain blood vessel growth for oxygen and nutrients supplies which are crucial for sustainable cancer growth, cellular function and survival (Hanahan & Weinberg, 2000). Cancer cells activate the “angiogenic switch” by altering the balance of angiogenesis inducers and countervailing inhibitors, probably involving gene transcription (Hanahan & Folkman, 1996). Acquisition of genetic alterations in cancer cells allow them to break free from the primary tumour, penetrate into lymphatic and blood vessels, circulate through the bloodstream, and then invade sites where nutrients and space are not limiting, forming secondary metastatic lesions. These distant settlements of tumour are known as metastasis; the final stage of cancerous development that cause 90% of human cancer deaths (Sporn, 1996). Alterations of cells

possessing invasive or metastatic capabilities in several classes of proteins such as cell–cell adhesion molecules (CAMs) and calcium-dependent cadherin families mediate cell-to-cell interactions via integrins during the tethering of cells to their surroundings in a tissue (Aplin, Howe, Alahari, & Juliano, 1998).

2.3.3 Apoptosis: A Cell Suicide Mechanism

Eukaryotic cells undergo programmed cell death during senescence or when committed to suicide by a genetically controlled, regulated response called apoptosis. It is a normal physiological form of cell death that plays a crucial role in during embryogenesis and adult tissue stem cells maintenance (Cooper & Hausman, 2004). Apoptosis kills and eliminates damaged and potentially cancerous cells. Hence, one of the fundamental processes of cancer is probably the loss of this programmed cell death, resulting in uncontrolled cell proliferation (van Heemst, den Reijer, & Westendorp, 2007).

Apoptosis is defined by its morphological changes which entail cell shrinkage and rounding, membrane blebbing, loss of cell membrane asymmetry and attachment, chromatin condensation (pyknosis), chromosomal DNA fragmentation, as well as nuclear DNA fragmentation (karyorrhexis) leading to nucleus disintegration (Cardoso & Leonhardt, 1999). Chromatin margination and condensation occurs in the presence of preserved cellular structures which culminates with apoptotic bodies budding, and thus resulting in phagocytosis of the apoptotic bodies by macrophages and neighbouring cells, without any inflammatory response (Chen-Scarabelli & Scarabelli, 2004).

Apoptosis is mediated by the integration of various signalling pathways, some acting to induce cell death while others to promote cell survival. There are two main signalling pathways which have been identified in the control of apoptosis: the intrinsic (core pathway) and the extrinsic pathway. The former involves the mitochondria and the release of proteins from that organelle, including cytochrome *c*, apoptosis-inducing factor (AIF), and endonucleases G whereas the extrinsic pathway involves death receptors (DRs) at the plasma membrane (Hancock, 2010).

2.3.3.1 Death Receptor (DR) Pathway: TNF- α -mediated Apoptosis

Tumour necrosis factor- α (TNF- α) is encoded by the *TNF* gene which is located at chromosome 6p21.3. TNF- α is a 233 amino acids-long, 25.6kDa, type II transmembrane protein arranged into stable homotrimers which plays a key role in immune cells regulation. It is also responsible for apoptosis induction, inflammation initiation, carcinogenesis inhibition and viral replication (Gaur & Aggarwal, 2003; Locksley, Killeen, & Lenardo, 2001).

TNF- α mediates death signalling pathway via the activation of TNF receptor type 1, TNF-R1 (CD120a; p55/60). Binding of TNF- α to the widely expressed, TNF-R1 triggered the conformation-dependent release of inhibitory protein, silencer of death domains (SODD) from the intracellular death domain and enables the binding of multifunctional adaptor protein, TNF-R1 associated death domain (TRADD) to FADD, the Fas-associated protein with death domain, which then recruits the cysteine protease, Caspase-8. Autoproteolytic

activation of Caspase-8 and subsequent cleaving of effector caspases leads to apoptosis (Gaur & Aggarwal, 2003; Wajant, Pfizenmaier, & Scheurich, 2003).

2.3.3.2 Intrinsic Pathway: Mitochondria-mediated Cell Death

Cell death signals such as DNA damage, oxidative stress, and ischaemia lead to the activation of intrinsic, mitochondria-mediated apoptotic pathway. The mitochondrial pathway is often characterized by the permeabilization of mitochondrial outer membrane, subsequent cytochrome *c* release and thereby resulting in the assembly of apoptosome, which is a caspase-activating complex between Caspase-9 and apoptosis protease activating factor (APAF1) (Green & Kroemer, 2004).

Mitochondrial outer membrane permeabilization (MOMP) is regulated by the expression of Bcl-2 family members, which can be either pro-apoptotic (Bax, BAD, Bak and Bok) or anti-apoptotic (Bcl-xL, Bcl-2, and Bcl-w) (Dejean, Martinez-Caballero, Manon, & Kinnally, 2006). Bcl-xL (B-cell lymphoma-extra large) is a potent inhibitor of apoptosis which inhibits cell death by either heterodimerization with death agonists such as Bax (Bcl-2-associated X protein) or binding to the voltage-dependent anion channel (VDAC) in order to prevent the release of caspase activator, the cytochrome *c* (Minn et al., 1999; Vander Heiden et al., 2001).

Oligomerization of Bax and/or Bak (Bcl-2 homologous antagonist/killer) stimulates MOMP, thus forming the mitochondrial apoptosis-induced channel

(MAC) that allows the release of apoptogenic proteins such as cytochrome *c*, apoptosis-inducing factor (AIF) and endonuclease G from the mitochondrial intermembrane space. Association of cytochrome *c* to APAF1 and pro-Caspase-9 leads to the formation of apoptosome complex, which in turn promotes the activation of Caspase-9. Activation of Caspase-9 leads to subsequent activation of effector Caspase-3 that directs the cascade of proteolytic reactions, resulting in cell death (Green & Kroemer, 2004; Hotchkiss & Nicholson, 2006). AIF and endonuclease G are involved in nuclear DNA fragmentation, which is the hallmark of apoptosis (Bajt, Cover, Lemasters, & Jaeschke, 2006).

2.3.3.3 Cross-talk between Extrinsic and Intrinsic Pathways

Both DR (extrinsic) and mitochondrial (intrinsic) pathways converge at the level of Caspase-3 activation which is tightly regulated by the caspase inhibitors, inhibitor of apoptosis proteins (IAPs). The Smac/DIABLO (second mitochondria-derived activator of caspases/direct IAP-associated binding protein with low pI) and Omi/HtrA2 (high temperature requirement A2) which is also released during MOMP antagonizes IAP activity and contribute to caspase-independent cell death (Adrain, Creagh, & Martin, 2001; Yang, Church-Hajduk, Ren, Newton, & Du, 2003).

Interconnection between the two apoptosis pathways is attributed to truncated Bid (tBid), which is a product of Bid, a widely expressed pro-apoptotic member of the Bcl-2 family, upon Caspase-8-mediated cleavage. Of note,

Caspase-8 is an enzyme that signals for the activation of extrinsic pathway (Section 2.3.3.1). The translocation of tBid to mitochondria upon cleavage facilitates the release of cytochrome *c* and thereby activating the intrinsic pathway (Esposti, Eler, Hickman, & Dive, 2001; Hengartner, 2000).

Recent studies have demonstrated that both extrinsic and intrinsic pathways can activate each other. Cleavage of Caspase-3 by active Caspase-9 triggered its activation, which in turn activates Caspase-8 in a feedback amplification loop. Few less firmly established studies have also hypothesized that the Caspase-3 activation might actually bring about the subsequent activation of Caspase-9 in a similar retrograde manner (Basu, Castle, Bouziane, Bhalla, & Haldar, 2006; Hotchkiss & Nicholson, 2006). Figure 2.4 illustrates the cross-talk of the two apoptosis pathways.

2.3.4 Cell Cycle Arrest and Apoptosis

Mitotic cell cycle progression is regulated by a wide range of positive and negative signals during cell proliferation. Interestingly, common morphological features such as cell shrinkage, chromatin condensation and membrane blebbing and the participation of cell cycle genes such as p53, retinoblastoma (RB) and E2F in apoptosis show a strong link between mitosis and apoptosis (Alenzi, 2004). Dysregulation of cell proliferation together with apoptosis suppression lead to further aberrant development in the contribution to malignancy (Evan & Vousden, 2001; R. Fotadar, Diederich, & A. Fotadar, 1996).

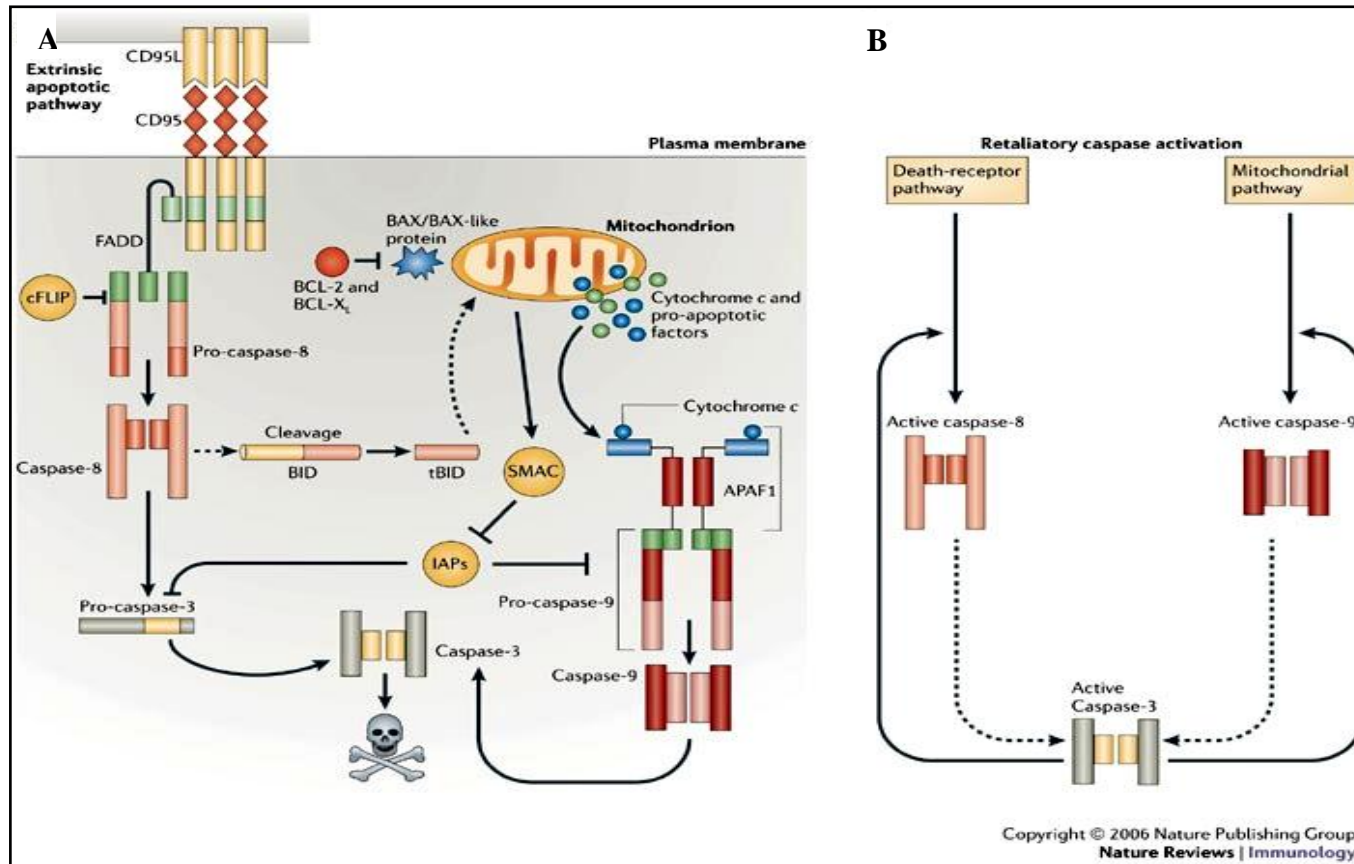


Figure 2.4: Cross-talk between extrinsic and intrinsic pathways. (A) In certain cell types, the extrinsic and intrinsic pathways are interconnected by tBID. (B) There is increasing evidence that, in certain cases, the two death pathways can activate each other via Caspase-3 activation. Figure taken from Hotchkiss and Nicholson, 2006.

2.3.4.1 Cell Cycle Regulation

The cell cycle clock or cell-division cycle is a series of events that governs cell replication upon receiving the growth regulatory signals (Foster, 2008). Cell cycle comprises of the four distinct phases: G₁-, S-, G₂- and M-phase. Cells, mostly eukaryotes, which are committed to replication shift from G₁-phase (the first gap) of the cycle, into S-phase (synthesis phase) for DNA synthesis, followed by G₂-phase, where cells prepare for duplication in the M-phase (mitotic phase) (De Souza & Osmani, 2007). Movement of cells from one phase to another is tightly regulated by the cyclin-dependent kinase (CDK) family of serine/threonine protein kinases.

Cells are only responsive to extracellular growth signals and specific mitogens at a discrete time in G₁-phase checkpoint, referred to as the restriction point, where subsequent absence of mitogens or growth signals will not affect cell cycle progression through the S-, G₂-, and M-phase unless cells return to their sensitive window in G₁-phase. In response to high cell density or mitogens and/or growth signal deprivation, cells with normal 2N DNA content will exit into the quiescent G₀-phase (Boye & Nordström, 2003; Zetterberg, Larsson, & Wiman, 1995).

2.3.5 Oxidative Stress and Apoptosis

Reactive oxygen species (ROS) such as hydroxyl radicals (OH[•]), superoxide anions (O₂⁻), and hydrogen peroxide (H₂O₂) are generated within the

mitochondria, which is the target of ROS itself. Imbalance between ROS-generating systems and ROS-detoxifying systems, the endogenous antioxidant defence mechanisms, will result in oxidative stress which ultimately leads to apoptosis (Buttke & Sandstrom, 1994).

For instance, hydrogen peroxide (H_2O_2) has been shown to act as a messenger in a variety of signalling pathways associated with apoptosis. H_2O_2 treatment in HeLa cells resulted in sustained activation of MAPK subfamilies such as the extracellular signal related protein kinase, c-Jun amino-terminal kinase/stress-activated protein kinase, and p38 (Wang, Martindale, Liu, & Holbrook, 1998). Besides, nitric oxide ($NO\cdot$) with a single unpaired electron has been implicated as an apoptosis inducer in macrophages and monocytes, epithelial cells, mesangial cells, and endothelial cells, as well as cancer cells (Albina, Cui, Mateo, & Reichner, 1993; Simon, Haj-Yehia, & Levi-Schaffer, 2000). However, the exact mechanism exerted by $NO\cdot$ during apoptosis induction remains vague.

ROS appears to be responsible for triggering the death receptor-mediated apoptosis (extrinsic pathway) in the subsequent mitochondrial events leading to full activation of the caspase cascade. It is postulated that the initial released ROS from mitochondria could augment the gating potential of the pore either directly or indirectly (via ceramide generation) upon oxidation of the mitochondrial pores, thus disrupting the mitochondrial membrane potential which in turn leads to cytochrome *c* release (Simon et al., 2000; Zamzami et al., 1995).

2.3.6 Unfolded Protein Response, ER Stress and Apoptosis

The folding pathway or final conformation of a protein in the ER can be altered by certain drugs that disrupt glycosylation (e.g. tunicamycin), disulphide bond formation and calcium homeostasis which in turn instigates ER stress and subsequent activation of a signalling network called the unfolded protein response (UPR) (Kaufman, 1999; Schröder & Kaufman, 2005). The UPR in mammalian cells brings about the activation of protein kinase RNA (PKR)-like ER kinase- (PERK-), activating transcription factor 6- (ATF6-), and inositol-requiring protein-1- (IRE1-) mediated signalling pathways to cope with the accumulation of unfolded ER protein and for normal cell function restoration. Consequently, UPR commits cells to apoptosis instead of promoting their survival during prolonged ER stress or when the protein-folding defect in the ER is irreversible (Walter, 2010; Xue et al., 2005).

In terms of apoptosis initiation, phosphorylation of eukaryotic translation initiation factor-2 (eIF2) induces the translation activating transcription factor 4 (ATF4) which in turn activates the translation of its target genes, CHOP (C/EBP-homologous protein) and subsequent GADD34 (growth arrest and DNA damage-inducible protein-34) activation (Harding et al., 2000; Welihinda & Kaufman, 1996). Association of GADD34 with protein phosphatase 1 (PP1) leads to eIF2 dephosphorylation and thus resulting in a negative feedback loop which recovers protein synthesis and stress-induced transcripts translation. CHOP is a pro-apoptotic, CCAAT/-enhancer-binding protein homologous protein which down-regulates Bcl-2 expression and subsequent activation of

the mitochondrial-dependent apoptotic pathway involving cytochrome *c* release and Caspase-3 activation (Ron & Walter, 2007; Yoshida, Haze, Yanagi, Yura, & Mori, 1998).

Alternatively, IRE1 may also initiate apoptosis. Association of phosphorylated IRE1 to TRAF2 (tumour necrosis factor receptor (TNFR)-associated factor-2) leads to JNK (Jun N-terminal kinase) pathway activation involving pro-Caspase-4 and subsequent downstream caspases activation to promote apoptosis. Formation of IRE1–TRAF2 complex has also been linked to Caspase-12 activation and intracellular signalling alterations, such as the suppression of insulin signalling, resulting in insulin resistance (Ron & Walter, 2007; Wang et al., 1996).

2.4 The Role of PrP^C in Cancer Biology

Although PrP^C is renowned as a highly expressing protein in the nervous system, existence of this protein has also been documented in other various systems throughout the body such as lymphoid cells, lung, heart, kidney, gastrointestinal tract, muscle, and mammary glands. Since then, new emerging data has revealed the implications of PrP^C in cancer biology for such that PrP^C may be involved in resistance to apoptosis, as well as proliferation and metastasis of human cancer cells.

2.4.1 The Anti-apoptotic Property of PrP^C

The anti-apoptotic activity of PrP^C has been demonstrated in a variety of experimental systems such as in mice, cultured mammalian cells, and yeast. However, the exact cellular and molecular pathways involved by PrP^C remain vague even though these diverse experimental systems suggest a common mechanism for its cytoprotective activity.

2.4.1.1 *In Vivo* Neuroprotection Evidences

Development of PrP knockout mice via homologous recombination in embryonic stem cells such as *Prnp*^{0/0} (Zürich I) and *Prnp*^{-/-} (Edinburgh) display distinct neurophysiological alterations and progressive demyelination in the peripheral nerves (Büeler, 1992; Mehrpour & Codogno, 2010). Subsequently generated PrP knockout mice lines such as *Prnp*^{-/-} (Nagasaki), Rcm0, and *Prnp*^{-/-} (Zürich II) have been shown to develop ataxia and age-related Purkinje cell loss. Noteworthy, these neurodegeneration phenotypes in Nagasaki, Zurich II, and Rcm0 PrP-null mice can be rescued by the reintroduction of *Prnp*-encoding transgenes, suggesting a neuroprotective function of PrP^C (Moore et al., 1999; Sakaguchi et al., 1996).

The neuroprotective activity of PrP^C is also demonstrated by an *in vivo* study using N-terminally deleted forms of PrP in transgenic mice. Severe ataxia and progressive neurodegeneration limited to the granular layer of the cerebellum was observed in mice with two larger PrP deletions (Δ 32–121 or Δ 32–134) as

early as 1-3 months after birth while introduction of single copy wild-type PrP gene completely abolishes the defect (Shmerling et al., 1998).

2.4.1.2 *In Vitro* Neuroprotection Evidences

Using human primary neurons, PrP in the presence of the octarepeat region has been shown to potently inhibit Bax-mediated neuronal apoptosis in spite of the GPI anchor signal peptide truncation (Bounhar et al., 2001). The octarepeat region of PrP^C is therefore proposed to be important for the anti-Bax function since the domain displays some similarity with the BH2 domain of Bcl-2. Moreover, familial PrP^C mutations D178N and T183A associated with the human prion diseases FFI and familial atypical spongiform encephalopathy has been shown to be partially or completely abolish PrP's neuroprotective function against Bax (Roucou et al., 2005).

The Bax inhibition activity has also been attributed to the cytosolic PrP, CyPrP which is uniquely expressed in the cytosol. Co-expression of various Syrian hamster PrP mutants in MCF-7 cells and primary human neurons has confirmed that the CyPrP is the anti-Bax PrP form in exclusion of transmembrane and secreted PrP forms (Lin et al., 2008; Roucou, Guo, Zhang, Goodyer, & LeBlanc, 2003). However, the physiological importance of CyPrP is yet to be assured since *in vivo* generation of this form from the wild-type molecule appears to be modest (Stewart & Harris, 2003).

Of note, the cytoprotective effect of PrP is very specific for Bax, since PrP cannot prevent cell death mediated by Bak (Bcl-2 antagonist killer 1), truncated Bid (tBid), staurosporine or thapsigargin. PrP has been shown to protect against Bax-mediated cell death in human primary neurons and MCF-7 cells by inhibiting Bax conformational change which is the first step in Bax activation and subsequent cytochrome *c* release. It has been proposed that PrP^C does not directly interact with Bax to prevent cell death. It is likely that PrP^C, together with Bcl-2 maintain Bax in an inactive state, thus conferring neuroprotection in mammalian cells (Roucou et al., 2005; Roucou & LeBlanc, 2005).

However, the neuroprotection evidences of PrP^C which circles around the involvement of Bax remain inconclusive. Using yeast *S.cerevisiae* as a model system, a form of mouse PrP encompassing a charged region of residues 23-31 and containing a modified signal peptide was shown to potently suppress cell death in yeast expressing mammalian Bax from a galactose-inducible promoter despite of octapeptide repeat region deletion (Li & Harris, 2005; Westergard et al., 2007). Furthermore, CyPrP-(23–231) has failed to show rescue effect in the growth of Bax-expressing yeast demonstrating that such protective activity requires targeting of PrP to destinations of the secretory pathway (Li & Harris, 2005; Westergard et al., 2007). Thus, the protective effect of PrP^C in yeast seems to be dependent on its interactions with endogenous yeast proteins that occur downstream of Bax during cellular stress or a toxicity pathway (Li & Harris, 2005).

2.4.1.3 Controversy of PrP^C Anti-apoptotic Property

The anti-apoptotic property of PrP^C is highly cell-specific and may be death stimuli-dependent. The hydrophobic, amyloid PrP fragment 106-126 (PrP106-126) has been shown to increase both *in vitro* and *in vivo* toxicity in cultured hippocampal neurons, primary cultures of mouse cerebral endothelial cells expressing PrP^C and retina (Deli et al., 2000; Ettaiche, Pichot, Vincent, & Chabry, 2000). Further investigation using primary culture of murine cortical neurons and transgenic mice 338 cortical neurons have been shown to exhibit substantial neuronal death within 24hr upon PrP106-126 exposure which may be due in part to the activation of c-Jun-N-terminal kinase (JNK) (Crozet, Beranger, & Lehmann, 2008). Additionally, overexpression of PrP^C in human embryonic kidney 293 cell line, rabbit epithelial Rov9 cell line, and murine cortical TSM1 cell line further sensitizes the cells to apoptotic inducer, staurosporine, a response involving Caspase-3 activation via transcriptional and post-transcriptional control of the tumour suppressor gene, p53 (Paitel et al., 2004; Paitel, Fahraeus, & Checler, 2003).

2.4.2 PrP^C, Copper Binding and Oxidative Stress

PrP^C is a copper-binding protein with an affinity that may be as high as 0.1nM depending on the binding site occupancy. Cu²⁺, and to a lesser extent Cu⁺, binds to the histidine-containing octarepeat region located at N-terminal region of the protein in a pH-dependent and negatively cooperative manner (Walter, Chattopadhyay, & Millhauser, 2006).

Hence, owing to the high affinity and number of Cu^{2+} -binding sites in PrP^{C} , it is suggested that PrP^{C} might act as an antioxidant via copper redox cycling by quenching the generated free radicals upon binding to the potentially harmful Cu^{2+} ions. Indeed, González-Iglesias et al. (2002) have demonstrated the formation of $\text{PrP}^{\text{C}}\text{-Cu}^{2+}$ glycosaminoglycan (GAG) complexes upon binding of PrP^{C} octarepeat region to GAGs which may be crucial entities in PrP^{C} metabolism. The formation of such oligomeric complexes is stabilized by Cu(II) bridges whereby His-bound Cu(II) may act as a cofactor for intermolecular recognition reactions. It has been further shown that up-regulation of ataxia-telangiectasia mutated (ATM)-mediated PrP^{C} transcription in murine N2a and human HeLa cells protects against copper-induced oxidative stresses and eventually cell death by reducing the intracellular copper concentration (Qin, L. Zhao, Ash, McDonough, & R. Y. Zhao, 2009).

Evidence supporting the role of PrP^{C} in copper metabolism has been documented in Brown's study that showed a reduced copper (but not any other transition metals) content and lower SOD activity in PrP^{C} -deficient cells. Hence, this further suggests that PrP^{C} modulates oxidative stress through SOD activity regulation in a copper-dependent manner (Brown et al., 1999; Brown & Besinger, 1998). Two distinct mechanisms have been proposed to elucidate the role of PrP^{C} in the cellular defence against oxidative stress. PrP^{C} may act directly as a copper-dependent SOD or indirectly by up-regulating the activities of other antioxidant proteins, such as Cu/Zn SOD that detoxify ROS to protect cells from oxidative stress (Brown et al., 1999; Brown & Besinger, 1998).

Besides, PrP^C may exert its protective mechanism towards oxidative stress by acting either upstream or downstream of ROS (Halliwell, 2006).

As mentioned in Section 2.2.2, ROS-mediated β -cleavage within or adjacent to the octarepeat region of PrP^C generates a 21kDa, GPI-anchored C-terminal fragment C2, and the corresponding 7kDa, N-terminal fragment N2 (residues 23–90) (Jiménez-Huete et al., 1998; Mangé et al., 2004; Watt et al., 2005). A study by Watt and Hooper (2005) shows increased sensitivity of human neuroblastoma cells to copper and H₂O₂ followed by reduced levels of glutathione peroxidase and increased amounts of intracellular oxygen radicals upon expression of two disease-associated mutants of PrP, namely PG14 and A116V (Ala(116)→Val) which are incapable of undergoing β -cleavage. This suggests that the β -cleavage event contributes to a pathway involved in cellular resistance against oxidative stress in neuronal cells (Watt & Hooper, 2005). Indeed, this is in accordance with a study by Malaisé, Schätzl, and Bürkle (2008) which proposed that the protective effect of PrP^C against oxidative stress in N2a mouse neuroblastoma involves the octarepeat region, and not the TM1 domain nor the high-affinity copper binding site described for human residues His96/His111.

2.4.3 PrP^C and Tumour Resistance

One of the distinct hallmarks of cancer cells is their capability to evade apoptosis (Hanahan & Weinberg, 2000). Supporting studies have shown the plausible implications of the anti-apoptotic role of PrP^C in cancer biology.

Silencing of PrP^C expression in human breast adenocarcinoma TRAIL sensitive MCF7 cell line and its two resistant counterparts; the multidrug resistant (MDR) MCF-7/ADR and TRAIL-resistant clone was shown to mediate Bax activation upon down-regulation of Bcl-2 expression. Eventually, this sensitizes breast cancer cells to TRAIL-induced apoptosis associated with caspase processing, Bid cleavage and Mcl-1 degradation (Clohessy, Zhuang, de Boer, Gil-Gómez, & Brady, 2006; Mehrpour & Codogno, 2010).

Liang et al. (2007) further demonstrated that siRNA knockdown of PrP^C expression in gastric cancer MKN28 cells sensitizes the cells to hypoxia-induced drug sensitivity. Instead, PrP^C expression was up-regulated in MKN28 gastric cancer cells during hypoxia resulting from the phosphorylation of several transcriptional factors by ERK1/2, which could in turn interact with the heat shock element (HSE) in PrP^C promoter (-2253 ~ +289) in MKN28 cells. Stress-inducible protein-1 (STI1) is a heatshock-related protein that produces neuroprotective activity in conjunction with PrP^C. Detection of STI1 secretion in human glioblastoma-derived cell line A172 via thymidine incorporation assays suggests the ability of STI1 to promote glioma proliferation via the MAPK and PI3K pathways (Erlich et al., 2007).

2.4.4 PrP^C and Tumour Progression

Expression of PrP^C has been shown to be associated with adjuvant chemotherapy resistance in patients with estrogen receptor (ER)-negative breast cancer where 15% patients displayed positive PrP^C expression in

primary breast cancer tissues. Thus, tumours expressing PrP^C did not seem to benefit from chemotherapy (Meslin et al., 2007).

Expression of PrP^C in gastric cancer cell lines SGC7901 and MKN45 significantly promotes adhesive, invasive, and *in vivo* metastatic capabilities of the cells in conjunction with increased promoter activity and up-regulation of matrix metalloproteinase-11 (MMP11) expression. The N-terminal fragment of PrP^C (amino acid 24-90) promotes invasion and metastasis at least in part of MEK/ERK pathway activation and subsequent MMP11 transactivation upon activation of Erk1/2 phosphorylation (Pan et al., 2006). As well, PrP^C overexpression has also been shown to promote carcinogenesis, G₁/S-phase transition, and proliferation in SGC7901 and AGS gastric cancer cells at least to some extent by mediating the PI3K/Akt pathway activation and subsequent CyclinD1 transactivation, in which the octapeptide repeat region might play an obligatory role (Liang et al., 2007).

2.5 RNA Interference

Post-transcriptional gene silencing (PTGS) which is more widely known as RNA interference (RNAi) was discovered by Dr. C. Mello and Dr. A. Fire in the nematode, *C.elegans* (Fire et al., 1998). It is a conserved biological mechanism to diminish or abolish gene expression, in which the incorporation of non-translated double stranded RNA (dsRNA) molecules called small interfering RNA (siRNA) into cells effectively directs the degradation of target messenger RNA (mRNA) in a highly sequence specific manner. RNAi has

been shown to occur in humans, animals, and plants (Dykxhoorn, Novina, & Sharp, 2003). This natural mechanism for gene silencing shows great importance in functional genomics for loss-of-function phenotypes systematic analysis; experimental biology revolution; therapeutic intervention against viral infections, dominant disorders, neurological disorders, and cancers via *in vivo* inactivation of disease-related gene products; as well as in agriculture and other areas (Agrawal et al., 2003; Walton, Wu, Gredell, & Chan, 2010).

The RNAi pathway consists of two main phases involving ribonucleases (RNases). Figure 2.5 shows the schematic overview of the RNAi mechanism. The first phase is initiated by the presence of silencing trigger of exogenous or endogenous origin such as short hairpin RNA (shRNA), which is transcribed from expression vector, dsRNA, or microRNA (miRNA) primary transcript. Trigger RNA, specifically dsRNA, is recognized and cleaved by RNase III-like enzyme Dicer to produce a short siRNA of 21- to 23-nucleotides (nt) in length with symmetric 2- to 3-nt overhangs on the 3' ends carrying hydroxyl groups and a phosphate at each 5' end. The highly specific structure of siRNA prevents erroneous gene silencing. Of note, exogenous shRNA enters gene silencing mechanism in the subsequent phase without having to undergo Dicer cleavage (Kim, Lee, Harris, Nakahara, & Carthew, 2006; Meister & Tuschl, 2004).

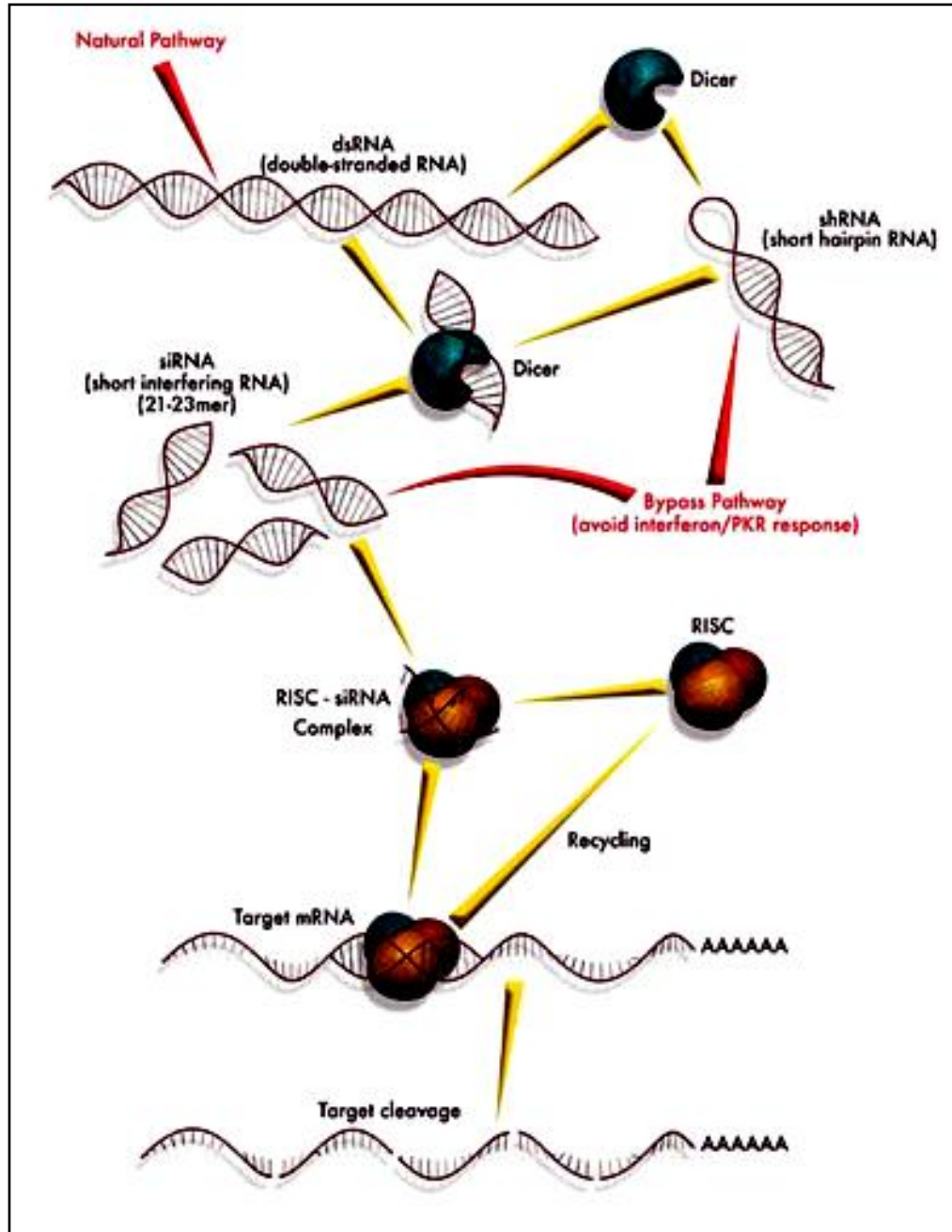


Figure 2.5: Mechanism of gene silencing by RNAi. Figure taken from Sarnow, Jopling, Norman, Schütz, and Wehner, 2006.

In the second phase, siRNA is integrated into multiprotein effector complex, RNA-induced silencing complex (RISC) which further directs its hybridization with mRNA target bearing the complementary sequences. The siRNA duplex is unwound by a helicase in RISC and the “antisense” strand remains bound to

RISC for subsequent degradation of the complementary mRNA sequence by nucleolytic cleavage. mRNA cleavage begins at single site 10-nt upstream of the 5'-most residue of the siRNA–target mRNA duplex by RNase H enzyme Argonaute family of proteins, specifically Argonaute 2 which is also known Slicer. Gene silencing is a result of translational inhibition upon degradation of the targeted mRNA (Ekwall, 2004; Hammond, 2005; Meister & Tuschl, 2004).

Initiation of RNAi response experimentally by dsRNA longer than 30-nt is unsuccessful in mammalian cells as they led to the induction of non-specific Type I interferon response (anti-viral response) and subsequent mRNA degradation as well as global inhibition of mRNA translation. Hence, protein expression is altered and eventually leads to cell death. These problems could be prevented by exogenous introduction of synthetic, short siRNA molecules that mimic Dicer products. As an alternative to the chemically synthesized of siRNA, plasmid vectors expressing shRNA molecules can be opted (Paddison, Caudy, Bernstein, Hannon, & Conklin, 2002; Sandy, Ventura, & Jacks, 2005).

CHAPTER 3

MATERIALS AND METHODS

3.1 Chemicals and Reagents

Tris and glycine were purchased from Vivantis (CA). Glacial acetic acid, ethylenediaminetetraacetic acid (EDTA), magnesium chloride (MgCl_2), calcium chloride (CaCl_2), sodium chloride (NaCl), sodium deoxycholate, glycerol and Tween-20 were purchased from SYSTERM (Selangor, Malaysia). Sodium dodecyl sulphate (SDS) and β -Mercaptoethanol were purchased from Merck (NJ). Bromophenol blue and Naphthol Blue Black were purchased from Sigma-Aldrich (MO). Gelatin was purchased from Agar Scientific (Stansted, England). Phenylmethanesulfonylfluoride (PMSF) was purchased from Bio Basic Inc. (Ontario, Canada). Nonidet P-40 was purchased from Roche (Basel, Switzerland). Methanol was purchased from QRecTM (Quebec, Canada). Phosphate buffered saline (PBS) was purchased from OXOID (Cambridge, UK). Hygromycin B and G-418 sulfate were purchased from A.G. Scientific (CA). Puromycin dihydrochloride was purchased from bioWORLD (OH). Pre-mix 30% acrylamide/bis solution, 37.5:1 was purchased from Bio-Rad (CA). Ammonium persulfate (APS) was purchased from Promega (WI).

3.2 List of Formula

Table 3.1 shows the list of formulations of buffers and solutions used in this study.

Table 3.1: Formulations of buffers and solutions

Buffers/Solutions	Formulations
Amido black dye	0.1% w/v Naphthol Blue Black, 10% v/v Methanol, 2% v/v Glacial acetic acid
Laemmli sample buffer	62.5mM Tris, pH 6.8, 25% v/v Glycerol, 2% w/v SDS, 0.01% w/v Bromophenol blue, 5% v/v β -Mercaptoethanol
MgCl ₂ -CaCl ₂ solution	80mM MgCl ₂ , 20mM CaCl ₂
NP-40 cell lysis buffer	10mM Tris, pH 7.8, 100mM NaCl, 10mM EDTA, 0.1mM PMSF, 0.5% w/v Sodium deoxycholate, 0.5% v/v Nonidet P-40
Phosphate buffered glycerol jelly	100ml 0.2M PBS, pH 7.0, 100ml Glycerol, 15g Gelatin
Phosphate buffered saline Tween-20	0.1% v/v Tween-20 in PBS
Stripping buffer	0.4M Glycine, 2% v/v Tween-20, 0.2% SDS, pH 2.2
Transfer buffer	150mM Glycine, 20mM Tris, 20% v/v Methanol
Tris buffered saline	50mM Tris, pH 7.4, 150mM NaCl
Tris-acetate-EDTA (TAE) buffer	20mM Tris, pH 8.0, 2mM Glacial acetic acid, 1mM EDTA
Tris-glycine electrophoresis buffer	25mM Tris, 190mM Glycine, 1% w/v SDS, pH 8.6

3.3 Molecular Biology

3.3.1 The pcDNATM 3.1 Vector

The pcDNATM 3.1 vector (InvitrogenTM, CA) as shown in Figure 3.1 consists of a human cytomegalovirus (CMV) immediate-early enhancer at bases 232 to 819 which is responsible for efficient and high-level expression of recombinant protein of interest (Andersson, Davis, Dahlbäck, Jörnvall, & Russell, 1989; Boshart et al., 1985; Nelson, Reynolds-Kohler, & Smith, 1987). Further downstream of the CMV promoter is the T7 promoter which allows *in vitro* “sense” transcription and DNA insert sequencing. The TOPO[®] cloning site 1 and 2 is important for directional cloning of PCR product in frame with the V5 epitope and polyhistidine C-terminal tag. Detection of recombinant protein using anti-V5 antibodies occurs at the V5 epitope which consists of Gly-Lys-Pro-Ile-Pro-Asn-Pro-Leu-Leu-Gly-Leu-Asp-Ser-Thr amino acid residues (Southern, Young, Heaney, Baumgartner, & Randall, 1991). At bases 1102 to 1119 is the bovine growth hormone (BGH) reverse priming site which plays a vital role during insert sequencing. Termination efficiency is enhanced in the presence of both BGH polyadenylation signal and SV40 early polyadenylation signal located at bases 1108 to 1332 and 3189 to 3319, respectively (Goodwin & Rottman, 1992). Located upstream of the SV40 early polyadenylation signal is the SV40 early promoter and origin which regulates the efficiency and high-level expression of the neomycin resistance gene and episomal replication in cells expressing the SV40 large T antigen. The neomycin resistance gene itself is important for selection of stable transfectants in mammalian cells. The selectable marker is located at bases 2217 to 3011.

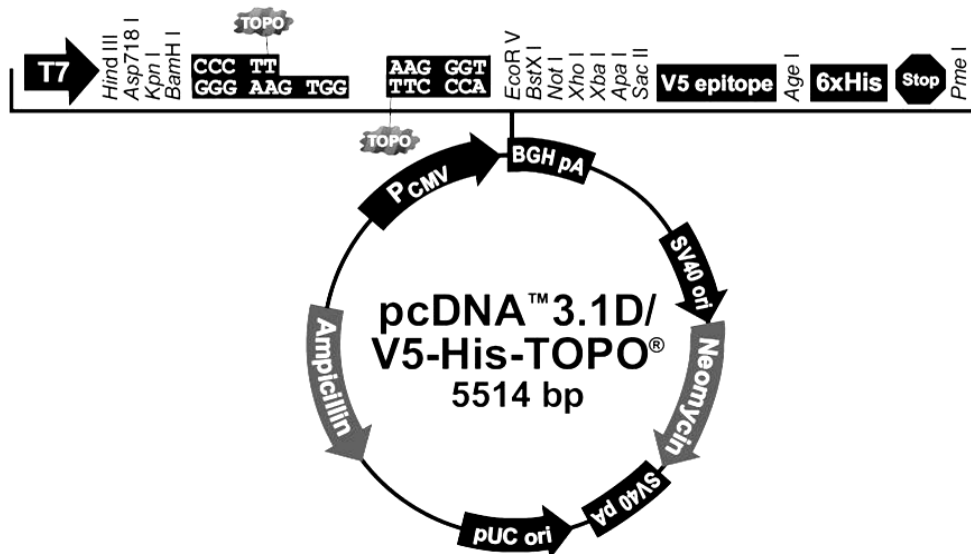


Figure 3.1: Map of pcDNA™ 3.1 vector. Figure taken from Invitrogen™.

3.3.1.1 Cloning of Human PrP^C cDNA into pcDNA™ 3.1 Vector

Blunt end PCR products were produced using PCR primers (Bio Basic Inc., Ontario, Canada) specific for human cellular prion protein (PrP^C). The PCR primers used were 5'-CACCATGGCGAACCTTGGC-3' (forward) and 5'-TCATCCCCTATCAGGAAGATGAG-3' (reverse). To ensure that the chosen sequences were not highly homologous with other genes, target sequences were aligned to the human genome database through Basic Local Alignment Search Tool (BLAST) from National Center for Biotechnology Information (NCBI, MD).

Full length human PrP^C (Accession no. BC012844) cDNA (Clone ID: 3863784, Open Biosystem, AL) was amplified by polymerase chain reaction (PCR) and subsequently cloned into the pcDNA™ 3.1 vector using pcDNA™ 3.1 Directional TOPO® Expression Kit (Invitrogen™, CA) according to

manufacturer's instructions. A total of 50µl of PCR reaction mixture was prepared as shown in Table 3.2.

Table 3.2: Preparation of PCR reaction mixture

PCR Mix Component	Volume/Reaction
10× <i>Pfu</i> Buffer (EURx, Przewodnikow, Poland)	5µl
10mM dNTP mix (GeneCraft, Cologne, Germany)	1µl
100µM Forward primer	0.25µl
100µM Reverse primer	0.25µl
Template DNA(1ng/µl)	10µl
Sterile distilled water (ddH ₂ O)	33µl
5U/µl <i>Pfu</i> Plus! DNA Polymerase (EURx)	0.5µl
Final volume	50µl

PCR cycles were carried out at the following conditions as shown in Table 3.3.

Table 3.3: Cycling conditions for PCR

Step	Temperature	Time	Number of Cycles
Initial denaturation	95°C	5min	1
Denaturation	95°C	30sec	}25
Annealing	53°C	30sec	
Extension	72°C	1min	
Final Extension	72°C	7min	1
Cooling	4°C	Indefinite	1

Samples were loaded on a 1% agarose gel completely covered with TAE buffer, electrophoresed at 95V for 25-30min, and visualized by GelRed™ (Biotium, CA) staining in order to check the integrity of the PCR products. To set up a 1% general purpose agarose gel for nucleic acid electrophoresis, gel solution was first prepared by adding 1g of agarose powder (Vivantis, CA) into 100ml of TAE buffer. The solution was then dissolved in microwave oven at

low medium to medium mode using 30-60sec intervals, where at each interval; the solution was stirred gently in order to resuspend the agarose. The cycle of heating and swirling were carried out throughout the heating process until the agarose was completely dissolved and no visible particles were present. Heated gel solution was cooled to about 70°C at room temperature (RT) or water bath and was then poured into a pre-set gel rack without generating bubbles. Gel solution was cooled to complete polymerization.

Purification of DNA was performed using GF-1 Gel DNA Recovery Kit (Vivantis, CA) where briefly, agarose gel band containing the DNA of interest was excised and solubilised in equal volume of Buffer GB (provided) at 50°C. Upon solubilisation of agarose, sample was transferred into a column assembled in a clean collection tube (provided) for binding of DNA onto the specially-treated glass filter membrane at pH 7.0 or below. Column was spun twice at 10,000g for 1min to remove the remaining sample followed by washing step with 750µl of Wash Buffer (provided) at 10,000g for 1min. Residual ethanol was removed by centrifugation at 10,000g for 1min. The purified DNA was eluted in 30µl of TE Buffer.

Determination of the DNA concentration and its purity were performed using SmartSpec™ Plus Spectrophotometer (Bio-Rad, CA) at 260nm and 280nm. A 260/280 ratio at 1.8 to 2.0 indicates DNA sample which is relatively free from protein contamination whereas sample DNA that is contaminated with protein will have a 260/280 ratio lower than 1.8. DNA concentration was calculated

using the formula below where 50µg/ml of double stranded DNA (dsDNA) has an absorbance of 1.000 at 260nm:

$$\text{DNA concentration } (\mu\text{g}/\mu\text{l}) = \frac{\text{Absorbance at 260nm} \times \text{Dilution factor} \times 50}{1000}$$

TOPO[®] Cloning Reaction was performed by transforming One Shot[®] TOP10 Chemically Competent Cells according to user's manual. The TOPO[®] Cloning Reaction was prepared as follows:

Reagents	Chemically Competent <i>E.coli</i>
Fresh PCR product	2µl
Salt solution	1µl
ddH ₂ O	2µl
TOPO [®] vector	1µl
Final volume	6µl

For positive clones screening, plasmids DNA were isolated from the transformants using PureLink[™] Quick Plasmid Miniprep Kit (Invitrogen[™], CA), according to the manufacturer's instruction. Upon transformation, bacterial cells were harvested and lysed using alkaline procedure. Plasmids DNA were purified from the lysates upon binding to the provided membrane column that selectively binds plasmid DNA. Contaminants such as RNA, proteins, dyes, and other impurities were then removed by subsequent washing steps. Elution of plasmids DNA was performed using high-salt buffer (provided) and the eluted plasmids DNA were then resuspended in TE Buffer (Invitrogen[™], CA).

Constructs were sequenced using T7 and BGH reverse primers in order to confirm the presence and exact orientation of the insert and its sequence. Once the correct positive clone of interest was obtained, it was transformed into self-prepared competent *E.coli* JM109 strains and plasmid purification was carried out using QIAGEN Plasmid Midi Kits (QIAGEN, WA). Stock of plasmid DNA was stocked at -20°C for future purposes. The empty vector, pcDNA™ 3.1 was employed as the negative control throughout the study.

3.3.2 The pCMV-SPORT6 Vector

The 4,396bp pCMV-SPORT6 mammalian/bacterial expression vector as shown in Figure 3.2 encompasses an enhancer of human CMV gene at bases 328 to 399 which allows constitutive expression of the protein of interest in mammalian cells (Andersson et al., 1989; Boshart et al., 1985; Nelson et al., 1987). The SV40 polyadenylation signal regulator which is located further downstream of the CMV promoter at bases 1304 to 1338 upholds competent transcription termination and polyadenylation of mRNA during and subsequent to transcription of DNA into RNA. A T7 priming site located at bases 16 to 34 promotes *in vitro* transcription in the “sense” orientation and sequencing through the insert. The pUC origin at bases 3333 to 3952 and ampicillin resistance selectable marker at bases 2117 to 2977 permits growth via high-copy number replication and selection of vector in *E.coli* cells, respectively.

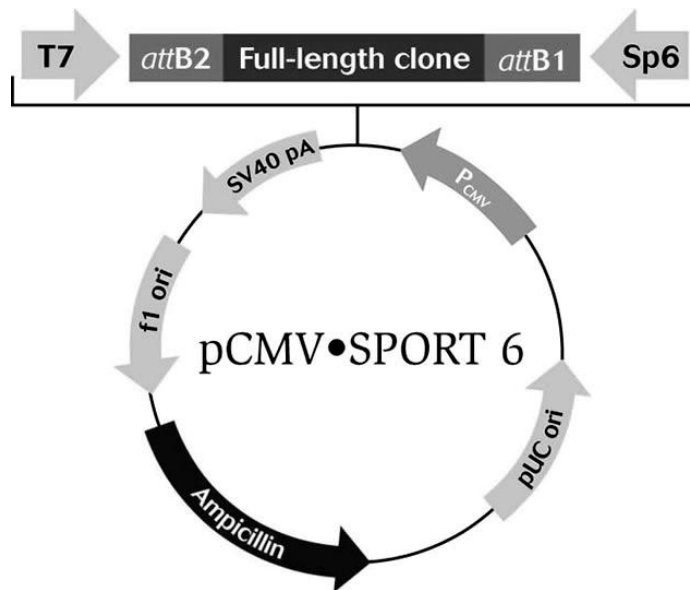


Figure 3.2: Map of pCMV-SPORT6 vector. Figure taken from Galerija SLU Niš.

3.3.2.1 Creating pCMV-SPORT6 Empty Vector

Briefly, pCMV-SPORT6 vector carrying the human PrP^C insert, designated as pCMV-SPORT6-PrP (Clone ID: 3863784, Open Biosystem, AL) was sequentially dual digested using the *SalI* (Vivantis, CA) and *XhoI* restriction enzymes (Vivantis, CA) to create compatible ends. The digested DNA was then electrophoresed on a 1% agarose gel until 2 bands were clearly visible, one 4,400bp band which is the vector backbone, and one 2,400bp band which is the PrP^C insert. The 4,400bp band was excised and purified using GF-1 Gel DNA Recovery Kit as described previously. The purified plasmid DNA was then re-ligated using T4 DNA ligase (Vivantis, CA) at 16°C for overnight incubation. An amount of 10µl T4 ligation mix was transformed into self-prepared competent *E.coli* DH5a cells. Positive transformants were analyzed through sequencing using M13 forward (-20) primer (5'-GTAAAACGACGGCCAGT-3') which was provided by 1st Base DNA

sequencing facilities. The pCMV-SPORT6 empty vector served as the negative control during the experimental co-transfection for pCMV-SPORT6-PrP and pBABE-hygro (Addgene, MA) where the latter carries a hygromycin resistance gene at bases 1921 to 2928 (Addgene).

3.3.3 The pLKO.1 TRC Cloning Vector

Figure 3.3 shows the map of pLKO.1 TRC cloning vector with a short hairpin RNA (shRNA) insert sourced from Addgene, MA. The vector is well established for cloning and expressing shRNA sequences. Once transfected into the mammalian cells, the puromycin resistance gene at bases 529 to 1128 encoded in the vector allows for convenient selection of stable transfectants. The expression of puromycin is regulated by human phosphoglycerate kinase promoter (hPGK) while human U6 promoter which resides at bases 6579 to 6811 directs the transcription of shRNA transcripts via RNA Polymerase III. The Central Polypurine Tract (cPPT) which is located at bases 1239 to 1254 plays vital role during transduction by facilitating nuclear import of the vector's preintegration complex into the transduced cells (Addgene, 2006). Both f1 origin and pUC origin were the bacterial origins of replication while the ampicillin selectable marker which is located downstream of f1 origin at bases 2650 to 3510 allows selection of plasmid in bacterial cells (Moffat et al., 2006). The original pLKO.1 TRC cloning vector contains a 1,900bp stuffer that would be replaced with shRNA oligos upon digestion with *AgeI* and *EcoRI*.

A total of 3 siRNA sequences which each consists of 21-nucleotide (nt) that matches the pattern AA(N₁₉)TT starting at 25-nt downstream of the start codon (ATG) with GC content between 36-52% were selected. The selected target sequences were then aligned to the human genome database using BLAST program (NCBI, MD) where at least 3-nt mismatches must be present in order to minimize degradation of off-target mRNA. Upon selection of the suitable 21-nt targets for *PRNP* gene, both its “sense” and “antisense” sequences were inserted into 5'-CCGG---21-nt “sense”---CTCGAG---21-nt “antisense”---TTTTTG-3' (forward oligo) and 5'-AATTCAAAA---21-nt “sense”---CTCGAG---21-nt “antisense”-3' (reverse oligo) to form the shRNA oligos.

shRNA were synthesized as a 21 “sense” bases separated by a 6-nt loop containing an *XhoI* restriction site followed by 21 “antisense” bases that are complementary to the “sense” bases (Figure 3.3). The polyadenylation signal consists of five consecutive T residues, which is the termination sequence for RNA Polymerase III. The designated shRNA oligos sequences are as shown in Table 3.4 and assisted screenshots are illustrated in Figure 3.4.

Table 3.4: shRNA oligos corresponding to siRNA sequences known to knockdown PrP^C

Designated Name	Forward Oligo (5'-3')	Reverse Oligo (3'-5')
HuPrPshRNA 1	CCGGAATGCCCTATCTT AGTAGAGACTCGAGTC TCTACTAAGATAGGGC ATTTTTTTG	AATTCAAAAAAATGCC CTATCTTAGTAGAGAC TCGAGTCTCTACTAAG ATAGGGCATT
HuPrPshRNA 2	CCGGAAGGCAAATCTC CTTTGTCCACTCGAGTG GACAAAGGAGATTTGC CTTTTTTTG	AATTCAAAAAAAGGCA AATCTCCTTTGTCCACT CGAGTGGACAAAGGAG ATTTGCCTT
HuPrPshRNA 3	CCGGAATCCTAGAGAT TCTTAGCTCCTCGAGG AGCTAAGAATCTCTAG GATTTTTTTG	AATTCAAAAAAATCCT AGAGATTCTTAGCTCCT CGAGGAGCTAAGAATC TCTAGGATT

Table 3.5 shows the target regions of each shRNA oligos which are indicated on the basis of the base sequences and nt numbering as shown in the human PrP^C mRNA (BC012844).

Table 3.5: shRNA oligos against human PrP^C mRNA sequence (BC012844)

Target region in human PrP^C mRNA		
	Base Sequences	Nucleotide Numbering
HuPrPshRNA 1	5'-AATGCCCTATCTTAGTAGAGA-3'	1194-1214
HuPrPshRNA 2	5'-AA GGCAAATCTCCTTTGTCCA-3'	1664-1684
HuPrPshRNA 3	5'-AATCCTAGAGATTCTTAGCTC-3'	1309-1329

A.

siRNA Selection Program

- * Enter your sequence in [Raw or FASTA format](#) below,
- OR enter [GI or Accession number](#)
- * [Choose the siRNA pattern:](#)

Recommended patterns	custom
<input type="radio"/> N2[CG]N8[AUT]N8[AUT]N2	<input type="radio"/>
<input checked="" type="radio"/> AAN19TT	<input type="text" value=""/> Enter pattern with 23 bases
<input type="radio"/> NAN21	
- Filter criteria:
 - *GC percentage: from to
 - *[exclude a run of](#) [or more T or A in a row](#)
 - *[exclude a run of](#) [or more Gs in a row](#)
 - *include less than consecutive GC in a row.
 - equal %(+/- %) for all 4 bases.
- *[End your siRNAs with](#)
-

Note: *: required parameters.

Copyright 2004 Whitehead Institute for Biomedical Research. All rights reserved.

Comments and suggestions to: siRNA-help@wi.mit.edu

Sequence was entered via Accession number: BC012844 of human PrP^C mRNA and the siRNA pattern: AANN19TT ended with TT at 3'-terminus was chosen. siRNA sequences which do not contain GC percentages of 36-52% was filtered out.

Figure legend on page 60.

Figure 3.4 continued.
B.

Choose siRNA Candidate(s)

1. siRNA candidates after filtering the base_run, gc%, and base_variation: (The more oligos you choose, the longer time for you to get results.)
Oligo patterns: A=AAN19TT; B=NANI9NN; C=N2[CG]N8[AU]N8[AU]N2; F=Custom

Position	Sequence	Patterns	GC%	Thermodynamic Values	SNPs	miRNA targets
<input checked="" type="checkbox"/> 1 1194-1216	S 5' : UGCCCUAUCUUAGUAGAGA dTdT mRNA: AA TGCCCTATCTTAGTAGAGA TT AS 3' : TdTd ACGGGAUAGAAUCAUCUCU	A,B	42	-3.1 (-12.6, -9.5)		89[43]
<input checked="" type="checkbox"/> 2 1664-1686	S 5' : GGCAAUUCUUUGUCCA dTdT mRNA: AA GGCAAAATCTCCTTTGTCCA TT AS 3' : TdTd CCGUUUAGAGGAAACAGGU	A,B	47	-0.3 (-10.9, -10.6)		177[72]
<input checked="" type="checkbox"/> 3 1309-1331	S 5' : UCCUAGAGAUUCUAGCUC dTdT mRNA: AA TCCTAGAGATTCTTAGCTC TT AS 3' : TdTd AGGAUCUCUAGAAUCGAG	A,B	42	1.5 (-9.6, -11.1)		122[56]
<input type="checkbox"/> 4 2261-2283	S 5' : GAUCCAAAGUGGACACCA dTdT mRNA: AA GAATCCAAAGTGGACACCA TT AS 3' : TdTd CUUAGGUUUCACCUUGUGU	A,B	47	2.4 (-7.9, -10.3)		72[37]
<input type="checkbox"/> 5 2043-2065	S 5' : UGUUUUUUUGGCUUGCAC dTdT mRNA: AA TGTATTATTGGCTTGCAC TT AS 3' : TdTd ACAUUAAUACCGAACGUG	A,B	37	3.9 (-7.2, -11.1)		167[70]

2. Choose the alignment tool:

3. Choose the species:

4. Choose the database you would like to BLAST against:

5. Receive result
 via email:
 on web browser.

6.

C.

View BLAST Results and Filter Results to reduce off-target effects

To eliminate siRNAs that may produce off-target effects, we provide several filtering methods:

by Number of Matches: [EXAMPLE](#)

Eliminate siRNAs with off-target BLAST hits sharing more than matched bases of the antisense strand

by Positions: [EXAMPLE](#)

Eliminate siRNAs with off-target BLAST hits aligning with its antisense strand at the specified positions

2	3	4	5	6	7	8	9	10	11	12	13	14	15	16	17	18	19
<input checked="" type="checkbox"/>																	

The entrez_gene ID for your specific target: [How to get entrez_gene ID?](#)

No.	pos	siRNA	type	GC%	thermodynamics	SNP	blast
<input checked="" type="checkbox"/> 1	1194-1216	S 5' : UGCCCUAUCUUAGUAGAGA dTdT mRNA: AA TGCCCTATCTTAGTAGAGA TT AS 3' : TdTd ACGGGAUAGAAUCAUCUCU	A,B	42	-3.1 (-12.6, -9.5)		LINK
<input checked="" type="checkbox"/> 2	1664-1686	S 5' : GGCAAUUCUUUGUCCA dTdT mRNA: AA GGCAAAATCTCCTTTGTCCA TT AS 3' : TdTd CCGUUUAGAGGAAACAGGU	A,B	47	-0.3 (-10.9, -10.6)		LINK
<input checked="" type="checkbox"/> 3	1309-1331	S 5' : UCCUAGAGAUUCUAGCUC dTdT mRNA: AA TCCTAGAGATTCTTAGCTC TT AS 3' : TdTd AGGAUCUCUAGAAUCGAG	A,B	42	1.5 (-9.6, -11.1)		LINK

Figure 3.4: Selection of siRNA targets in PRNP gene. (A) siRNA sequences were designed based on the selected criteria. (B) The 3 top-scoring 21-nt siRNA sequences were chosen. (C) siRNA sequences that have at least 3-nt mismatches to all unrelated genes were selected after a BLAST search. Screenshots were adapted from using siRNA Selection Program hosted by the Whitehead Institute for Biomedical Research.

Cloning procedure of shRNA oligos into pLKO.1 TRC (Addgene, MA) were performed according to the manufacturer's manual. Oligos were annealed at 95°C for 4min in a pre-heated water bath which were then slowly cooled down to RT. Preparation of 50µl oligos suspension mixture was as shown:

Oligos Mixture Component	Volume/Reaction
100µM Forward oligo	5µl
100µM Reverse oligo	5µl
10× NEB buffer 2	5µl
ddH ₂ O	35µl
Final volume	50µl

On the other hand, pLKO.1 TRC were dual digested using *AgeI* and *EcoRI* restriction enzymes which were purchased from New England Biolabs (NEB, MA). Digested DNA was electrophoresed on a 0.8% low melting point agarose gel. The 7,000bp DNA was purified using GF-1 Gel DNA Recovery Kit.

The 20µl of T4 ligation reactions below were performed overnight at 16°C using Mastercycler[®] Gradient (Eppendorf, Hamburg, Germany).

Ligation Mix Component	Amount/Reaction
Annealed oligo	0.5-2µl
Digested pLKO.1 TRC	50ng
10× NEB T4 DNA ligase buffer	2µl
NEB T4 DNA ligase	1µl
ddH ₂ O	Top up to 20µl
Final volume	20µl

Five microlitres of the ligation mix were then transformed into self-prepared competent *E.coli* JM109 strains. Positive clones screening were performed as described in the user's manual where restriction enzyme digestion were

conducted on the miniprep DNA with *EcoRI* (NEB, MA) and *NcoI* (NEB, MA). Positive clones which showed two fragments, a 2,000bp fragment and a 5,000bp fragment on 1% agarose gel were sequenced with pLKO.1 sequencing primer (5'-CAAGGCTGTTAGAGAGATAATTGGA-3'). The successfully ligated plasmids were then stably transfected into target cells for *PRNP* gene knockdown. Plasmids pLKO.1 TRC control and pLKO.1 scramble shRNA, both purchased from Addgene (MA) were used to serve as transfection controls.

3.3.4 Preparation of Competent *E.coli* Cells using Calcium Chloride

Fresh single colony of DH5 α or JM109 *E.coli* strains were streaked on Luria Bertani (LB) agar (Merck, NJ) plate and incubated overnight at 37°C. Single colony was picked on the next day from the LB plate and grown overnight in 50ml of LB broth (Merck, NJ) at 37°C and 200rpm. On the subsequent day, 500 μ l of the *E.coli* culture was added into 25ml of LB broth and incubated for 2-3hr to reach optical density of 0.600 to 1.000 at 600nm where 1_{OD600} equals 1 \times 10⁹ cells/ml. Cells were then transferred to pre-chilled sterile centrifuge tube where the culture was cooled to 0°C by storing the tube on ice for 10min. Bacterial cells were pelleted with a 9,000rpm spin for 10min at 4°C. The cells pellet was resuspended with 10ml of cold MgCl₂-CaCl₂ solution and further pelleted at 9,000rpm for 10min at 4°C. The supernatant was discarded and cells pellet was resuspended with 2ml of 0.1M CaCl₂. Cells were stored on ice for 2hr in order to increase competency. Cells were finally mixed with 40% v/v glycerol at 1:1 ratio and stored at -80°C for future use. To check for

contamination, a small aliquot of competent cells were spreaded on LB agar containing 0.025mg/ml of ampicillin (AMRESCO, OH).

3.3.4.1 Transformation of DNA into Competent *E.coli* Cells

An amount of 2-5µl DNA/ligation mix was added to 100µl of thawed competent cells, gently mixed, and was incubated on ice for 30min. The cell suspensions were then subjected to heat shock at 42°C for exactly 90sec, after which they were rapidly transferred to ice for 2-5min. An amount of 900µl fresh LB broth was added into cell suspension and was incubated for an hour at 37°C and 200rpm. The transformed cells were then pelleted at 10,000g for 10min. An amount of 900µl supernatant was discarded and the remaining 100µl transformant suspension was then plated onto selective ampicillin-containing LB agar plates, and incubated overnight at 37°C. Single colony was picked and grown overnight in LB broth containing 0.025mg/ml of ampicillin. The bacterial cultures were then used for plasmid purification using PureLink™ Quick Plasmid Miniprep Kit according to manufacturer's instruction.

3.4 Cell Culture

3.4.1 The Cell Lines

3.4.1.1 Oral Squamous Carcinoma, HSC-2 (JCRB0622)

The HSC-2 cell line (Figure 3.5) which was derived from the mouth of a 69yr old male diagnosed with squamous carcinoma at the Tokyo Medical and Dental University (Momose et al., 1989) is the most familiar neoplasm of the head and neck. The adherence epithelial-like cells proliferate in Eagle's Minimum Essential Medium with 10% calf serum and grew in synthetic medium PF86-1. This cell line has neither invasive nor metastatic potential (Rikimaru, Toda, Tachikawa, Enomoto, & Kamata, 1990).

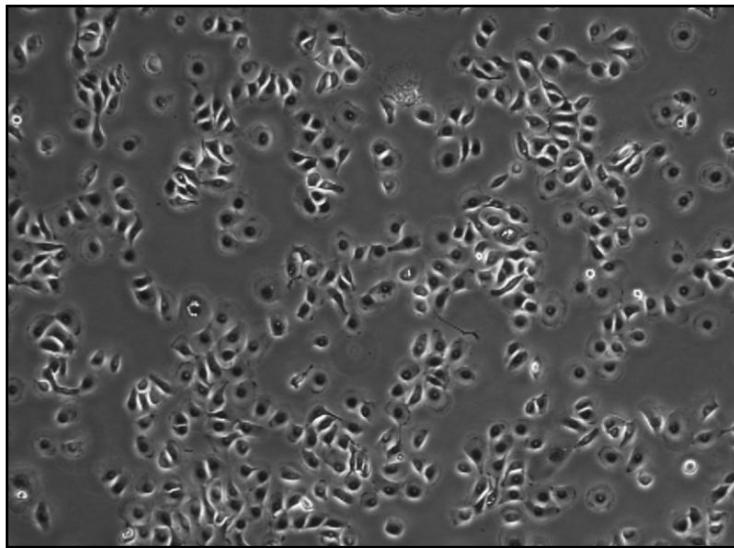


Figure 3.5: Cell morphology of HSC-2. Photograph of cells was taken with NIS-Elements BR 3.0 software under Nikon Eclipse TS100 inverted microscope at 40× magnification in the same exposure.

3.4.1.2 Renal Cell Adenocarcinoma, ACHN (CRL-1611)

ACHN cell line (Figure 3.6) was isolated from pleural effusion of a 22yr old Caucasian male patient with renal cell adenocarcinoma. The adherence epithelial-like ACHN cells grew in close contact with each other in the presence of Eagle's Minimum Essential Medium supplemented with 10% fetal bovine serum. ACHN cells were mostly applied in antiproliferative studies using human interferons or interferon inducers as its growth can be inhibited by the latter (Kochevar, 1990).

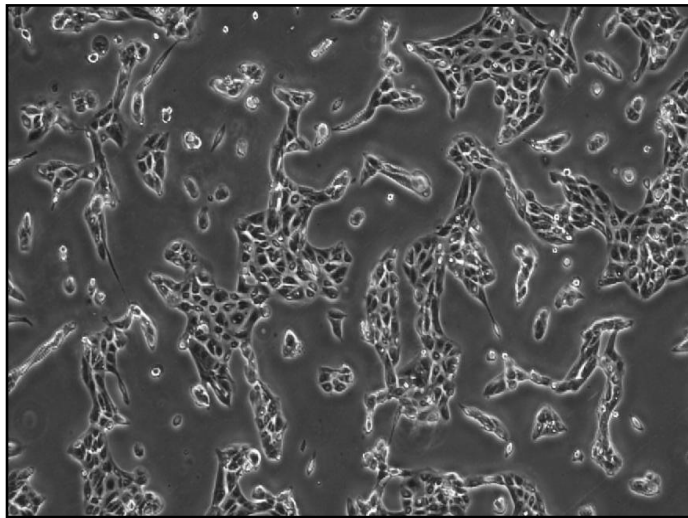


Figure 3.6: Cell morphology of ACHN. Photograph of cells was taken with NIS-Elements BR 3.0 software under Nikon Eclipse TS100 inverted microscope at 40× magnification in the same exposure.

3.4.1.3 Colorectal Adenocarcinoma, LS 174T (CL-188)

LS 174T cell line (Figure 3.7) was deposited by Northwestern University from a 59yr old Caucasian female who is diagnosed with Dukes' type B colorectal adenocarcinoma. The colon-originated adherence cells appear to be epithelial-like with abundance of microvilli and intracytoplasmic mucin vacuoles (Tom et al., 1976). LS 174T cell line proliferates in Eagle's Minimum Essential Medium supplemented with 10% fetal bovine serum and worth noting, the cells are positive for c-myc, N-myc, H-ras, N-ras, Myb, and fos oncogenes expression whereas K-ras and sis oncogene expression were not detected. Interestingly, they are negative for expression of p53 antigen but positive for mRNA expression (Trainer et al., 1988).

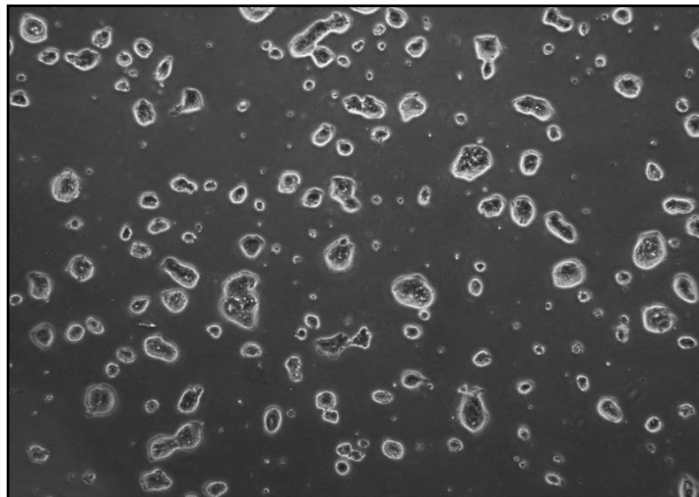


Figure 3.7: Cell morphology of LS 174T. Photograph of cells was taken with NIS-Elements BR 3.0 software under Nikon Eclipse TS100 inverted microscope at 40× magnification in the same exposure.

3.4.2 Cell Lines Maintenance

HSC-2, ACHN and LS 174T cell lines were generous gift from Dr. Lim Yang Mooi, Faculty of Medicine and Health Sciences, Universiti Tunku Abdul Rahman. The cells were grown in complete culture Minimum Essential Medium (MEM, Cellgro, VA) supplemented with 10% v/v heat-inactivated fetal bovine serum (FBS, i-DNA Biotechnology, Singapore) and antibiotics, 1% v/v Penicillin-Streptomycin (Pen-Strep, Millipore, MA). All cells were maintained in a humidified atmosphere of 95% air and 5% CO₂ at 37°C. Sub-culturing of cells was performed every 3-4 days depending on the cells' confluency state. CKX31 inverted microscope (OLYMPUS, PA) was used to check the cell cultures for any contamination and cell morphology changes.

3.4.2.1 Preparation of Complete Culture MEM Medium

An amount of 9.53g MEM powder and 2.2g of sodium bicarbonate (NaHCO₃, SYSTERM, Selangor, Malaysia) were dissolved in 1litre of deionized water. pH value range was adjusted to 7.2-7.6. The culture media was then sterilized by filtration with a 0.2µm membrane (Sartorius, Goettingen, Germany) filtration unit using vacuum filter system into sterile autoclaved Schott bottle. A total of 2ml medium was incubated in a 37°C, 5% CO₂ humidified incubator for 2 days to test for sterility while the remainder was stored at 4°C for future use.

3.4.2.2 Preparation of OPTI-MEM

For the preparation of OPTI-MEM (GIBCO™, CA) for cationic lipids transfection, a packet of 13.6g powdered OPTI-MEM and 2.4g of NaHCO₃ was dissolved in 1litre of deionized water. The pH value of the medium was initially adjusted to 7.0 ± 0.1 using 10M of sodium hydroxide (NaOH, SYSTERM, Selangor, Malaysia) as pH value will generally rise 0.1-0.3 units upon filtration. The medium mixture was then sterilized using membrane filtration method. Positive pressure and 0.2µm membrane porosity were applied.

3.4.3 Sub-culturing of Adherent Cell Lines

Spent medium were first removed and cells were washed with PBS prior to trypsinization with adequate amount of 0.05% trypsin-EDTA (GIBCO™, CA). Cells were incubated for 5-10min at 37°C to allow detachment of cells. Fresh serum-containing medium was then added onto the trypsinized cells to inactivate the trypsin. Cells were spun down at 1,500rpm for 5min and the pelleted cells were resuspended with complete culture medium and seeded at preferred density.

3.4.4 Freezing and Thawing of Cells

For cryopreservation, cells reaching 60-80% confluency were brought into suspension by trypsinization and were later pelleted at 1,500rpm for 5min. Freezing media containing 950µl of fresh culture medium and 50µl of dimethyl sulfoxide (DMSO, Merck, NJ) were added onto cells pellet, resuspended, and finally transferred to cryovial (Nalgene, NY) for storage at -80°C overnight prior to permanent storage in liquid nitrogen.

Cryopreserved vial was removed from liquid nitrogen and thawed instantly in a pre-heated 37°C water bath. Thawed cells were then rapidly transferred to a culture flask containing complete culture media and incubated at 37°C, 5% CO₂. Medium was replaced the next day with fresh medium in order to remove the DMSO remnants which are cytotoxic.

3.4.5 Cell Counting

Neubauer-improved haemocytometer (Marienfeld, Lauda-Königshofen) was used for cell counting purposes. Cells were trypsinized and spun down for 5min at 1,500rpm. Supernatant was discarded and adequate amount of medium was added to resuspend the cells. An amount of 10µl cells suspension were taken and gently mixed with 10µl of trypan blue dye (Sigma-Aldrich, MO) on a parafilm. Later on, 10µl of the mixture was transferred to the underside of the coverslip by capillary action. The slide was observed under inverted microscope at 100× magnification of. Cells were counted using a cell counter.

Only cells fall within the 16 corner square and any positioned on the right hand or bottom boundary line were counted. Viable cells were unstained and clear with a refractile ring around them while dead cells were stained with trypan blue and have no refractile ring. The cell concentration was calculated as follows:

$$\text{Cell concentration} = \frac{\text{Number of viable cells counted}}{4} \times \text{Dilution factor (2)} \times 10^4$$

The calculated cell concentration was adjusted according to the optimal seeding density of each cell lines during plating.

3.5 Cells Transfection

Cells were subjected to two modes of transfection: transient and stable. Transient transfection was performed as a preliminary study to generally characterize the properties of PrP^C while PrP^C-overexpressing and PrP^C-knockdown cells were created using stable transfection to further investigate the underlying physiological functions of PrP^C. Two methods to create stable cell lines were attempted using electroporation and cationic lipid-vesicles formulation.

Co-transfection to create cell lines overexpressing PrP^C was performed beforehand using pCMV-SPORT6-PrP and pBABE-hygro, where the latter served as a hygromycin-selectable marker. However, due to continuous unsuccessful transfection, pcDNATM 3.1 were opted instead.

3.5.1 Linearization of Plasmid DNA for Transfection Purposes

Targeting vectors or plasmids DNA were freshly linearized prior to stable transfection in order to enhance the integration of all essential gene elements of the plasmid DNA into host genome (Stuchbury & Munch, 2010). The vectors, irrespective of their inserts, were linearized as follows: pBABE-hygro with *EcoRI* (NEB, MA); pCMV-SPORT6 with *SalI* (Vivantis, CA); pcDNATM 3.1 with *XhoI* (EURx, Przewodnikow, Poland) and pLKO.1 TRC with *NcoI* (Fermentas, Vilnius, Lithuania). Vectors linearization was omitted during transient transfection.

3.5.2 Electroporation Method for the Transfection of Cells

Cells were seeded and transfected with 30µg of DNA by electroporation method using ECM830 electroporation generator (BTX[®] Harvard Apparatus, MA) which will create an electro-magnetic field in the cell solution to increase the electrical conductivity and permeability of the cell plasma membrane. Cells reaching 80% confluency in T₂₅-flask were trypsinized, pelleted and resuspended in 1ml of MEM culture medium. Cell suspensions were transferred to a 4mm cuvette, followed by the addition of DNA, which were then mixed carefully by inverting 5 times prior to electroporation. Optimization of electroporation parameters for better transfection efficiency was carried out by adjusting the field strengths, pulse length, and the number of pulses as shown in Table 3.6.

Table 3.6: Attempted electroporation parameters for human HSC-2, ACHN, and LS 174T cancer cell lines

Cell line	Electroporation Settings	
	1 st Attempt	2 nd Attempt
HSC-2	Voltage: 1,200V Pulse Length: 40µsec Number of Pulses: 1 Chamber: 4mm gap	Voltage: 200V Pulse Length: 4msec Number of Pulses: 2 Chamber: 4mm gap
ACHN	Voltage: 145V Pulse Length: 15msec Number of Pulses: 1 Chamber: 4mm gap	Voltage: 200V Pulse Length: 7msec Number of Pulses: 1 Chamber: 4mm gap
LS 174T	Voltage: 180V Pulse Length: 70msec Number of Pulses: 1 Chamber: 4mm gap	Voltage: 165V Pulse Length: 70msec Number of Pulses: 1 Chamber: 4mm gap

Electroporated cells were rapidly transferred into T-flask containing fresh MEM culture medium and incubated at 37°C, 5% CO₂. After 48hr post-transfection, stably transfected cells were selected as shown in Table 3.7.

Table 3.7: Effective working concentrations of selective antibiotics towards human cancer cell lines

	Selectable Marker	Selective Antibiotic	Working Concentration
pBABE-hygro	Hygromycin	Hygromycin B	200µg/ml for 10 days
pcDNA TM 3.1	Neomycin	G-418 sulfate	1mg/ml for 3wk
pLKO.1 TRC	Puromycin	Puromycin dihydrochloride	3µg/ml for 2wk

3.5.3 Cells Transfection using Cationic Lipids

Cells transfection using TransPass D1 Transfection Reagent (TPD1TR, NEB, MA) were performed in the absence of serum. Protocol as described in the manufacturer's instructions was modified accordingly. Cells were seeded on a 100mm cell culture dish (BD Biosciences, NJ) to reach 60-90% confluency by the time of transfection. An amount of 5µg DNA was added into 4ml of serum-free OPTI-MEM in a 15ml centrifuge tube for each transfection reaction. TPD1TR was vortexed just before use to thoroughly mix the frozen suspension. An amount of 12.5µl TPD1TR was added into each reaction and was then mixed well by finger flicking the tube. The mixture was allowed to form transfection complexes by incubating at RT for 30min. Prior to transfection, cells were washed once with OPTI-MEM. The medium were immediately replaced with the transfection mixture and were subjected to gently rocking to evenly disperse the complex mixture. Cells were then incubated for 4hr at 37°C, 5% CO₂. After incubation, transfection medium was aspirated and replaced with fresh complete culture MEM medium. Following transfection, cells were harvested and assayed after 48hr. However, in order to obtain stable clones, transfected cells were selected in medium containing selective antibiotic as shown in Table 3.7 after 24hr post-transfection. PrP^C expression of the resultant stable transfectants was assessed by immunofluorescence microscopy (IFM) and Western blotting.

3.6 Immunofluorescence Microscopy

For surface detection of PrP^C, cells were seeded and allowed to attach on coverslips for 4-5hr. Upon attachment to coverslips, cells were fixed with 4% w/v paraformaldehyde (Sigma-Aldrich, MO) in PBS for 15min at RT and further permeabilized with 0.2% v/v Triton X-100 (Thermo Scientific, MA) in PBS for 2min at RT. Coverslips were then blocked with 10% goat serum (Sigma-Aldrich, MO) in PBS for 20min at RT prior to incubation with primary antibodies. PrP^C was detected with anti-PrP mouse antibody (mAB) clone 3F4 (Millipore, MA) in 5% goat serum at 1:500 dilution. After overnight incubation with primary antibodies at 4°C, cells were treated with Dylight 488 goat anti-mouse IgG (Thermo Scientific, MA) in 5% goat serum at a dilution of 1:100 for an hour at RT. Prior to imaging, coverslips were mounted onto glass slides with the monolayer facing downward using self-prepared water-based mounting media, phosphate buffered glycerol jelly. Cells were visualized using Nikon Eclipse TS100 inverted fluorescence microscope (Nikon, Tokyo, Japan) and images were captured with NIS-Elements BR 3.0 software.

3.7 Sodium dodecyl sulphate polyacrylamide gel electrophoresis (SDS-PAGE) and Western Blot Analysis

3.7.1 Preparation of Cell Lysate

In brief, cell lysates for SDS-PAGE were prepared as follows: Adherent cells were collected through scraping, washed twice with ice-cold PBS and lysed with NP-40 cell lysis buffer containing Protease inhibitor cocktail (PIC, Sigma-Aldrich, MO) where lysis buffer to PIC ratio = 100:1. Cell lysates were allowed to stand on ice for an hour prior to centrifugation. Supernatant form of lysates was collected. Concentration of protein lysates were quantified using Bicinchoninic acid (BCA) based on colorimetric detection at 562nm using BCATM Protein Assay Kit (Thermo Scientific, MA).

3.7.1.1 Quantitation of Total Protein

BCA protein assay was performed in a 96-well plate where 10µl of each standard at 0.2, 0.4, 0.6, 0.8 and 1mg/ml or unknown samples diluted at 1:10 and 1:5 was loaded into single well separately. BCA Working Reagent (WR) which was prepared by mixing 50 parts of BCA Reagent A with 1 part of BCA Reagent B (50:1, Reagent A:B) was then added into each well at 200µl. Plate was mixed thoroughly on a plate shaker for 30sec followed by incubation at 37°C for 30min. The purple coloured product of this assay which strongly absorbs light at 562nm is produced by the chelation of two BCA molecules with one cuprous ion. Absorbance was measured using Infinite 200 PRO

multimode reader (Tecan, Männedorf, Switzerland) and data analysis was performed using Magellan™ software (Tecan, Männedorf, Switzerland).

3.7.2 Sodium dodecyl sulphate polyacrylamide gel electrophoresis

Lysates containing desired amount of proteins were mixed with Laemmli sample buffer in 1:1 ratio and pre-heated at 95°C for 5min. Heated samples were then separated by electrophoresis on a 15% polyacrylamide gel at 170V for approximately 2hr in a electrophoresis tank filled with Tris-glycine electrophoresis buffer. Formulations of stacking gel and resolving gel are shown in Table 3.8.

Table 3.8: Protocol for 15% polyacrylamide gel

	Stacking Gel (4%)	Resolving Gel (15%)
30% Acrylamide/bis solution, 37.5:1	660µl	4.95ml
0.5 M Tris-HCl, pH 6.8	1.26ml	-
1.5 M Tris-HCl, pH 8.8	-	2.5ml
10% SDS	50µl	100µl
ddH ₂ O	3ml	2.4ml
TEMED (Bio Basic Inc., Ontario, Canada)	5µl	5µl
10% Ammonium persulfate (APS)	25µl	50µl
Total volume	5ml	10ml

3.7.3 Western Blotting

The resolved proteins were transferred onto methanol-soaked BioTrace™ Polyvinylidene fluoride (PVDF) membrane (Pall Corp., NY) by semi-dry transfer system via Trans-Blot SD Semi-Dry Transfer Cell (Bio-Rad, CA) at 15V for 30min. Transfer buffer was used to pre-wet the SDS-PAGE gel and

thick filter paper (Bio-Rad, CA). Gel sandwich was arranged in the following order from the bottom platinum anode to top stainless steel cathode: pre-wet thick filter paper → pre-wet PVDF membrane → transfer buffer-equilibrated SDS-PAGE gel → pre-wet thick filter paper.

Transferred membrane was blocked with 5% w/v Skim milk powder (OXOID, Cambridge, UK) in PBS-T, followed by hybridization with primary antibody, anti-PrP clone 3F4 diluted in PBS-T containing 3% Bovine Serum Albumin (BSA) Fraction V (Bio Basic Inc., Ontario, Canada) for overnight incubation at 4°C. The membrane was then incubated in PBS-T containing IgG-horseradish peroxidase (HRP) conjugate and 3% BSA at RT for an hour. After extensive washing with PBS-T, reactive bands were visualized using enhanced luminal-based chemiluminescent (ECL) detection system via the highly sensitive nonradioactive Pierce ECL Western Blotting Substrate (Thermo Scientific, MA). Membrane was covered in 2ml of substrate working solution which was prepared by mixing equal parts of Detection Reagents 1 and 2. Image acquisition was performed using FluorChem FC2 System (Alpha Innotech, CA). ImageJ 1.43U software hosted by National Institutes of Health at <http://rsb.info.nih.gov/ij/index.html> was used for densitometry analysis. Summary of antibody dilutions are described in Table 3.9.

Table 3.9: Antibodies for Western blotting analysis

Antibodies	Source	Supplier	Dilution
anti-PrP clone 3F4	Mouse	Millipore (MA)	1:10,000
anti-actin clone C4	Mouse	Millipore (MA)	1:5,000
anti-Bax	Rabbit	Cell Signaling Technology Inc. (MA)	1:1,000
anti-Bcl-xL	Rabbit	Cell Signaling Technology Inc. (MA)	1:1,000
anti-mouse IgG- HRP conjugate	Rabbit	Thermo Scientific (MA)	1:10,000
anti-rabbit IgG-HRP conjugate	Goat	Nacalai Tesque, Inc., (Kyoto, Japan)	1:10,000

3.7.3.1 Stripping of PVDF Membrane for Repeated Hybridization

For repeated hybridization with anti-actin clone C4 as loading control, the blot was stripped in stripping buffer at RT for 10min upon image acquisition. Membrane was washed twice with PBS-T for 5min and further incubated in anti-actin clone C4 which was pre-diluted in PBS-T containing 3% BSA for an hour at RT.

3.7.3.2 Amido Black Staining of PVDF Membrane

Amido black dye was used to stain the total proteins on transferred membrane. Membrane was stained for 5-10min before rinsing it under running water for 1-2min. The membrane was then dried at RT and kept for future reference.

3.8 Treatment Paradigm

HSC-2, ACHN and LS 174T cell lines were seeded at a density of 2.5×10^5 cells/ml, 1×10^5 cells/ml and 3×10^5 cells/ml, respectively into 6-, 12- or 96-well plates (Table 3.10). To induce cell death, cells were plated in culture plates, allowed to adhere overnight, and then given the indicated concentrations of recombinant human tumour necrosis factor α (TNF- α , Millipore, MA), tunicamycin (TUN, Santa Cruz Biotech., CA) and hydrogen peroxide (H_2O_2 , SYSTERM, Selangor, Malaysia). The cells were incubated for 48hr during 100ng/ml of TNF- α treatment and 24hr for both TUN and H_2O_2 treatment at half maximal inhibitory concentration (IC_{50}), unless otherwise stated. In order to block glycosylation of PrP^C, HSC-2 and LS 174T cells were treated with TUN at 6 μ g/ml and 2 μ g/ml for 24hr, respectively. Oxidative stress was induced by exposing the cells to 3mM of H_2O_2 for 30min. After treatment, cells were harvested and assayed. TNF- α and H_2O_2 were dissolved in deionized water while TUN was dissolved in DMSO, filter sterilized with 0.2 μ m membrane, before added into cell culture medium for treatment purposes. The reconstituted TNF- α aliquots and TUN solutions were stored at $-20^\circ C$ while diluted H_2O_2 was stored at RT.

Table 3.10: Seeding density for cell lines in various types of culture vessels

Cell Lines	Culture Vessel/Volume Plating Medium		
	6-well/2ml	12-well/1ml	96-well/100 μ l
HSC-2	5×10^5 cells/well	2.5×10^5 cells/well	2.5×10^4 cells/well
ACHN	2×10^5 cells/well	1×10^5 cells/well	1×10^4 cells/well
LS 174T	6×10^5 cells/well	3×10^5 cells/well	3×10^4 cells/well

3.9 Cell Viability Assessment using MTT Assay

A total of 100µl cells were seeded into each well of the 96-well plate (Table 3.10). Twenty-four hours after plating, cells were treated and cultured at 37°C, 5% CO₂. Following 24 or 48hr incubation, depending on the drug treatment, morphology of treated cells was assessed using Nikon Eclipse TS100 inverted microscope equipment prior to the addition of 20µl 3-(4,5-dimethylthiazol-2-yl)-2,5-diphenyltetrazolium bromide (MTT, Calbiochem[®], Darmstadt, Germany) stock solution of 5mg/ml in PBS into each well. The plate was then incubated for 4hr at 37°C until purple formazan crystal developed. Seventy-five percent of the medium-containing MTT were pipetted out and 150µl of DMSO (Fisher Scientific, MA) was added in order to dissolve the formazan crystals. Following 10-30min of incubation in the dark, absorbance was determined by Model 680 Microplate Reader (Bio-Rad, CA) at 550nm. Cell viability was compared. Cell viability was determined by using the formula below:

$$\text{Cell viability} = \frac{\text{Corrected Value}}{\text{Dynamic Range}} \times 100\%$$

Corrected Value = Average OD of transfected cells – Average OD of blank

Dynamic Range = Average OD of control cells – Average OD of blank

3.10 Apoptotic Markers Detection by Western Blot Analysis

Following SDS-PAGE, treated cells were blotted on PVDF membrane using semi-dry transfer system as described in Section 3.7.3. Membrane was then blocked for an hour at RT with 5% w/v Skim milk powder in PBS-T followed by incubation with rabbit monoclonal anti-Bax antibodies or rabbit monoclonal anti-Bcl-xL antibodies diluted in Tris buffered saline (TBS) containing 5% BSA and 0.1% v/v Tween-20 for overnight incubation at 4°C. Primary antibodies were labelled with goat anti-rabbit IgG-HRP conjugate diluted in PBS-T containing 2% BSA for an hour at RT. Summary of antibody dilutions are shown in Table 3.9. Immunoreactive bands were visualized by ECL detection system and image acquisition was performed using FluorChem FC2 System.

3.10.1 Bax/Bcl-xL Ratio Quantification

Detection of Bax and Bcl-xL was performed separately on the same PVDF membrane to ensure consistency of protein loading was achieved. Densitometry analysis of the Bax or Bcl-xL protein expression was performed using ImageJ 1.43U software where the relative intensity of Bax or Bcl-xL in each sample was quantified by comparing the relative intensity of actin in each sample (on the same lane of the PVDF membrane).

3.11 Cell Cycle Analysis by Flow Cytometry

Cells growing in 6-well plate were harvested by centrifugation for 5min at 1,500rpm, washed with PBS, and finally resuspended in 300 μ l of PBS. Cells were then fixed in 700 μ l of ice-cold 100% absolute ethanol (HmbG[®] Chemicals, Hamburg, Germany) and stored at -20°C for at least 2hr. Prior to storage, tubes were inverted a few times to ensure proper mixing and good fixing of cells. Cells were then centrifuged for 5min at 5,000rpm and washed with PBS to remove any ethanol residue. The supernatants were discarded and cells were incubated in DNA staining solution (10 μ g/ml Propidium iodide (PI, Sigma-Aldrich, MO) and 100 μ g/ml RNase A (Fermentas, Vilnius, Lithuania) in PBS) for 30min at 37°C, in the dark. RNase A specifically degrades single stranded RNA (ssRNA) which will interrupt with PI binding to DNA. Fluorescence of cell was measured with BD FACSCalibur[™] flow cytometer (BD Biosciences, NJ) using BD CellQuest Pro software. PI was excited with the 488 line of an argon-ion laser and its fluorescence was detected in the 623nm emission filter, FL2 channel. A total of 10,000 cells were collected for each sample. Percentages of cells were analyzed and the data analysis was performed using WinMDI 2.8 software by J. Trotter which was downloaded from <http://facs.scripps.edu/software.html>. Proliferative index (PrIn) was computed using the formula $PrIn = (S+G_2)/(S+G_2+G_1)$ to determine the number of cancer cells which are proliferating (Liang et al., 2007).

3.11.1 Cell Cycle Synchronization

Cell cycle synchronization was carried out using TUN which was able to trigger suppression of S-phase and arrest cell cycle in late G₁-phase. Cells were initially exposed to TUN for 24hr at IC₂₀ to initiate cell cycle arrest. Subsequently, TUN was quenched off and the post-treated cells were then washed twice and incubated in fresh culture MEM media for an additional 24hr. Cells in MEM medium were harvested at 4hr intervals throughout the next 24hr after 1 day incubation with MEM in the absence of TUN and each time point were analyzed for DNA content using flow cytometer. The fraction of cells in G₁-phase, S-phase, G₂/M-phase and sub G₁-phase were evaluated using WinMDI 2.8 software.

3.12 FITC Annexin V-PI Dual Staining

Apoptotic cells were detected by flow cytometry with a combination of Annexin V-Fluorescein isothiocyanate (FITC)/PI staining using FITC Annexin V Apoptosis Detection Kit I (BD Biosciences, NJ) according to manufacturer's manual. Treated cells were harvested and washed twice with ice-cold PBS. Cells were then resuspended in 500µl of 1× Binding buffer. A total of 10µl of 5µl FITC Annexin V and 5µl PI were added into the cells suspension prior to incubation at RT for 5-15min in the dark. Samples were then transferred to FACS tube, analyzed by flow cytometer. Fluorescence was detected via 530/30 band filter (FL1) and 585/42 band filter (FL2) to monitor FITC Annexin V binding and PI uptake, respectively. A total of 10,000 events per sample were

recorded. Data collected were later analyzed with WinMDI 2.8 software. The following controls were used to set up compensation and quadrants: unstained cells, cells stained with FITC Annexin V only and cells stained with PI only.

3.13 Determination of Antioxidant Activity using DCFH-DA

ROS, H₂O₂ generated within cells were detected using fluorescent probe 2',7'-dichlorofluorescein diacetate (DCFH-DA, Sigma-Aldrich, MO). Cells were harvested, washed twice and resuspended in 500µl of PBS. Later on, cells were treated in 3mM of H₂O₂ for 30min at 37°C. Treated cells were then washed once with ice-cold PBS and incubated with 10µM DCFH-DA in 500µl of PBS for 30min at 37°C. The fluorescence of 2',7'-Dichlorofluorescein (DCF) (excitation 488nm, emission 525nm) was measured using BD FACSCalibur™ flow cytometer on FL1 channel. A total of 10,000 cells were analyzed. Fluorescence intensity of the data was expressed as the mean logarithm of green DCF fluorescence. Data acquired was analyzed using WinMDI 2.8 software.

Negative control along with fluorescence baseline control was prepared for the setting up of template. The negative control was loaded with DCFH-DA alone, without H₂O₂ treatment whereas the fluorescence baseline shows the distribution of untreated control cells, which was not loaded with both DCFH-DA and H₂O₂.

3.14 Statistical Analysis

Results presented are from representative experiments and data were expressed as mean \pm standard error of the mean (SEM) of at least two independent experiments which were performed in triplicates, unless otherwise stated. Statistical Package for the Social Sciences (SPSS) version 15.0 (SPSS Inc., IL) with one-way ANOVA followed by the LSD's post hoc test for multiple comparisons was used to compare mean values. Data of cell cycle analysis which was presented as percentages and the significance of Bax/Bcl-xL expression in each samples were compared with Microsoft Excel[®] 2007 (Microsoft Corp., WA) using unpaired two-tailed Student's t-Test. A *p* value of less than 0.05 was considered as statistically significant, as per indicated by asterisks in the graphs.

CHAPTER 4

RESULTS

4.1 Molecular Biology

4.1.1 The pCMV-SPORT6 Empty Vector Construction

pCMV-SPORT6 vector carrying the human PrP^C insert, designated as pCMV-SPORT6-PrP was initially used to create cell lines overexpressing PrP^C. Empty vector of pCMV-SPORT6 was created as described in Materials and Methods to serve as negative control. Cells were co-transfected with pCMV-SPORT6-PrP and mammalian selection marker-containing pBABE-hygro to overexpress PrP^C. Upon stable transfection, cells were selected in medium containing 200µg/ml of Hygromycin B for 10 days.

Figure 4.1A shows the sizes of pCMV-SPORT6 empty vector, pCMV-SPORT6-PrP and pBABE-hygro. To ensure proper migration of DNA, pCMV-SPORT6 and pBABE-hygro were first linearized with *SalI* and *EcoRI* respectively prior to agarose gel electrophoresis. The sequence alignment of a single positive transformant of pCMV-SPORT 6 empty vector using Multiple sequence alignment (Corpet, 1988) hosted by Plateforme Bioinformatique Genotoul is shown in Figure 4.1B. Positive transformants were verified by DNA sequencing using the M13 forward (-20) primer in order to confirm the presence and exact orientation of the insert and its sequence.

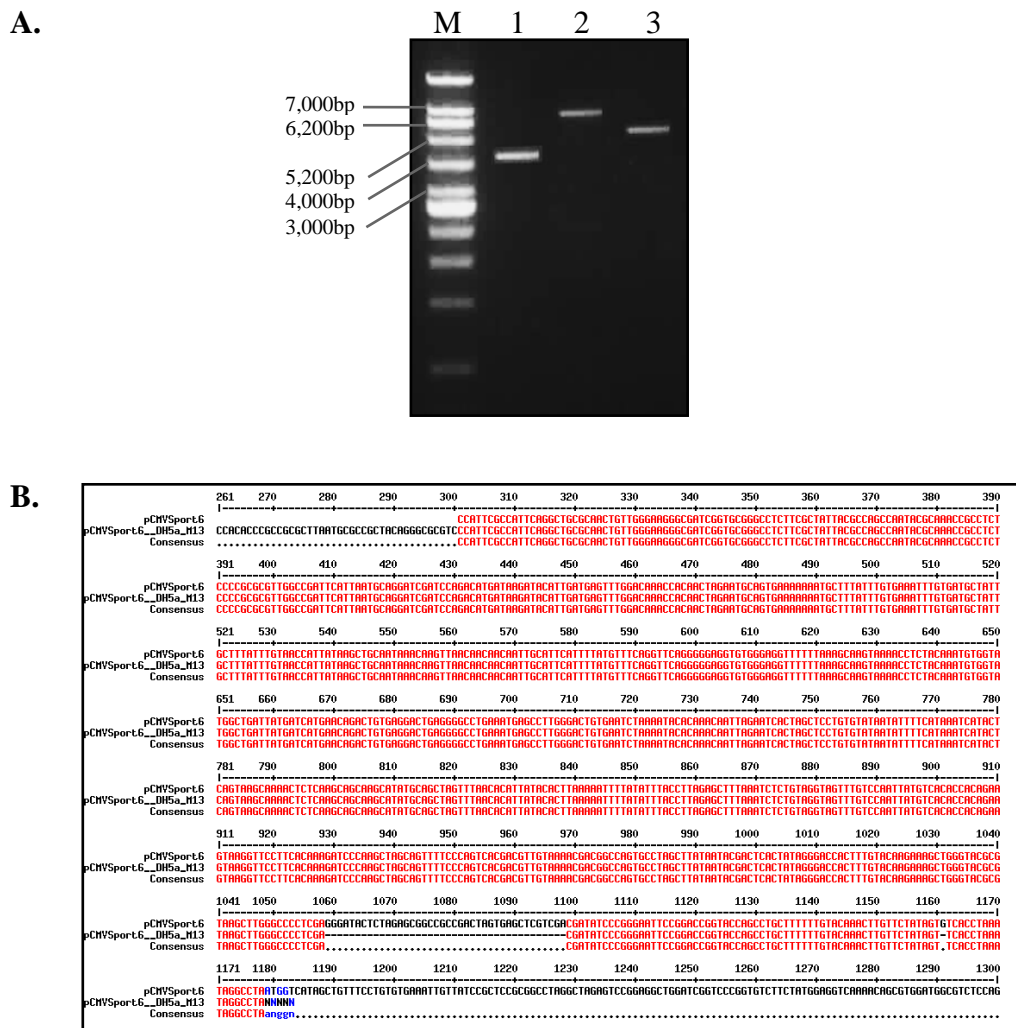


Figure 4.1: The construction of pCMV-SPORT6 empty vector. (A) Agarose gel analysis. Lane 1, pCMV-SPORT6 (4,396bp); lane 2, pCMV-SPORT6-PrP (6,827bp); lane 3, pBABE-hygro (5,558bp); and lane M, 1kb DNA ladder (Vivantis, CA). Sizes of markers are indicated on the left. (B) Multiple sequence alignment (Multalin) of a positive transformant with pCMV-SPORT6 sequence which was designated as “pCMVSPORT6” while “pCMVSPORT6__DH5a_M13” was the sequence of positive transformant. The red one-letter nucleic acid abbreviations represent fit match.

4.1.2 Cloning of Human PrP^C cDNA into pcDNATM 3.1 Construct

Upon linearization with *Xho*I, cloned inserts were screened using agarose gel electrophoresis. DNA linearization is necessary to ensure proper migration of the DNA according to its size during electrophoresis. A single positive clone and the pcDNATM 3.1 empty vector are shown in Figure 4.2A.

The linearized purified plasmid DNA carrying the positive clone was then transfected into cancer cells to overexpress the PrP^C. For selection of cell lines stably expressing PrP^C, G-418 sulfate was used as described in Materials and Methods.

4.1.3 Short Hairpin RNA (shRNA) Cloning into pLKO.1 TRC Cloning Vector

The 1,900bp stuffer of the pLKO.1 TRC cloning vector which was replaced with the shRNA oligos was released by dual digestion using *AgeI* and *EcoRI*. The digested pLKO.1 TRC vector is shown in Figure 4.3A. The shRNA oligos: HuPrPshRNA 1, HuPrPshRNA 2 and HuPrPshRNA 3 were then ligated into the 7,000bp pLKO.1 TRC cloning vector as described in Materials and Methods. The positive transformants which produce two fragments, a 2,000bp fragment and a 5,000bp fragment as shown in Figure 4.3B after restriction digest with *EcoRI* and *NcoI* were verified by conducting a sequencing reaction using pLKO.1 sequencing primer (5'-CAAGGCTGTTAGAGAGATAATTGGA-3') as shown in Figure 4.3C.

The successfully ligated oligos with pLKO.1 TRC vector were transfected into HSC-2 cells and selected with puromycin dihydrochloride to create stable cell lines. Plasmids pLKO.1 TRC control and pLKO.1 scramble shRNA served as transfection controls and the PrP^C expression was then confirmed by Western blotting.

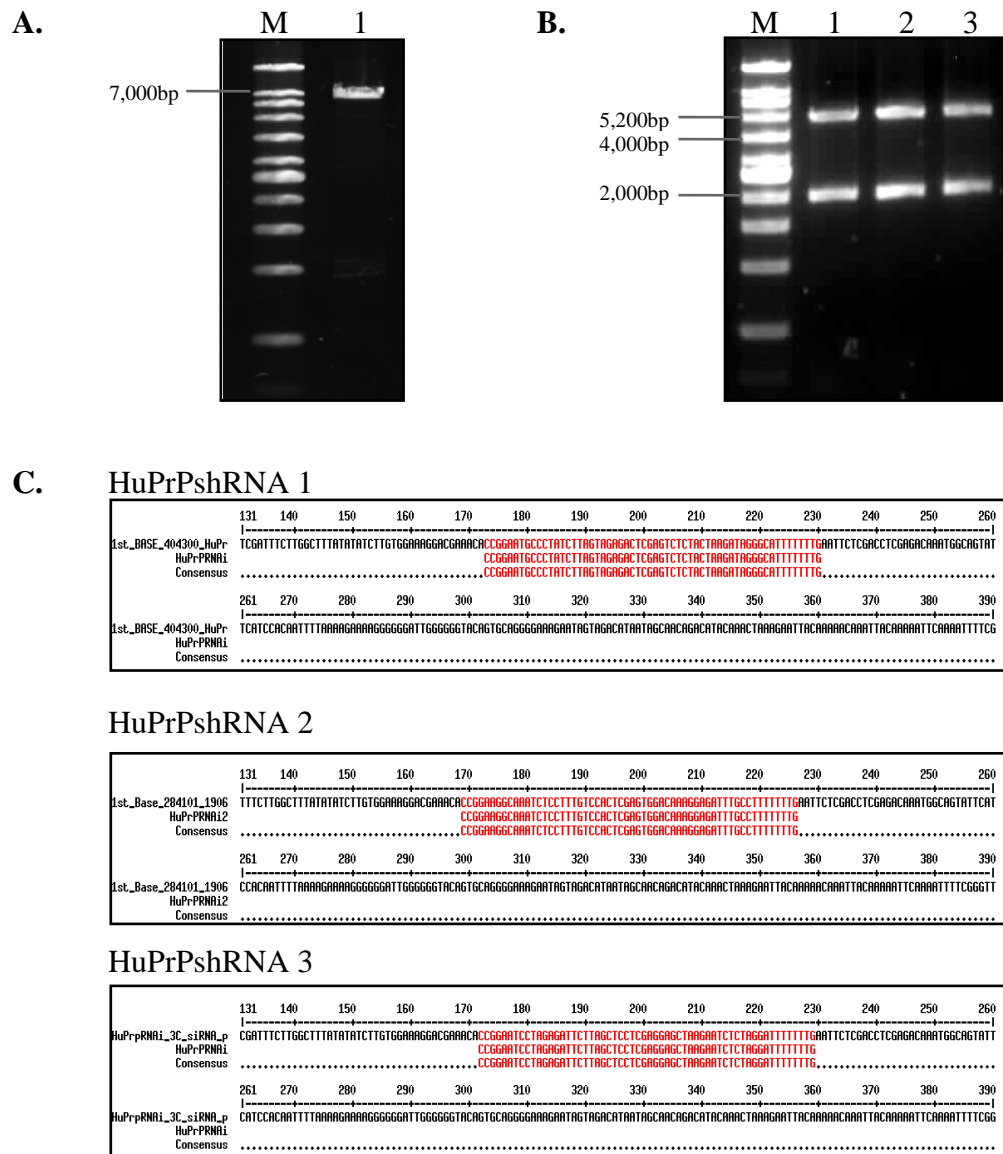


Figure 4.3: shRNA cloning into pLKO.1 TRC cloning vector. (A) Agarose gel analysis. Lane 1, dual-digested pLKO.1 TRC vector (7,000bp); and lane M, 1kb DNA ladder. (B) Agarose gel analysis. Lane 1, 2 and 3, screening for inserts HuPrPshRNA 1, HuPrPshRNA 2 and HuPrPshRNA 3, respectively on transformants subsequent to restriction digest with *EcoRI* and *NcoI*; and lane M, 1kb DNA ladder. Sizes of markers are indicated on the left. (C) Positive clones sequencing with pLKO.1 sequencing primer. The red one-letter nucleic acid abbreviations represent fit match.

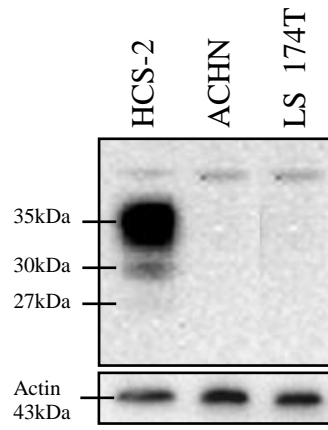
4.2 Assessment of PrP^C Expression in Cancer Cells

4.2.1 PrP^C Expression in Transiently Transfected Cancer Cells

Cells overexpressing PrP^C were initially created via co-transfection using pCMV-SPORT6 and pBABE-hygro. However, due to repeatedly unsuccessful transfections (Figure 4.4B), pcDNATM 3.1 cloning vector which is designated as pcDNA 3.1 were utilized. Introduction of pcDNA 3.1 into cells was performed using cationic lipid formulations, TransPass D1 Transfection Reagent (TPD1TR) as a replacement for electroporation method due to low transfection success rate of the latter.

PrP^C expression was assessed through Western blot analysis upon 24hr after transient transfection with empty vector pcDNA 3.1 and pcDNA 3.1 carrying the insert PrP^C, designated as pcDNA 3.1-PrP, into selected cancer cell lines, ACHN, HSC-2 and LS 174T (Figure 4.4C). Basal PrP^C expression which ranged from 27-35kDa in the 3 cancer cell lines are shown in Figure 4.4A. HSC-2 cell line expressed high endogenous levels of PrP^C while ACHN and LS 174T cells did not. Transiently pcDNA 3.1-PrP transfected-HSC-2, -ACHN and -LS 174T cells are annotated as Tr-HSC-2-pcDNA 3.1/PrP, Tr-ACHN-pcDNA 3.1/PrP and Tr-LS 174T-pcDNA 3.1/PrP, respectively. To confirm equal protein loading in each lane, membranes were reprobed with actin antibody and image analysis was performed by densitometry using ImageJ 1.43U software.

A.



B.

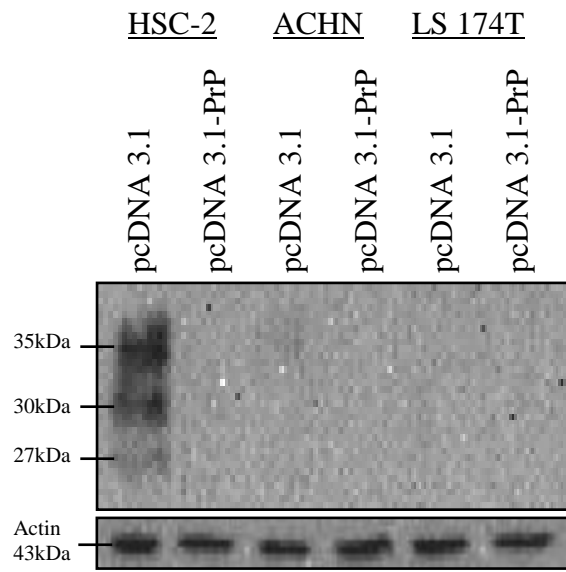
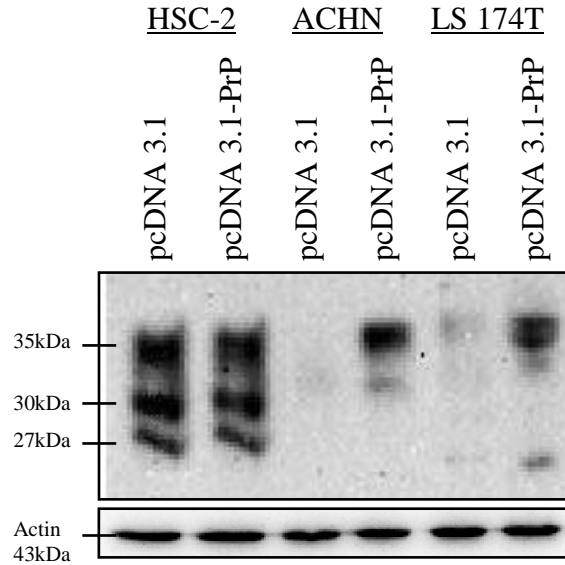


Figure legend on page 93.

Figure 4.4 continued.

C.



D.

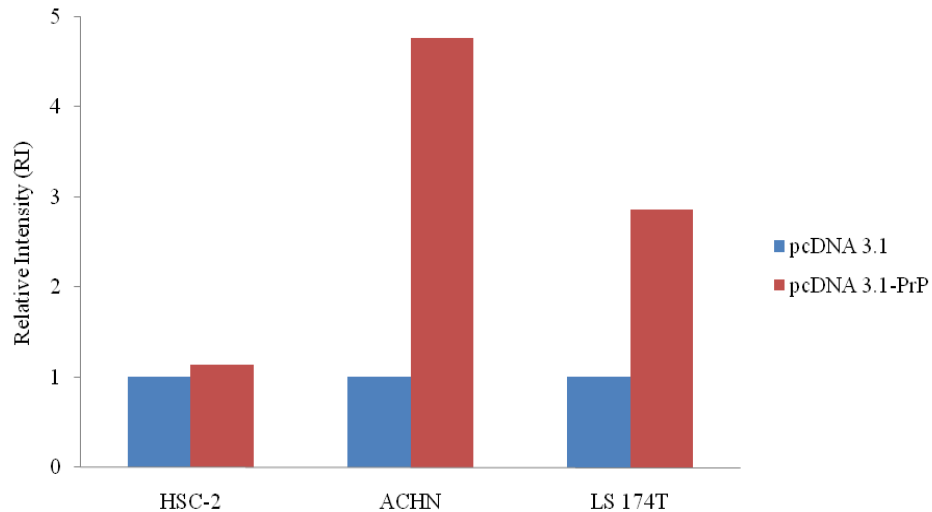


Figure 4.4: Western blot analysis on transiently pcDNA 3.1-PrP-transfected cancer cell lines. (A) Basal expression of PrP^C (27-35kDa) in untransfected HSC-2, ACHN and LS 174T cells. (B) Unsuccessful co-transfection using pCMV-SPORT6 and pBABE-hygro. Only endogenous PrP^C in HSC-2 was detected. (C) PrP^C expression in transiently transfected HSC-2, ACHN and LS 174T cells. Molecular weights are indicated on the left. The immunoblot presented is representative from two independent experiments. (D) Densitometry of protein expression in Western blot shown in C was performed using ImageJ 1.43U software. The total relative intensity (RI) of the PrP^C bands (27-35kDa) was normalized to the pcDNA 3.1-transfected control of each respective cell line which was set at 1.

Western blot analysis shows that the three isoforms of PrP^C, namely unglycosylated PrP (27kDa), monoglycosylated PrP (30kDa) and diglycosylated PrP (35kDa) which were detected using anti-PrP mAB clone 3F4 occurred in unison indicating normal synthesis and processing of PrP^C. The greater band intensities at 30kDa and 35kDa further revealed that PrP^C is predominantly glycosylated which is contrary to the often unglycosylated pathogenic PrP^{Sc} (Müller, Strom, Hunsmann, & Stuke, 2005).

It was shown that HSC-2 cells express high endogenous levels of PrP^C (Figure 4.4B) which even after subjected to transient transfection; the PrP^C level did not show any significant overexpression. On the other hand, PrP^C expression in both pcDNA 3.1-PrP-transfected ACHN and LS 174T increased approximately 5- (RI value of 4.76 vs. 1.00) and 3-fold (RI value of 2.85 vs. 1.00), respectively, compared to the vector-transfected cells. The transiently PrP^C expressing cell line was evaluated for its anti-cytotoxicity properties after TNF- α treatment using MTT assay and basal cell cycle analysis.

4.2.2 Stably-transfected LS 174T Cells Overexpress PrP^C

To further elucidate the general properties of PrP^C, cell lines which stably express PrP^C were created in order to ensure long-term, reproducible gene expression compared to the transiently transfected cells which is more for fast analysis of genes and small scale protein production.

HSC-2 and LS 174T cells were selected as to our knowledge, these cell lines have by no means been reported in literature on their establishment in prion research and due to the high endogenous PrP^C level in HSC-2, this study was also attempted to knockdown the PrP^C using shRNA. Thus, the two digestive system cancer cell lines, LS 174T and HSC-2, were subjected to stable transfection for advance study purposes where glycosylation status of PrP^C in the stable transfectants was modified to investigate its association with apoptosis and oxidative stress. PrP^C expressing stable transfectants were also studied for its involvement in cell proliferation and progression.

LS 174T were transfected with pcDNA 3.1-PrP and empty vector itself, which the latter was served as the negative control throughout the study. Assessment of PrP^C expression was performed using IFM as shown in Figure 4.5A. PrP^C expression was further confirmed with Western blot analysis using anti-PrP mAB clone 3F4. Membranes were reprobbed with actin antibody to confirm equal protein loading in each lane. The stably overexpressing PrP^C LS 174T cells is annotated as sT-LS 174T-pcDNA 3.1/PrP while vector-transfected cells is designated as sT-LS 174T-pcDNA 3.1.

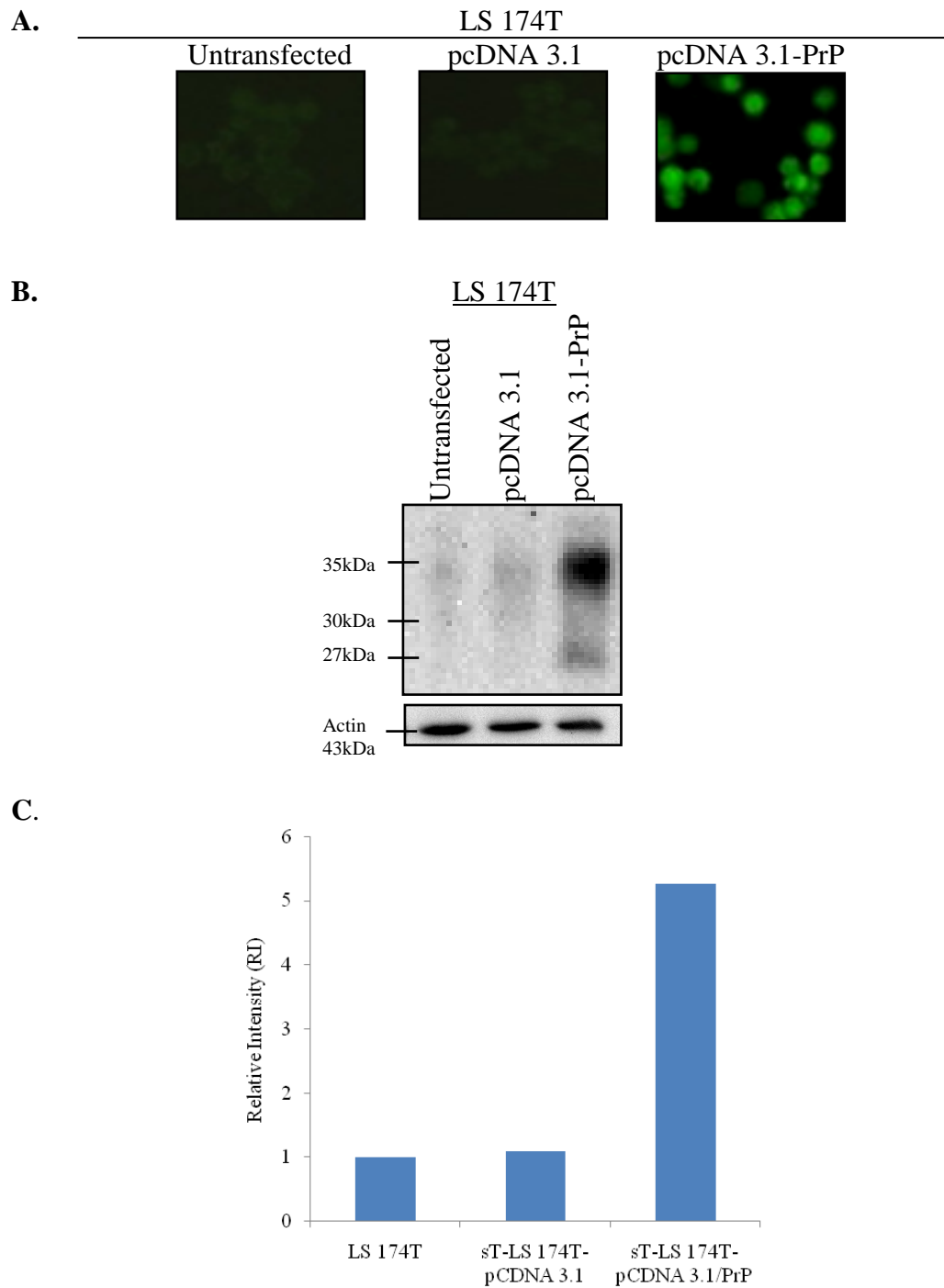


Figure 4.5: PrP^C overexpression in LS 174T cells. (A) Immunofluorescence staining of PrP^C in LS 174T using 3F4 antibody. Images were captured using NIS-Elements BR 3.0 at 200× magnification in the same exposure. (B) PrP^C expression in stably transfected LS 174T cells. Molecular weights are indicated on the left. The immunoblot presented is representative from three independent experiments. (C) Densitometry of protein expression in Western blot shown in B was performed using ImageJ 1.43U software. The total relative intensity (RI) of the PrP^C bands (27-35kDa) was normalized to the untransfected group which was set at 1.

Upon stable transfection with pcDNA 3.1-PrP, Western blots revealed similar PrP^C expression, diglycosylated (35kDa), monoglycosylated (30kDa) and unglycosylated (27kDa). The expression of PrP^C in LS 174T was increased 5-fold surplus, with RI value of 5.27 compared to the untransfected cells and sT-LS 174T-pcDNA 3.1 cells. Untransfected LS 174T and sT-LS 174T-pcDNA 3.1 cells were negative for PrP^C expression. By performing IFM, PrP^C on LS 174T cells transfected with pcDNA 3.1-PrP was revealed by emission of bright green fluorescence signals. There was almost null or weak staining in both the untransfected and vector-transfected cells.

4.2.3 Depletion of Endogenous PrP^C in *PRNP* Gene Knockdown HSC-2

Knockdown efficiencies of each shRNA oligos were assessed using Western blot analysis as shown in Figure 4.6. The RI of the PrP^C bands were normalized to the untransfected HSC-2 cells which were set at 1. Plasmids pLKO.1 TRC control and pLKO.1 scramble shRNA were used as transfection controls. Membranes were reprobed with actin antibody to confirm equal protein loading in each lane.

The quantification of bands at Figure 4.6B indicates that shRNA oligos HuPrPshRNA 1 possessed the highest knockdown efficiency at RI value equal to 0.27, followed by HuPrPshRNA 3 and HuPrPshRNA 2 at 0.43 and 0.78, respectively. There was least PrP^C detected in HSC-2 cells expressing HuPrPshRNA 1 and all three isoforms of PrP^C were efficiently inhibited.

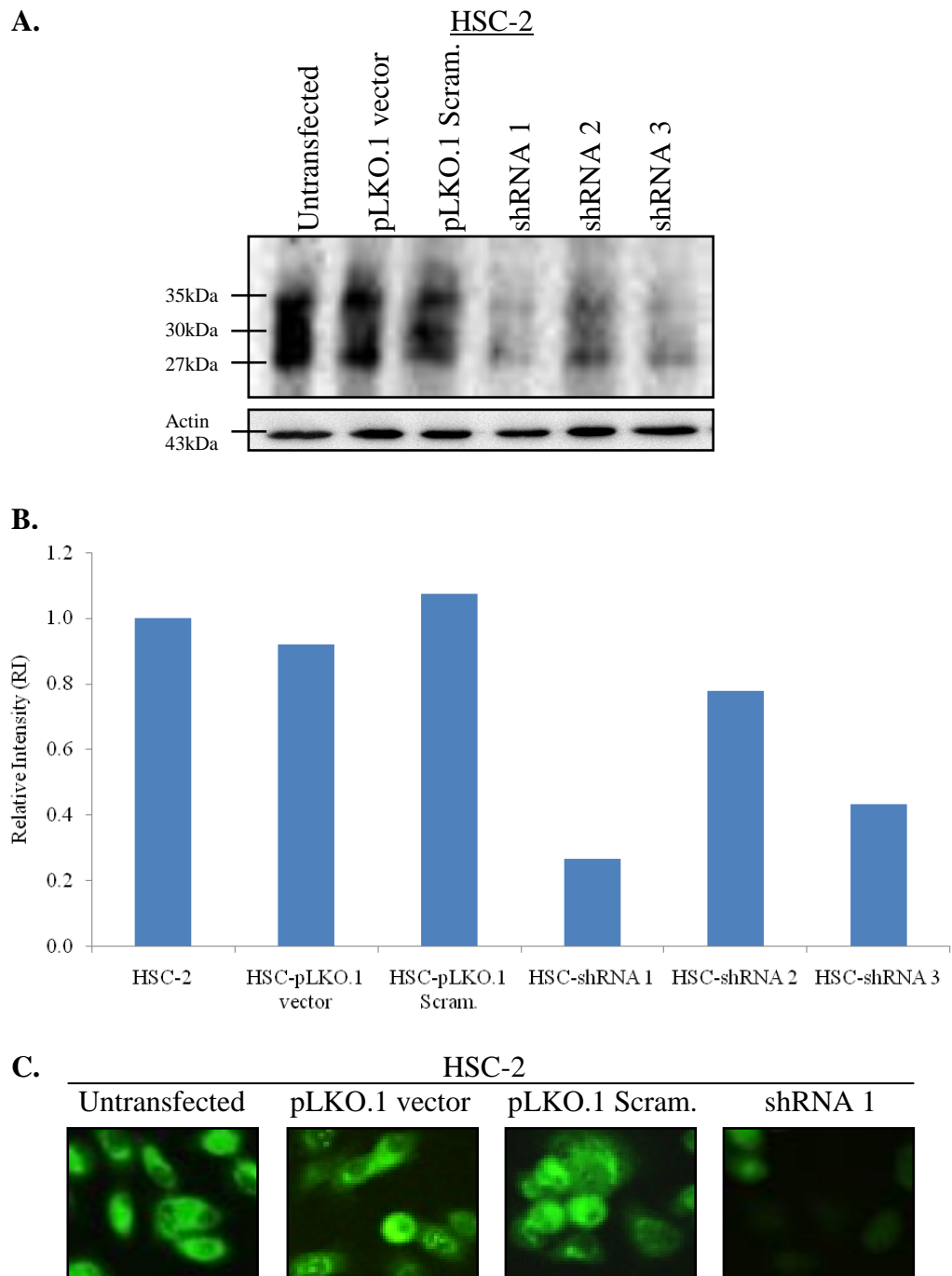


Figure 4.6: Inhibition of PrP^C expression using shRNA oligonucleotide. (A) Assessment of PrP^C expression in *PRNP* knockdown HSC-2 cells. Molecular weights are indicated on the left. The immunoblot presented is representative from two independent experiments. (B) Densitometry of protein expression in Western blot shown in A was performed using ImageJ 1.43U. The total relative intensity (RI) of the PrP^C bands (27-35kDa) was normalized to the untransfected group which was set at 1. (C) Immunofluorescence staining of *PRNP* knockdown HSC-2 cells using 3F4 antibody. Images were captured using NIS-Elements BR 3.0 software at 200× magnification in the same exposure.

To further confirm the efficiency of *PRNP* gene knockdown using HuPrPshRNA 1, transfected cells were subjected to immunofluorescence microscopy. As expected, the cells were weakly stained and significant reduction of the bright green fluorescence was observed compared to the untransfected HSC-2 cells, pLKO.1 TRC control- and pLKO.1 scramble shRNA-transfected HSC-2 cells. Hence, it is demonstrated that expression of pLKO.1 carrying the HuPrPshRNA 1 can capably down-regulate expression of the endogenous PrP^C in HSC-2 cells in a specific manner.

Consequently, HSC-2 cells transfected with pLKO.1 TRC vector carrying the HuPrPshRNA 1, annotated as HSC-shRNA 1 was then chosen to be used in the subsequent assays to study the properties of PrP^C. pLKO.1 TRC control- and pLKO.1 scramble shRNA-transfected HSC-2 cells are designated as HSC-pLKO.1 vector and HSC-pLKO.1 Scram., respectively.

4.3 PrP^C Expression in Cells Suppresses TNF- α -induced Cell Death

To determine the protective effects of PrP^C towards cancer cells in TNF- α -induced cell death, HSC-2, ACHN and LS 174T cells were plated in 96-well plates and transiently transfected with vector pcDNA 3.1 or pcDNA 3.1-PrP prior to 100ng/ml of human recombinant TNF- α treatment for 48hr. To test the anti-cytotoxicity activity of PrP^C, cells were subjected to TNF- α treatment and cell viability was assessed using MTT dye reduction assay. In metabolically active cells, the membrane-permeable yellow MTT dye is reduced by

mitochondrial reductases to form the purple crystalline product, MTT-formazan.

Assays were performed in triplicates of three independent experiments. Relative survival in comparison with untreated vector-transfected control was determined. Effect of PrP^C on cell viability is represented in Figure 4.7.

The percentage (%) of cellular cell death in non-PrP^C expressing cells increased significantly, with the MTT signal reduced to an estimated 50% after 48hr in comparison to the untreated control cells as shown in Figure 4.7 upon TNF- α treatment. MTT analysis revealed that transfection of pcDNA 3.1-PrP group showed significantly higher cell viability upon treatment with TNF- α compared to the vector-transfected group. There was a larger increment of cell viability differences between the treated pcDNA 3.1-PrP-transfected cells and treated vector-transfected control in ACHN cell line (81.2% \pm 4.3 vs. 65.2% \pm 2.9) compared to LS 174T (54.2% \pm 0.7 vs. 45.3% \pm 2.7). No significant difference was observed in HSC-2 cells as the cell line itself overexpresses PrP^C. Thus, these results suggest that PrP^C resists the cytotoxic activity of TNF- α in a cell-dependent manner, by displaying statistically significant increase in cell viability compared to vector-transfected cells.

Morphological changes in cells upon treatment with TNF- α were shown in Figure 4.8. Cell rounding was monitored with a Nikon Eclipse TS100 inverted microscope. Phase contrast images were acquired at 200 \times magnification with NIS-Elements BR 3.0 software.

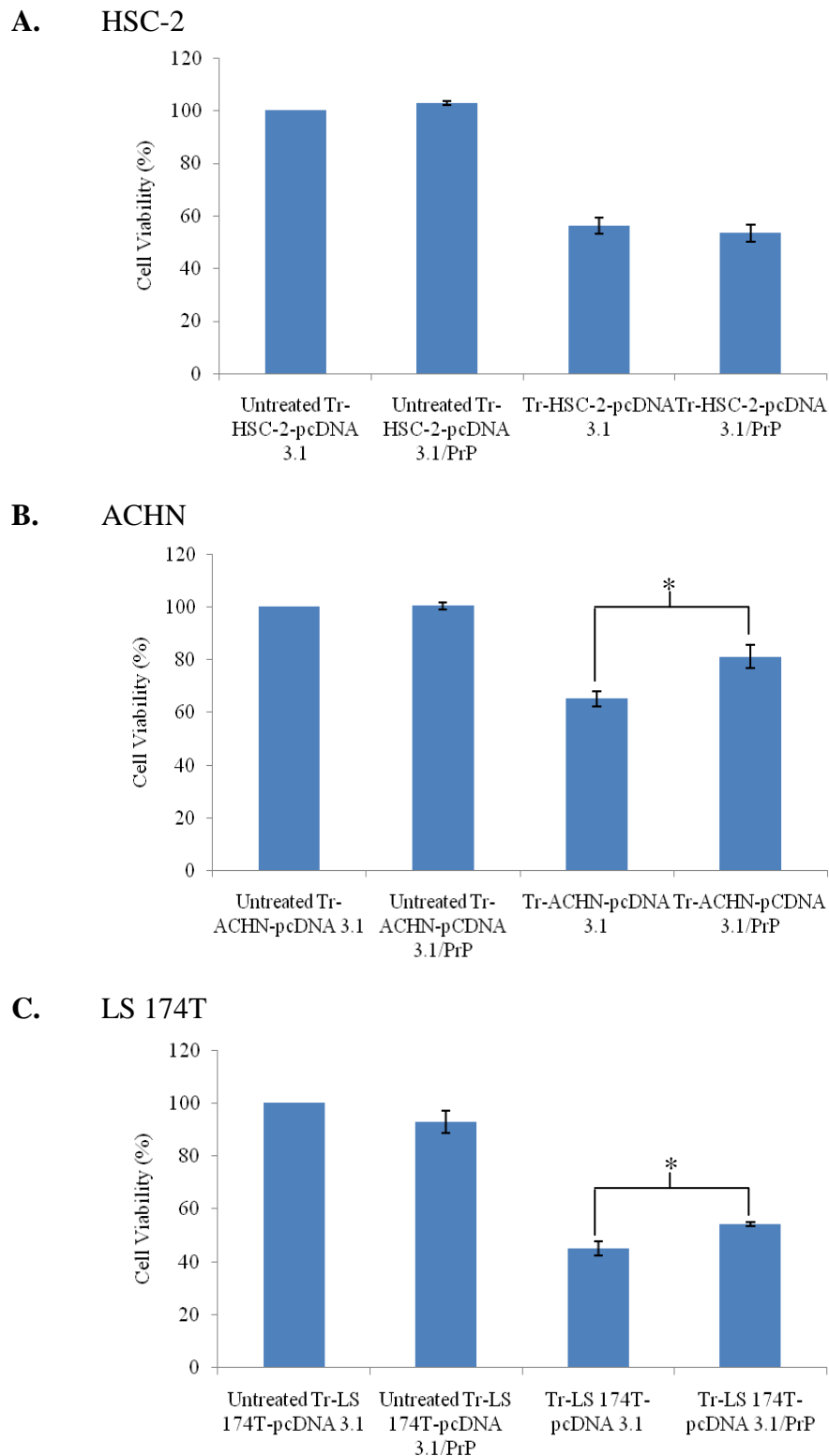


Figure 4.7: PrP^C in transiently transfected cells suppresses TNF- α -induced cell death. Cell viability was determined by MTT assay following treatment with 100ng/ml of TNF- α in (A) HSC-2, (B) ACHN and (C) LS 174T cells. Data of cell viability was expressed in % and representing the mean \pm SEM of 3 independent experiments as compared to the untreated vector-transfected cells. Mean values were compared using ANOVA followed by LSD's post hoc test for comparison of the means, via SPSS software. * $p < 0.05$ in treated pcDNA 3.1-PrP-transfected cells vs. treated vector-transfected cells.

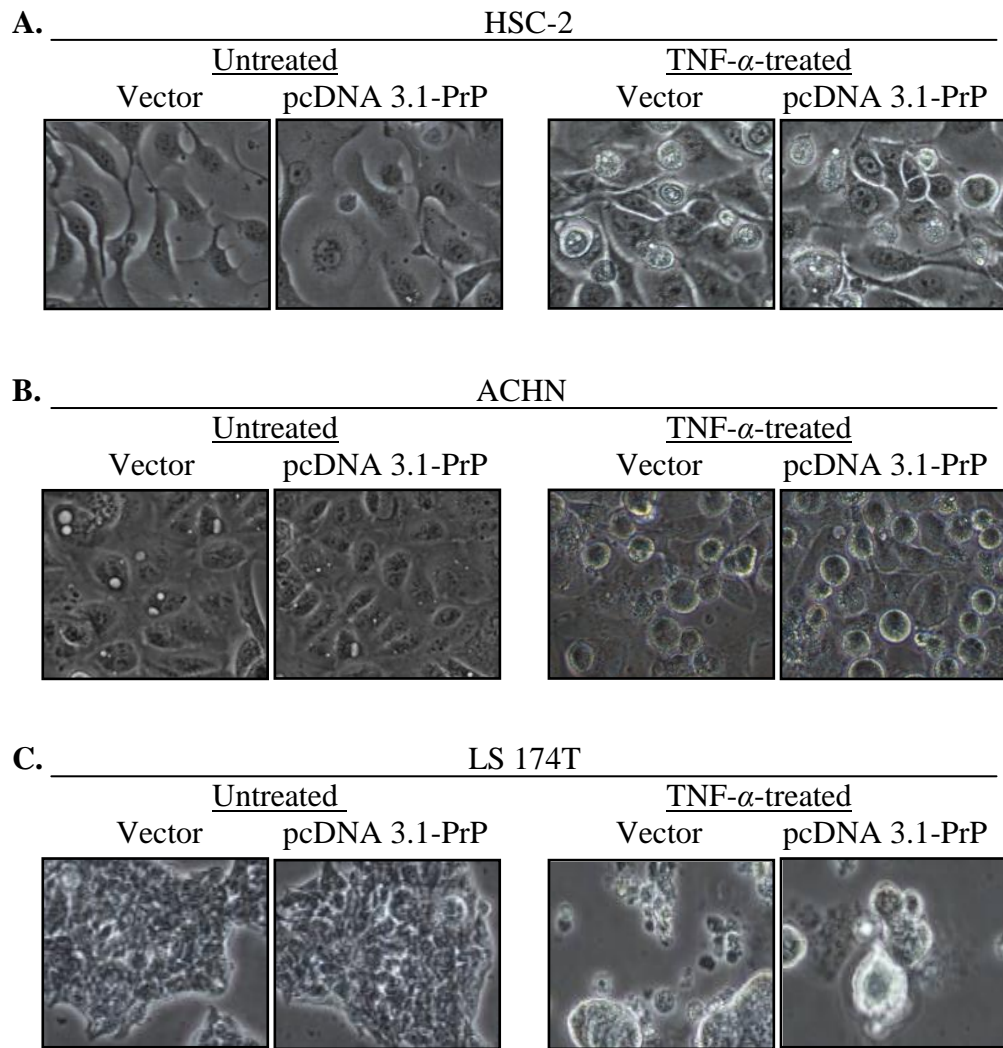


Figure 4.8: PrP^C resists cytotoxicity of TNF- α in cancer cells. Cell morphology alterations of (A) HSC-2, (B) ACHN and (C) LS 174T with/without TNF- α treatment at 100ng/ml were shown. Apoptotic bodies were visibly distinguished in the TNF- α -treated cells. Photographs of cells were taken with NIS-Elements BR 3.0 software under Nikon Eclipse TS100 inverted microscope at 200 \times magnification in the same exposure.

To further validate the protective effect of PrP^C towards TNF- α -induced cell death, morphological analysis was performed using Nikon Eclipse TS100 inverted microscope. Cells were recognized as healthy or apoptotic by their morphological status, where the presence of chromatin condensation, nuclear fragmentation and cytoplasm blebbing indicates apoptosis.

Normal cell morphology was observed in cells without TNF- α treatment. Cells were grown in high confluency and adhered to each other with a relatively uniform monolayer. pcDNA 3.1-transfected ACHN and LS 174T cells treated with TNF- α under light microscope showed a lot more of shrunken and rounded cells compared to PrP^C expressing cells. Other abnormal morphologies, including condensation of chromatin and nuclear fragmentation were also detected. Apparently, no differences in morphological changes were observed between the treated vector-transfected and treated pcDNA 3.1-PrP-transfected HSC-2 cells. These findings correspond with the MTT analysis performed earlier.

4.3.1 PrP^C Exerts Its Protective Effect in TNF- α -induced Cell Death through Bax Regulation

Previous data shows that PrP^C resists cytotoxicity of TNF- α in cancer cells. To further elucidate the underlying mechanism of PrP^C in TNF- α -induced cell death, treated cells were examined for the expression of apoptotic markers, Bax and Bcl-xL through Western blotting. Bax was chosen as it is a key component for cellular induced apoptosis through mitochondrial stress (Wei et al., 2001). Additionally, PrP^C was shown to specifically inhibit Bax (Roucou et al., 2005). On the other hand, Bcl-xL was preferred as it was the endogenous regulator of cell resistance/sensitivity to TNF- α -induced apoptosis (Gozzelino et al., 2008).

Upon transient transfection with pcDNA 3.1-PrP in 100mm cell culture dish, cells were treated with 100ng/ml of TNF- α for 48hr. Upon treatment, collected

cell lysates were electrophoresed on 15% polyacrylamide SDS-PAGE prior to Western blotting. The immunoblots which derived from the same PVDF membrane are shown in Figure 4.9A. Blots were visualized by ECL detection system and image acquisition was performed using FluorChem FC2 System. Data presented in Figure 4.9B and Figure 4.9C was expressed as mean \pm SEM.

A significant difference in protein expression between the PrP^C expressing cells and vector-transfected cells was observed. As shown in Figure 4.9, Bax expression in both Tr-HSC-2-pcDNA 3.1/PrP and Tr-ACHN-pcDNA 3.1/PrP was significantly lower compared to the vector-transfected cells whereas Bcl-xL expression was not affected. Hence, this illustrates that PrP^C might play a prominent role in modulating the expression of the pro-apoptotic protein, Bax, without interfering with the regulation of anti-apoptotic protein, Bcl-xL expression. The quantitative Bax and Bcl-xL protein expression levels and the Bax/Bcl-2 ratios are listed in Table 4.1.

Table 4.1: Quantification of the Bax/Bcl-xL ratio in TNF- α -treated cells

	Bax (RV)	Bcl-xL (RV)	Bax/Bcl-xL
Untransfected HSC-2	1.92 \pm 0.35	1.67 \pm 0.58	1.22 \pm 0.21
Tr-HSC-2-pcDNA 3.1	1.83 \pm 0.01	1.47 \pm 0.29	1.29 \pm 0.25
Tr-HSC-2-pcDNA 3.1/PrP	1.26 \pm 0.05	1.06 \pm 0.02	1.19 \pm 0.02
Untransfected ACHN	1.93 \pm 0.13	1.66 \pm 0.11	1.17 \pm 0.15
Tr-ACHN-pcDNA 3.1	1.97 \pm 0.23	1.92 \pm 0.06	1.02 \pm 0.09
Tr-ACHN-pcDNA 3.1/PrP	0.53 \pm 0.21	1.39 \pm 0.25	0.37 \pm 0.08*

Relative value (RV) was enumerated subsequent to densitometry analysis of the Western blot shown in Figure 4.9A. RV was normalized to the band intensity of actin in each lane which was set at 1. Data represented as mean \pm SEM from 2 independent experiments. An unpaired two-tailed Student's t-Test using Microsoft Excel® 2007 was used for statistical analysis. * $p < 0.05$ in treated pcDNA 3.1-PrP transfected cells vs. treated vector-transfected cells.

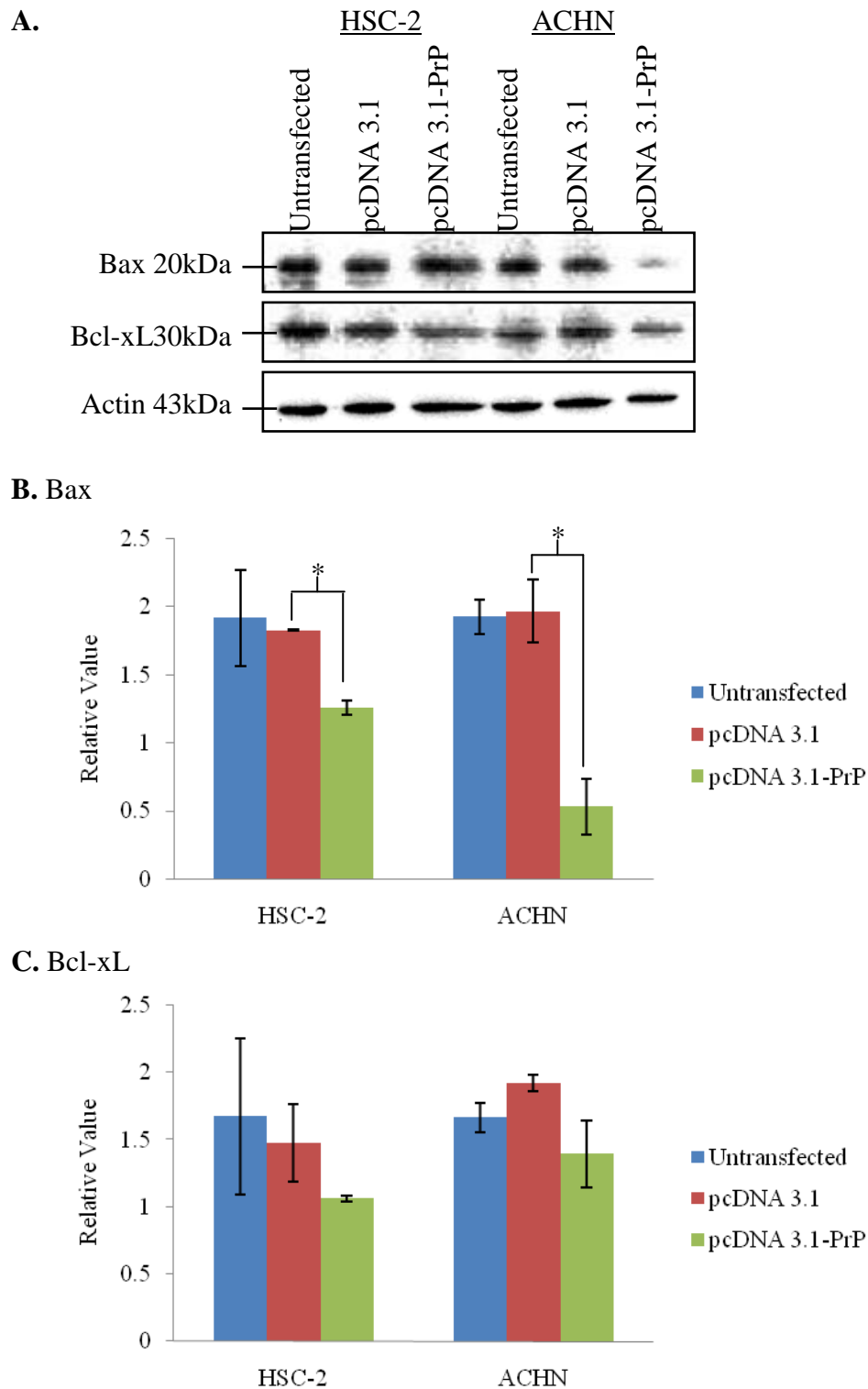


Figure 4.9: Western blot analysis of Bax and Bcl-xL in TNF- α -treated cells. (A) The expression levels of Bax and Bcl-xL were compared by Western blotting among the transiently transfected cells. Molecular weights are indicated on the left. The calculated relative value (mean \pm SEM) of protein intensities were shown in (B) Bax and (C) Bcl-xL. An unpaired two-tailed Student's t-Test using Microsoft Excel[®] 2007 was used for statistical analysis. * $p < 0.05$ in treated pcDNA 3.1-PrP-transfected cells vs. treated vector-transfected cells where $n = 2$.

From Table 4.1, the PrP^C expressing ACHN cells revealed a significantly lower expression of Bax in relation to Bcl-xL, 0.37 ± 0.08 , compared to other cells which have a Bax/Bcl-2 ratio of more than 1.00. These findings are paralleled with the higher resistance of Tr-ACHN-pcDNA 3.1/PrP towards TNF- α as compared with the non-PrP^C expressing cells in MTT analysis.

4.3.2 LS 174T Cells are Bax-deficient

Interestingly, Bax protein was not detectable by Western blot analysis in LS 174T cells (Figure 4.10).

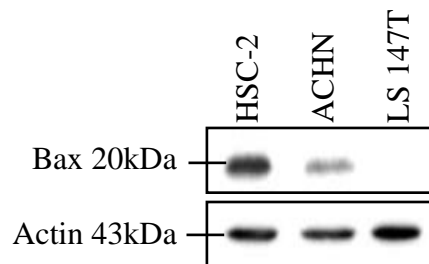


Figure 4.10: Analysis of Bax status in HSC-2, ACHN and LS 174T. Molecular weights are indicated on the left. Data correspond to a representative experiment out of 3 replicates with similar findings. Membranes were reprobed with actin antibody to confirm equal protein loading in each lane.

For this reason, it is speculated that there might be the presence of other pathways engaged by PrP^C to exert its protective activity against TNF- α -mediated cell death, which does not involve the participation of Bax.

4.4 Glycosylation Inhibition of PrP^C Promotes Endoplasmic Reticulum stress-induced Cell Death in Cells

In the fully matured protein, three forms of the PrP^C namely diglycosylated, monoglycosylated and unglycosylated co-exist. Thus, in this study, the glycosylation status of PrP^C and its relation to apoptosis induction was examined. The characterization of modified PrP^C glycosylation status in cells upon TUN treatment is described in Figure 4.11.

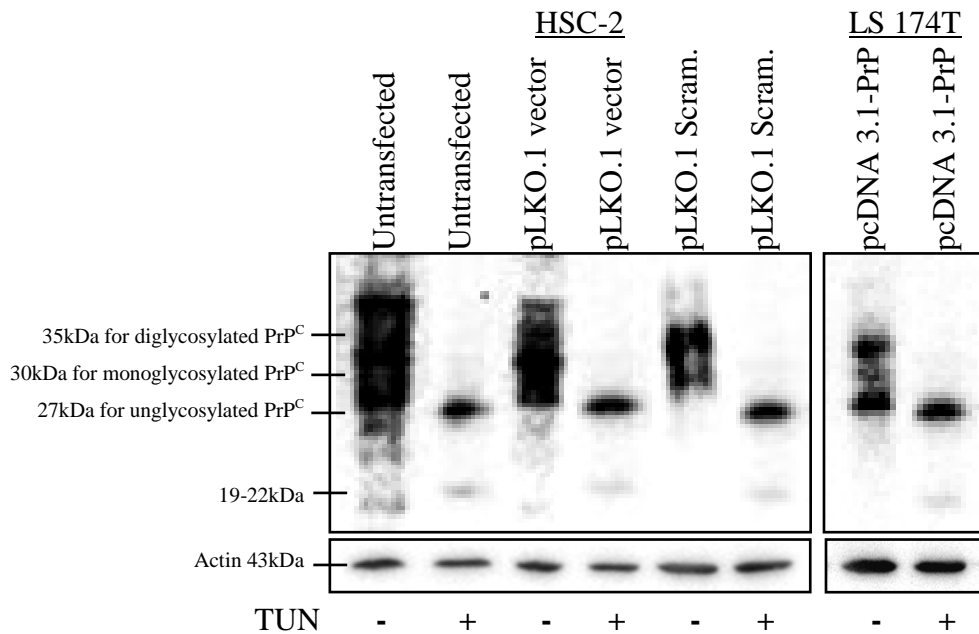


Figure 4.11: Effects of TUN on PrP^C expressing HSC-2 and LS 174T cells. PrP^C-expressing HSC-2 (Untransfected, pLKO.1 vector, pLKO.1 Scram.) and pcDNA 3.1-PrP-transfected LS 174T cell lines at lanes labelled with + represents TUN-treated cells at IC₅₀ for 24hr, whereas - were untreated group. Molecular weights are indicated on the left. Data correspond to a representative experiment out of 3 replicates with similar findings.

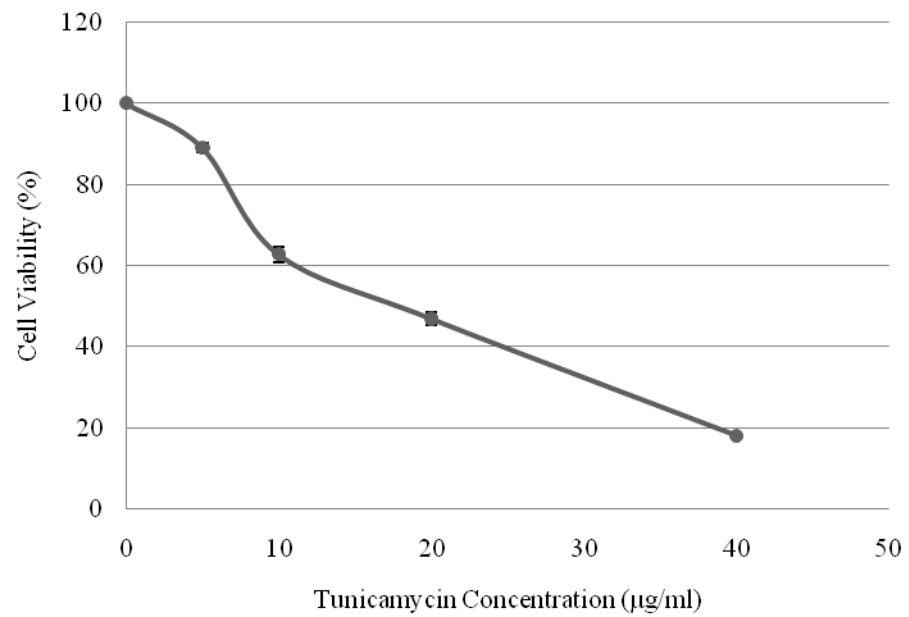
Following TUN treatment on the stably PrP^C expressing HSC-2 and LS 174T cells, the di- and monoglycosylated isoforms of PrP^C which reside at the 35-30kDa region were completely diminished and only the unglycosylated PrP

isoform at 27kDa was expressed. Besides, a dim yet notable band of approximately 19-22kDa was observed in the presence of the N-linked inhibitor, TUN. The appearance of this 19-22kDa species is consistent and no such singular species was detected in the untreated PrP^C expressing cells.

To determine the concentration of 50% cytotoxicity (IC₅₀) of TUN for each respective cancer cell lines, HSC-2 and LS 174T cells were initially treated with a serial dilution of TUN for 24hr and the measured cell viability was plotted against its corresponding concentration. IC₅₀ was then determined from the concentration–response curve as shown in Figure 4.12. TUN was able to provoke cell death in both HSC-2 and LS 174T in a dose-dependent manner. Increasing concentrations of TUN significantly diminished the cell viability of HSC-2 cells in 24hr. A similar course of cell death was observed in LS 174T cells.

IC₅₀ and IC₂₀ values of both HSC-2 and LS 174T cells were determined by identifying the concentration that has caused 50% and 20% inhibition on cell viability, respectively. From the concentration–response curve in Figure 4.12, IC₅₀ and IC₂₀ value of TUN on HSC-2 cells were 16µg/ml and 6µg/ml, respectively whereas for LS 174T, the IC₅₀ and IC₂₀ values were 24µg/ml and 2µg/ml, respectively. Alterations in cell viability towards glycosylation modification of PrP^C were measured and were represented in Figure 4.13.

A. Untransfected HSC-2



B. Untransfected LS 174T

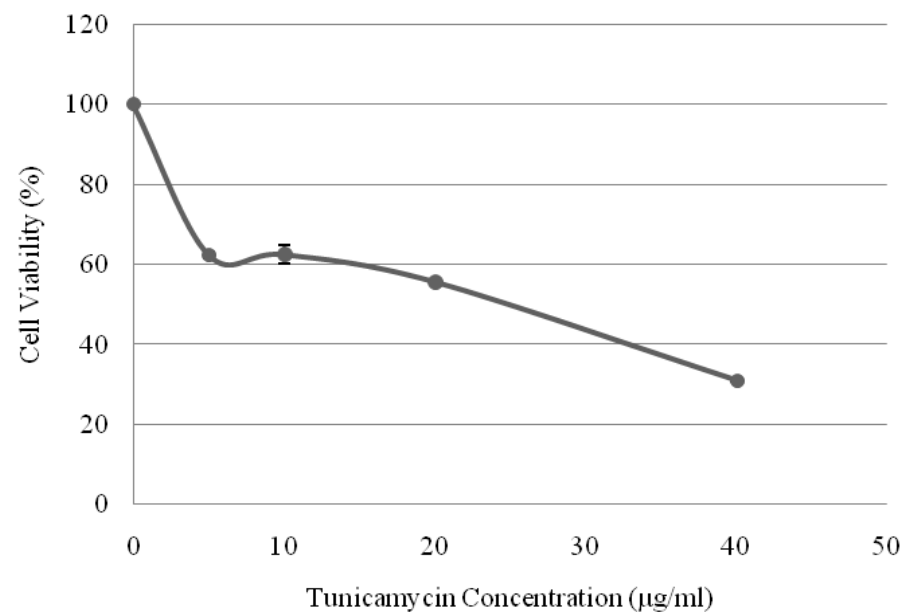
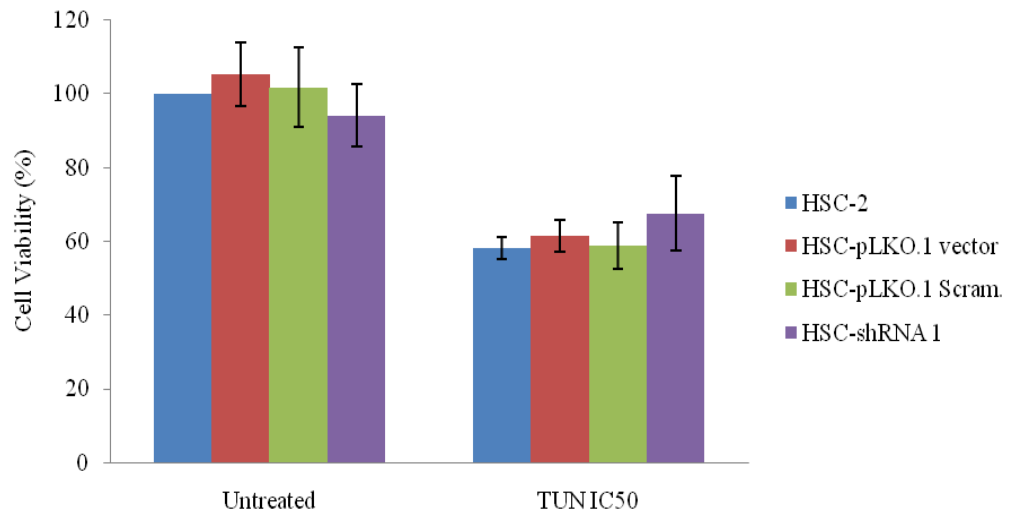


Figure 4.12: Induction of cell death following treatment with TUN. Effects of TUN on the viability of (A) untransfected HSC-2 and (B) untransfected LS 174T cells were determined. Cells were treated with various concentrations of TUN at 5, 10, 20 and 40µg/ml. Data of cell viability was expressed in % and representing the mean \pm SEM of 2 independent experiments as compared to the untreated and untransfected cells.

A. HSC-2



B. LS 174T

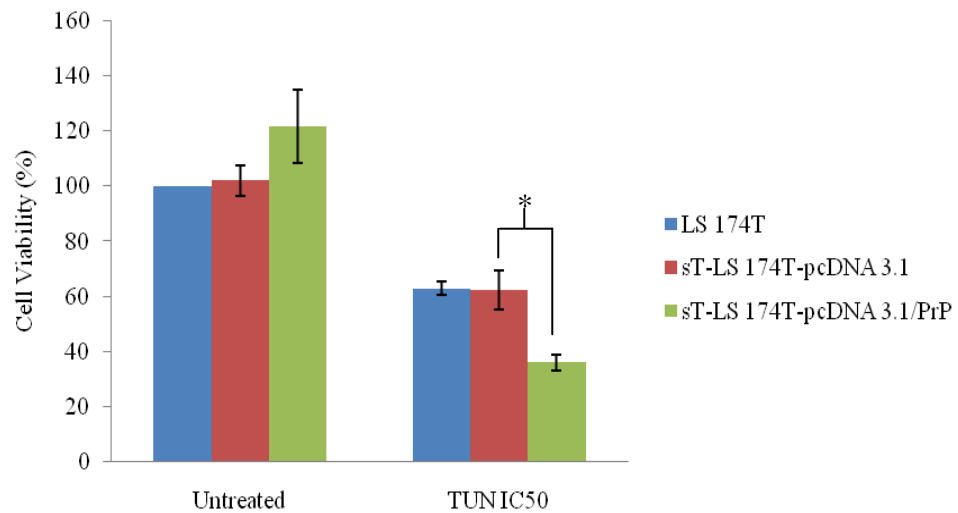


Figure 4.13: Blocking of PrP^C glycosylation by TUN promotes cell death. Cell viability was determined by MTT assay following treatment with TUN at IC₅₀ (TUN IC₅₀) in (A) HSC-2 and (B) LS 174T cells. Data of cell viability was expressed in % and representing the mean \pm SEM of 3 independent experiments as compared to the untreated and untransfected control cells. Mean values were compared using ANOVA followed by LSD's post hoc test for comparison of the means, via SPSS software. * $p < 0.05$ in treated sT-LS 174T-pcDNA 3.1/PrP vs. treated sT-LS 174T-pcDNA 3.1.

MTT data in Figure 4.13 indicate that the cell viability of sT-LS 174T-pcDNA 3.1/PrP was significantly reduced compared to those of pcDNA 3.1 group upon TUN treatment while a small, insignificant difference was observed in TUN-treated PrP^C expressing HSC-2, HSC-pLKO.1 vector and HSC-pLKO.1 Scram.

as compared to the TUN-treated HSC-shRNA 1 cells, which its PrP^C expression has been suppressed.

Interestingly, LS 174T cells which stably expressing wild type PrP^C showed significantly ($p < 0.05$) enhancement in cell proliferation on the growth after 24hr compared to the untreated, untransfected LS 174T which does not express PrP^C. Then again, a fairly increment on the growth of PrP^C expressing HSC-2 group; HSC-2, HSC-pLKO.1 vector and HSC-pLKO.1 Scram.; as compared to the HSC-shRNA 1 cells was observed. The cell viability differences between the untreated and TUN-treated group were compared. Cell viability differences of sT-LS 174T-pcDNA 3.1/PrP (85.6%) was significantly higher compared to sT-LS 174T pcDNA 3.1 group (39.6%), while PrP^C-deficient HSC-shRNA 1 had significantly lower cell viability differences or less cell death (26.6%) compared to the PrP^C-expressing HSC-2 cells with cell viability differences of 42.0-44.0%. Hence, the results indicated that the unglycosylated PrP^C in cells provoked cell death.

To further elucidate the effect of glycosylation inhibition in PrP^C towards cell viability, cells were subjected to flow cytometry analysis with FITC Annexin V-PI dual staining. The induction of apoptosis upon treatment with TUN in PrP^C expressing HSC-2 and LS 174T cells are displayed in Figure 4.14 and Figure 4.15, respectively.

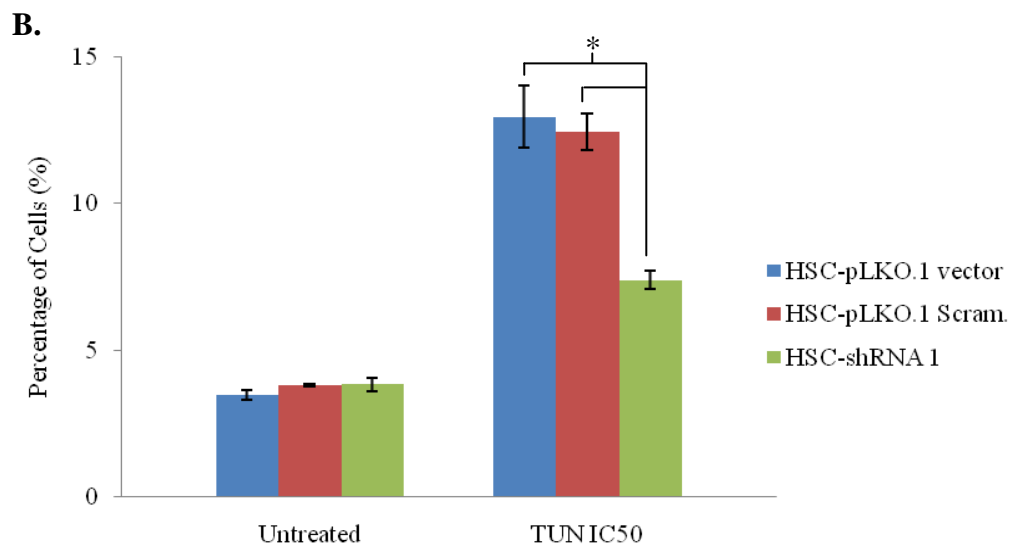
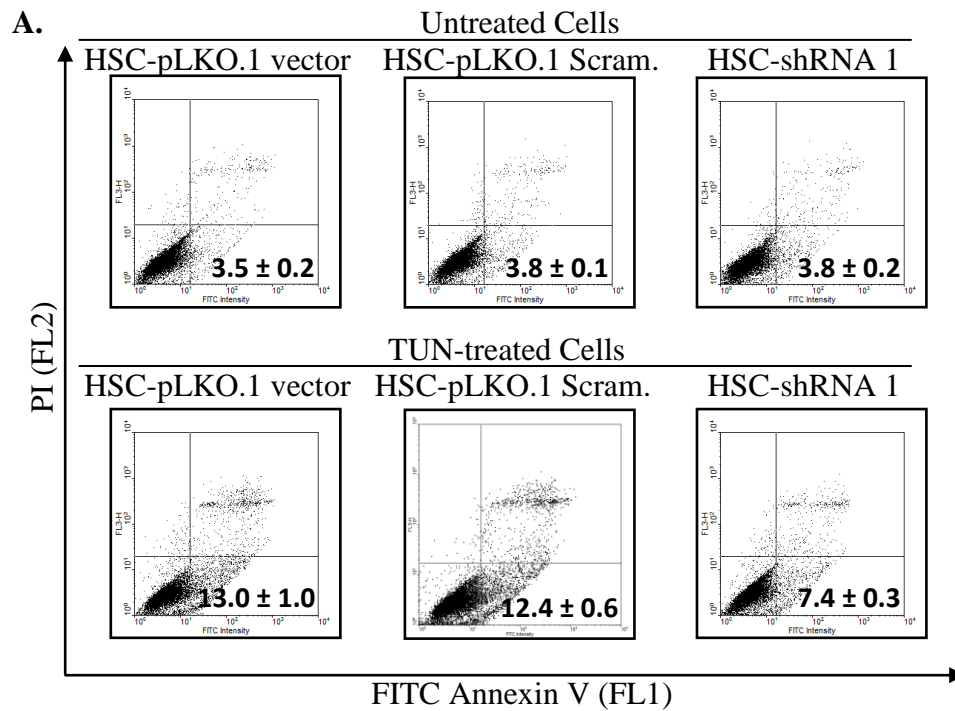


Figure 4.14: Apoptosis induction in PrP^C expressing HSC-2 cells treated with TUN. (A) Flow cytometry analysis of FITC Annexin V–PI dual staining. Cells were plated in 6-well plates, allowed to adhere overnight and treated with TUN at IC₅₀ (TUN IC₅₀) for 24hr prior to flow cytometry analysis FITC Annexin V–PI dual staining. X-axis indicates the number of FITC Annexin V-labelled cells. Y-axis indicates the number of PI-labelled cells. The % of cells in lower right quadrant is shown in each figure. (B) Statistical graph of FITC Annexin V–PI dual staining. Data is expressed in % of cells in the lower right quadrant and representing the mean ± SEM of 3 independent experiments. Mean values were compared using ANOVA followed by LSD's post hoc test for comparison of the means, via SPSS software. * *p* < 0.05 in treated HSC-shRNA 1 vs. treated PrP^C expressing HSC-2 group; HSC-pLKO.1 vector and HSC-pLKO.1 Scram..

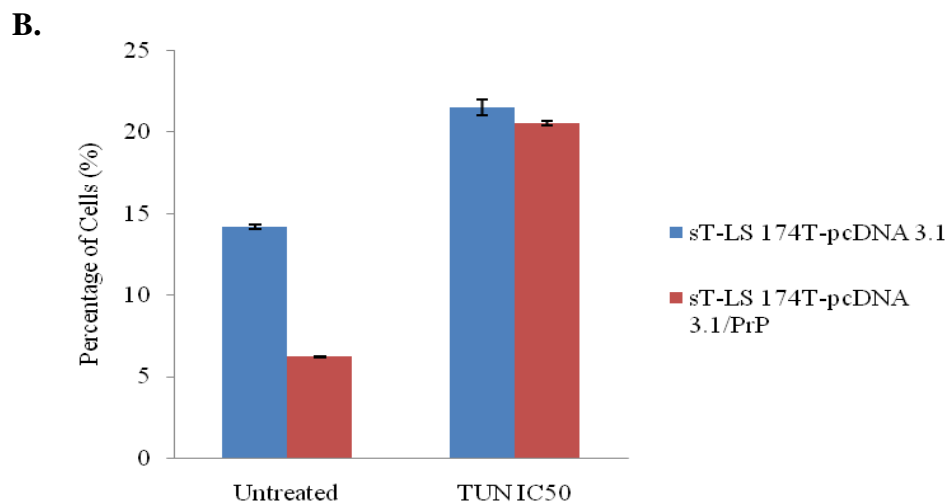
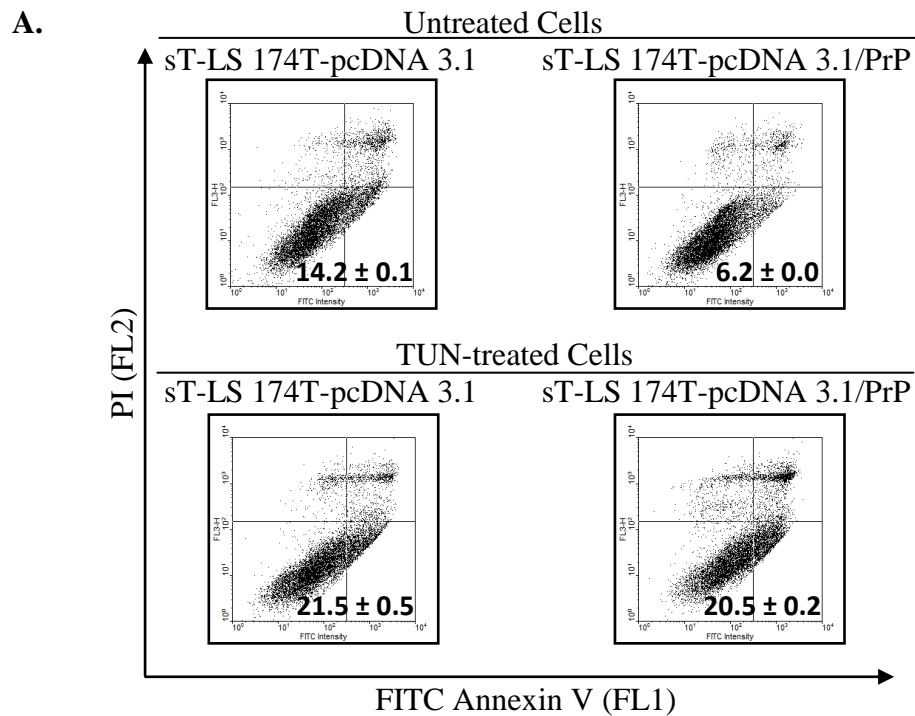


Figure 4.15: Apoptosis induction in PrP^C expressing LS 174T cells treated with TUN. (A) Flow cytometry analysis of FITC Annexin V–PI dual staining. Cells were plated in 6-well plates, allowed to adhere overnight and treated with TUN at IC₅₀ (TUN IC₅₀) for 24hr prior to flow cytometry analysis FITC Annexin V-PI dual staining. X-axis indicates the number of FITC Annexin V-labelled cells. Y-axis indicates the number of PI-labelled cells. The % of cells in lower right quadrant is shown in each figure. (B) Statistical graph of FITC Annexin V-PI dual staining. Data is expressed in % of cells in the lower right quadrant and representing the mean ± SEM of 3 independent experiments.

Binding of FITC Annexin V to the phosphatidylserine which normally resides within the plasma membrane in living cells was then used as a parameter to detect and measure apoptosis. Unlabelled cells in the lower left (LL) quadrant represent viable cells while FITC Annexin V-labelled cells in the lower right (LR) quadrant are the apoptotic population. Upper right (UR) quadrant represents FITC Annexin V/PI-dual labelled cells, indicative of membrane permeability and late apoptosis. Thus, in this assay, the apoptotic cell population in the LR quadrant, which is only labelled with FITC Annexin V, was accounted.

The single binding of FITC Annexin V to cells indicates an early phase of apoptosis. Hence, the mechanism of cell death induced by unglycosylated PrP using TUN is via apoptosis as shown by FITC Annexin V binding. As shown in Figure 4.14, there were significantly lower proportions of FITC Annexin V-labelled cells in TUN-treated HSC-shRNA 1 compared to the treated PrP^C expressing group; HSC-pLKO.1 vector and HSC-pLKO.1 Scram.. No significant difference was detected between the treated sT-LS 174T-pcDNA 3.1 and treated sT-LS 174T-pcDNA 3.1/PrP. However, in comparison to the untreated LS 174T cells transfected with pcDNA3.1-PrP, the treated sT-LS 174T-pcDNA 3.1/PrP showed a remarkable increment in the % of cells in early apoptosis. The % differences of the untreated sT-LS 174T-pcDNA 3.1 and untreated sT-LS 174T-pcDNA 3.1/PrP were significant. These data suggest that in the presence of wild type PrP^C, cells were more likely to endure stress which causes basal apoptosis. Due to this reason, differences in apoptotic fraction between the untreated and TUN-treated group were compared. The

TUN-treated LS 174T cells expressing PrP^C had almost 2-fold increment of apoptotic cell death compared to the mock transfected cells (14.3% vs. 7.3%). To get more evidences on the apoptosis phenomenon in the cells with unglycosylated PrP, cellular morphology was examined via inverted microscope (Figure 4.16).

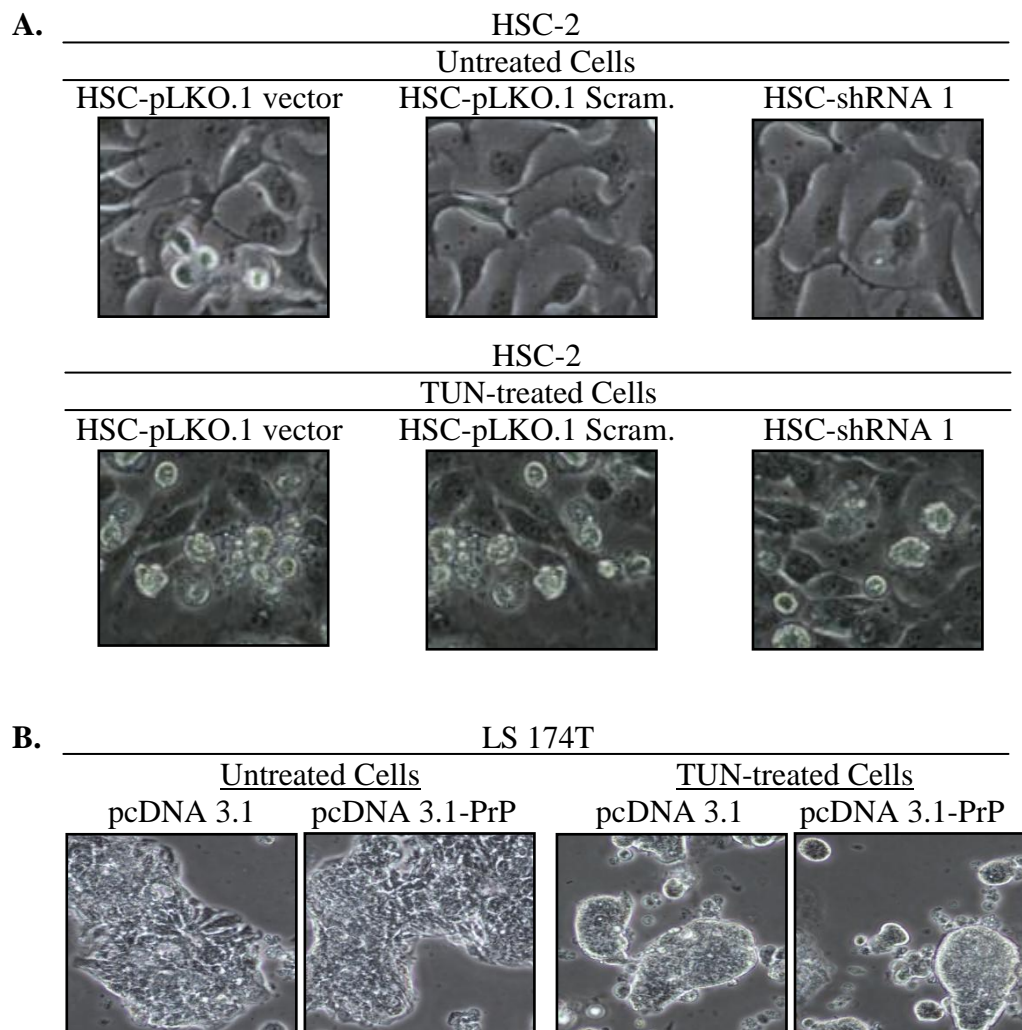


Figure 4.16: Inhibition of glycosylation of PrP^C induces apoptosis in cancer cells. Cell morphology alterations of (A) HSC-2 and (B) LS 174T with/without TUN treatment at IC₅₀ were shown. Apoptotic bodies were visibly distinguished in the TUN-treated PrP^C expressing cells. Photographs of cells were taken with NIS-Elements BR 3.0 software under Nikon Eclipse TS100 inverted microscope at 200× magnification in the same exposure.

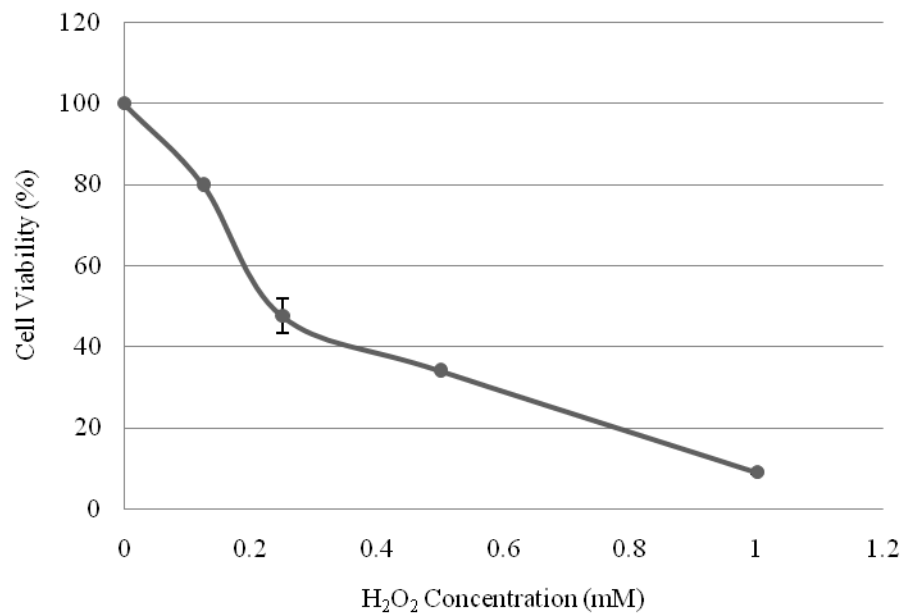
As shown in Figure 4.16, upon treatment with TUN, HSC-pLKO.1 vector and HSC-pLKO.1 Scram. possessed higher number of apoptotic bodies compared to HSC-shRNA 1 which has PrP^C expression knocked-down. Notable cell morphology alterations were also detected in treated sT-LS 174T-pcDNA 3.1/PrP compared to the treated vector-transfected LS 174T cells. Taken together, there were a lot more of shrunken and rounded cells were detected in PrP^C-expressing group. No significant changes on cell morphology were detected in cells without TUN treatment.

Results shown from each assessment were in accord to each other. Hence, as a whole, these findings suggest that induction of apoptosis in PrP^C expressing cells upon TUN treatment were due to the formation of unglycosylated PrP through inhibition of N-linked glycosylation.

4.5 PrP^C is Anti-apoptotic During Oxidative Stress-induced Cancer Cell Death

Previous findings have shown the protective effects of PrP^C towards TNF- α -mediated cell death (Section 4.3). Inquisitively, this study was also intended to ascertain the protective activity of PrP^C during oxidative stress-induced cell death as the role of PrP^C as an antioxidant has been well established in previous studies. The concentration of H₂O₂ required to kill 50% of the cells (IC₅₀) was determined from the concentration–response curve (Figure 4.17).

A. Untransfected HSC-2



B. Untransfected LS 174T

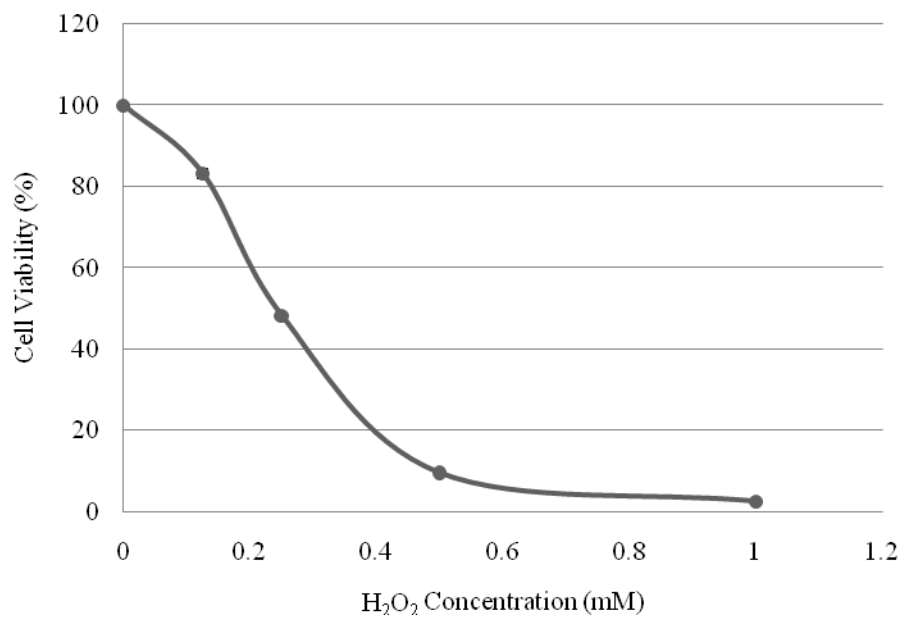


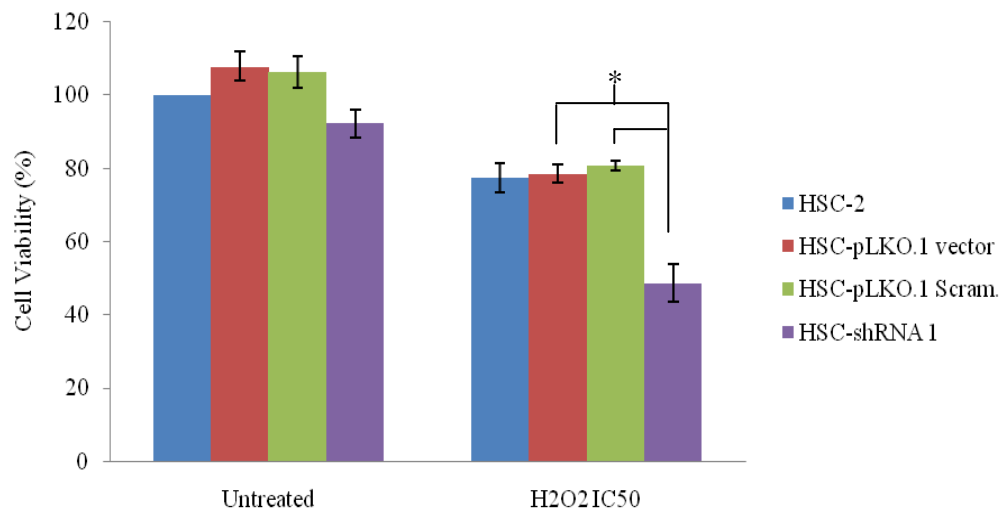
Figure 4.17: Induction of cell death following treatment with H₂O₂. Effects of H₂O₂ on the viability of (A) untransfected HSC-2 and (B) untransfected LS 174T cells were determined. Cells were treated with various concentrations of H₂O₂ at 0.125, 0.25, 0.5 and 1mM. Data of cell viability was expressed in % and representing the mean ± SEM of 2 independent experiments as compared to the untreated and untransfected cells.

Exposure of cells to increasing concentrations of H₂O₂ resulted in dose-dependent cell death, which was easily detectable 24hr after the insults. LS 174T were shown to be more susceptible to H₂O₂-induced cell death as the cells almost died off by 90% compared to HSC-2 cells which had higher cell viability at 0.5mM of H₂O₂. As shown in Figure 4.17, the effective concentration for 50% reduction of cells over 24hr for both HSC-2 and LS 174T was 0.2mM.

The involvement of PrP^C in exerting its protective effect towards oxidative stress-induced cell death was investigated by subjecting cells to H₂O₂ treatment at 0.2mM for 24hr. Cell viability (%) of each respective cell lines was enumerated in relative to the untreated control cells. Effects of H₂O₂ at 0.2mM on cell viability in the presence or absence of PrP^C or not are represented in Figure 4.18.

There was an overall significant increment on cell viability in the PrP^C expressing cells. PrP^C-depleted HSC-shRNA1 cells showed an estimated of 30% reduction in cell viability compared to the untransfected, HSC-pLKO.1 vector and HSC-pLKO.1 Scram. upon H₂O₂ treatment. In parallel, the % of cell death in treated LS 174T cells stably transfected with pcDNA 3.1-PrP was significantly lower than the treated vector-transfected cells as well as the untransfected cells as shown in Figure 4.18. Besides, in the absence of H₂O₂, the viabilities of cells, both PrP^C-expressing and non-PrP^C expressing, remained unchanged. These results implicate a profound role of PrP^C in attenuating H₂O₂-induced cell death in cultured cell.

A. HSC-2



B. LS 174T

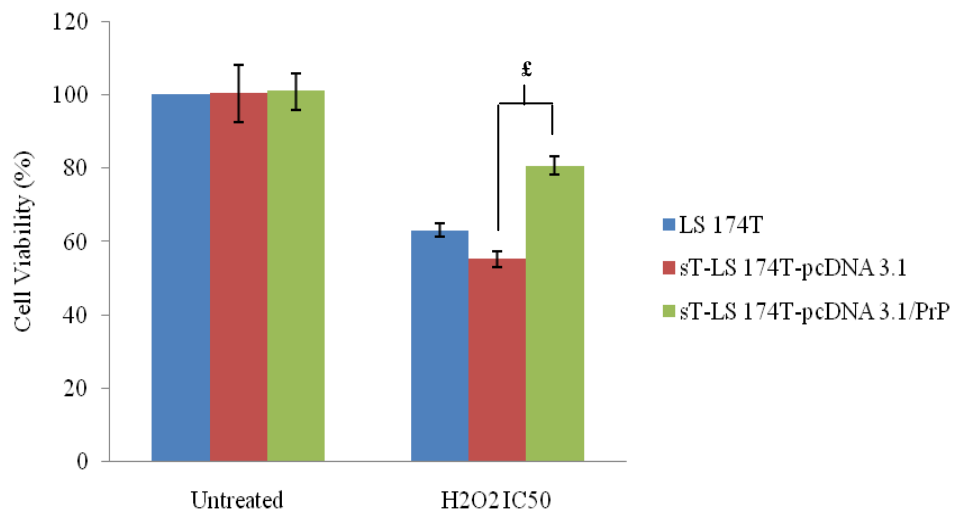


Figure 4.18: PrP^C exerts its protective effect towards oxidative stress-induced cell death in cultured cancer cells. Cell viability was determined by MTT assay following treatment with H₂O₂ at 0.2mM (H₂O₂ IC₅₀) in (A) HSC-2 and (B) LS 174T cells. Data of cell viability was expressed in % and representing the mean \pm SEM of 3 independent experiments as compared to the untreated and untransfected control cells. Mean values were compared using ANOVA followed by LSD's post hoc test for comparison of the means, via SPSS software. * $p < 0.05$ in treated HSC-shRNA 1 vs. treated PrP^C expressing HSC-2 group; HSC-pLKO.1 vector and HSC-pLKO.1 Scram.. £ $p < 0.05$ in treated sT-LS 174T-pcDNA 3.1/PrP vs. treated sT-LS 174T-pcDNA 3.1.

Further extension of study using FITC Annexin V-PI dual staining via flow cytometry was performed to confirm the protective effect of PrP^C towards oxidative stress-induced cell death in cancer cells. Data from the flow cytometry analysis of FITC Annexin V-PI dual staining is presented Figure 4.19 and Figure 4.20.

As shown in Figure 4.20A, existence of notable cells population in the UR quadrant of the treated LS 174T cells was observed. An explanation to this might be due to the prolonged incubation of H₂O₂ which further promotes late apoptosis in the cells as this study has previously demonstrated that the LS 174T cells were shown to be more vulnerable to H₂O₂ (Figure 4.17B) compared to HSC-2 cells. The shift in FL2 up to the UR quadrant represents FITC Annexin V/PI-labelled cells, indicative of membrane permeability and late apoptosis. Nevertheless, the dual stained cells might also correspond to necrosis since H₂O₂ is capable to induce both necrosis and apoptosis in a dose- and time-dependent manner (Saito et al., 2006; Takeda, Shirato, Kobayashi, & Endou, 1999; Watson, Askew, & Benson, 1995). Hence, owing to the almost comparable % of cells in the LR quadrant of LS 174T in both treated and untreated group, the % of cells in the UR quadrant were compared as well.

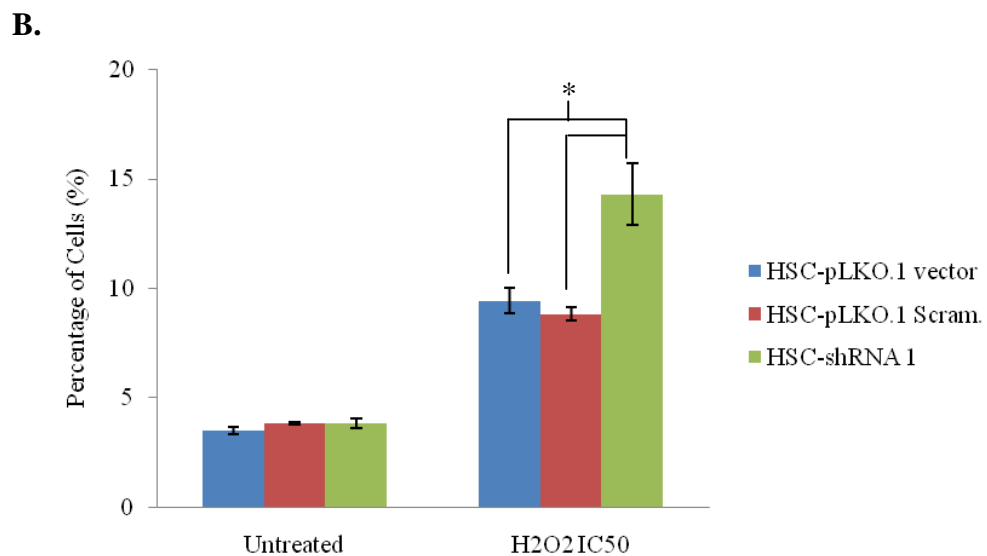
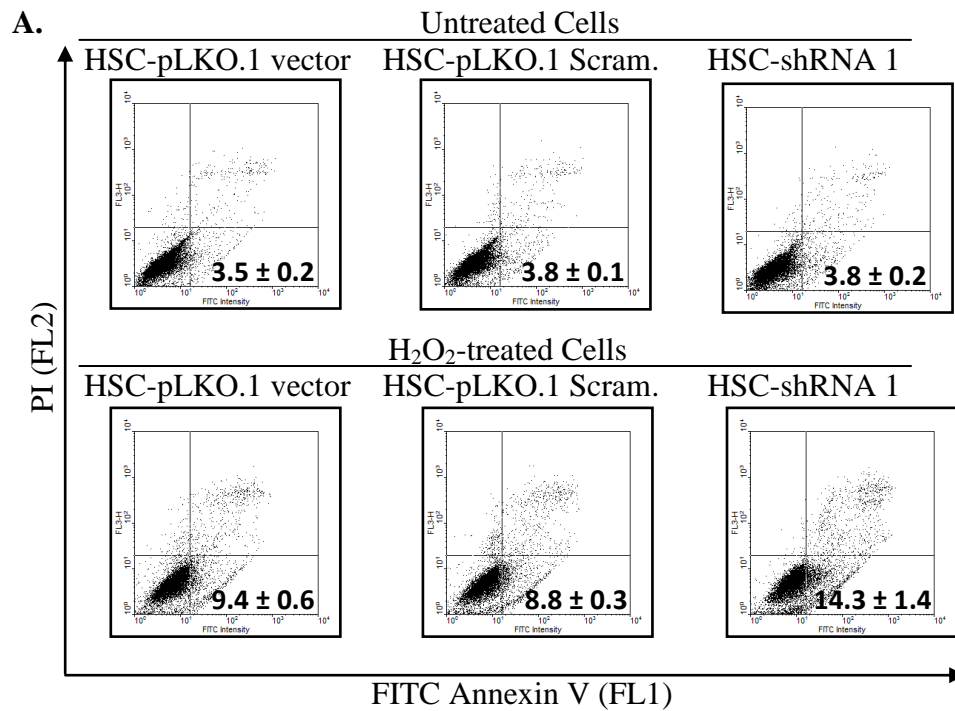


Figure 4.19: Protective effects of PrP^C in HSC-2 cells treated with H₂O₂. (A) Flow cytometry analysis of FITC Annexin V–PI dual staining. Cells were plated in 6-well plates, allowed to adhere overnight and treated with H₂O₂ at IC₅₀ (H2O2 IC50) for 24hr prior to flow cytometry analysis FITC Annexin V-PI dual staining. X-axis indicates the number of FITC Annexin V-labelled cells. Y-axis indicates the number of PI-labelled cells. The % of cells in LR quadrant is shown in each figure. (B) Statistical graph of FITC Annexin V-PI dual staining. Data is expressed in % of cells in the LR quadrant and representing the mean \pm SEM of 3 independent experiments. Mean values were compared using ANOVA followed by LSD's post hoc test for comparison of the means, via SPSS software. * $p < 0.05$ in treated HSC-shRNA 1 vs. treated PrP^C expressing HSC-2 group; HSC-pLKO.1 vector and HSC-pLKO.1 Scram..

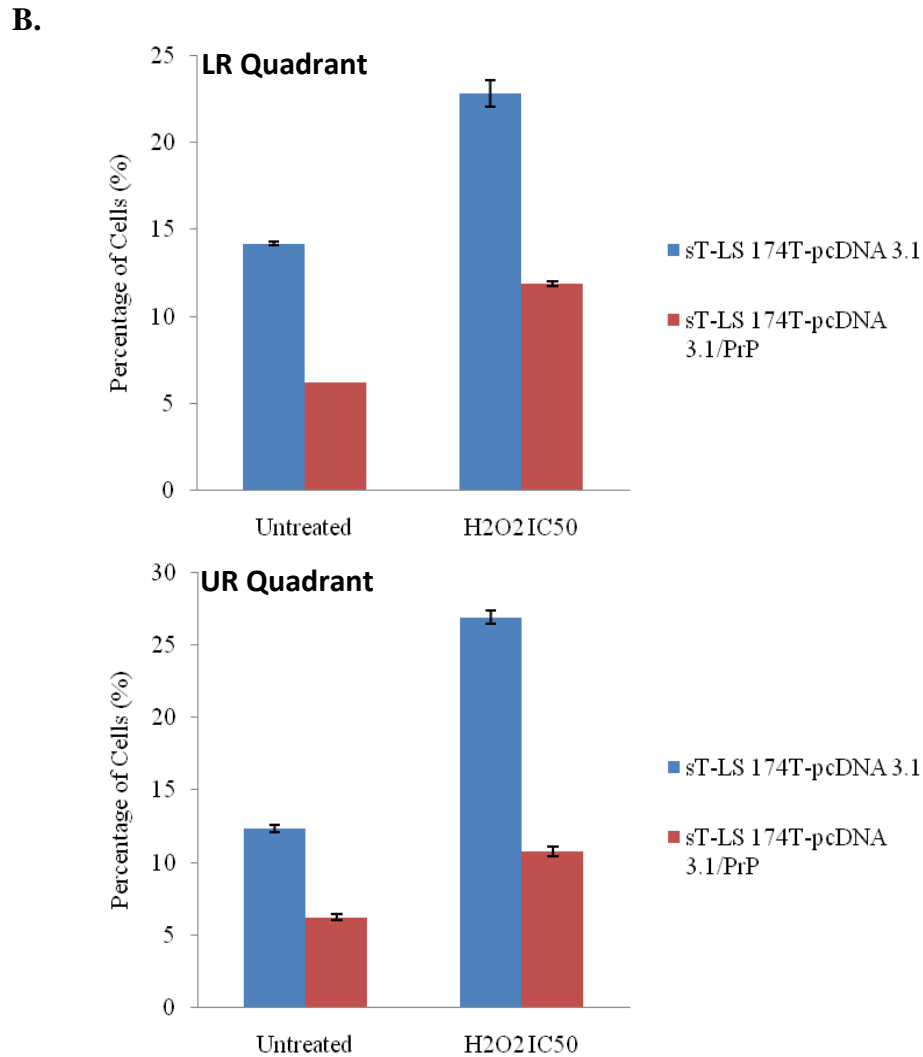
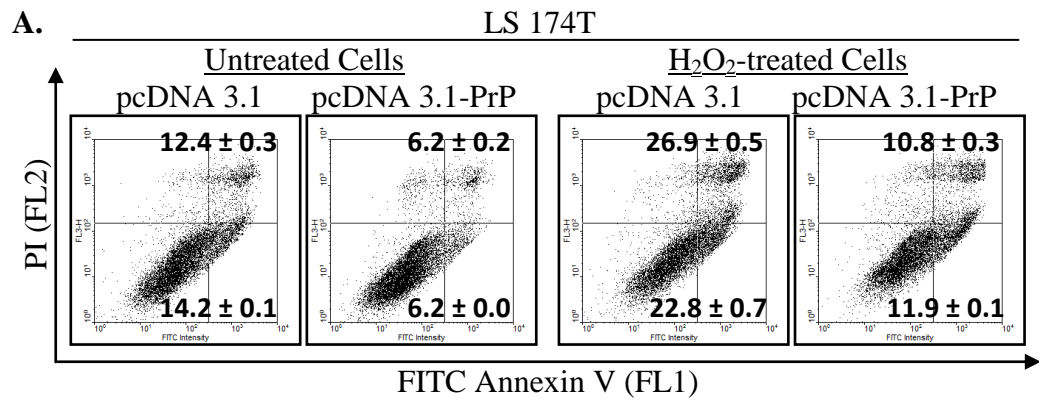


Figure 4.20: Protective effects of PrP^C in LS 174T cells treated with H₂O₂. (A) Flow cytometry analysis of FITC Annexin V–PI dual staining. Cells were plated in 6-well plates, allowed to adhere overnight and treated with H₂O₂ at IC₅₀ (H2O2 IC50) for 24hr prior to flow cytometry analysis FITC Annexin V-PI dual staining. X-axis indicates the number of FITC Annexin V-labelled cells. Y-axis indicates the number of PI-labelled cells. The % of cells in LR and UR quadrants are shown in each figure. (B) Statistical graph of FITC Annexin V-PI dual staining. Data in the LR and UR quadrants which were expressed in % of cells represents the mean ± SEM of 3 independent experiments.

From Figure 4.19, depletion of PrP^C in H₂O₂-treated HSC-shRNA 1 resulted in a significantly higher % of cells in LR quadrant compared to the PrP^C expressing HSC-2 cells. On the other hand, greater differences in the number of apoptotic cells were also observed between the sT-LS 174T-pcDNA 3.1 (8.6%, 14.5%) and sT-LS 174T-pcDNA 3.1/PrP (5.7%, 4.5%) in both LR and UR quadrants, respectively. Of note, the comparison were made between the treated and untreated group of each respective cell lines, either vector-transfected or pcDNA 3.1-PrP-transfected. Hence, these data suggested that PrP^C possessed an anti-apoptotic effect towards H₂O₂-induced cell death with its ability to lessen the susceptibility of cells to oxidative insults, probably acting as an antioxidant agent.

Eventually, the mechanism of cell death induced by H₂O₂ was proposed to be apoptosis instead of necrosis. The population of cells in the UR quadrant might apparently undergo a transition from apoptosis to the necrotic state (Saito et al., 2006; Takeda, Shirato, Kobayashi, & Endou, 1999; Watson, Askew, & Benson, 1995), since there were no significant PI-labelled cells observed in the UL quadrant, which is known to be necrotic.

The mechanism of cell death mediated by H₂O₂ was further confirmed to be apoptotic via inverted microscope to detect morphology alterations as revealed in Figure 4.21. As expected, shrinkage of cell, membrane blebbing, cell rounding and loss of cell membrane asymmetry were observed in group of cells treated with H₂O₂.

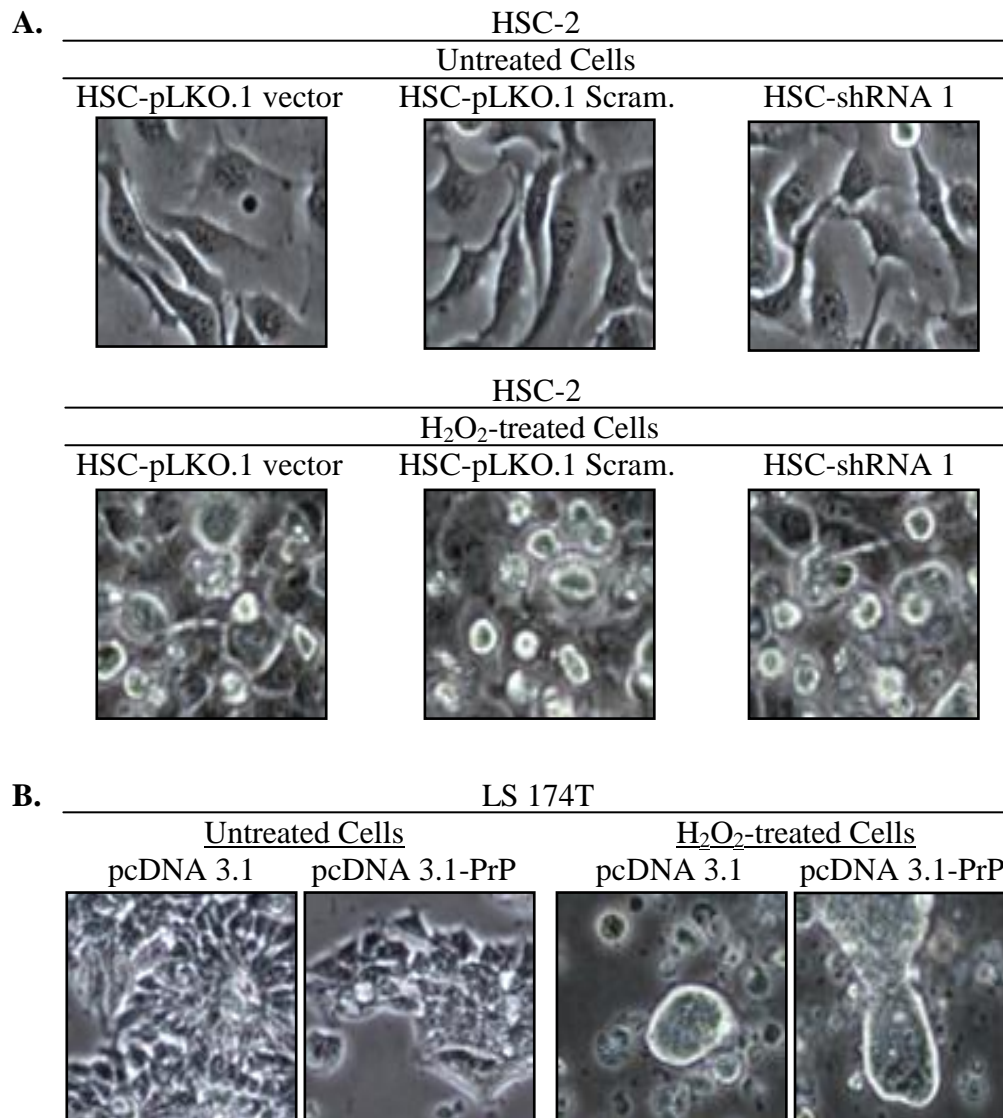


Figure 4.21: PrP^C exerts its anti-apoptotic effects in H₂O₂-induced cell death. Cell morphology alterations of (A) HSC-2 and (B) LS 174T with/without H₂O₂ treatment at IC₅₀ were shown. Apoptotic bodies were visibly distinguished in the H₂O₂-treated non-PrP^C expressing cells. Photographs of cells were taken with NIS-Elements BR 3.0 software under Nikon Eclipse TS100 inverted microscope at 200× magnification in the same exposure.

Both HSC-pLKO.1 vector and HSC-pLKO.1 Scram. exhibited higher number of apoptotic cells compared to HSC-shRNA 1 upon treatment with H₂O₂. The typical morphological alterations were more prominent in the treated vector-transfected LS 174T cells as compared to the H₂O₂-treated sT-LS 174T-

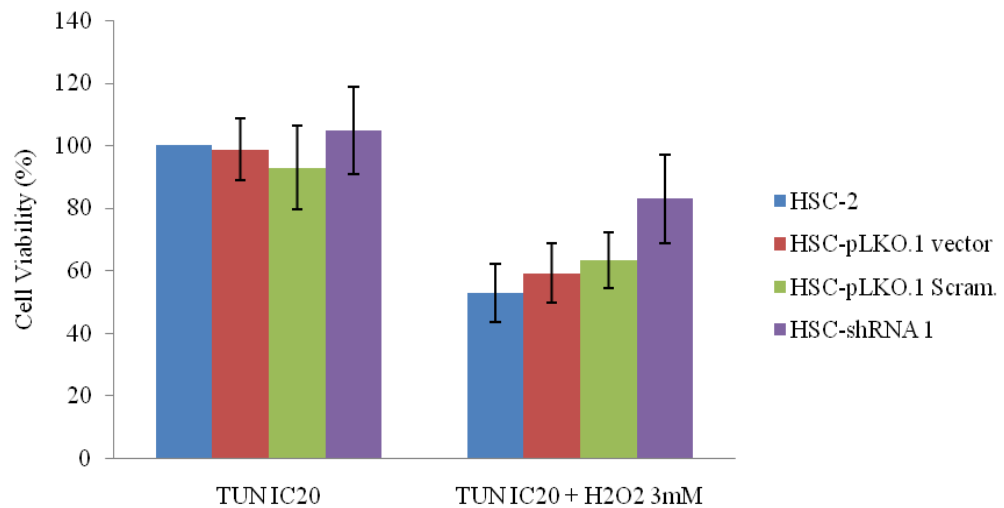
pcDNA 3.1/PrP. Sensibly, no cell morphological changes were shown in untreated cells.

4.6 Blocking of PrP^C Glycosylation Impedes its ROS Scavenging Activity

On account of the previously shown opposing roles of PrP^C during ER stress and oxidative stress-mediated apoptosis via TUN and H₂O₂, respectively, this study has also intended to further examine the effect of glycosylation inhibition of PrP^C towards H₂O₂-induced ROS generation. Both PrP^C-expressing and PrP^C-negative HSC-2 and LS 174T cells were also subjected to TUN treatment for 24hr at IC₂₀ (6µg/ml and 2µg/ml, respectively), as it has the ability to inhibit N-linked glycosylation as efficient as IC₅₀, while minimizing cell death. It was then followed by H₂O₂ treatment at 3mM for 30min to generate exogenous ROS which triggered oxidative stress within a short period of time.

The effect of glycosylation modification of PrP^C towards H₂O₂-induced oxidative stress is shown in Figure 4.22. Upon glycosylation suppression of PrP^C followed by induction of oxidative stress, the cell viability in both HSC-2 and LS 174T PrP^C expressing group dropped remarkably compared to the non-PrP^C expressing group. There was at least a 20% of reduction in cell viability detected. No significant difference was observed between the groups of cells after treatment with TUN at IC₂₀ alone.

A. HSC-2



B. LS 174T

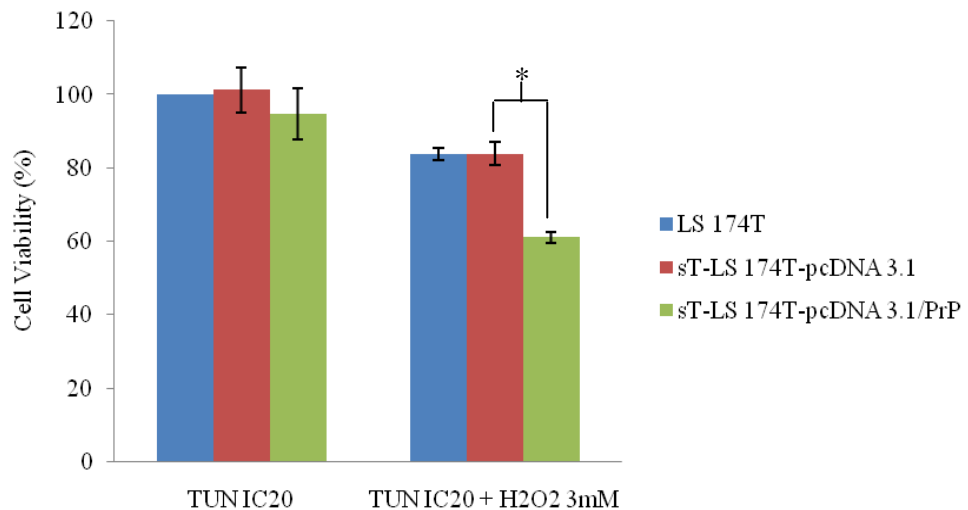


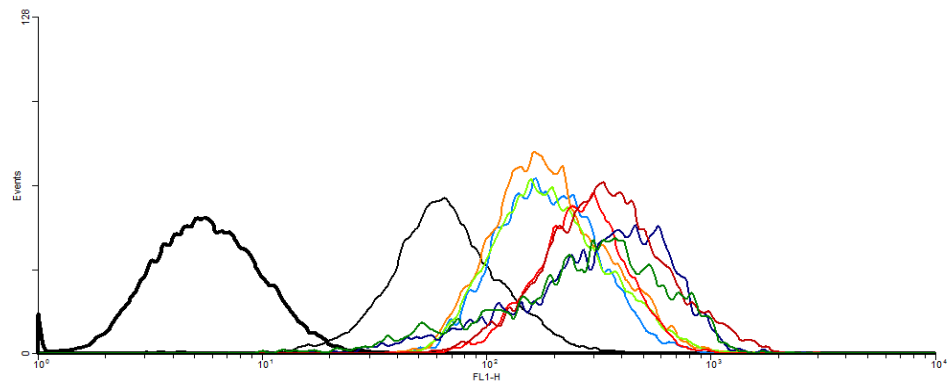
Figure 4.22: Inhibition of glycosylation in PrP^C provokes cell death in H₂O₂-induced oxidative stress in cultured cells. Cell viability was determined by MTT assay following treatment with TUN at IC₂₀ and H₂O₂ at 3mM for 30min (TUN IC₂₀ + H₂O₂ 3mM) in (A) HSC-2 and (B) LS 174T cells. Data of cell viability was expressed in % and representing the mean \pm SEM of 3 independent experiments as compared to the untreated control cells. Mean values were compared using ANOVA followed by LSD's post hoc test for comparison of the means, via SPSS software. * $p < 0.05$ in treated sT-LS 174T-pcDNA 3.1/PrP vs. treated sT-LS 174T-pcDNA 3.1.

The unglycosylated sT-LS 174T-pcDNA 3.1/PrP^C cells showed a lower % of cell viability compared to both untransfected and sT-LS 174T-pcDNA 3.1 cells upon treatment with H₂O₂. As well as for HCS-2 cells, although was not statistically significant, exposure of the unglycosylated PrP^C expressing group of cells which consists of the untransfected, HSC-pLKO.1 vector and HSC-pLKO.1 Scram. to 3mM H₂O₂ resulted in a decrease in cell viability compared to TUN IC₂₀-treated PrP^C depleted HSC-shRNA 1 cells. These MTT results imply that unglycosylated PrP induced a rapid loss of metabolic activity of cells during H₂O₂-induced oxidative stress. This is opposed to the protective role of fully glycosylated PrP^C during oxidative stress-induced cell death as shown in Section 4.5.

Subsequently, the ability of both wild type PrP^C and the unglycosylated PrP to scavenge ROS production was investigated. Assessment was performed using 2',7'-dichlorofluorescein diacetate (DCFH-DA) as an intracellular probe. Cells were seeded in 12-well plate and the selected PrP^C expressing cells were treated with TUN at IC₂₀ for 24hr to block glycosylation prior to flow cytometric analysis. Results were expressed in fluorescence intensity (FI) unit which is proportional to the amount of ROS generated, particularly H₂O₂. Figure 4.23 and Figure 4.24 show the flow cytometric fluorescence distribution of HSC-2 and LS 174T cells, respectively.

HSC-2

A.



B.

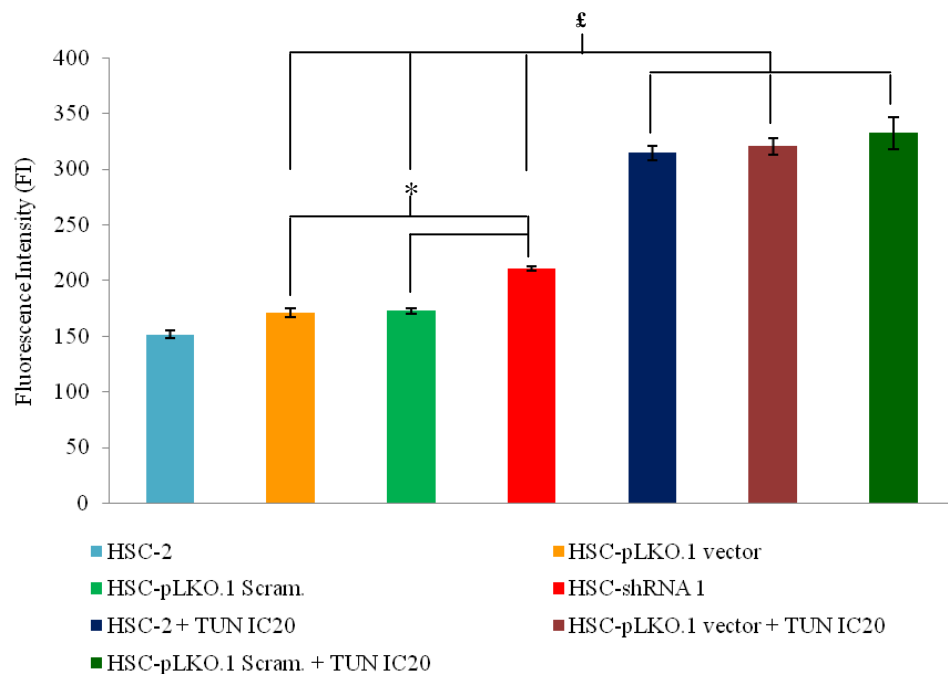
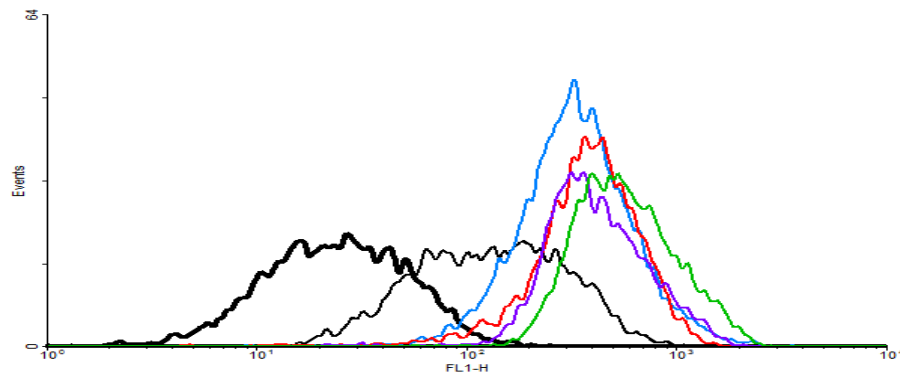


Figure 4.23: PrP^C modulates H₂O₂-induced burst of ROS in HSC-2 cells. ROS generated within cells was detected using fluorescent probe DCFH-DA upon treatment with 3mM of H₂O₂ for 30min. (A) Flow cytometric fluorescence distributions of HSC-2 cells with/without DCFH-DA. Fluorescence baseline and negative control were represented with broad and fine black line, respectively. Each sample was depicted according to the colour legend shown in B. (B) Graphical representation of flow cytometric analysis shown in A. Data are represented as mean fluorescence intensity (FI) ± SEM of triplicate from 3 independent experiments. Mean values were compared by ANOVA followed by LSD's post hoc test for comparison of the means, via SPSS software. * $p < 0.05$ in HSC-shRNA 1 vs. HSC-pLKO.1 vector & HSC-pLKO.1 Scram.. ‡ $p < 0.05$ in unglycosylated PrP expressing group of cells vs. glycosylated PrP expressing group of cells and HSC-shRNA 1.

LS 174T

A.



B.

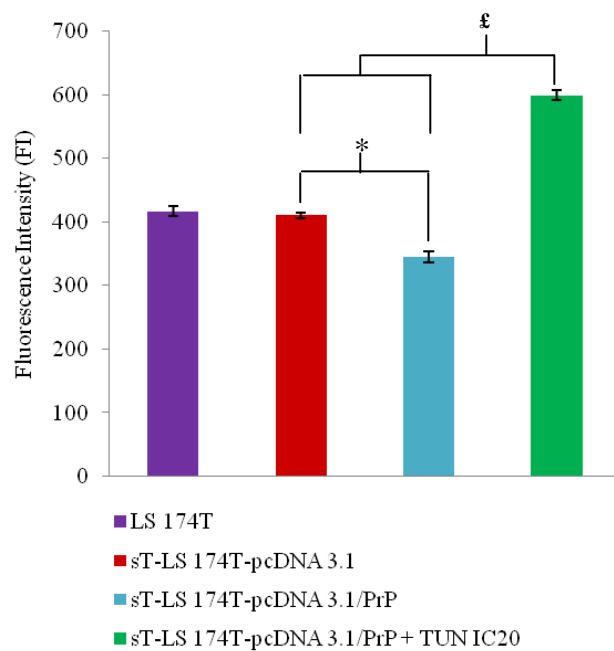


Figure 4.24: PrP^C modulates H₂O₂-induced burst of ROS in LS 174T cells. ROS generated within cells was detected using fluorescent probe DCFH-DA upon treatment with 3mM of H₂O₂ for 30min. (A) Flow cytometric fluorescence distributions of LS 174T cells with/without DCFH-DA. Fluorescence baseline and negative control were represented with broad and fine black line, respectively. Each sample were depicted according to the colour legend shown in B. (B) Graphical representation of flow cytometric analysis shown in A. Data are represented as mean fluorescence intensity (FI) \pm SEM of triplicate from 3 independent experiments. Mean values were compared by using ANOVA followed by LSD's post hoc test for comparison of the means, using the SPSS software. * $p < 0.05$ in sT-LS 174T-pcDNA 3.1/PrP vs. sT-LS 174T-pcDNA 3.1. £ $p < 0.05$ unglycosylated sT-LS 174T-pcDNA 3.1/PrP vs. sT-LS 174T-pcDNA 3.1/PrP and sT-LS 174T-pcDNA 3.1.

The fluorescence baseline and negative control were used for flow cytometer setting as described under Materials and Methods. The generation of ROS were monitored using the DCFH-DA, a well-established compound to detect and quantify intracellular produced H_2O_2 . The non-fluorescent DCFH-DA probe is lipophilic and cell-permeable. It is deacetylated intracellularly by cytosolic enzymes e.g. esterases to form polar, non-fluorescent 2',7'-dichlorofluorescein (DCFH) which, due to its polarity, will be trapped either within the cytoplasm or in myeloperoxidase (MPO)-positive intracellular granules. Upon oxidation by ROS such as H_2O_2 , it will turn to the highly fluorescent 2',7'-dichlorofluorescein (DCF) (Robinson, Carter, & Narayanan, 1997).

The amount of DCF formed is proportional to the cellular oxidant production, particularly H_2O_2 . As shown in Figure 4.23, the unglycosylated PrP expressing group of cells (TUN IC₂₀-treated HSC-2, -treated HSC-pLKO.1 vector and –treated HSC-pLKO.1 Scram.) had significantly elevated ROS levels upon H_2O_2 treatment compared to HSC-shRNA 1 which have knocked-down PrP^C. On the other hand, the wild type PrP^C expressing group: HSC-2, HSC-pLKO.1 vector and HSC-pLKO.1 Scram. showed a remarkable decrement of ROS level compared to the PrP^C depleted cells (HSC-shRNA 1) upon exposure to 3mM of H_2O_2 for 30min. A similar trend was also observed in the LS 174T cells where the stable expression of wild type PrP^C, sT-LS 174T-pcDNA 3.1/PrP, significantly decreased ROS production from 410.56 ± 4.04 in sT-LS 174T-pcDNA 3.1 to 345.72 ± 8.85 . Then again, once sT-LS 174T-pcDNA 3.1/PrP was treated with TUN in order to block glycosylation PrP^C, ROS generation

was apparently observed. ROS levels were significantly increased from 410.56 ± 4.04 to 598.84 ± 8.03 .

Thus, these results demonstrate that wild type PrP^C has the ability to effectively scavenge ROS production by acting as an antioxidant, either directly or indirectly during H₂O₂ treatment. Conversely, upon glycosylation inhibition with TUN, the unglycosylated PrP isoform increases ROS production to a great extent. The ability of PrP^C in modulating ROS generation might be an explanation for its protective effects during oxidative stress-induced apoptosis.

4.7 PrP^C Regulates Cell Cycle Progression and Cell Proliferation in Cultured Cancer Cells

It has been previously demonstrated in MTT assay (Figure 4.13) that the PrP^C expressing sT-LS 174T-pcDNA 3.1/PrP cells showed significantly augmentation on cell proliferation compared to the non-PrP^C expressing group; untransfected LS 174T and vector-transfected sT-LS 174T-pcDNA 3.1. Besides, akin but not as significant phenomenon was too observed in the HSC-2 cell line where the PrP^C depleted cells, HSC-shRNA 1 showed trivial reduction on cell growth compared to the PrP^C expressing group: Untransfected HSC-2, HSC-pLKO.1 vector and HSC-pLKO.1 Scram.. This observation is almost consistent throughout the study which thus indicates that PrP^C might promote cell proliferation in cultured cancer cells.

To determine whether PrP^C promotes growth by modulating cell cycle progression, its effects on cell cycle distribution in asynchronous transiently transfected-HSC-2, -ACHN and -LS 174T cells with pcDNA 3.1-PrP was examined using flow cytometric analysis. Distribution of cellular DNA contents throughout the cell was measured using Propidium iodide (PI), a fluorescent stain for nucleic acids. The flow cytometry profiles are shown in Figure 4.25 whilst Table 4.2 gives an account of the overall data shown in Figure 4.25.

Table 4.2: Effects of PrP^C on cell proliferation in cancer cell lines

	% of Cells		
	G ₁ -phase	S-phase	G ₂ /M-phase
Tr-HSC-2-pcDNA 3.1	55.2 ± 0.0	22.3 ± 0.1	22.7 ± 0.2
Tr-HSC-2-pcDNA 3.1/PrP	54.9 ± 0.1	22.5 ± 0.0	22.7 ± 0.2
Tr-ACHN-pcDNA 3.1	60.6 ± 0.1	25.6 ± 0.8	14.0 ± 0.9
Tr-ACHN-pcDNA 3.1/PrP	53.9 ± 0.4	30.6 ± 0.2*	15.6 ± 0.2
Tr-LS 174T-pcDNA 3.1	56.2 ± 0.1	28.1 ± 0.2	15.8 ± 0.1
Tr-LS 174T-pcDNA 3.1/PrP	52.8 ± 0.2	30.2 ± 0.4*	16.7 ± 0.9

Data presented in % of cells in G₁-phase, S-phase, G₂/M-phase are mean ± SEM of triplicates from 2 independent experiments. An unpaired two-tailed Student's t-Test using Microsoft Excel[®] 2007 was used for statistical analysis. * $p < 0.05$ in pcDNA 3.1-PrP-transfected cells vs. vector-transfected cells.

As shown in Table 4.2, there was a minor but statistically significant increment on the population of both PrP^C expressing ACHN and LS 174T cells in the S-phase, indicating a G₁ to S-phase transition. PrP^C prompted cells (Tr-ACHN-pcDNA 3.1/PrP and Tr-LS 174T-pcDNA 3.1/PrP) in G₁-phase while increasing the accumulation of cells in the S-phase. No effect was observed on the fraction of cells occupying the G₂/M-phase. As expected, there were no changes observed in the cell cycle distribution of HSC-2 cells since the cells overexpress PrP^C endogenously.

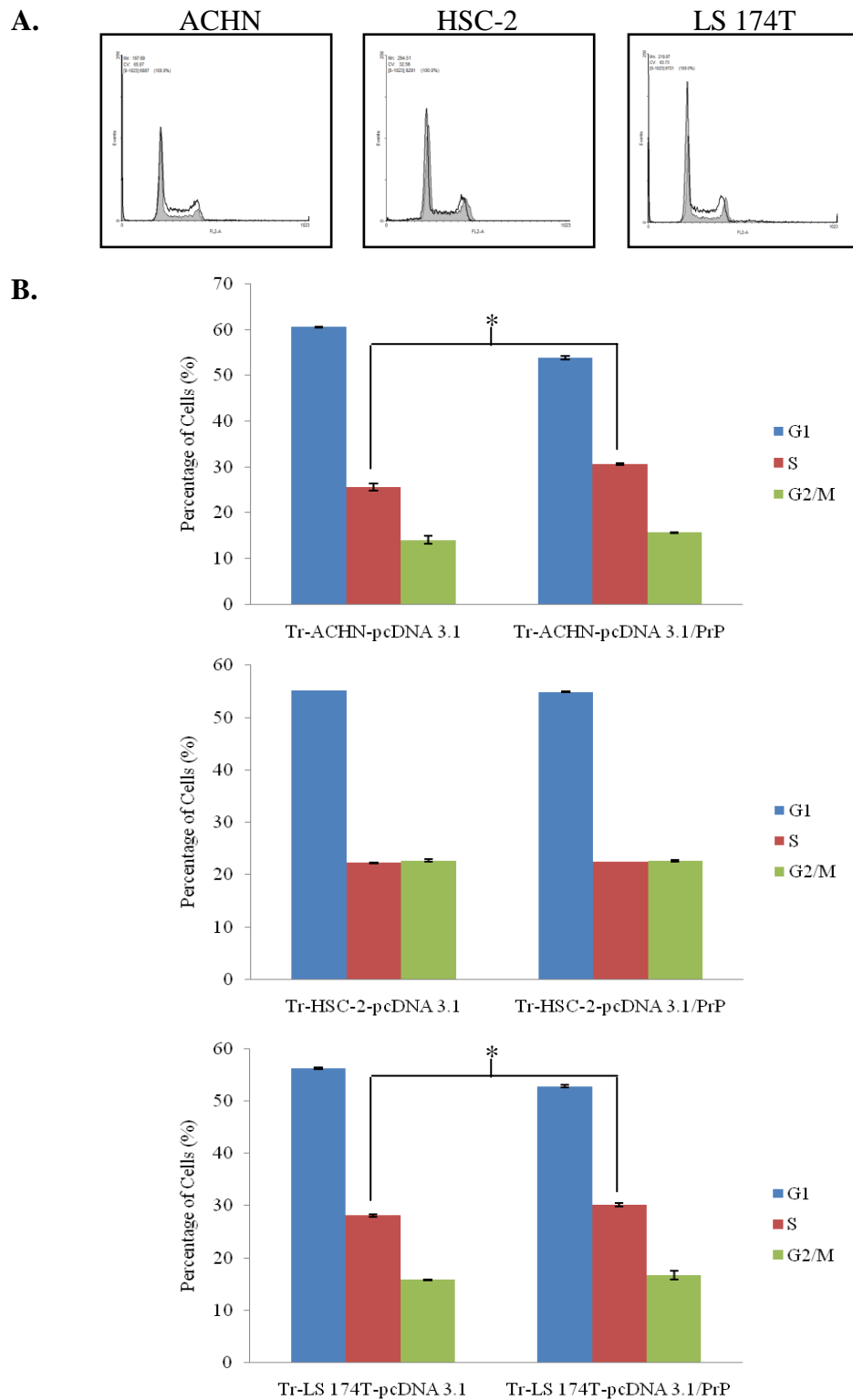


Figure 4.25: PrP^C expression increases the growth rate of cancer cells. (A) Cell cycle distribution of PrP^C expressing cells (Black line) overlay to vector-transfected cells (Grey region). (B) Graphical representation of A for each respective cell lines. Fractions (%) of cells in G₁-phase, S-phase, G₂/M-phase are mean ± SEM of triplicates from 2 independent experiments. An unpaired two-tailed Student's t-Test using Microsoft Excel[®] 2007 was used for statistical analysis. * $p < 0.05$ in pcDNA 3.1-PrP-transfected cells vs. vector-transfected cells.

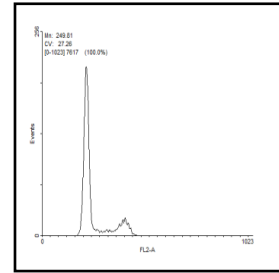
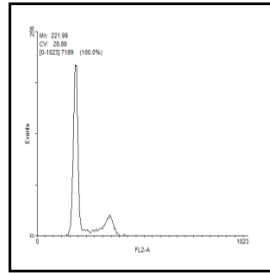
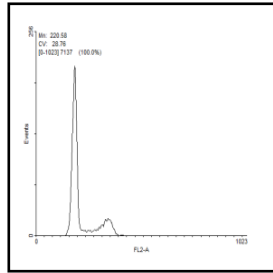
Proliferative indexes (PrIn) for each respective cell lines were calculated using the formula $\text{PrIn} = (\text{S} + \text{G}_2) / (\text{S} + \text{G}_2 + \text{G}_1)$. PrIn, in account of the fractions of cells in S-phase, was used as a tool to measure the number of cancer cells that are actively dividing as it provides a more comprehensive understanding of the proliferation rate (National Cancer Institute [NCI], 2010). The computed mean PrIn of PrP^C expressing Tr-ACHN-pcDNA 3.1/PrP, 0.46, was significantly higher than Tr-ACHN-pcDNA 3.1 with PrIn of 0.40 and as for LS 174T cells, the pcDNA 3.1-PrP-transfected cells showed higher PrIn value at 0.47 compared to vector transfected cells with PrIn value at 0.44. As expected, no variation in PrIn value was detected between Tr-HSC-2-pcDNA 3.1/PrP (0.45) and Tr-HSC-2-pcDNA 3.1 (0.45). The augmentation of PrIn value in PrP^C expressing cells is parallel with the role of PrP^C in promoting G₁- to S-phase transition.

To gain insight into the role of PrP^C in cell cycle progression, the kinetics of cell cycle progression induced by PrP^C were further investigated using synchronized cells. Synchronizing of cells in G₁-phase was performed using TUN which was able to trigger suppression of S-phase and arrest cell cycle in late G₁-phase. The stably pcDNA 3.1-PrP-transfected LS 174T and PrP^C depleted HSC-2 cells were used in this study. Flow cytometric DNA histograms showing cell cycle distribution of HSC-2 and LS 174T cells upon synchronization are represented in Figure 4.26 and Figure 4.27 respectively. The data shown is corresponding to a representative experiment; which was performed in triplicate; out of two with similar findings.

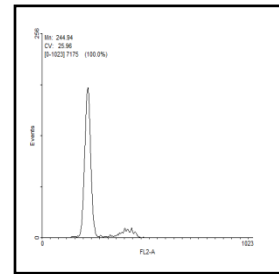
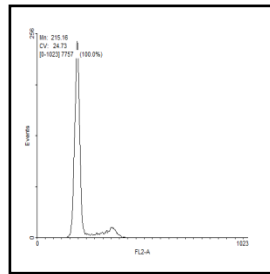
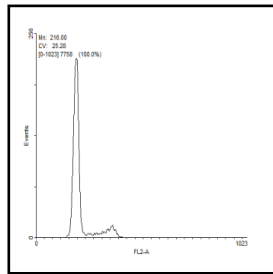
A.

Asynchronous

HSC-pLKO.1 vector HSC-pLKO.1 Scram. HSC-shRNA 1
0hr

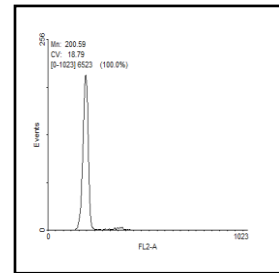
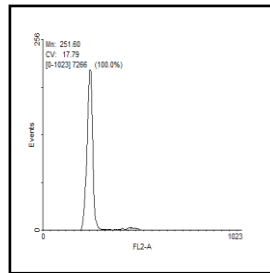
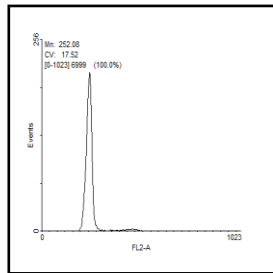


24hr

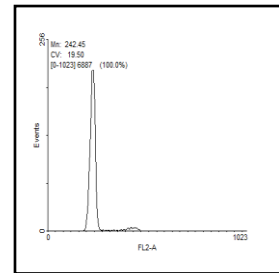
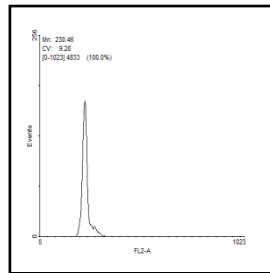
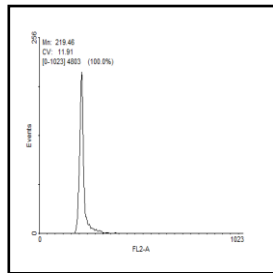


Synchronous

HSC-pLKO.1 vector HSC-pLKO.1 Scram. HSC-shRNA 1
0hr



4hr



8hr

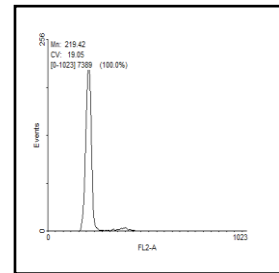
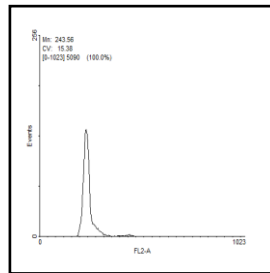
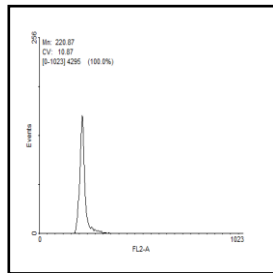


Figure 4.26 continued.

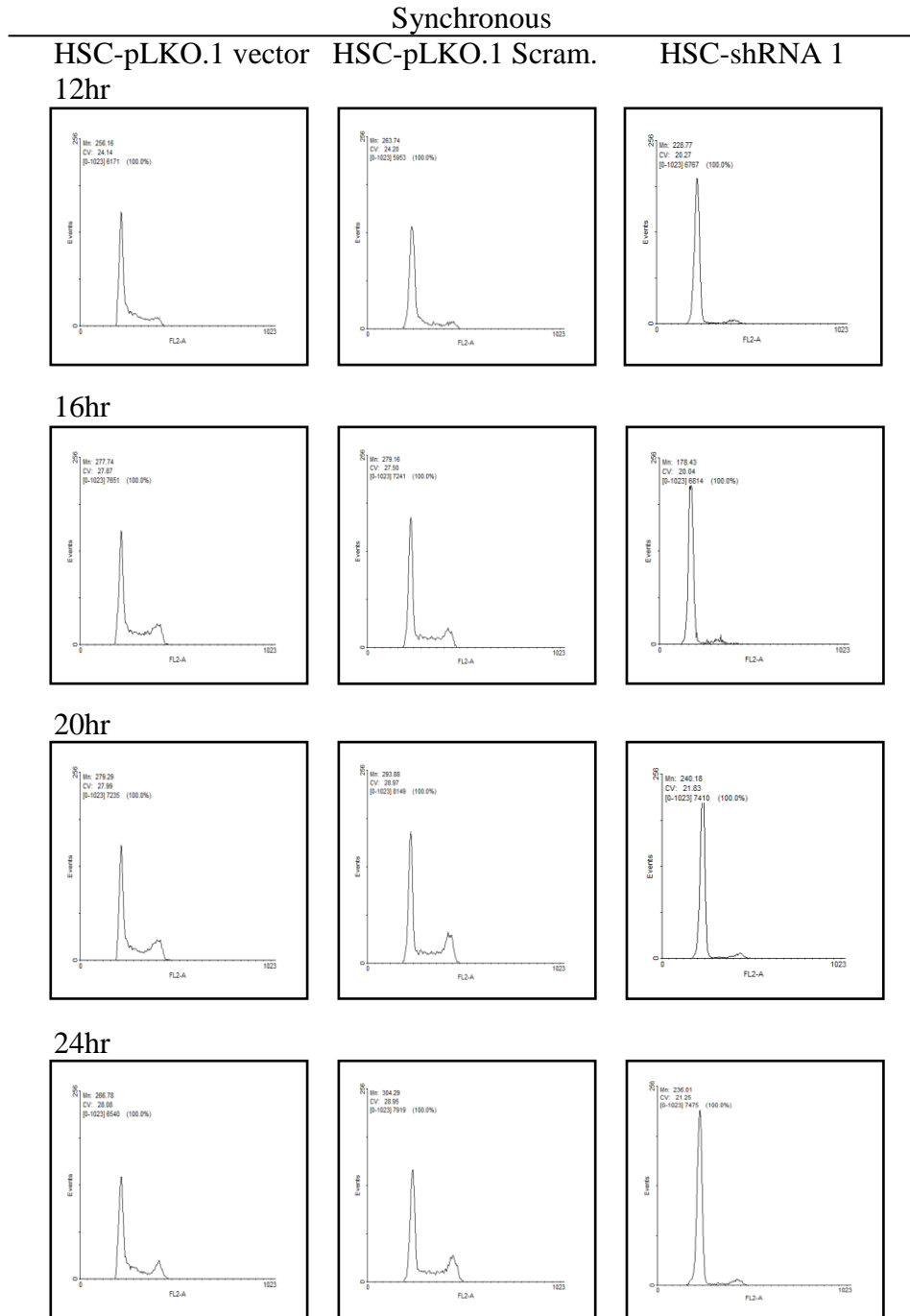


Figure legend on page 137.

Figure 4.26 continued.

B.

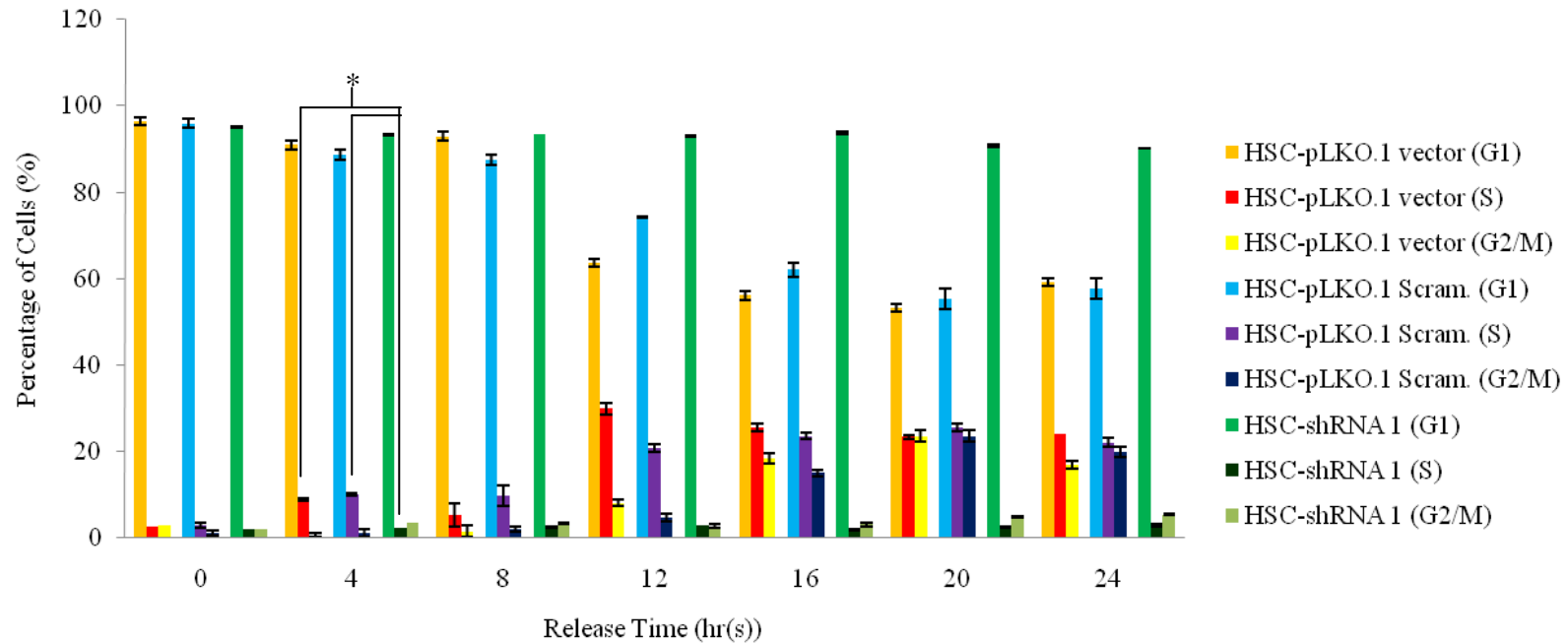
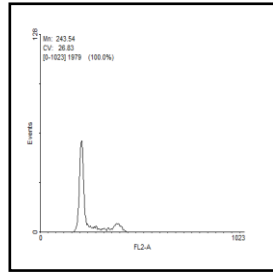


Figure 4.26: Effects of PrP^C on cell cycle distribution in HSC-2 cells upon synchronization. Cells were arrested in mitosis by synchronization using TUN followed by release into MEM medium. The post-released cells were harvested at 4hr intervals for 24hr in MEM medium. As a control treatment, asynchronous cells at 0hr and 24hr were collected to monitor the effectiveness of experimental procedure. (A) Flow cytometric analysis of cell cycle distribution in asynchronous and synchronous cells. (B) Graphical representation of synchronous HSC-2 in A. % of cells in G₁-phase, S-phase, G₂/M-phase are mean ± SEM of triplicates from 2 independent experiments. An unpaired two-tailed Student's t-Test using Microsoft Excel[®] 2007 was used for statistical analysis. * $p < 0.05$ in HSC-shRNA 1 vs. HSC-pLKO.1 vector and HSC-pLKO.1 Scram..

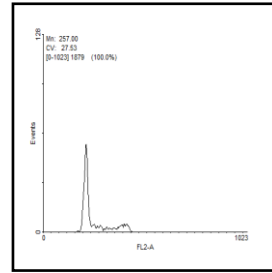
A.

Asynchronous

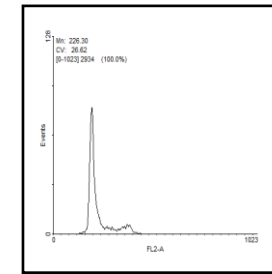
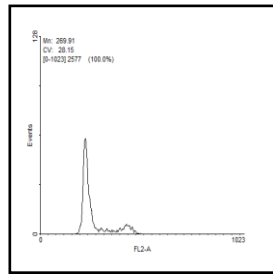
sT-LS 174T-pcDNA 3.1
0hr



sT-LS 174T-pcDNA 3.1/PrP

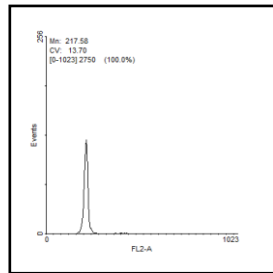


24hr

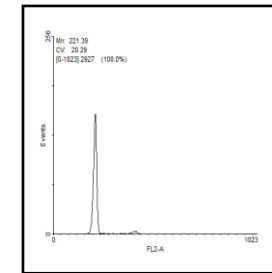


Synchronous

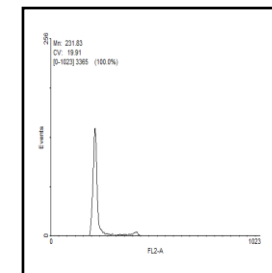
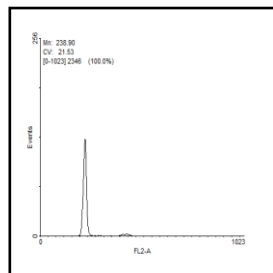
sT-LS 174T-pcDNA 3.1
0hr



sT-LS 174T-pcDNA 3.1/PrP



4hr



8hr

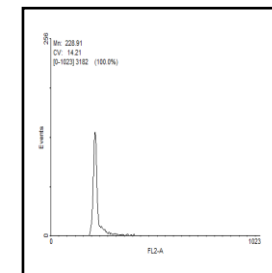
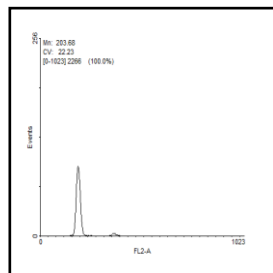


Figure 4.27 continued.

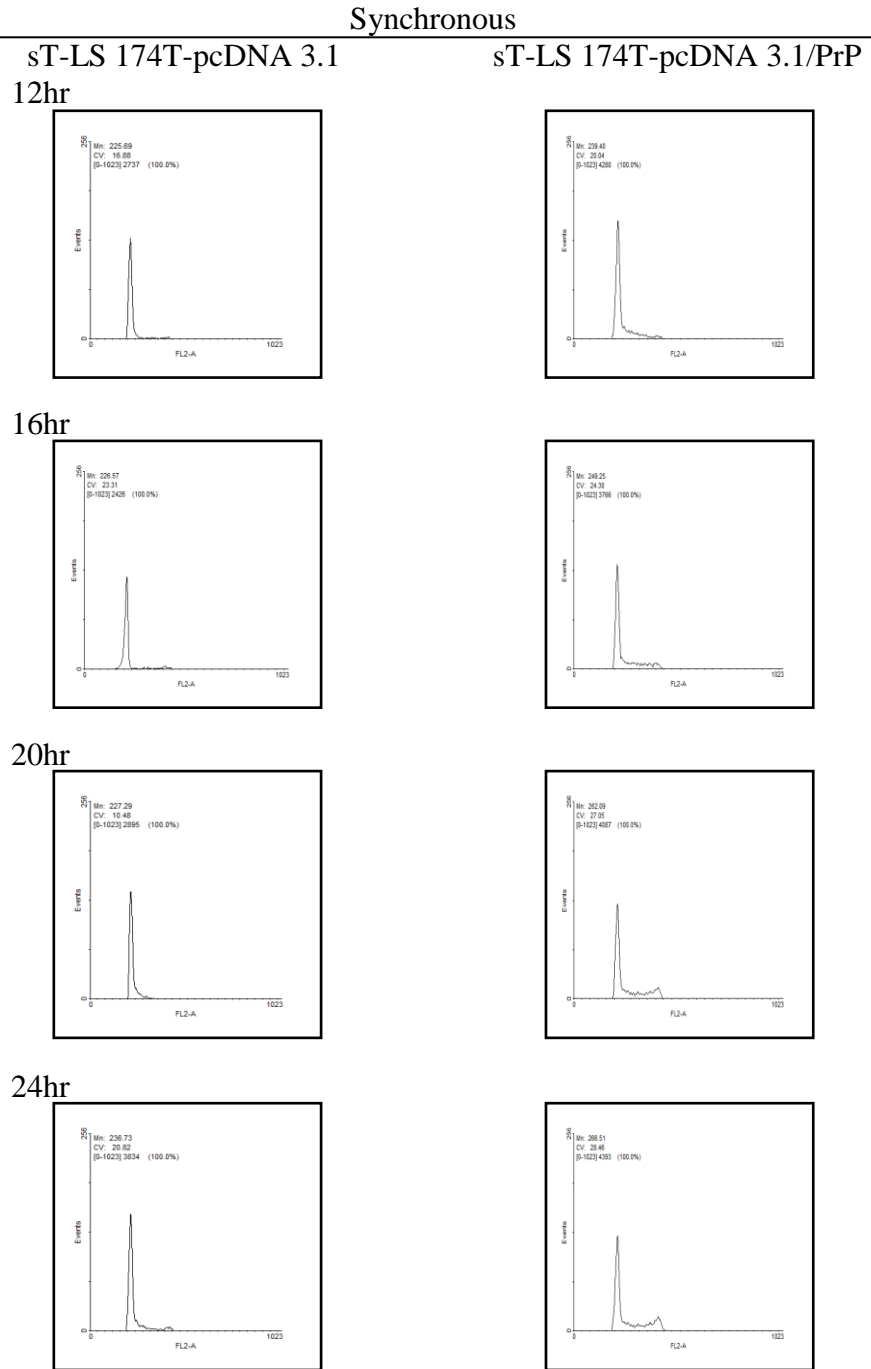


Figure legend on page 140.

Figure 4.27 continued.

B.

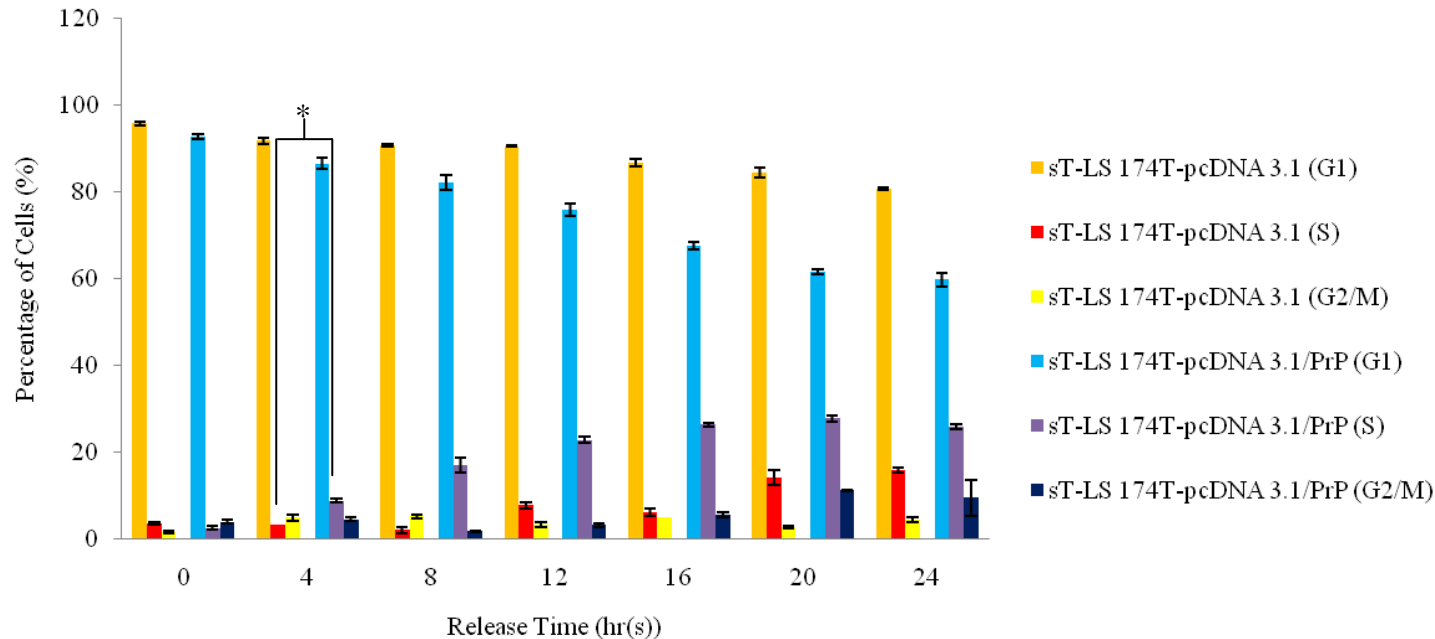


Figure 4.27: Effects of PrP^C on cell cycle distribution in LS 174T cells upon synchronization. Cells were arrested in mitosis by synchronization using TUN followed by release into MEM medium. The post-released cells were harvested at 4hr intervals for 24hr in MEM medium. As a control treatment, asynchronous cells at 0hr and 24hr were collected to monitor the effectiveness of experimental procedure. (A) Flow cytometric analysis of cell cycle distribution in asynchronous and synchronous cells. (B) Graphical representation of synchronous LS 174T in A. % of cells in G₁-phase, S-phase, G₂/M-phase are mean ± SEM of triplicates from 2 independent experiments. An unpaired two-tailed Student's t-Test using Microsoft Excel[®] 2007 was used for statistical analysis. * $p < 0.05$ in sT-LS 174T-pcDNA 3.1/PrP vs. sT-LS 174T-pcDNA 3.1.

There was almost 95% of the cancer cells were arrested in G₁-phase at the end of the synchronization period. The asynchronous cells did not show any influence on cell cycle distribution, as expected.

The PrP^C expressing group in synchronous HSC-2 cells, HSC-pLKO.1 vector (8.9% ± 0.3) and HSC-pLKO.1 Scram. (10.1% ± 0.3) began entering S-phase 4hr after post-releasing. This G₁ to S-phase transition event occurs significantly much earlier compared to the PrP^C depleted HSC-shRNA 1 (2.5% ± 0.0). By 12hr post-release, most HSC-pLKO.1 vector and HSC-pLKO.1 Scram. cells have shifted to S-phase and cells entered a new cell cycle at 16hr post-release. As for HSC-shRNA 1 cells, there was no notable cell cycle phase transition observed within the 24hr post-release. The event might occur at later time point which was not investigated in this study.

Synchronized sT-LS 174T-pcDNA 3.1/PrP cells (8.8% ± 0.4) released from G₁- to S-phase in the presence of PrP^C exhibited a prompted cell cycle progression by 4hr post-release compared to the synchronized sT-LS 174T-pcDNA 3.1 cells (3.3% ± 0.1). At 12 to 16hr, many of the synchronized sT-LS 174T-pcDNA 3.1/PrP cells were in S phase and probably after 24hr post-release, most of the cells were in G₁-phase of the next cycle. On the other hand, most of the synchronized sT-LS 174T-pcDNA 3.1 cells, which do not express PrP^C, were still in G₁-phase at 4hr post-release. A G₁- to S-phase transition of the cells was observed later on at 12hr post-release, which was much delayed than that of sT-LS 174T-pcDNA 3.1/PrP cells. Cells were still in a transition state at 24hr post-release.

Taken together, these data demonstrated that PrP^C promotes growth through cell cycle progression by regulating G₁- to S-phase transition in a cell- and time-dependent manner.

CHAPTER 5

DISCUSSION

5.1 Inefficient Co-transfection using Electroporation Method

A few attempts using electroporation method have been carried out as described in Materials and Methods. Unfortunately, it was ineffective. The strength of the applied electrical field, the length of the pulses, temperature and the composition of the buffered medium are important parameters for efficient gene delivery via electroporation method (Knutson & Yee, 1987). Therefore, substantial optimization is required in order to obtain efficient delivery and minimize cell death as high field strengths, long pulses and multiple pulsing might decrease the survival rate of cells. Yet, in this study, although the cells survived the parameters attempted, low % or almost none of the cells were expressing PrP^C upon selection. Hence, transfection failure was likely attributed to the approach of using co-transfection with two plasmid vectors simultaneously.

Unsuccessful development of cultured cancer cells overexpressing PrP^C may be due in part to inefficient co-transfection with pCMV-SPORT6-PrP and pBABE-hygro. Plasmid carrying the gene of interest, in this case, pCMV-SPORT6-PrP, must be accompanied by at least one other gene that acts as a selectable marker e.g. pBABE-hygro in order for co-transfection to be successful. As the selectable marker and the gene of interest are under control

of two separated vectors, it is uncertain whether these hygromycin resistant colonies-forming cells have taken up pCMV-SPORT6-PrP, and vice-versa. For this reason, efficient delivery of both vectors at once to target cells merely occurred by chance.

To further exacerbate the situation, in the presence of both vectors within the same cell, trans effects might occur when either one of the vector or both possess very strong promoter/enhancer elements (Farr & Roman, 1992). This cell-specific experimental artifact can in turn potentially affect gene expression and the incidence and enormity of such effects will be depending on the combination and activities of genetic regulatory elements present on the vectors. Therefore, optimization of the best possible amount and relative ratio of pCMV-SPORT6-PrP to pBABE-hygro is necessary in order to ensure self-regulating genetic expression of both vectors independently.

Thus, in this study, transfection of single pcDNATM 3.1 vector carrying the neomycin resistance gene using cationic lipids was chosen in order to achieve higher transfection efficiencies and to minimize the time needed for optimization of the wide ranging electroporation parameters. Problems such as cell toxicity and off-target effects can be reduced as lower amount of DNA is needed for cationic lipids transfection method. These added advantages will provide a good model for *in vitro* study purposes. Besides, due to the well established formation of lipophilic complexes between shRNA plasmid DNA and cationic carriers (Promega, 2009), cationic lipid-mediated delivery of shRNA oligos into cultured cells was also opted in this study.

5.2 Protective Effect of PrP^C towards TNF- α -induced Cell Death

The defensive role of PrP^C towards TNF- α -mediated cell death in the TNF- α resistant human breast carcinoma MCF-7 clone has been well described previously by Diarra-Mehrpour et al. (2004). Detection of PrP^C expression via DNA microarray analysis showed that the 17-fold and 10-fold up-regulation of PrP^C at both mRNA and protein levels, respectively, further converts the TNF- α sensitive MCF-7 to its TNF- α resistant clone. These investigators then showed that the resistance of PrP^C overexpressing MCF-7 cells towards TNF- α is more or less linked to the alteration of cytochrome *c* release from the mitochondria and nuclear condensation. This cytoprotective effect of PrP^C was re-examined by Christensen and Harris (2008), showing a more modest effect in comparison to the latter. This suggests that the protective effect of PrP^C is strain variant-specific and cell-specific.

Hence in this study, the reproducibility of such phenomenon in other cell culture system particularly in HSC-2, ACHN and LS 174T cell lines was examined. Transiently transfected cells overexpressing PrP^C were treated with 100ng/ml TNF- α for 48hr. MTT analysis revealed that there was merely about 10-15% increment of cell viability between the PrP^C expressing group and vector-transfected group, showing transient overexpression of PrP^C in ACHN and LS 174T suppresses TNF- α -induced cell death in a mild but statistically significant manner. No significant difference was observed in HSC-2 cells as the cell line itself overexpresses PrP^C.

The feeble results attained from this study might be due to several reasons as discussed earlier by Christensen and Harris (2008), such as genetic deviation and differences in the magnitude of response towards TNF- α between cell lines. On top of that, different methods used during gene delivery might play a key role. In this study, transient transfection was opted for fast analysis of gene function and further minimizes the risk of artifacts based on clonal effects (Malaisé et al., 2008). Therefore, DNA is not integrated into the nuclear genome during transient transfection and consequently, *PRNP* gene might be gradually lost from the daughter cells after a period of time; affected by the mitotic rate of the cancer cells and other environmental factors (Miura & Yuan, 2000). Owing to this, expression of PrP^C was up-regulated merely 3-fold and 5-fold in LS 174T and ACHN cells, respectively whereby in both Diarra-Mehrpour et al. (2004) and Christensen and Harris (2008) studies, as high as 25-fold up-regulation of PrP^C was achieved via adenovirus-mediated transduction and stable transfection, respectively.

5.2.1 Protective Effect of PrP^C in TNF- α -mediated Apoptosis Involves the Suppression of Bax

TNF- α has been shown to activate apoptotic signalling through a Bid-dependent conformational change in Bax (Perez & White, 2000). Hence, to further clarify the causal mechanism of PrP^C on TNF- α -mediated cell death, protein expression level of Bax and Bcl-xL in treated cells was measured. Bid expression was not considered in the study as PrP^C was shown to be very specific for Bax and does not prevent truncated Bid-mediated cell death

(Roucou et al., 2005). Of note, truncated Bid (tBid) is the active form of the pro-death protein, Bid. Likewise, Bcl-xL was preferred over Bcl-2 as the former is reported to rescue cells from apoptosis 10 times more effectively than Bcl-2 in a highly cell-specific manner (Fiebig, Zhu, Hollerbach, Leber, & Andrews, 2006).

In this study, pcDNA 3.1-PrP transfected LS 174T showed significantly higher cell viability upon TNF- α treatment compared to the vector-transfected cells. Interestingly, LS 174T is null for Bax expression. Hence, it is speculated that there might be the presence of other pathways that is engaged by PrP^C to exert its protective activity against TNF- α -mediated cell death which does not involve the participation of Bax. On the other hand, Bax expression was down-regulated 4-fold in PrP^C expressing ACHN cells upon TNF- α treatment while a small but notable reduction of Bax level was observed in the pcDNA 3.1-PrP-transfected HSC-2 cells compared to the vector-transfected HSC-2. The relative Bax/Bcl-xL ratio gives an indication to the degree of sensitivity in cells towards an applied insult (Raisova et al., 2001). Thus, the low Bax/Bcl-xL ratio of less than 1 in the PrP^C expressing ACHN cells shows that the cells were TNF- α -resistant while the Bax/Bcl-xL ratio of more than 1 in both vector-transfected ACHN and HSC-2 cells indicates that they were TNF- α -sensitive. This finding is comparable to the MTT analysis performed earlier.

Although Bax expression was highly modulated during TNF- α -induced cell death, the expression of Bcl-xL was not affected. This suggests that PrP^C exerts its protective effect in TNF- α -mediated cell death through Bax regulation

independent of the anti-apoptotic Bcl-2 family protein, Bcl-xL. This finding is further supported by a previous study which demonstrated that PrP protects against Bax-mediated mitochondria-dependent apoptosis and growth arrest in *S.cerevisiae* yeast cells lacking Bcl-2 genes (Bounhar, Mann, Roucou, & LeBlanc, 2006).

Upon binding of TNF- α to tumour necrosis factor- α receptor 1, TNF-R1, Bax is activated and subsequently translocated from the cytosol to mitochondria to induce the release of cytochrome *c* and caspase activation which results in apoptotic cell death. Hence, PrP^C may be involved in the PI3K/Akt pathway and executes its anti-Bax function by preventing the pro-apoptotic conformational changes of Bax at the early step of Bax activation (Diarra-Mehrpour et al., 2004; Roucou et al., 2005). The participation of PrP^C in PI3K/Akt pathway is further supported by Weise et al. (2006) who demonstrated that deletion of PrP^C impairs the anti-apoptotic PI3K/Akt pathway and further leads to exacerbation of neuronal injury in Prnp^{0/0} mice upon transient and permanent cerebral ischaemia.

5.2.2 A Plausible Protective Role of Cytosolic PrP Which Involves Bax

The interaction between PrP^C (which is most abundantly expressed on the cell membrane) and Bax is indirect since inhibition of Bax activation takes place in the cytosol, where Bax is localized. Although the transmembrane PrP isoforms; CtmPrP and NtmPrP may act indirectly through other cellular components on Bax, the anti-Bax function might attribute partly to the uncommon cytosolic

form of PrP^C (CyPrP) which arises either from the retrotranslocation of endogenous PrP^C from endoplasmic reticulum (ER) into the cytosol or from impaired translocation into the ER due to intrinsic weakness of the PrP signal peptide sequence (Lin et al., 2008; Orsi, Fioriti, Chiesa, & Sitia, 2006; Roucou et al., 2003). CyPrP is shown to be protective against Bax-mediated cell death in human primary neurons and MCF-7 cells where the loss of CyPrP expression leads to perturbed anti-Bax function in familial PrP mutants associated with Creutzfeldt-Jakob disease, Gerstmann-Sträussler-Scheinker syndrome and FFI (Jodoin, Laroche-Pierre, Goodyer, & LeBlanc, 2007; Jodoin et al., 2009; Roucou et al., 2003). Thus, these suggest the modulation of PrP's anti-Bax function in the manifestation of prion diseases.

LeBlanc's team has further investigated the anti-Bax function of the CyPrP via structure-function analysis using MCF-7 cells transfected with wild type or mutants PrP, and showed that the helix 3 region of PrP is essential and adequate for CyPrP's protection against Bax-mediated cell death. In their study, it is demonstrated that the deletion of C-terminal amino acid residues from 200 to 227 of PrP and the substitution of amino acid residues K204, V210, and E219 in helix 3 by Proline prevents CyPrP's anti-Bax function. Besides, substitution of helix 3 K204 alone by Alanine residues also inhibits the anti-Bax function of CyPrP (Laroche-Pierre, Jodoin, & LeBlanc, 2009).

5.3 Stable Knockdown of PrP^C Expression Using HuPrPshRNA 1

In this study, RNA interference (RNAi) was applied in the gene knockdown experiments to further analyze the loss of function of PrP^C and its insinuation in cultured HSC-2 cells. The plasmid pLKO.1 TRC cloning vector with RNA Polymerase III promoter has been employed to express shRNA oligos in the cancer cells. Of all the 3 sequences employed to knockdown PrP^C expression, HuPrPshRNA 1 was shown to acquire the highest knockdown efficiency. On the other hand, HuPrPshRNA 2 showed low or almost no reduction of PrP^C expression.

The varied gene knockdown efficacy is attributed to the uniqueness of the 21-nt within the genome, thermodynamic stability of the dsRNA duplex, GC content and the presence of single nucleotide polymorphisms (SNPs) in each shRNA oligos' sequences (Yuan et al., 2004). Reynolds et al. (2004) further identified the specific characteristics associated with siRNA functionality, such as low GC content, low internal stability at the “sense” strand 3'-terminus, lack of inverted repeats, and “sense” strand base preferences at positions 3, 10, 13 and 19. The potency of siRNA selection is remarkably improved upon an algorithm integration of all the stated criteria above. Although the position of the siRNA within the input sequence plays a key role in determining the gene knockdown efficacy, Zhou and Zeng (2009) reported that functional shRNA oligos prefer high free energy states with low stability at both terminals. In fact, the thermodynamic stability status was found to be a crucial influence aspect on shRNA efficacy, as the low stability of the “sense” or “antisense”

strand at 5'-terminus of siRNA duplex facilitates its incorporation into the RISC complex and further leads to higher gene silencing efficacy. As well, the accessibility of the 3'-terminus is another criterion to shRNA functionality (Yuan et al., 2004; Zhou & Zeng 2009).

Therefore, in this study, a lower GC content of 42.0% and the close proximity to the target gene region of both HuPrPshRNA 1 (bases 1194-1214) and HuPrPshRNA 3 (bases 1309-1329) were shown to be more effective in suppressing the expression of endogenous PrP^C in HSC-2 cells compared to HuPrPshRNA 2 with a higher GC content of 47.0% which targeted at bases 1664 to 1684 of the human PrP mRNA. Moreover, HuPrPshRNA 1 was shown to acquire the lowest thermodynamic value of -3.1 followed by HuPrPshRNA 2 and HuPrPshRNA 3 at -0.3 and 1.5, respectively. The lower thermodynamic stability of HuPrPshRNA 1 contributes to its higher *PRNP* gene knockdown efficiency.

5.4 PrP^C is Protective during Oxidative Stress-induced Apoptosis

The role of PrP^C as an antioxidant, especially in the nervous system, has been well established in extensive studies. Anantharam et al. (2008) have previously reported that PrP^C exerts its anti-apoptotic role during oxidative stress-induced cell death in mouse neural cells by decreasing the cells' vulnerability to oxidative insults such as H₂O₂. In their study, DNA fragmentation was increased by 152% and 244% in PrP^C and PrP^{ko} cells, respectively, upon H₂O₂ treatment at 100µM for 24hr, compared to the untreated controls.

Emphasizing the need to further elucidate the role of PrP^C as a competent antioxidant during H₂O₂-induced cell death especially in cancer cell lines, the stably transfected PrP^C LS 174T and shRNA-mediated PrP^C knockdown HSC-2 cells were chosen to undergo H₂O₂ treatment at high concentration in order to provoke oxidative stress-induced cell death. Endogenous PrP^C in HSC-2 cells was depleted via shRNA-mediated stable transfection. Stable transfection is preferred over transient transfection as the former is vital to the analysis of gene function and in order to ensure long-term, reproducible as well as defined gene expression/depletion since the gene/shRNA of interest is incorporated into the target cell's chromosome (Bernards, 2006; Miura & Yuan, 2000).

The robust cytoprotective effect of PrP^C towards H₂O₂-induced cell death was further confirmed with FITC Annexin V–PI dual staining where it showed that the protective effect of PrP against H₂O₂-mediated cell death was via an anti-apoptotic mechanism, instead of anti-necrotic. DCFH-DA based assay demonstrated that PrP^C acts as a free radical scavenger during oxidative stress. H₂O₂-induced ROS generation was significantly attenuated in PrP^C expressing LS 174T. Conversely, a considerably higher ROS level was observed in HSC-2 cells upon depletion of endogenous PrP^C via shRNA. These findings drew attention to the undisputable antioxidant role of PrP^C during oxidative stress-induced cell death and were supported by Yam, Gao, Wang, Wu, and Peretz (2010) who demonstrated that PrP^C protects against ROS-mediated DNA damage in SH-SY5Y cells under basal conditions and upon infection of PrP^{Sc} into N2a cells (ScN2a), DNA damage was elevated.

5.4.1 Association of PrP^C with Copper Metabolism and SOD Activity

Malaisé et al. (2008) demonstrated that intracellular ROS production was significantly attenuated in a deletion mutant N2a cells affecting the transmembrane domain 1 (TM1), $\Delta 8\text{TM1-PrP}$, but not in cells lacking the octarepeat region ($\Delta\text{octa-PrP}$) during oxidative stress. The defensive effect of PrP^C towards oxidative stress requires the specific octarepeat region (amino acid residues 51-91), which is conformationally altered during PrP^C conversion to PrP^{Sc}, and not the TM1 region located at amino acid residues 110-135 nor the high-affinity copper-binding site described for human residues His96/His111 (Malaisé et al., 2008; Watt, Routledge, Wild, & Hooper, 2007). The octarepeat region located at the N-terminal region is composed of four or more tandem PHGGGWGQ segments and is shown to be responsible for the high affinity copper binding by PrP^C, where the affinity can be as high as 0.1 nanomolar depending on binding site occupancy (Walter et al., 2006). Moreover, PrP^C in conjunction with its binding to copper, possesses SOD-like activity which contributes to its direct protective effects towards H₂O₂-induced oxidative stress, as proposed by Brown et al. (1999).

Devotion of copper metabolism regulated by PrP^C to cellular resistance towards oxidative stress has been clearly postulated in previous studies. Kralovicova et al. (2009) showed an increased expression of PrP^C specific to SODs knockout such as Cu/Zn SOD, MnSOD and EC-SOD; but not in any other proteins in the brains of transgenic mice. This implicates that the loss of antioxidant activity during SODs depletion was compensated by up-regulation

of PrP expression together with association of copper metabolism. Modulation by PrP^C as a copper-binding protein of intracellular H₂O₂ level has been shown to protect primary cerebellar granular neurons (CGNs) from apoptotic cell death where upon copper sensitization, the *PRNP* gene-deficient, Prnp^{-/-} CGNs were more readily underwent apoptotic cell death as compared to the wild type CGNs (Nishimura et al., 2004).

Likewise, Brown and Besinger (1998) have previously demonstrated that the protective mechanism of PrP^C against oxidative stress may be indirect by its ability to up-regulate expression of other proteins, such as Cu/Zn SOD and glutathione reductase which are responsible for ROS detoxification. This is in agreement with data from previous study which showed that attenuation of glutathione reductase activity in PrP-deficient neurons (PrP^{-/-} neurons) greatly sensitized the cells to H₂O₂ toxicity (White et al., 1999).

It is likely that the protective effect of PrP^C towards oxidative stress occurs either upstream or downstream of ROS where during activation of apoptotic pathway via oxidative stress, the anti-apoptotic effects of PrP^C may be accredited to its ability to protect cells against oxidative stress (Halliwell, 2006). ROS may play a direct or indirect role by mediating the mitochondria-dependent apoptosis via caspase activation through the release of cytochrome *c* from mitochondria (Simon et al., 2000). This is supported by the study of Choi et al. (2007) which demonstrated that PrP protects against H₂O₂- and manganese (Mn)-mediated oxidative stress and apoptotic cell death in PrP^C- and PrP^{KO}-mouse neural cells by hampering divalent metal Mn uptake.

Consequently, this is coherent with the present study which shows that PrP^C exerts its protective effects in PrP^C overexpressing LS 174T and HSC-2 cells towards H₂O₂-mediated apoptosis by attenuating ROS levels.

5.4.2 PrP^C Downregulation, Copper Elevation, and Oxidative Stress: A Targeted Cancer Therapy

Although there is limited research reporting on the defensive antioxidant effect of PrP^C in cancer cell lines compared to the neuronal cells, recent data has emerged showing the implication of PrP^C and its overexpression in the cancer biology of neuroblastoma, breast cancer, and gastric cancer. It has been demonstrated that PrP^C decelerates apoptosis in gastric cancer cell line AGS by suppressing ROS generation and up-regulating the expression of Bcl-2 (Liang et al., 2006). Hence, PrP^C may act as an antioxidant enzyme such as SOD to endure increased ROS stress, and helps to protect the cancer cells against intrinsic oxidative stress (Pelicano, Carney, & Huang, 2004).

Consequently, the up-regulation of antioxidant capacity in adaptation to intrinsic oxidative stress in cancer cells can confer drug resistance. It has been shown that down-regulation of PrP^C expression sensitized the breast carcinoma cells, MCF-7, to TRAIL-mediated cell death (Diarra-Mehrpour et al., 2004). A close association was also observed between chemotherapy resistance and PrP^C expression in the cells. Overexpression of PrP^C in cancer cells could in turn lead to the development of resistance to antitumour drugs such as paclitaxel and anthracyclines (Diarra-Mehrpour et al., 2004). Thus, modulation of the

unique redox regulatory mechanisms of PrP^C might be an effective strategy to eliminate cancer cells (Hileman, Liu, Albitar, Keating, & Huang, 2004).

In fact, a potential pharmacological application of PrP antibodies together with combination chemotherapy has been well documented by McEwan, Windsor, and Cullis-Hill (2009), where they showed that antibodies to PrP improved the upshot of multiple anticancer drugs such as irinotecan, 5-FU, cisplatin and doxorubicin to varying extents. Besides, PrP antibodies treatment alone was shown to have different magnitude of anti-proliferative activity and an increased apoptosis *in vitro*. Their study further showed significant inhibition of tumour growth in an *in vivo* nude mouse bearing human HCT 116 xenografts upon treatment with anti-PrP antibody and in combination with irinotecan. Hence, this makes PrP^C a promising target for future drug development.

A plausible cancer therapeutic strategy by involving the perturbation of PrP^C expression might also relate to the defect in copper transport systems, as PrP^C is a high-affinity copper binding protein. This is encouraging since there are evidences showing that copper transport mechanisms may play a role in drug resistance. Yoshizawa et al. (2007) showed that the overexpression of copper efflux transporter, ATP7B, contributes to the acquisition of cisplatin-resistance in various types of invasive human oral squamous cell lines, while the knockdown of ATP7B sensitizes the cells to cisplatin. Meanwhile, Owatari et al. (2007) demonstrated that another type of the copper efflux transporter, ATP7A, confers multidrug resistance to the Chinese hamster ovary cells

(CHO-K1) and fibroblasts isolated from Menkes disease patients via the trans-Golgi network, by compartmentalizing drugs in the Golgi apparatus and subsequently promoting efflux of the anticancer drugs. ATP7A expressing colon cancer cells were also shown to be more resistant to SN-38, an active metabolite of irinotecan, than the ATP7A-negative cells.

5.5 Glycosylation Inhibition in PrP^C Provokes ER Stress-induced Apoptosis in Cancer Cells

PrP^C has been shown to have a protective effect against oxidative stress induced-apoptosis by attenuating the ROS generation. In cervical cancer HeLa cells transiently expressing *PRNP* gene glycosylation mutants, N181Q N197Q and T183A T199A, the ROS scavenging properties of PrP^C was diminished and further sensitized the HeLa cells to mitochondria mediated-cell death (Yang, Chen, Pan, Kou, & Xu, 2009). Hence, this study was intended to validate the reproducibility of the above effect using a different cancer cell culture models. Instead of generating PrP^C glycosylated mutant cells, inhibition of N-glycosylation using TUN was employed. Tunicamycin is a member of the nucleoside antibiotics family which is of uridine, an 11-carbon disaccharide called aminodeoxydialdose, and a fatty acid of variable length (13–17 carbons), branching, and unsaturation. In eukaryotes, tunicamycin acts as a tight binding competitive inhibitor which inhibits N-glycosylation by blocking the transfer of GlcNAc-1-P from UDP-GlcNAc to dolichyl-P (catalyzed by GlcNAc phosphotransferase, GPT), thereby decreasing dolichyl-PP-GlcNAc in the first step of glycoprotein synthesis (Esko, 1999).

Western blot analysis showed that only the unglycosylated PrP isoform at 27kDa was expressed upon glycosylation inhibition as expected. Noteworthy, a 19-22kDa species (p19-22) was detected in the presence of TUN. The generation of this 19-22kDa species, possibly the C-terminal fragment C2 that has the 3F4 epitope intact, resulting from the β -cleavage of PrP^C (Mangé et al., 2004). ROS has been shown to be responsible for the β -cleavage that takes place within the unstructured region of the molecule, near or within the octarepeat region of PrP^C (McMahon et al., 2001; Watt et al., 2005). Thus, these studies offer a supportive explanation to the occurrence of p19-22 since TUN is also able to induce oxidative stress regulated by protein degradation (Hsieh et al., 2007), as described in Section 5.5.1.

β -cleavage has been shown to be protective against oxidative stress (Lewis & Collins, 2008; Watt & Hooper, 2005). Hence, aberrant or compromised PrP^C processing could instigate an event of oxidative damage and further cellular injury that may be implicated in neurodegenerative as observed in prion diseases, or possibly influences susceptibility to prion infection by facilitating the conversion of PrP^C to PrP^{Sc} (Lewis & Collins, 2008). More extensive research should be conducted in order to elucidate the underlying mechanism as well as the biochemical properties of p19-22 occurrence in uninfected PrP^C expressing cells.

In the present study, MTT analysis revealed that cells expressing glycosylated PrP exhibit higher viable cells population compared to the unglycosylated PrP expressing cells. Accumulation of death cells in the LR and UR quadrant, but

not in UL quadrant, via FITC Annexin V-PI flow cytometry analysis further confirms that the cell death mechanism induced by unglycosylated PrP upon TUN treatment is via apoptosis. However, the anti-apoptotic property seems to differ from one cell line to another, with less profound apoptosis in PrP^C-depleted and glycosylation-inhibited oral squamous cell carcinoma HSC-2 cells, and more profound general cell death (less profound proliferative effect) in PrP^C-overexpressing and glycosylation-inhibited colon adenocarcinoma LS 174T cells in this study.

The initiation of apoptosis upon PrP^C N-linked glycosylation inhibition via TUN has been described in a few extensive studies, although the approach used may not be similar. Dricu, Carlberg, Wang, and Larsson (1997) have reported that continuous presence of TUN for 24-48hr provokes cell death in SK-MEL-2 melanoma cells. Specifically, the mechanism of cell death upon inhibition of N-linked glycosylation using TUN has been shown to be via apoptosis due to the detection of oligonucleosomally fragmented DNA in gel electrophoresis. TUN exerts its apoptotic effect in a time- and cell-dependent manner since Carlberg et al. (1996) showed that a short exposure of 7min of TUN to SV40-transformed fibroblasts (line 90VAVI) triggered significant reduction in the cell viability and subsequently leading to apoptosis.

5.5.1 Accumulation of Unglycosylated PrP^C Triggers Oxidative Stress-related Unfolded Protein Response

The association between the ER stressor cum N-linked glycosylation inhibitor TUN and apoptosis is attributed to the unfolded protein response (UPR). Orsi et al. (2006) reported that UPR was activated upon ER stress induction in TUN-treated PrP expressing HeLa transfectants. They further proved that the translocation of the misfolded PrP^C into ER involves multifaceted interaction between oxidative folding, glycosylation, and calcium homeostasis.

In accord, the connection between ER stress and oxidative stress has been proposed in a review by Malhotra and Kaufman (2007) which stated that generation of ROS as a byproduct of protein oxidation during protein misfolding in the ER are coupled events that cause the activation of UPR and subsequent cell death. Malhotra et al. (2008) further testified the protective role of antioxidant during ER stress by showing a marked reduction in UPR activation and oxidative stress-mediated apoptosis in both *in vitro* and *in vivo* in mice upon subjected to antioxidant. However, the exact mechanism on how oxidative stress affects protein misfolding and vice versa is still a question mark.

Owing to the relation between ROS and ER stress, the ROS level in PrP^C expressing cells upon TUN treatment was measured using DCFH-DA based assay. The ROS scavenging activity of PrP^C was suppressed upon ER stress induction in cells. There was almost a 2-fold increment of ROS level in the

unglycosylated PrP^C expressing HSC-2 and LS 174T cells compared to the glycosylated PrP^C expressing cells. In conclusion, the present study has demonstrated that upon induction of ER stress, apoptosis was aggravated in the presence of unglycosylated variant of PrP which does not exhibit the antioxidant activity as described in the fully glycosylated PrP^C.

Due to the participation of ROS elevation during ER stress-induced apoptosis as been shown in the current study, it is likely that the underlying mechanism behind the induction of apoptosis in unglycosylated PrP is highly allied to the mitochondria-mediated signal transduction pathway. In fact, Yang et al. (2009) showed that upon apoptosis instigation in the non-glycosylated PrP expressing HeLa cells, pro-apoptotic trends were observed, such as cell growth retardation, reduction in mitochondrial membrane potential, elevated ROS generation, along with lower levels of apoptosis-related Bcl-xL and cleaved Caspase-9 was activated. The involvement of Bcl-2 family proteins and mitochondrial membrane potential diminution during apoptosis in transiently-expressing unglycosylated PrP^C mutants - N181Q/N197Q and T183A/T199A in human astrocytoma SF-126 cells further supported the observations (Chen et al., 2007). The experimental settings above using mutant PrP^C devoid of the glycosylation sites could be extended as our future studies, whereby these mutants could be stably transfected into HSC-2 cells with a knock-downed endogenous PrP^C background, and further subjecting the cells to apoptotic and oxidative stress insults. This could directly answer the role of PrP^C glycosylation in the survival of cancer cells besides HeLa and SF-126 cells, as well as HSC-2 and LS 174T cells.

5.5.2 Glycosylation Inhibition of PrP^C via TUN: A Promising Anticancer Strategy

The aggravation of apoptosis and induction of oxidative stress in cancer cells expressing the unglycosylated variant of PrP implicates the potential role of TUN as an anticancer agent or a potent enhancer during cancer therapy, especially in cancer cells overexpressing PrP^C. Since it has been shown in this study that PrP^C is responsible for ROS scavenging (mainly H₂O₂), the suppression of this antioxidant activity upon glycosylation inhibition - probably by down-regulating SOD - may further lead to a severe accumulation of ROS and ultimately oxidative stress-induced apoptosis via superoxide- and mitochondria-dependent pathways in cancer cells. Hence, glycosylation inhibition of PrP^C via TUN may provide a novel approach for the selective killing of cancer cells.

In fact, the promising strategy of using TUN to induce sensitization of cancer cells during cancer therapy has been well established. Combined treatment with TUN and TRAIL has been shown to enhance apoptosis in human prostate cancer cells by cooperatively activating Caspase-8, -10, -9, and -3 and Bid cleavage (Shiraishi et al., 2005). TUN remarkably sensitized the androgen-independent human prostate cancer cells, PC-3 cells to TRAIL-induced apoptosis by up-regulating the expression DR5 at the mRNA and protein levels in a dose-dependent manner (Shiraishi et al., 2005). Zhang et al. (2009) further demonstrated that TUN potently enhanced TRAIL-mediated apoptosis by

down-regulating the expression of CyclinD1 and subsequent survivin in thyroid carcinoma.

Moreover, an earlier study by Noda et al. (1999) suggested that the glycosylation modification by TUN in human head-and-neck carcinoma cells might be a constructive therapeutic approach for successful chemotherapy using cisplatin both *in vivo* and *in vitro*. Increased *in vivo* apoptosis of tumour cells and remarkable local tumour growth inhibition was observed upon TUN treatment in conjunction with cisplatin in the cisplatin-resistant C3H/He mouse model as compared with the control group. Besides, a pharmacomodulatory effect was observed in combination of TUN with anticancer drugs on multidrug-resistant (MDR) human UWOV2 ovarian cancer cells. TUN enhances drug cytotoxicity by effectively decreasing the EC₅₀ and further prolonging the intracellular drug retention time. It as well increases the binding of both [¹⁴C]doxorubicin and [³H]azidopine, where the latter is a photoaffinity label of the multidrug transporter, P-glycoprotein (P-gp). This proves that the pharmacomodulatory effects of TUN are intervened by global inhibition of protein as well as glycoprotein synthesis via N-glycosylation suppression and synergistic interaction with anticancer drugs (Hiss, Gabriels, & Folb, 2007).

The P-gp is an ATP-dependent efflux pump that prevents intracellular accumulation of cytotoxic anticancer drugs in tumour cells where proper processing and maturation of the protein bring to its structural-functional integrity and mediation of MDR (Di Pietro et al., 1999). The interaction between PrP^C and P-gp has been documented in a recent study by Li et al.

(2009) in MDR breast cancer cells treated with paclitaxel, a P-gp substrate. Induction of paclitaxel-mediated invasion upon up-regulation of P-gp activity or PrP^C expression further facilitated the formation of P-gp/PrP^C complex which is important in initiating the anti-apoptotic activity of adriamycin-resistant MCF7/ADR cells. Up-regulation of PrP^C and its significance in MDR gastric carcinoma cell line SGC7901/ADR has also been reported by Du et al. (2005). Their study demonstrated that the expression of the classical MDR-related molecule P-gp was significantly up-regulated by PrP^C, where the protein itself is resistant to both P-gp-related and P-gp-nonrelated drugs on SGC7901 cells. Besides, PrP^C was shown to inhibit adriamycin-induced apoptosis by modulating the expression of Bcl-2 and Bax, which might be the other pathway contributing to PrP^C-related MDR. Upon inhibition of PrP^C expression, the MDR phenotype of SGC7901/ADR was partially reversed. Once again, PrP^C shows promise as a potential therapeutic target molecule not only in prion diseases but as well as in PrP^C related carcinoma treatment.

5.6 A Role of PrP^C in Cell Cycle Progression

PrP^C has been shown to be abundantly expressed in the actively dividing hippocampus, hypothalamus, and olfactory bulb of the CNS (Mironov et al., 2003). Moreover, the expression of PrP^C has been documented in other non-neuronal tissues such as lymphoid cells, lung, heart, kidney, gastrointestinal tract, muscle, and mammary glands (Mehrpour & Codogno, 2010). Up-regulation of PrP^C expression in the cytoplasm and plasma membrane of gastric cancer cells, particularly in the innermost mucous lining of

gastrointestinal tract, upon *H.pylori* infection has also been reported previously (Konturek et al., 2005; Pammer, Suchy, Rendl, & Tschachler, 1999). Hence, owing to the abundance of PrP^C in these regions which is constantly undergo cell division, it is sensible to relate an association of PrP^C to cell proliferation, specifically in cancer cells.

In this study, MTT analysis showed an increase of cell growth in PrP^C expressing cells compared to the non-PrP^C expressing cells at the basal level, which indicates the proliferative ability of PrP^C in cancer cells. Hence, this study explores the potential proliferative ability of PrP^C by performing a basal cell cycle analysis screening in HSC-2, ACHN and LS 174T cancer cells. PrIn = $(S+G_2)/(S+G_2+G_1)$ was calculated to access the proliferation rate as defined by the S-phase cell cycle (Rytwiński, Wnuk, Woźniak, Rychłowska, & Bieńkowska, 2004). A small but significant increment of PrIn was observed in the PrP^C expressing group of cells. Further cell cycle synchronization using TUN in PrP^C overexpressing sT-LS 174T-pcDNA 3.1/PrP cancer cells showed that PrP^C modulates the cell cycle progression, which enhances cell proliferation by promoting G₁- to S-phase transition in a cell- and time-dependent manner. Conversely, the PrP^C depleted HSC-shRNA 1 cells showed the reverse effect.

These findings are coherent to Liang's team which reported that overexpression of PrP^C promoted G₁- to S-phase transition and subsequently led to cell proliferation and carcinogenesis in thymidine-synchronized human gastric cancer SGC7901 and AGS cell lines. PrP^C was shown to modulate G₁-

to S-phase transition in cell cycle progression in the course of PI3K/Akt pathway activation where the octarepeat region of PrP^C might play an obligatory role. Following the activation of PI3K/Akt pathway, expression of CyclinD1 was up-regulated upon its transactivation (Liang et al., 2007). This is further supported by Satoh, Kuroda, and Katamine (2000) who described a down-regulation of a series of genes responsible for cell proliferation, differentiation, and survival in PrP-knockout (PrP^(-/-)) mice-derived skin fibroblast SFK cell lines prior to basic fibroblast growth factor (bFGF) exposure. In their study, the receptor tyrosine kinase substrate Eps8, CyclinD1, and CD44 mRNAs expression was down-regulated whereas considerable up-regulation of PI3K p85, IGF-I, and serine protease inhibitor-2.2 mRNAs expression was demonstrated via Northern blot analysis in the SFK cells.

The association of CyclinD1 with G₁- to S-phase transition initiation in PrP^C expressing cells is plausible since CyclinD1 itself is mainly responsible for G₁- to S-phase transition regulation. The G₁/S-specific proto-oncogene is also an important cofactor which regulates the activity of several transcription factors as well as histone acetylation and chromatin remodeling proteins in numerous cell types (Fu, Wang, Li, Sakamaki, & Pestell, 2004). Likewise, Alao et al. (2006) has shown that the sequestration of the cytoplasmic protein CyclinD1 impedes apoptosis in neuronal cells.

5.7 Concluding Remarks and Future Directions

In this study, overexpression of PrP^C in HSC-2, ACHN and LS 174T cancer cell lines confers resistant towards TNF- α -induced apoptosis by mediating Bax regulation and exhibits antioxidant activity during H₂O₂-induced oxidative stress. On contrary, such protective effect of PrP^C was diminished upon TUN-induced ER stress. Adding on to that, the sialoglycoprotein PrP^C was also shown to be implicated in cell proliferation and G₁- to S-phase transition. Taken together, the apparent physiological role of PrP^C observed from this study seems to portray a close connection of PrP^C to cancer progression.

However, we are now still at the initial stages of understanding the complex interplay between PrP^C and cancer biology. Investigating the underlying mechanism which relates to the physiological role of PrP^C remains an imperative source to comprehend its relation to carcinogenesis as well as in prion diseases. Hence, it would be desirable to extend the finding of this study to *in vivo* models as this is indispensable since the development of an animal study *in vivo* will greatly aid in deciphering the molecular mechanisms of the role ascribed to PrP^C, and how it might be subverted during carcinogenesis and prion diseases.

It has been shown that HSC-2 cells highly expresses endogenous PrP^C. Effectively, overexpression of endogenous PrP^C has also been documented in other cancer cells as described earlier. Hence, studying the association of PrP^C as well as its polymorphic variants such as those which involved in prion

diseases with cancer might shed new light in finding a potential early tumour marker to improve cancer prognosis. Moreover, it is worthwhile to study the degree of proliferation and pattern of invasiveness in PrP^C and its polymorphic variants via behavioural profiling as to determine the likelihood of carcinogenesis.

Pan et al. (2006) has previously demonstrated that in the presence of the N-terminal fragment (bases 24-90), PrP^C promotes invasion and metastasis in gastric cancer cell lines: SGC7901 and MKN45 through at least in part of, MEK/ERK pathway activation followed by transcriptional activation of matrix metalloproteinase-11 (MMP11). Thus, attributable to PrP^C insinuation in cancer biology by promoting cell proliferation, invasion and metastasis, suppression of PrP^C expression specifically the octarepeat region and the N-terminal fragment via RNAi might be a possible approach for therapeutic intervention in human cancer especially in the PrP^C overexpressing human gastric and oral cancer cell lines.

It is demonstrated in this study that PrP^C resists TNF- α -mediated cell death in the absence of Bax in LS 174T cells, although the exact mechanism has yet to be identified. Thus, it might be an interest to further elucidate the preferable signalling pathway activated by PrP^C in LS 174T upon TNF- α treatment. RNAi might be a merit approach for screening of cellular pathways involved. Upon having the targeted pathway, further study such as DNA microarray, real time-PCR (RT-PCR), reporter assay as well as Western blot analysis can be applied.

The occurrence of the fragment p19-22 upon glycosylation inhibition of PrP^C and its association to the unglycosylated PrP isoform at 27kDa remains elusive. Future study should be extended to characterize the biochemical properties and possibly the physiological role of the 19-22kDa species during glycosylation inhibition of PrP^C. Proteinase K digestion and detergent solubility assay should be performed for this fragment to determine whether it has PrP^{Sc}-like properties or not (Taraboulos et al., 1990).

CHAPTER 6

CONCLUSIONS

In this study, MTT analysis revealed that there was 10-15% increment of cell viability between the PrP^C expressing group and vector-transfected group in ACHN and LS 174T upon TNF- α treatment at 100ng/ml for 48hr. It has been shown that PrP^C exerts its protective effect in TNF- α -mediated cell death through Bax regulation independent of the anti-apoptotic Bcl-xL. It is speculated that there might be the presence of other pathways that are engaged by PrP^C to exert its protective activity against TNF- α -mediated cell death which does not involve the participation of Bax, since LS 174T is negative for Bax expression.

These findings further drew attention to the undisputable antioxidant role of PrP^C during oxidative stress-induced cell death. Upon H₂O₂ treatment at 0.2mM for 24hr, MTT analysis showed up to 80% of PrP^C expressing LS 174T cells remained viable compared to 60% of untransfected control cells while down-regulation of endogenous PrP^C sensitizes HSC-2 to H₂O₂ toxicity by reducing the cell viability to 50% compared with 80% viability in the non-PrP^C depleted HSC-2 cells. FITC Annexin V–PI dual staining showed that the protective effect of PrP against H₂O₂-mediated cell death was via an anti-apoptotic mechanism while DCFH-DA based assay demonstrated that PrP^C acts as a free radical scavenger during oxidative stress.

The initiation of apoptosis upon PrP^C N-linked glycosylation inhibition using TUN has been demonstrated in MTT analysis. Accumulation of death cells in the LR and UR quadrant via FITC Annexin V-PI flow cytometry analysis further confirms that the cell death mechanism induced by unglycosylated PrP upon TUN treatment is via apoptosis. DCFH-DA based assay revealed that the ROS scavenging activity of PrP^C was suppressed upon ER stress induction in cells.

A basal cell cycle analysis screening in transiently pcDNA 3.1-PrP transfected HSC-2, ACHN and LS 174T cancer cells revealed the proliferative ability of PrP^C. Further cell cycle synchronization using TUN in PrP^C overexpressing LS 174T cancer cells showed that PrP^C modulates cell cycle progression, which in turn, enhances cell proliferation by promoting G₁- to S-phase transition in a cell- and time-dependent manner. Conversely, the PrP^C depleted HSC-2 cells showed the reverse effect.

Taken together, the apparent physiological role of PrP^C observed from this study seems to portray a close connection between PrP^C and cancer progression. Inhibition of PrP^C expression in cancer cells may provide a new therapeutic strategy. A plausible cancer therapeutic strategy by involving the perturbation of PrP^C expression might as well relate to the defect in copper transport systems, as PrP^C is a high-affinity copper binding protein itself. This is encouraging since there are evidences that copper transport mechanisms may play a role in drug resistance. Besides, the aggravation of apoptosis and induction of oxidative stress in cancer cells expressing the unglycosylated

variant of PrP implicates the potential role of TUN as an anticancer agent or a potent enhancer during cancer therapy especially in cancer cells overexpressing PrP^C.

Based on the findings, it is concluded that PrP^C might have numerous important implications for carcinogenesis. Although the exact mechanism involved in the anti-apoptotic and cell cycle progression were not extensively explored in this study, the results here provide a stimulus for further studies on the role of PrP^C in cancer biology not just in the apoptotic and cell cycle pathways, but also in other hallmarks of cancer involving replicative potential, angiogenesis, and tissue invasion and metastasis.

REFERENCES

- Addgene. (2006). *pLKO.1 - TRC Cloning Vector*. Retrieved November 26, 2010, from <http://www.addgene.org/pgvec1?f=c&cmd=showcol&colid=170&page=2>
- Addgene. (n.d.). *Plasmid 1765: pBABE-hygro*. Retrieved November 10, 2010, from <http://www.addgene.org/pgvec1?f=c&cmd=findpl&identifier=1765>
- Adrain, C., Creagh, E. M., & Martin, S. J. (2001). Apoptosis-associated release of Smac/DIABLO from mitochondria requires active caspases and is blocked by Bcl-2. *The EMBO Journal*, 20(23), 6627-6636.
- Agrawal, N., Dasaradhi, P. V., Mohammed, A., Malhotra, P., Bhatnagar, R. K., & Mukherjee, S. K. (2003). RNA interference: Biology, mechanism, and applications. *Microbiology and Molecular Biology Reviews*, 67(4), 657-685.
- Alao, J. P., Gamble, S. C., Stavropoulou, A. V., Pomeranz, K. M., Lam, E. W., Coombes, R. C., et al. (2006). The cyclin D1 proto-oncogene is sequestered in the cytoplasm of mammalian cancer cell lines. *Molecular Cancer*, 5, 7.
- Albina, J. E., Cui, S., Mateo, R. B., & Reichner, J. S. (1993). Nitric oxide-mediated apoptosis in murine peritoneal macrophages. *The Journal of Immunology*, 150(11), 5080-5085.
- Alenzi, F. Q. (2004). Links between apoptosis, proliferation and the cell cycle. *British Journal of Biomedical Science*, 61(2), 99-102.
- Anantharam, V., Kanthasamy, A., Choi, C. J., Martin, D. P., Latchoumycandane, C., Richt, J. A., et al. (2008). Opposing roles of prion protein in oxidative stress- and ER stress-induced apoptotic signaling. *Free Radical Biology & Medicine*, 45(11), 1530-1541.
- Andersson, S., Davis, D. L., Dahlbäck, H., Jörnvall, H., & Russell, D. W. (1989). Cloning, structure, and expression of the mitochondrial cytochrome P-450 sterol 26-hydroxylase, a bile acid biosynthetic enzyme. *The Journal of Biological Chemistry*, 264(14), 8222-8229.
- Aplin, A. E., Howe, A., Alahari, S. K., & Juliano, R. L. (1998). Signal transduction and signal modulation by cell adhesion receptors: The role of integrins, cadherins, immunoglobulin-cell adhesion molecules, and selectins. *Pharmacology Reviews*, 50(2), 197-263.

- Aronoff-Spencer, E., Burns, C. S., Avdievich, N. I., Gerfen, G. J., Peisach, J., Antholine, W. E., et al. (2000). Identification of the Cu²⁺ binding sites in the N-terminal domain of the prion protein by EPR and CD spectroscopy. *Biochemistry*, 39(45), 13760-13771.
- Bajt, M. L., Cover, C., Lemasters, J. J., & Jaeschke, H. (2006). Nuclear translocation of endonuclease G and apoptosis-inducing factor during acetaminophen-induced liver cell injury. *Toxicological Sciences*, 94(1), 217-225.
- Basler, K., Oesch, B., Scott, M., Westaway, D., Walchli, M., Groth, D. F., et al. (1986). Scrapie and cellular PrP isoforms are encoded by the same chromosomal gene. *Cell*, 46(3), 417-428.
- Basu, A., Castle, V. P., Bouziane, M., Bhalla, K., & Haldar, S. (2006). Crosstalk between extrinsic and intrinsic cell death pathways in pancreatic cancer: Synergistic action of estrogen metabolite and ligands of death receptor family. *Cancer Research*, 66(8), 4309-4318.
- Bernards, R. (2006). Exploring the uses of RNAi--gene knockdown and the Nobel Prize. *The New England Journal of Medicine*, 355(23), 2391-2393.
- Boshart, M., Weber, F., Jahn, G., Dorsch-Häsler, K., Fleckenstein, B., & Schaffner, W. (1985). A very strong enhancer is located upstream of an immediate early gene of human cytomegalovirus. *Cell*, 41(2), 521-530.
- Bounhar, Y., Mann, K. K., Roucou, X., & LeBlanc, A. C. (2006). Prion protein prevents Bax-mediated cell death in the absence of other Bcl-2 family members in *Saccharomyces cerevisiae*. *FEMS Yeast Research*, 6(8), 1204-1212.
- Bounhar, Y., Zhang, Y., Goodyer, C. G., & LeBlanc, A. (2001). Prion protein protects human neurons against Bax-mediated apoptosis. *The Journal of Biological Chemistry*, 276(42), 39145-39149.
- Boye, E., & Nordström, K. (2003). Coupling the cell cycle to cell growth. *EMBO Reports*, 4(8), 757-760.
- Brown, D. R., & Besinger, A. (1998). Prion protein expression and superoxide dismutase activity. *Biochemical Journal*, 334(Pt 2), 423-429.
- Brown, D. R., Wong, B. S., Hafiz, F., Clive, C., Haswell, S. J., & Jones, I. M. (1999). Normal prion protein has an activity like that of superoxide dismutase. *Biochemical Journal*, 344(Pt 1), 1-5.
- Brown, K., & Mastrianni, J. A. (2010). The prion diseases. *Journal of Geriatric Psychiatry and Neurology*, 23(4), 277-298.

- Bryan, T. M., & Cech, T. R. (1999). Telomerase and the maintenance of chromosome ends. *Current Opinion in Cell Biology*, *11*(3), 318-324.
- Büeler, H., Fischer, M., Lang, Y., Bluethmann, H., Lipp, H. P., DeArmond, S. J., et al. (1992). Normal development and behaviour of mice lacking the neuronal cell-surface PrP protein. *Nature*, *356*(6370), 577-582.
- Buttke, T. M., & Sandstrom, P. A. (1994). Oxidative stress as a mediator of apoptosis. *Immunology Today*, *15*(1), 7-10.
- Capellari, S., Parchi, P., Russo, C. M., Sanford, J., Sy, M. S., Gambetti, P., et al. (2000). Effect of the E200K mutation on prion protein metabolism. Comparative study of a cell model and human brain. *The American Journal of Pathology*, *157*(2), 613-622.
- Cardoso, M. C., & Leonhardt, H. (1999). Differentiation, Development, and Programmed Cell Death. In G. S. Stein, R. Baserga, A. Giordano, & D. T. Denhardt (Eds.), *The Molecular Basis of Cell Cycle and Growth Control* (pp. 305-347). New York, NY: John Wiley & Sons.
- Carimalo, J., Cronier, S., Petit, G., Peyrin, J. M., Boukhtouche, F., Arbez, N., et al. (2005). Activation of the JNK-c-Jun pathway during the early phase of neuronal apoptosis induced by PrP106-126 and prion infection. *European Journal of Neuroscience*, *21*(9), 2311-2319.
- Carlberg, M., Dricu, A., Blegen, H., Kass, G. E. N., Orrenius, S., & Larsson, O. (1996). Short exposures to tunicamycin induce apoptosis in SV40-transformed but not in normal human fibroblasts. *Carcinogenesis*, *17*(12), 2589-2596.
- Castilla, J., Saá, P., Hetz, C., & Soto, C. (2005). *In vitro* generation of infectious scrapie prions. *Cell*, *121*(2), 195-206.
- Caughey, B., Baron, G. S., Chesebro, B., & Jeffrey, M. (2009). Getting a grip on prions: Oligomers, amyloids, and pathological membrane interactions. *Annual Review of Biochemistry*, *78*, 177-204.
- Caughey, B., Kocisko, D. A., Raymond, G. J., & Lansbury, P. T. Jr. (1995). Aggregates of scrapie-associated prion protein induce the cell-free conversion of protease-sensitive prion protein to the protease-resistant state. *Chemistry & Biology*, *2*(12), 807-817.
- Chen, L., Yang, Y., Han, J., Zhang, B. Y., Zhao, L., Nie, K., et al. (2007). Removal of the glycosylation of prion protein provokes apoptosis in SF126. *Journal of Biochemistry & Molecular Biology*, *40*(5), 662-669.
- Chen, S. G., Teplow, D. B., Parchi, P., Teller, J. K., Gambetti, P., & Autilio-Gambetti, L. (1995). Truncated forms of the human prion protein in normal brain and in prion diseases. *The Journal of Biological Chemistry*, *270*(32), 19173-19180.

- Chen-Scarabelli, C., & Scarabelli, T. M. (2004). Turning necrosis into apoptosis: The exacting task that can enhance survival. *American Heart Journal*, 148(2), 196-199.
- Choi, C. J., Anantharam, V., Saetveit, N. J., Houk, R. S., Kanthasamy, A., & Kanthasamy, A. G. (2007). Normal cellular prion protein protects against manganese-induced oxidative stress and apoptotic cell death. *Toxicological Sciences*, 98(2), 495-509.
- Christensen, H. M., & Harris, D. A. (2008). Prion protein lacks robust cytoprotective activity in cultured cells. *Molecular Neurodegeneration*, 3, 11.
- Clohessy, J. G., Zhuang, J., de Boer, J., Gil-Gómez, G., & Brady, H. J. (2006). Mcl-1 interacts with truncated Bid and inhibits its induction of cytochrome *c* release and its role in receptor-mediated apoptosis. *The Journal of Biological Chemistry*, 281(9), 5750-5759.
- Cobb, N. J., & Surewicz, W. K. (2009). Prion diseases and their biochemical mechanisms. *Biochemistry*, 48(12), 2574-2585.
- Colling, S. B., Khana, M., Collinge, J., & Jefferys, J. G. (1997). Mossy fibre reorganization in the hippocampus of prion protein null mice. *Brain Research*, 755(1), 28-35.
- Cooper, G. M., & Hausman, R. E. (2004). Regulation of programmed cell death. In *The Cell: A Molecular Approach* (3rd ed., pp. 579-582). Sunderland, MA: Sinauer Associates.
- Corpet, F. (1988). Multiple sequence alignment with hierarchical clustering. *Nucleic Acids Research*, 16(22), 10881-10890.
- Counter, C. M., Avilion, A. A., LeFeuvre, C. E., Stewart, N. G., Greider, C. W., Harley, C. B., et al. (1992). Telomere shortening associated with chromosome instability is arrested in immortal cells which express telomerase activity. *The EMBO Journal*, 11(5), 1921-1929.
- Criado, J. R., Sánchez-Alavez, M., Conti, B., Giacchino, J. L., Wills, D. N., Henriksen, S. J., et al. (2005). Mice devoid of prion protein have cognitive deficits that are rescued by reconstitution of PrP in neurons. *Neurobiology of Disease*, 19(1-2), 255-265.
- Crozet, C., Beranger, F., & Lehmann, S. (2008). Cellular pathogenesis in prion diseases. *Veterinary Research*, 39(4), 44.
- De Souza, C. P., & Osmani, S. A. (2007). Mitosis, not just open or closed. *Eukaryotic Cell*, 6(9), 1521-1527.

- Dejean, L. M., Martinez-Caballero, S., Manon, S., & Kinnally, K. W. (2006). Regulation of the mitochondrial apoptosis-induced channel, MAC, by BCL-2 family proteins. *Biochimica et Biophysica Acta*, 1762(2), 191-201.
- Deleault, N. R., Harris, B. T., Rees, J. R., & Supattapone, S. (2007). Formation of native prions from minimal components *in vitro*. *Proceedings of the National Academy of Sciences of the USA*, 104(23), 9741-9746.
- Deli, M. A., Sakaguchi, S., Nakaoke, R., Abrahám, C. S., Takahata, H., Kopacek, J., et al. (2000). PrP fragment 106-126 is toxic to cerebral endothelial cells expressing PrP(C). *NeuroReport*, 11(17), 3931-3936.
- Di Pietro, A., Dayan, G., Conseil, G., Steinfels, E., Krell, T., Trompier, D., et al. (1999). P-glycoprotein-mediated resistance to chemotherapy in cancer cells: Using recombinant cytosolic domains to establish structure-function relationships. *Brazilian Journal of Medical and Biological Research*, 32(8), 925-939.
- Diarra-Mehrpour, M., Arrabal, S., Jalil, A., Pinson, X., Gaudin, C., Piétu, G., et al. (2004). Prion protein prevents human breast carcinoma cell line from tumor necrosis factor alpha-induced cell death. *Cancer Research*, 64(2), 719-727.
- Dricu, A., Carlberg, M., Wang, M., & Larsson, O. (1997). Inhibition of N-linked glycosylation using tunicamycin causes cell death in malignant cells: Role of down-regulation of the insulin-like growth factor 1 receptor in induction of apoptosis. *Cancer Research*, 57(3), 543-548.
- Drisaldi, B., Stewart, R. S., Adles, C., Stewart, L. R., Quaglio, E., Biasini, E., et al. (2003). Mutant PrP is delayed in its exit from the endoplasmic reticulum, but neither wild-type nor mutant PrP undergoes retrotranslocation prior to proteasomal degradation. *The Journal of Biological Chemistry*, 278(24), 21732-21743.
- Du, J., Pan, Y., Shi, Y., Guo, C., Jin, X., Sun, L., et al. (2005). Overexpression and significance of prion protein in gastric cancer and multidrug-resistant gastric carcinoma cell line SGC7901/ADR. *International Journal of Cancer*, 113(2), 213-220.
- Dyxhoorn, D. M., Novina, C. D., & Sharp, P. A. (2003). Killing the messenger: Short RNAs that silence gene expression. *Nature Reviews Molecular Cell Biology*, 4(6), 457-467.
- Ekwall, K. (2004). The RITS complex-A direct link between small RNA and heterochromatin. *Molecular Cell*, 13(3), 304-305.
- Endo, T., Groth, D., Prusiner, S. B., & Kobata, A. (1989). Diversity of oligosaccharide structures linked to asparagines of the scrapie prion protein. *Biochemistry*, 28(21), 8380-8388.

- Erlich, R. B., Kahn, S. A., Lima, F. R., Muras, A. G., Martins, R. A., Linden, R., et al. (2007). STI1 promotes glioma proliferation through MAPK and PI3K pathways. *Glia*, 55(16), 1690-1698.
- Ermonval, M., Mouillet-Richard, S., Codogno, P., Kellermann, O., & Botti, J. (2003). Evolving views in prion glycosylation: Functional and pathological implications. *Biochimie*, 85(1-2), 33-45.
- Esko, J. (1999). Natural and Synthetic Inhibitors of Glycosylation. In A. Varki, R. Cummings, J. Esko, H. Freeze, G. Hart, & J. Marth (Eds.), *Essentials of Glycobiology*. Cold Spring Harbor, NY: Cold Spring Harbor Laboratory Press.
- Esposti, M. D., Erler, J. T., Hickman, J. A., & Dive, C. (2001). Bid, a widely expressed proapoptotic protein of the Bcl-2 family, displays lipid transfer activity. *Molecular and Cellular Biology*, 21(21), 7268-7276.
- Ettaiche, M., Pichot, R., Vincent, J. P., & Chabry, J. (2000). *In vivo* cytotoxicity of the prion protein fragment 106-126. *The Journal of Biological Chemistry*, 275(47), 36487-36490.
- Evan, G. I., & Vousden, K. H. (2001). Proliferation, cell cycle and apoptosis in cancer. *Nature*, 411(6835), 342-348.
- Farr, A., & Roman, A. (1992). A pitfall of using a second plasmid to determine transfection efficiency. *Nucleic Acids Research*, 20(4), 920.
- Fedi, P., Tronick, S. R., & Aaronson, S. A. (1997). Growth Factors. In J. F. Holland, R. C. Bast, D. L. Morton, E. Frei, D. W. Kufe, & R. R. Weichselbaum (Eds.), *Cancer Medicine* (pp. 41-64). Baltimore, MD: WilliamsWilkins.
- Fiebig, A. A., Zhu, W., Hollerbach, C., Leber, B., & Andrews, D. W. (2006). Bcl-XL is qualitatively different from and ten times more effective than Bcl-2 when expressed in a breast cancer cell line. *BMC Cancer*, 6, 213.
- Fiedler, K., & Simons, K. (1995). The role of N-glycans in the secretory pathway. *Cell*, 81(3), 309-312.
- Fire, A., Xu, S., Montgomery, M. K., Kostas, S. A., Driver, S. E., & Mello, C. C. (1998). Potent and specific genetic interference by double-stranded RNA in *Caenorhabditis elegans*. *Nature*, 391(6669), 806-811.
- Foster, I. (2008). Cancer: A cell cycle defect. *Radiography*, 14(2), 144-149.
- Fotedar, R., Diederich, L., & Fotedar, A. (1996). Apoptosis and the cell cycle. *Progress in Cell Cycle Research*, 2, 147-163.

- Fu, M., Wang, C., Li, Z., Sakamaki, T., & Pestell, R. G. (2004). Minireview: Cyclin D1: Normal and abnormal functions. *Endocrinology*, *145*(12), 5439-5447.
- Galerija SLU Niš. (n.d.). *PCMV SPORT6*. Retrieved June 13, 2011, from <http://gslunis.org/palanski-skulpture/pcmv-sport6&page=7>
- Gaur, U., & Aggarwal, B. B. (2003). Regulation of proliferation, survival and apoptosis by members of the TNF superfamily. *Biochemical Pharmacology*, *66*(8), 1403-1408.
- Ghobrial, I. M., Witzig, T. E., & Adjei, A. A. (2005). Targeting apoptosis pathways in cancer therapy. *CA: A Cancer Journal for Clinicians*, *55*(3), 178-194.
- Giménez-Bonafé, P., Tortosa, A., & Pérez-Tomás, R. (2009). Overcoming drug resistance by enhancing apoptosis of tumor cells. *Current Cancer Drug Targets*, *9*(3), 320-340.
- González-Iglesias, R., Pajares, M. A., Ocal, C., Espinosa, J. C., Oesch, B., & Gasset, M. (2002). Prion protein interaction with glycosaminoglycan occurs with the formation of oligomeric complexes stabilized by Cu(II) bridges. *Journal of Molecular Biology*, *319*(2), 527-540.
- Goodwin, E. C., & Rottman, F. M. (1992). The 3'-flanking sequence of the bovine growth hormone gene contains novel elements required for efficient and accurate polyadenylation. *The Journal of Biology Chemistry*, *267*(23), 16330-16334.
- Govaerts, C., Wille, H., Prusiner, S. B., & Cohen, F. E. (2004). Evidence for assembly of prions with left-handed beta-helices into trimers. *Proceedings of the National Academy of Sciences of the USA*, *101*(22), 8342-8347.
- Gozzelino, R., Sole, C., Llecha, N., Segura, M. F., Moubarak, R. S., Iglesias-Guimaraes, V., et al. (2008). BCL-XL regulates TNF-alpha-mediated cell death independently of NF-kappaB, FLIP and IAPs. *Cell Research*, *18*(10), 1020-1036.
- Graner, E., Mercadante, A. F., Zanata, S. M., Forlenza, O. V., Cabral, A. L., Veiga, S. S., et al. (2000). Cellular prion protein binds laminin and mediates neuritogenesis. *Molecular Brain Research*, *76*(1), 85-92.
- Green, D. R., & Kroemer, G. (2004). The pathophysiology of mitochondrial cell death. *Science*, *305*(5684), 626-629.
- Halliwell, B. (2006). Oxidative stress and neurodegeneration: Where are we now? *Journal of Neurochemistry*, *97*(6), 1634-1658.

- Hammond, S. M. (2005). Dicing and slicing: The core machinery of the RNA interference pathway. *FEBS Letters*, 579(26), 5822-5829.
- Hanahan, D., & Folkman, J. (1996). Patterns and emerging mechanisms of the angiogenic switch during tumorigenesis. *Cell*, 86(3), 353-364.
- Hanahan, D., & Weinberg, R. A. (2000). The hallmarks of cancer. *Cell*, 100(1), 57-70.
- Hancock, J. T. (2010). Life, Death, and Apoptosis. In *Cell Signalling* (3rd ed., pp. 314-324). Lavis, TN: Oxford University Press.
- Harding, H. P., Novoa, I., Zhang, Y., Zeng, H., Wek, R., Schapira, M., et al. (2000). Regulated translation initiation controls stress-induced gene expression in mammalian cells. *Molecular Cell*, 6(5), 1099-1108.
- Harris, C. C. (1996). p53 tumor suppressor gene: From the basic research laboratory to the clinician abridged historical perspective. *Carcinogenesis*, 17(6), 1187-1198.
- Harris, D. A. (1999). Cellular biology of prion diseases. *Clinical Microbiology Review*, 12(3), 429-444.
- Hegde, R. S., Mastrianni, J. A., Scott, M. R., DeFea, K. A., Tremblay, P., Torchia, M., et al. (1998). A transmembrane form of the prion protein in neurodegenerative disease. *Science*, 279(5352), 827-834.
- Helenius, A. (1994). How N-linked oligosaccharides affect glycoprotein folding in the endoplasmic reticulum. *Molecular Biology of the Cell*, 5(3), 253-265.
- Hengartner, M. O. (2000). The biochemistry of apoptosis. *Nature*, 407(6805), 770-776.
- Hileman, E. O., Liu, J., Albitar, M., Keating, M. J., & Huang, P. (2004). Intrinsic oxidative stress in cancer cells: A biochemical basis for therapeutic selectivity. *Cancer Chemotherapy & Pharmacology*, 53(3), 209-219.
- Hiss, D. C., Gabriels, G. A., & Folb, P. I. (2007). Combination of tunicamycin with anticancer drugs synergistically enhances their toxicity in multidrug-resistant human ovarian cystadenocarcinoma cells. *Cancer Cell International*, 7, 5.
- Holada, K., Simak, J., Risitano, A. M., Maciejewski, J., Young, N. S., & Vostal, J. G. (2002). Activated platelets of patients with paroxysmal nocturnal hemoglobinuria express cellular prion protein. *Blood*, 100(1), 341-343.

- Holscher, C., Bach, U. C., & Dobberstein, B. (2001). Prion protein contains a second endoplasmic reticulum targeting signal sequence located at its C terminus. *The Journal of Biological Chemistry*, 276(16), 13388–13394.
- Hotchkiss, R. S., & Nicholson, D. W. (2006). Apoptosis and caspases regulate death and inflammation in sepsis. *Nature Reviews Immunology*, 6(11), 813-822.
- Hsieh, Y. H., Su, I. J., Lei, H. Y., Lai, M. D., Chang, W. W., & Huang, W. (2007). Differential endoplasmic reticulum stress signaling pathways mediated by iNOS. *Biochemical and Biophysical Research Communications*, 359(3), 643-648.
- Invitrogen™. (n.d.). *pcDNA™ 3.1D/V5-His-TOPO® 5514 bp*. Retrieved November 10, 2010, from http://tools.invitrogen.com/content/sfs/vectors/pcdna3_1dv5histopo_map.pdf
- Jiménez-Huete, A., Lievens, P. M., Vidal, R., Piccardo, P., Ghetti, B., Tagliavini, F., et al. (1998). Endogenous proteolytic cleavage of normal and disease-associated isoforms of the human prion protein in neural and non-neural tissues. *The American Journal of Pathology*, 153(5), 1561-1572.
- Joao, H. C., & Dwek, R. A. (1993). Effects of glycosylation on protein structure and dynamics in ribonuclease B and some of its individual glycoforms. *European Journal of Biochemistry*, 218(1), 239-244.
- Jodoin, J., Laroche-Pierre, S., Goodyer, C. G., & LeBlanc, A. C. (2007). Defective retrotranslocation causes loss of anti-Bax function in human familial prion protein mutants. *The Journal of Neuroscience*, 27(19), 5081-5091.
- Jodoin, J., Misiewicz, M., Makhijani, P., Giannopoulos, P. N., Hammond, J., Goodyer, C. G., et al. (2009). Loss of anti-Bax function in Gerstmann-Sträussler-Scheinker syndrome-associated prion protein mutants. *PLoS One*, 4(8), e6647.
- Kanaani, J., Prusiner, S. B., Diacovo, J., Baekkeskov, S., & Legname, G. (2005). Recombinant prion protein induces rapid polarization and development of synapses in embryonic rat hippocampal neurons *in vitro*. *Journal of Neurochemistry*, 95(5), 1373-1386.
- Kaufman, R. J. (1999). Stress signaling from the lumen of the endoplasmic reticulum: Coordination of gene transcriptional and translational controls. *Genes & Development*, 13(10), 1211-1233.
- Kim, K., Lee, Y. S., Harris, D., Nakahara, K., & Carthew, R. W. (2006). The RNAi pathway initiated by Dicer-2 in *Drosophila*. *Cold Spring Harbor Symposia on Quantitative Biology*, 71, 39-44.

- Kim, S. J., & Hegde, R. S. (2002). Cotranslational partitioning of nascent prion protein into multiple populations at the translocation channel. *Molecular Biology of the Cell*, 13(11), 3775–3786.
- Kim, S. J., Rahbar, R., & Hegde, R. S. (2001). Combinatorial control of prion protein biogenesis by the signal sequence and transmembrane domain. *The Journal of Biological Chemistry*, 276(28), 26132–26140.
- Knutson, J. C., & Yee, D. (1987). Electroporation: Parameters affecting transfer of DNA into mammalian cells. *Analytical Biochemistry*, 164(1), 44-52.
- Kochevar, J. (1990). Blockage of autonomous growth of ACHN cells by anti renal cell carcinoma monoclonal antibody 5F4. *Cancer Research*, 50(10), 2968-2972.
- Konturek, P. C., Bazela, K., Kukharsky, V., Bauer, M., Hahn, E. G., & Schuppa, D. (2005). *Helicobacter pylori* upregulates prion protein expression in gastric mucosa: A possible link to prion disease. *World Journal of Gastroenterology*, 11(48), 7651–7656.
- Korth, C., Kaneko, K., & Prusiner, S. B. (2000). Expression of unglycosylated mutated prion protein facilitates PrP(Sc) formation in neuroblastoma cells infected with different prion strains. *Journal of General Virology*, 81(Pt 10), 2555-2563.
- Kralovicova, S., Fontaine, S. N., Alderton, A., Alderman, J., Ragnarsdottir, K. V., Collins, S. J., et al. (2009). The effects of prion protein expression on metal metabolism. *Molecular and Cellular Neuroscience*, 41(2), 135-147.
- Laroche-Pierre, S., Jodoin, J., & LeBlanc, A. C. (2009). Helix 3 is necessary and sufficient for prion protein's anti-Bax function. *Journal of Neurochemistry*, 108(4), 1019-10131.
- Lawson, V. A., Collins, S. J., Masters, C. L., & Hill, A. F. (2005). Prion protein glycosylation. *Journal of Neurochemistry*, 93(4), 793-801.
- Lehmann, S., & Harris, D. A. (1997). Blockade of glycosylation promotes acquisition of scrapie-like properties by the prion protein in cultured cells. *The Journal of Biological Chemistry*, 272(34), 21479-21487.
- Lehmann, S., Milhavet, O., & Mangé, A. (1999). Trafficking of the cellular isoform of the prion protein. *Biomedicine & Pharmacotherapy*, 53(1), 39-46.
- Lewis, V., & Collins, S. J. (2008). Analysis of endogenous PrPC processing in neuronal and non-neuronal cell lines. *Methods in Molecular Biology*, 459, 229-239.

- Li, A., & Harris, D. A. (2005). Mammalian prion protein suppresses Bax-induced cell death in yeast. *The Journal of Biological Chemistry*, 280(17), 17430-17434.
- Li, C., Yu, S., Nakamura, F., Yin, S., Xu, J., Petrolla, A. A., et al. (2009). Binding of pro-prion to filamin A disrupts cytoskeleton and correlates with poor prognosis in pancreatic cancer. *The Journal of Clinical Investigation*, 119(9), 2725-2736.
- Li, Q. Q., Cao, X. X., Xu, J. D., Chen, Q., Wang, W. J., Tang, F., et al. (2009). The role of P-glycoprotein/cellular prion protein interaction in multidrug-resistant breast cancer cells treated with paclitaxel. *Cellular and Molecular Life Sciences*, 66(3), 504-515.
- Liang, J., Bai, F., Luo, G., Wang, J., Liu, J., Ge, F., et al. (2007). Hypoxia induced overexpression of PrP(C) in gastric cancer cell lines. *Cancer Biology and Therapy*, 6(5), 769-774.
- Liang, J., Ge, F. L., Lu, Y. Y., Wang, J., Zhai, H. H., Yao, L. P., et al. (2006). Role of PrPc related to apoptosis. *EXCLI Journal*, 5, 11-24.
- Liang, J., Pan, Y. L., Ning, X. X., Sun, L. J., Lan, M., Hong, L., et al. (2006). Overexpression of PrPC and its antiapoptosis function in gastric cancer. *Tumour Biology*, 27(2), 84-91.
- Liang, J., Pan, Y., Zhang, D., Guo, C., Shi, Y. Wang, J., et al. (2007). Cellular prion protein promotes proliferation and G1/S transition of human gastric cancer cells SGC7901 and AGS. *The FASEB Journal*, 21(9), 2247-2256.
- Lin, D. T., Jodoin, J., Baril, M., Goodyer, C. G., & Leblanc, A. C. (2008). Cytosolic prion protein is the predominant anti-Bax prion protein form: Exclusion of transmembrane and secreted prion protein forms in the anti-Bax function. *Biochimica et Biophysica Acta*, 1783(10), 2001-2012.
- Locksley, R. M., Killeen, N., & Lenardo, M. J. (2001). The TNF and TNF receptor superfamilies: Integrating mammalian biology. *Cell*, 104(4), 487-501.
- Malaisé, M., Schätzl, H. M., & Bürkle, A. (2008). The octarepeat region of prion protein, but not the TM1 domain, is important for the antioxidant effect of prion protein. *Free Radical Biology & Medicine*, 45(12), 1622-1630.
- Malhotra, J. D., & Kaufman, R. J. (2007). Endoplasmic reticulum stress and oxidative stress: A vicious cycle or a double-edged sword? *Antioxidants & Redox Signaling*, 9(12), 2277-2293.

- Malhotra, J. D., Miao, H., Zhang, K., Wolfson, A., Pennathur, S., Pipe, S. W., et al. (2008). Antioxidants reduce endoplasmic reticulum stress and improve protein secretion. *Proceedings of the National Academy of Sciences of the USA*, 105(47), 18525-18530.
- Mangé, A., Béranger, F., Peoc'h, K., Onodera, T., Frobert, Y., & Lehmann, S. (2004). Alpha- and beta- cleavages of the amino-terminus of the cellular prion protein. *Biology of the Cell*, 96(2), 125-132.
- Manuelidis, L. (2007). A 25 nm virion is the likely cause of transmissible spongiform encephalopathies. *Journal of Cellular Biochemistry*, 100(4), 897-915.
- Manuelidis, L., Yu, Z. X., Barquero, N., & Mullins, B. (2007). Cells infected with scrapie and Creutzfeldt-Jakob disease agents produce intracellular 25-nm virus-like particles. *Proceedings of the National Academy of Sciences of the USA*, 104(6), 1965-1970.
- McEwan, J. F., Windsor, M. L., & Cullis-Hill, S. D. (2009). Antibodies to prion protein inhibit human colon cancer cell growth. *Tumour Biology*, 30(3), 141-147.
- McMahon, H. E., Mangé, A., Nishida, N., Créminon, C., Casanova, D., & Lehmann, S. (2001). Cleavage of the amino terminus of the prion protein by reactive oxygen species. *Journal of Cellular Biochemistry*, 276(3), 2286-2291.
- McNally, K. L., Ward, A. E., & Priola, S. A. (2009). Cells expressing anchorless prion protein are resistant to scrapie infection. *The Journal of Virology*, 83(9), 4469-4475.
- Mehrpour, M., & Codogno, P. (2010). Prion protein: From physiology to cancer biology. *Cancer Letters*, 290(1), 1-23.
- Meister, G., & Tuschl, T. (2004). Mechanisms of gene silencing by double-stranded RNA. *Nature*, 431(7006), 343-349.
- Meslin, F., Conforti, R., Mazouni, C., Morel, N., Tomasic, G., Drusch, F., et al. (2007). Efficacy of adjuvant chemotherapy according to prion protein expression in patients with estrogen receptor-negative breast cancer. *Annals of Oncology*, 18(11), 1793-1798.
- Minn, A. J., Kettlun, C. S., Liang, H., Kelekar, A., Vander Heiden, M. G., Chang, B. S., et al. (1999). Bcl-xL regulates apoptosis by heterodimerization-dependent and -independent mechanisms. *The EMBO Journal*, 18(3), 632-643.
- Mironov, A. Jr., Latawiec, D., Wille, H., Bouzamondo-Bernstein, E., Legname, G., Williamson, R. A., et al. (2003). Cytosolic prion protein in neurons. *The Journal of Neuroscience*, 23(18), 7183-7193.

- Miura, M., & Yuan, J. (2000). Transient transfection assay of cell death genes. *Methods in Enzymology*, 322, 480-492.
- Moffat, J., Grueneberg, D. A., Yang, X., Kim, S. Y., Kloepfer, A. M., Hinkle, G., et al. (2006). A lentiviral RNAi library for human and mouse genes applied to an arrayed viral high-content screen. *Cell*, 124(6), 1283-1298.
- Momose, F., Araida, T., Negishi, A., Ichijo, H., Shioda, S., & Sasaki, S. (1989). Variant sublines with different metastatic potentials selected in nude mice from human oral squamous cell carcinomas. *Journal of Oral Pathology & Medicine*, 18(7), 391-395.
- Moore, R. C., Lee, I. Y., Silverman, G. L., Harrison, P. M., Strome, R., Heinrich, C., et al. (1999). Ataxia in prion protein (PrP)-deficient mice is associated with upregulation of the novel PrP-like protein doppel. *Journal of Molecular Biology*, 292(4), 797-817.
- Müller, H., Strom, A., Hunsmann, G., & Stuke, A. W. (2005). Separation of native prion protein (PrP) glycoforms by copper-binding using immobilized metal affinity chromatography (IMAC). *Biochemical Journal*, 388(Pt 1), 371-378.
- National Cancer Institute. (2010). *Dictionary of Cancer Terms*. Retrieved November 21, 2010, from <http://www.cancer.gov/dictionary/?CdrID=44769>
- National Cancer Registry. (2006). *Malaysia Cancer Statistics, Data and Figure Peninsular Malaysia 2006*. Retrieved December 23, 2010, from http://www.moh.gov.my/images/gallery/Report/Cancer/MalaysiaCancerStatistics_2006.pdf
- Nelson, J. A., Reynolds-Kohler, C., & Smith, B. A. (1987). Negative and positive regulation by a short segment in the 5'-flanking region of the human cytomegalovirus major immediate-early gene. *Molecular and Cellular Biology*, 7(11), 4125-4129.
- Nicolas, O., Gavín, R., & del Río, J. A. (2009). New insights into cellular prion protein (PrP^c) functions: The "ying and yang" of a relevant protein. *Brain Research Reviews*, 61(2), 170-184.
- Nishimura, T., Sakudo, A., Nakamura, I., Lee, D. C., Taniuchi, Y., Saeki, K., et al. (2004). Cellular prion protein regulates intracellular hydrogen peroxide level and prevents copper-induced apoptosis. *Biochemical and Biophysical Research Communications*, 323(1), 218-222.
- Noda, I., Fujieda, S., Seki, M., Tanaka, N., Sunaga, H., Ohtsubo, T., et al. (1999). Inhibition of N-linked glycosylation by tunicamycin enhances sensitivity to cisplatin in human head-and-neck carcinoma cells. *International Journal of Cancer*, 80(2), 279-284.

- Orsi, A., Fioriti, L., Chiesa, R., & Sitia, R. (2006). Conditions of endoplasmic reticulum stress favor the accumulation of cytosolic prion protein. *The Journal of Biological Chemistry*, 281(41), 30431-30438.
- Owatari, S., Akune, S., Komatsu, M., Ikeda, R., Firth, S. D., Che, X. F., et al. (2007). Copper-transporting P-type ATPase, ATP7A, confers multidrug resistance and its expression is related to resistance to SN-38 in clinical colon cancer. *Cancer Research*, 67(10), 4860-4868.
- Paddison, P. J., Caudy, A. A., Bernstein, E., Hannon, G. J., Conklin, D. S. (2002). Short hairpin RNAs (shRNAs) induce sequence-specific silencing in mammalian cells. *Genes & Development*, 16(8), 948-958.
- Paitel, E., Fahraeus, R., & Checler, F. (2003). Cellular prion protein sensitizes neurons to apoptotic stimuli through Mdm2-regulated and p53-dependent caspase 3-like activation. *The Journal of Biological Chemistry*, 278(12), 10061-10066.
- Paitel, E., Sunyach, C., Alves da Costa, C., Bourdon, J. C., Vincent, B., & Checler, F. (2004). Primary cultured neurons devoid of cellular prion display lower responsiveness to staurosporine through the control of p53 at both transcriptional and post-transcriptional levels. *The Journal of Biological Chemistry*, 279(1), 612-618.
- Pammer, J., Suchy, A., Rendl, M., & Tschachler, E. (1999). Cellular prion protein expressed by bovine squamous epithelia of skin and upper gastrointestinal tract. *Lancet*, 354(9191), 1702-1703.
- Pan, Y., Zhao, L., Liang, J., Liu, J., Shi, Y., Liu, N., et al. (2006). Cellular prion protein promotes invasion and metastasis of gastric cancer. *The FASEB Journal*, 20(11), 1886-1888.
- Parodi, A. J. (2000). Role of N-oligosaccharide endoplasmic reticulum processing reactions in glycoprotein folding and degradation. *Biochemical Journal*, 348(Pt 1), 1-13.
- Pelicano, H., Carney, D., & Huang, P. (2004). ROS stress in cancer cells and therapeutic implications. *Drug Resistance Updates*, 7(2), 97-110.
- Perez, D., & White, E. (2000). TNF- α signals apoptosis through a Bid-dependent conformational change in Bax that is inhibited by E1B 19K. *Molecular Cell*, 6(1), 53-63.
- Perini, F., Vidal, R., Ghetti, B., Tagliavini, F., Frangione, B., & Prelli, F. (1996). PrP27-30 is a normal soluble prion protein fragment released by human platelets. *Biochemical and Biophysical Research Communications*, 223(3), 572-577.

- Petersen, R. B., Parchi, P., Richardson, S. L., Urig, C. B., & Gambetti, P. (1996). Effect of the D178N mutation and the codon 129 polymorphism on the metabolism of the prion protein. *The Journal of Biological Chemistry*, 271(21), 12661-12668.
- Petrakis, S., & Sklaviadis, T. (2006). Identification of proteins with high affinity for refolded and native PrPC. *Proteomics*, 6(24), 6476-6484.
- Pietri, M., Caprini, A., Mouillet-Richard, S., Pradines, E., Ermonval, M., Grassi J., et al. (2006). Overstimulation of PrPC signaling pathways by prion peptide 106-126 causes oxidative injury of bioaminergic neuronal cells. *The Journal of Biological Chemistry*, 281(38), 28470-28479.
- Promega. (2009). *Protocols & Applications Guide: Transfection*. Retrieved November 26, 2010, from <http://www.promega.com/paguide/chap12.htm>
- Prusiner, S. B. (1982). Novel proteinaceous infectious particles cause scrapie. *Science*, 216(4542), 136-144.
- Prusiner, S. B. (1998). Prions. *Proceedings of the National Academy of Sciences of the USA*, 95(23), 13363-13383.
- Qin, K., Zhao, L., Ash, R. D., McDonough, W. F., & Zhao, R. Y. (2009). ATM-mediated transcriptional elevation of prion in response to copper-induced oxidative stress. *The Journal of Biological Chemistry*, 284(7), 4582-4593.
- Raisova, M., Hossini, A. M., Eberle, J., Riebeling, C., Wieder, T., Sturm, I., et al. (2001). The Bax/Bcl-2 ratio determines the susceptibility of human melanoma cells to CD95/Fas-mediated apoptosis. *Journal of Investigative Dermatology*, 7(2), 333-340.
- Rane, N. S., Yonkovich, J. L., & Hegde, R. S. (2004). Protection from cytosolic prion protein toxicity by modulation of protein translocation. *The EMBO Journal*, 23(23), 4550-4559.
- Re, L., Rossini, F., Re, F., Bordicchia, M., Mercanti, A., Fernandez, O. S., et al. (2006). Prion protein potentiates acetylcholine release at the neuromuscular junction. *Pharmacological Research*, 53(1), 62-68.
- Reynolds, A., Leake, D., Boese, Q., Scaringe, S., Marshall, W. S., & Khvorova, A. (2004). Rational siRNA design for RNA interference. *Nature Biotechnology*, 22(3), 326-330.
- Riek, R., Hornemann, S., Wider, G., Billeter, M., Glockshuber, R., & Wüthrich, K. (1996). NMR structure of the mouse prion protein domain PrP (121-321). *Nature*, 382(6587), 180-182.

- Rikimaru, K., Toda, H., Tachikawa, N., Enomoto, S., & Kamata, N. (1990). Growth of the malignant and nonmalignant human squamous cells in a protein-free defined medium. *In Vitro Cellular & Developmental Biology*, 26(9), 849-856.
- Robinson, J. P., Carter, W. O., & Narayanan, P. (1997). Functional Assays by Flow Cytometry. In N. R. Rose, E. Marcario, J. D. Folds, H. C. Lane & R. Nakumura (Eds.), *Manual of Clinical Laboratory Immunology - Immune cell phenotyping and flow cytometric analysis* (5th ed., pp. 245-254). Washington, DC: ASM Press.
- Ron, D., & Walter, P. (2007). Signal integration in the endoplasmic reticulum unfolded protein response. *Nature Reviews Molecular Cell Biology*, 8(7), 519-529.
- Roucou, X., & LeBlanc, A. C. (2005). Cellular prion protein neuroprotective function: Implications in prion diseases. *Journal of Molecular Medicine*, 83(1), 3-11.
- Roucou, X., Giannopoulos, P. N., Zhang, Y., Jodoin, J., Goodyer, C. G., & LeBlanc, A. (2005). Cellular prion protein inhibits proapoptotic Bax conformational change in human neurons and in breast carcinoma MCF-7 cells. *Cell Death & Differentiation*, 12(7), 783-795.
- Roucou, X., Guo, Q., Zhang, Y., Goodyer, C. G., & LeBlanc, A. C. (2003). Cytosolic prion protein is not toxic and protects against Bax-mediated cell death in human primary neurons. *The Journal of Biological Chemistry*, 278(42), 40877-40881.
- Rudd, P. M., Endo, T., Colominas, C., Groth, D., Wheeler, S. F., Harvey, D. J., et al. (1999). Glycosylation differences between the normal and pathogenic prion protein isoforms. *Proceedings of the National Academy of Sciences of the USA*, 96(23), 13044-13049.
- Rytwiński, K., Wnuk, A., Woźniak, W., Rychłowska, M., & Bieńkowska, M. (2004). Assessment of the correlation between proliferation defined by S-phase cell cycle and apoptosis after preoperative chemotherapy in osteosarcomas of children and adolescents. *Medycyna Wieku Rozwojowego*, 8(4Pt2), 1029-1036.
- Saito, Y., Nishio, K., Ogawa, Y., Kimata, J., Kinumi, T., Yoshida, Y., et al. (2006). Turning point in apoptosis/necrosis induced by hydrogen peroxide. *Free Radical Research*, 40(6), 619-630.
- Sakaguchi, S., Katamine, S., Nishida, N., Moriuchi, R., Shigematsu, K., Sugimoto, T., et al. (1996). Loss of cerebellar Purkinje cells in aged mice homozygous for a disrupted PrP gene. *Nature*, 380(6574), 528-531.

- Sandy, P., Ventura, A., & Jacks, T. (2005). Mammalian RNAi: A practical guide. *BioTechniques*, 39(2), 215-224.
- Santuccione, A., Sytnyk, V., Leshchyn'ska, I., & Schachner, M. (2005). Prion protein recruits its neuronal receptor NCAM to lipid rafts to activate p59^{fyn} and to enhance neurite outgrowth. *The Journal of Cell Biology*, 169(2), 341-354.
- Sargh, M. J., & Gross, A. D. (2007). *The Cancer Dictionary* (3rd ed.). New York, NY: Checkmark Books.
- Sarnow, P., Jopling, C. L., Norman, K. L., Schütz, S., & Wehner, K. A. (2006). MicroRNAs: Expression, avoidance and subversion by vertebrate viruses. *Nature Reviews Microbiology*, 4(9), 651-659.
- Satoh, J., Kuroda, Y., & Katamine, S. (2000). Gene expression profile in prion protein-deficient fibroblasts in culture. *The American Journal of Pathology*, 157(1), 59-68.
- Schröder, M., & Kaufman, R. J. (2005). ER stress and the unfolded protein response. *Mutation Research*, 569(1-2), 29-63.
- Shiraishi, T., Yoshida, T., Nakata, S., Horinaka, M., Wakada, M., Mizutani, Y., et al. (2005). Tunicamycin enhances tumor necrosis factor-related apoptosis-inducing ligand-induced apoptosis in human prostate cancer cells. *Cancer Research*, 65(14), 6364-6370.
- Shmerling, D., Hegyi, I., Fischer, M., Blättler, T., Brandner, S., Götz, J., et al. (1998). Expression of amino-terminally truncated PrP in the mouse leading to ataxia and specific cerebellar lesions. *Cell*, 93(2), 203-214.
- Shyng, S. L., Heuser, J. E., & Harris, D. A. (1994). A glycolipid-anchored prion protein is endocytosed via clathrin-coated pits. *The Journal of Cell Biology*, 125(6), 1239-1250.
- Simon, H. U., Haj-Yehia, A., & Levi-Schaffer, F. (2000). Role of reactive oxygen species (ROS) in apoptosis induction. *Apoptosis*, 5(5), 415-418.
- Singh, N., Gu, Y., Bose, S., Basu, S., Luo, X., Ojha, A., et al. (2006). The Paradoxical Role of Proteasomes in Prion Diseases. In J. N. Keller & L. Stefanis (Eds.), *The Proteasome in Neurodegeneration* (pp. 265-284). New York, NY: Springer Science + Business Media.
- Smart, R. C. (2010). Chemical Carcinogenesis and Mutagenesis. In E. Hodgson (Ed.), *A Textbook of Modern Toxicology* (4th ed., pp. 237-264). Hoboken, NJ: John Wiley & Sons.

- Southern, J. A., Young, D. F., Heaney, F., Baumgartner, W., & Randall, R. E. (1991). Identification of an epitope on the P and V proteins of simian virus 5 that distinguishes between two isolates with different biological characteristics. *Journal of General Virology*, 72(Pt 7), 1551-1557.
- Sporn, M. B. (1996). The war on cancer. *Lancet*, 347(9012), 1377-1381.
- Stahl, N., Borchelt, D. R., Hsiao, K., & Prusiner, S. B. (1987). Scrapie prion protein contains a phosphatidylinositol glycolipid. *Cell*, 51(2), 229-240.
- Stewart, R. S., & Harris, D. A. (2003). Mutational analysis of topological determinants in prion protein (PrP) and measurement of transmembrane and cytosolic PrP during prion infection. *The Journal of Biological Chemistry*, 278(46), 45960-45968.
- Stewart, R. S., Drisaldi, B., & Harris, D. A. (2001). A transmembrane form of the prion protein contains an uncleaved signal peptide and is retained in the endoplasmic reticulum. *Molecular Biology of the Cell*, 12(4), 881-889.
- Stöhr, J., Weinmann, N., Wille, H., Kaimann, T., Nagel-Steger, L., Birkmann, E., et al. (2008). Mechanisms of prion protein assembly into amyloid. *Proceedings of the National Academy of Sciences of the USA*, 105(7), 2409-2414.
- Stuchbury, G., & Munch, G. (2010). Optimizing the generation of stable neuronal cell lines via pre-transfection restriction enzyme digestion of plasmid DNA. *Cytotechnology*, 62(3), 189-194.
- Sunyach, C., Jen, A., Deng, J., Fitzgerald, K. T., Frobert, Y., Grassi, J., et al. (2003). The mechanism of internalization of glycosylphosphatidylinositol-anchored prion protein. *The EMBO Journal*, 22(14), 3591-3601.
- Sy, M. (2003). Prion diseases. *Clinical Microbiology Newsletter*, 25(14), 105-111.
- Takeda, M., Shirato, I., Kobayashi, M., & Endou, H. (1999). Hydrogen peroxide induces necrosis, apoptosis, oncosis and apoptotic oncosis of mouse terminal proximal straight tubule cells. *Nephron*, 81(2), 234-238.
- Taraboulos, A., Rogers, M., Borchelt, D. R., McKinley, M. P., Scott, M., Serban, D., et al. (1990). Acquisition of protease resistance by prion proteins in scrapie-infected cells does not require asparagine-linked glycosylation. *Proceedings of the National Academy of Sciences of the USA*, 87(21), 8262-8266.

- Tobler, I., Gaus, S. E., Deboer, T., Achermann, P., Fischer, M., Rülicke, T., et al. (1996). Altered circadian activity rhythms and sleep in mice devoid of prion protein. *Nature*, *380*(6575), 639-642.
- Tom, B. H., Rutzky, L. P., Jakstys, M. M., Oyasu, R., Kaye, C. I., & Kahan, B. D. (1976). Human colonic adenocarcinoma cells. I. Establishment and description of a new line. *In Vitro*, *12*(3), 180-191.
- Trainer, D. L., Kline, T., McCabe, F. L., Faucette, L. F., Feild, J., Chaikin, M., et al. (1988). Biological characterization and oncogene expression in human colorectal carcinoma cell lines. *International Journal of Cancer*, *41*(2), 287-296.
- van Heemst, D., den Reijer, P. M., & Westendorp, R. G. (2007). Ageing or cancer: A review on the role of caretakers and gatekeepers. *European Journal of Cancer*, *43*(15), 2144-2152.
- Vander Heiden, M. G., Li, X. X., Gottlieb, E., Hill, R. B., Thompson, C. B., & Colombini, M. (2001). Bcl-xL promotes the open configuration of the voltage-dependent anion channel and metabolite passage through the outer mitochondrial membrane. *The Journal of Biological Chemistry*, *276*(22), 19414-19419.
- Varki, A. (1993). Biological roles of oligosaccharides: All of the theories are correct. *Glycobiology*, *3*(2), 97-130.
- Vey, M., Pilkuhn, S., Wille, H., Nixon, R., DeArmond, S. J., Smart, E. J., et al. (1996). Subcellular colocalization of the cellular and scrapie prion proteins in caveolae-like membranous domains. *Proceedings of the National Academy of Sciences of the USA*, *93*(25), 14945-14949.
- Wajant, H., Pfizenmaier, K., & Scheurich, P. (2003). Tumor necrosis factor signaling. *Cell Death & Differentiation*, *10*(1), 45-65.
- Walmsley, A. R., Watt, N. T., Taylor, D. R., Perera, W. S., & Hooper, N. M. (2009). alpha-cleavage of the prion protein occurs in a late compartment of the secretory pathway and is independent of lipid rafts. *Molecular and Cellular Neurosciences*, *40*(2), 242-248.
- Walter, E. D., Chattopadhyay, M., & Millhauser, G. L. (2006). The affinity of copper binding to the prion protein octarepeat domain: Evidence for negative cooperativity. *Biochemistry*, *45*(43), 13083-13092.
- Walter, P. (2010). Walking along the serendipitous path of discovery. *Molecular Biology of the Cell*, *21*(1), 15-17.
- Walton, S. P., Wu, M., Gredell, J. A., & Chan, C. (2010). Designing highly active siRNAs for therapeutic applications. *The FEBS Journal*, *277*(23), 4806-4813.

- Wang, F., Wang, X., Yuan, C. G., & Ma, J. (2010). Generating a prion with bacterially expressed recombinant prion protein. *Science*, 327(5969), 1132-1135.
- Wang, V., Chuang, T. C., Soong, B. W., Shan, D. E., & Kao, M. C. (2009). Octarepeat changes of prion protein in Parkinson's disease. *Parkinsonism & Related Disorders*, 15(1), 53-58.
- Wang, X. Z., Lawson, B., Brewer, J. W., Zinszner, H., Sanjay, A., Mi, L. J., et al. (1996). Signals from the stressed endoplasmic reticulum induce C/EBP-homologous protein (CHOP/GADD153). *Molecular and Cellular Biology*, 16(8), 4273-4280.
- Wang, X., Martindale, J. L., Liu, Y., & Holbrook, N. J. (1998). The cellular response to oxidative stress: Influences of mitogen-activated protein kinase signalling pathways on cell survival. *Biochemical Journal*, 333(Pt 2), 291-300.
- Watson, A. J. M., Askew, J. N., & Benson, R. S. P. (1995). Poly(adenosine diphosphate ribose) polymerase inhibition prevents necrosis induced by H₂O₂ but not apoptosis. *Gastroenterology*, 109(2), 472-482.
- Watt, N. T., & Hooper, N. M. (2005). Reactive oxygen species (ROS)-mediated beta-cleavage of the prion protein in the mechanism of the cellular response to oxidative stress. *Biochemical Society Transactions*, 33(Pt 5), 1123-1125.
- Watt, N. T., Routledge, M. N., Wild, C. P., & Hooper, N. M. (2007). Cellular prion protein protects against reactive-oxygen-species-induced DNA damage. *Free Radical Biology & Medicine*, 43(6), 959-967.
- Watt, N. T., Taylor, D. R., Gillott, A., Thomas, D. A., Perera, W. S., & Hooper, N. M. (2005). Reactive oxygen species-mediated beta-cleavage of the prion protein in the cellular response to oxidative stress. *The Journal of Biological Chemistry*, 280(43), 35914-35921.
- Wei, M. C., Zong, W. X., Cheng, E. H., Lindsten, T., Panoutsakopoulou, V., Ross, A. J., et al. (2001). Proapoptotic BAX and BAK: A requisite gateway to mitochondrial dysfunction and death. *Science*, 292(5517), 727-730.
- Weise, J., Sandau, R., Schwarting, S., Crome, O., Wrede, A., Schulz-Schaeffer, W., et al. (2006). Deletion of cellular prion protein results in reduced Akt activation, enhanced postischemic caspase-3 activation, and exacerbation of ischemic brain injury. *Stroke*, 37(5), 1296-1300.
- Welihinda, A. A., & Kaufman, R. J. (1996). The unfolded protein response pathway in *Saccharomyces cerevisiae*. Oligomerization and transphosphorylation of Ire1p (Ern1p) are required for kinase activation. *The Journal of Biological Chemistry*, 271(30), 18181-18187.

- Westergard, L., Christensen, H. M., & Harris, D. A. (2007). The cellular prion protein (PrP(C)): Its physiological function and role in disease. *Biochimica et Biophysica Acta*, 1772(6), 629-644.
- White, A. R., Collins, S. J., Maher, F., Jobling, M. F., Stewart, L. R., Thyer, J. M., et al. (1999). Prion protein-deficient neurons reveal lower glutathione reductase activity and increased susceptibility to hydrogen peroxide toxicity. *The American Journal of Pathology*, 155(5), 1723-1730.
- World Health Organization. (2009). *Cancer Fact Sheet*. Retrieved December 23, 2010, from <http://www.who.int/mediacentre/factsheets/fs297/en/index.html>
- Xue, X., Piao, J., Nakajima, A., Sakon-Komazawa, S., Kojima, Y., Mori, K., et al. (2005). Tumor necrosis factor (TNF) induces the unfolded protein response (UPR) in a reactive oxygen species (ROS)-dependent fashion, and the UPR counteracts ROS accumulation by TNF. *The Journal of Biological Chemistry*, 280(40), 33917–33925.
- Yam, A. Y., Gao, C. M., Wang, X., Wu, P., & Peretz, D. (2010). The octarepeat region of the prion protein is conformationally altered in PrP^{Sc}. *PLoS One*, 5(2), e9316.
- Yang, Q. H., Church-Hajduk, R., Ren, J., Newton, M. L., & Du, C. (2003). Omi/HtrA2 catalytic cleavage of inhibitor of apoptosis (IAP) irreversibly inactivates IAPs and facilitates caspase activity in apoptosis. *Genes & Development*, 17(12), 1487-1496.
- Yang, Y., Chen, L., Pan, H. Z., Kou, Y., & Xu, C. M. (2009). Glycosylation modification of human prion protein provokes apoptosis in HeLa cells *in vitro*. *BMB Reports*, 42(6), 331-337.
- Yoshida, H., Haze, K., Yanagi, H., Yura, T., & Mori, K. (1998). Identification of the cis-acting endoplasmic reticulum stress response element responsible for transcriptional induction of mammalian glucose-regulated proteins. Involvement of basic leucine zipper transcription factors. *The Journal of Biological Chemistry*, 273(50), 33741-33749.
- Yoshizawa, K., Nozaki, S., Kitahara, H., Ohara, T., Kato, K., Kawashiri, S., et al. (2007). Copper efflux transporter (ATP7B) contributes to the acquisition of cisplatin-resistance in human oral squamous cell lines. *Oncology Reports*, 18(4), 987-991.
- Yuan, B., Latek, R., Hossbach, M., Tuschl, T., & Lewitter, F. (2004). siRNA Selection Server: An automated siRNA oligonucleotide prediction server. *Nucleic Acids Research*, 32(Web Server issue), W130-W134.

- Zahn, R., Liu, A., Lührs, T., Riek, R., von Schroetter, C., López García, F., et al. (2000). NMR solution structure of the human prion protein. *Proceedings of the National Academy of Sciences of the USA*, 97(1), 145-150.
- Zamzami, N., Marchetti, P., Castedo, M., Decaudin, D., Macho, A., Hirsch, T., et al. (1995). Sequential reduction of mitochondrial transmembrane potential and generation of reactive oxygen species in early programmed cell death. *The Journal of Experimental Medicine*, 182(2), 367-377.
- Zetterberg, A., Larsson, O., & Wiman, K. G. (1995). What is the restriction point? *Current Opinion in Cell Biology*, 7(6), 835-842.
- Zhang, H. Y., Du, Z. X., Liu, B. Q., Gao, Y. Y., Meng, X., Guan, Y., et al. (2009). Tunicamycin enhances TRAIL-induced apoptosis by inhibition of cyclin D1 and the subsequent downregulation of survivin. *Experimental and Molecular Medicine*, 41(5), 362-369.
- Zhou, H., & Zeng, X. (2009). Energy profile and secondary structure impact shRNA efficacy. *BMC Genomics*, 10 Suppl 1, S9.



Resistance against apoptosis by the cellular prion protein is dependent on its glycosylation status in oral HSC-2 and colon LS 174T cancer cells

Yeannie Hui-Yeng Yap, Yee-How Say*

Department of Biomedical Science, Faculty of Science, Universiti Tunku Abdul Rahman (UTAR) Perak Campus, 31900 Kampar, Perak, Malaysia

ARTICLE INFO

Article history:

Received 21 January 2011

Received in revised form 23 February 2011

Accepted 24 February 2011

Keywords:

Cellular prion protein

N-linked glycosylation

Tunicamycin

Cancer

Oxidative stress

ABSTRACT

Most studies have focused on the role of the cellular prion protein (PrP^C) in neurodegenerative diseases, whereas the function of this ubiquitous protein outside the nervous system remains elusive. Therefore, the anti-apoptotic property of PrP^C in oral squamous cell carcinoma (HSC-2) and colon adenocarcinoma (LS 174T) was evaluated in this study, by stable shRNA knockdown and overexpression, respectively. PrP^C confers resistance against oxidative stress-apoptosis as indicated by MTT assay, Annexin V-FITC/PI and DCFH-DA staining, but this property is abolished upon N-glycosylation inhibition by tunicamycin. Our results indicate that the inhibition of glycosylation in cancer cells overexpressing PrP^C could represent a potential therapeutic target.

© 2011 Elsevier Ireland Ltd. All rights reserved.

1. Introduction

Scrapie prion (PrP^{Sc}) is the causative agent of prion diseases, which are also known as transmissible spongiform encephalopathies (TSEs), a group of rare neurodegenerative diseases which include bovine spongiform encephalopathy (BSE) in cattles and Creutzfeldt–Jakob disease (CJD) in humans [1]. These diseases are characterized by spongiform change, neuronal degeneration and protein aggregation which lead to further amyloid plaque formation, along with gliosis [1]. Sporadic prion diseases are thought to be triggered by a rare and stochastic change of the normal cellular prion protein (PrP^C) conformation, leading to the formation of PrP^{Sc} which forms insoluble aggregates and is partially resistant to proteinase K [2].

The biogenesis of PrP^C yields a final protein of 209 amino acid residues which may be present as di-, mono-, or unglycosylated species upon glycosylation, depending on the number of glycosylation sites (Asn181IleThr and Asn197PheThr in humans) occupied with N-linked oligosaccharide [3,4]. N-glycans play structural role by confer-

ring stability on the proteins to which they are attached where upon N-linked glycosylation inhibition, conversion of PrP^C to PrP^{Sc} occurs more readily [5,6]. Diglycosylated PrP^C carrying two N-linked glycans is expected to increase the free energy barrier to the transition state and further delays the conversion [7]. Lehmann and Harris [8] reported that PrP molecules with properties similar to PrP^{Sc} such as non-ionic detergent insolubility and partially resistant to digestion by proteinase K have been generated upon mutation of glycosylation consensus sites (AsnXaaThr) or by tunicamycin (TUN) treatment in cells expressing recombinant PrP^C. This suggests that the absence of N-linked glycosylation favors the likeliness of PrP^C sequence to adopt a β -sheet conformation [9].

The initiation of apoptosis upon PrP^C N-linked glycosylation inhibition via TUN has been described in a few extensive studies, although the approach used may not be similar. Dricu, Carlberg, Wang, and Larsson [10] have reported that continuous presence of TUN for 24–48 h provoked cell death in SK-MEL-2 melanoma cells. Specifically, the mechanism of cell death upon inhibition of N-linked glycosylation using TUN has been shown to be via apoptosis due to the detection of oligonucleosomally fragmented DNA in gel electrophoresis. TUN exerts its apoptotic effect

* Corresponding author. Tel.: +60 5 4688888; fax: +60 5 4661676.

E-mail address: sayyh@utar.edu.my (Y.-H. Say).

in a time- and cell-dependent manner since Carlberg et al. [11] showed that a short exposure of 7 min of TUN to SV40-transformed fibroblasts (line 90VAVI) triggered significant reduction in the cell viability and subsequently led to apoptosis. Moreover, in cervical cancer HeLa cells transiently expressing *PRNP* gene glycosylation mutants – N181Q N197Q and T183A T199A, the ROS scavenging properties of PrP^C was diminished and further sensitized the HeLa cells to mitochondria-mediated cell death [12]. Hence, this study was intended to validate the reproducibility of the above effect using different cancer cell lines – oral squamous cell carcinoma (HSC-2) and colon adenocarcinoma (LS 174T), by inhibition of PrP^C N-glycosylation using TUN.

2. Materials and methods

2.1. Cell culture, transfection and treatment paradigm

Full length human PrP^C (Accession No. BC012844) cDNA (Clone ID: 3863784, Open Biosystem, AL) was subcloned into the pcDNATM 3.1 vector using the pcDNATM 3.1 Directional TOPO[®] Expression Kit (InvitrogenTM, CA) according to manufacturer's instructions. Oligonucleotide sequences to knock down PrP^C in HSC-2 cell lines were designed using siRNA Selection Program hosted by the Whitehead Institute for Biomedical Research at <http://jura.wi.mit.edu/bioc/siRNAext/> [13]. Cloning procedure of shRNA oligos into pLKO.1 TRC vector [14] sourced from Addgene, MA was performed according to the recommended procedures. Table 1 shows the target regions of each designated shRNA oligos which are indicated on the basis of the base sequences and nucleotide numbering as shown in the human PrP mRNA (BC012844). HSC-2 and LS 174T cancer cell lines (kindly donated by Dr. Yang-Mooi Lim, Faculty of Medicine and Health Sciences, UTAR) were maintained at 37 °C and 5% CO₂ in Minimum Essential Medium (Cellgro, VA) supplemented with 10% v/v heat-inactivated fetal bovine serum (i-DNA, Singapore) and 1% v/v Penicillin–Streptomycin (Millipore, MA). Transfection was performed using TransPass D1 Transfection Reagent (New England Biolabs, MA) in serum-free OPTI-MEM with 5 µg of DNA, according to the manufacturer's instruction. After 48 h, stably transfected LS 174T cells and HSC-2 cells were selected using G-418 sulfate (A.G. Scientific, CA) and puromycin dihydrochloride (bioWORLD, OH) at 1 mg/ml for 3 wk and 3 µg/ml for 2 wk, respectively. In order to block glycosylation of PrP^C, HSC-2 and LS 174T cells were treated with TUN (Sigma, MO) at half maximal inhibitory concentration (IC₅₀); 16 µg/ml and 24 µg/ml or IC₂₀; 6 µg/ml and 2 µg/ml, respectively, for 24 h. Cells were also subjected to reac-

tive oxygen species (ROS) oxidative stress insult by subjecting the cells to 0.2 mM H₂O₂ for 24 h, or 3 mM H₂O₂ for 30 min after TUN IC₂₀ treatment, as per indicated in the figure legend.

2.2. Western blot analysis

Cells were collected through scraping and lysed with lysis buffer (10 mM Tris, pH 7.8, 100 mM NaCl, 10 mM EDTA, 0.1 mM PMSF, 0.5% w/v sodium deoxycholate, 0.5% v/v Nonidet P-40) containing protease inhibitor cocktail (Sigma, MO). Concentration of supernatant protein lysates were quantified using bicinchoninic acid (BCA) based on colorimetric detection at 562 nm using the BCATM Protein Assay Kit (Thermo Scientific, MA). Equal amounts of total protein (20–60 µg/well) were then subjected to electrophoresis using 15% sodium dodecyl sulfate–polyacrylamide gels. Transferred membrane was blocked with 5% w/v skim milk powder in Phosphate-Buffered Saline–Tween (PBS-T), followed by overnight incubation at 4 °C with primary antibody, anti-PrP clone 3F4 (Millipore) diluted to 1:10,000 in PBS-T containing 3% BSA. The membrane was then incubated for 1 h in 3% BSA/PBS-T containing a 1:10,000 dilution of rabbit anti-mouse horseradish peroxidase-conjugated IgG (Calbiochem, Germany). Bands were visualized via enhanced chemiluminescence (ECL) detection system (Thermo Scientific) according to the manufacturer's instructions and image acquisition was performed using FluorChem FC2 System (Alpha Innotech, CA). For repeated hybridization with anti-actin clone C4 as loading control, the membrane was stripped in stripping buffer (0.4 M glycine, 2% v/v Tween-20, 0.2% SDS, pH2.2) for 10 min upon image acquisition, washed twice with PBS-T for 5 min and further incubated in anti-actin (Millipore) at 1:5000 dilution for 1 h. The NIH ImageJ 1.43U software was used for densitometry analysis.

2.3. MTT cell viability assay

A total of 2.5×10^4 cells/well and 3×10^4 cells/well for HSC-2 and LS 174T, respectively, were seeded into 96-well plates. A total of 20 µl 3-(4,5-dimethylthiazol-2-yl)-2,5-diphenyltetrazolium bromide (MTT; Calbiochem) stock solution of 5 mg/ml in PBS was added into each well of treated or untreated cells. The plate was then incubated for 4 h at 37 °C until purple formazan crystal developed. Dimethyl sulfoxide (DMSO) was added in order to dissolve the formazan crystals. Absorbance was determined by Model 680 Microplate Reader (Bio-Rad, CA) at 550 nm.

2.4. Annexin V-FITC/PI dual staining

Apoptotic cells were detected by flow cytometry using Annexin V-FITC Apoptosis Detection Kit I (BD Biosciences, NJ) according to manufacturer's instructions. Treated cells were harvested and resuspended in 500 µl of 1× Binding buffer. A total of 10 µl of 5 µl Annexin V-FITC and 5 µl PI were added into the cells suspension prior to incubation at RT for 5–15 min in the dark. Fluorescence was detected via 530/30 band filter (FL1) and 585/42 band filter (FL2) to monitor Annexin V-FITC binding and PI uptake, respec-

Table 1
shRNA Oligonucleotides against human PrP mRNA sequence (BC012844).

Name	Target region in human PrP mRNA	
	Base sequences	Nucleotide numbering
HuPrPshRNA1	5'-AATGCCTATCT TAGTAGAGA-3'	1194–1214
HuPrPshRNA2	5'-AA GCGAAATCTCCTTTGTCCA-3'	1664–1684
HuPrPshRNA3	5'-AATCTA GAGATTCCTAGCTC-3'	1309–1329

tively. A total of 10,000 events per sample were recorded. Data collected were later analyzed with Scripps Research Institute's WinMDI 2.8 software.

2.5. Determination of antioxidant activity using DCFH-DA

Reactive oxygen species (ROS) – H₂O₂ generated within cells were detected using fluorescent probe 2',7'-dichlorofluorescein diacetate (DCFH-DA; Sigma, MO). Cells were harvested, resuspended in 500 µl of PBS and treated or untreated with 3 mM of H₂O₂ for 30 min at 37 °C. Cells were then incubated with 10 µM DCFH-DA in 500 µl of PBS for 30 min at 37 °C. The fluorescence of 2',7'-Dichlorofluorescein (DCF) (excitation 488 nm, emission 525 nm) was measured using BD FACSCalibur™ flow cytometer on FL1 channel. A total of 10,000 cells were analyzed. The negative control was loaded with DCFH-DA alone, without H₂O₂ treatment whereas the baseline fluorescence shows the distribution of untreated control cells, which was not loaded with both DCFH-DA and H₂O₂. Fluorescence intensity of the data was expressed as the mean logarithm of green DCF fluorescence. Data acquired was analyzed using WinMDI 2.8 software.

2.6. Statistical analysis

Data were expressed as mean ± standard error of the mean (SEM) of three independent experiments which were performed in triplicates, unless otherwise stated. Statistical analysis was performed by one-way analysis of variance (ANOVA) followed by LSD's post hoc test for multiple comparisons using the SPSS 15.0 software (SPSS Inc., IL). A *p* value of less than 0.05 was considered as statistically significant.

3. Results

3.1. PrP^C expression in stably transfected cancer cells

A few cancer cell lines were selected from our cancer cell line library for the evaluation of endogenous PrP^C expression, so that it could be knocked-down or over-expressed by stable transfection. As shown in

Fig. 1, untransfected LS 174T had negligible while HSC-2 cells had high endogenous PrP^C expression. After stable transfection, PrP^C overexpression was increased 5-fold surplus compared to the untransfected or mock-transfected LS 174T cells. Knockdown efficiency of three HuPrPshRNA sequences was also assessed, where HuPrPshRNA1 possessed the lowest Relative Intensity (RI), followed by HuPrPshRNA3 and HuPrPshRNA2. This indicates that stable expression of pLKO.1 carrying the HuPrPshRNA1 can capably down-regulate expression of endogenous PrP^C in HSC-2 cells in a long-term and specific manner, and thus was chosen to be used in the subsequent assays. HSC-2 cells transfected with pLKO.1 vector and pLKO.1 scramble shRNA served as controls.

3.2. Glycosylation inhibition of PrP^C promotes cell death in cancer cells

To investigate the effect of N-glycosylation on the conferment of anti-apoptotic property by PrP^C in HSC-2 and LS 174T cells, cells were treated with TUN. Following TUN treatment, the di- and monoglycosylated isoforms of PrP^C which resides at the 35–30 kDa region were completely diminished and only the unglycosylated PrP isoform at 27 kDa was expressed (Fig. 2A). Besides, a dim but yet notable band of approximately 19–22 kDa was observed too, which appearance was consistent and no such singular species was detected in the untreated PrP^C-expressing cells. Upon establishment of the IC₅₀ value, the sensitivity of PrP^C in cultured cells towards glycosylation inhibition was assessed using MTT assay. As seen in Fig. 2B, LS 174T cells which stably expresses wild type PrP^C showed significantly (*p* < 0.05) enhancement in cell proliferation after 24 h compared to the untransfected LS 174T, while only a fair increment on the growth of PrP^C-expressing HSC-2 group (HSC-2, HSC-pLKO.1 vector and HSC-pLKO.1 Scram.) was observed, compared to HSC-shRNA1 cells. The cell viability differences between the untreated and TUN-treated group were also compared. Cell viability differences of sT-LS 174T-pcDNA 3.1/PrP (85.6%) was significantly higher compared to sT-LS 174T pcDNA 3.1 group (39.6%), while PrP^C-deficient HSC-shRNA 1 had significantly lower cell viability differences or less cell death (26.6%) compared to the PrP^C-expressing HSC-2 cells with cell viability differences of 42.0–44.0%. The cell viability of LS 174T stably-expressing PrP^C was significantly reduced upon TUN treatment, compared to the untransfected or mock-transfected cells. However, a small and insignificant difference was observed in TUN-treated PrP^C-expressing HSC-2 cells, compared to the shRNA-knocked-down or shRNA-controls.

To further elucidate the mechanism of cell death by glycosylation inhibition of PrP^C, cells were subjected to flow cytometry analysis with Annexin V-FITC/PI dual staining. The percentages of viable cell population in the LL quadrant – not labeled with Annexin V-FITC or PI, and apoptotic cell population in the LR quadrant – labeled with Annexin V-FITC, were accounted. The induction of apoptosis upon treatment with TUN in PrP^C expressing HSC-2 and LS 174T cells is displayed in Fig. 3A and B, respectively. The single binding of Annexin V-FITC to cells indicates an early phase of apoptosis. Hence, the mechanism of cell death induced by glyco-

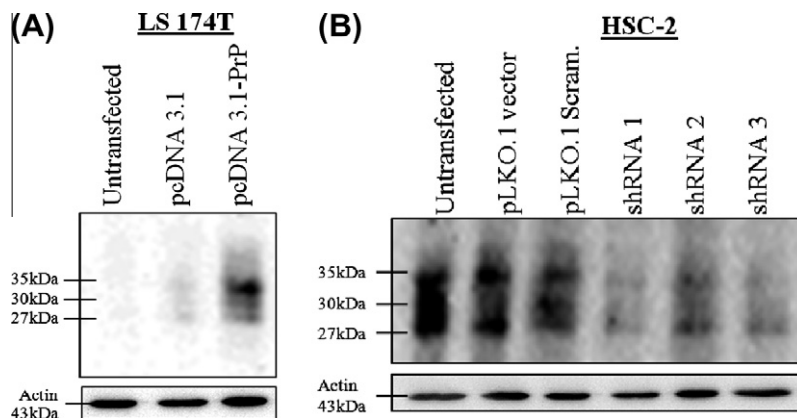


Fig. 1. Assessment of PrP^C expression in stably transfected cancer cell lines. (A) PrP^C overexpression in LS 174T cells. (B) Inhibition of PrP^C expression using shRNA oligonucleotide in HSC-2 cells. The LS 174T cells stably-overexpressing PrP^C is annotated as sT-LS 174T-pcDNA 3.1/PrP while mock vector-transfected cells – sT-LS 174T-pcDNA 3.1. Molecular weights are indicated on the left of Western blots. Membranes were reprobed with actin antibody to confirm equal protein loading in each lane.

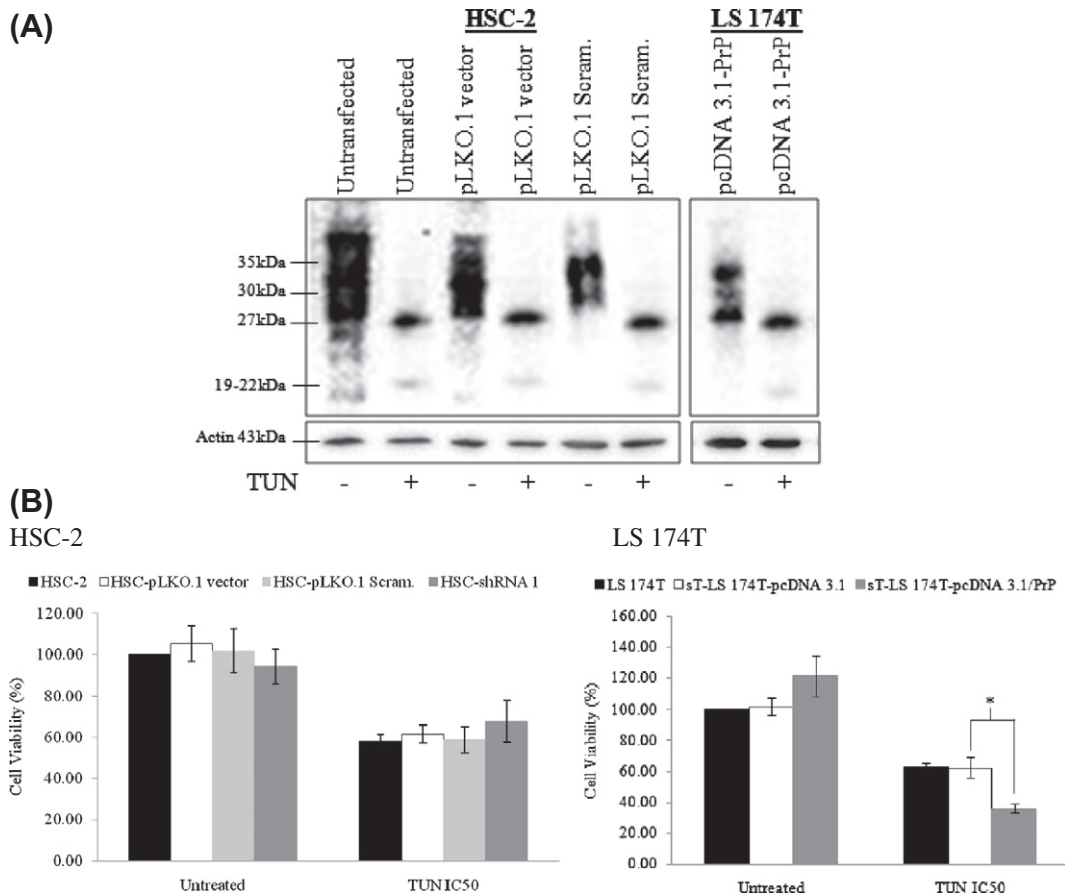


Fig. 2. TUN treatment in PrP^C expressing HSC-2 and LS 174T cells promotes cell death. (A) Effects of TUN on PrP^C expressing HSC-2 and LS 174T cells. The lanes labeled with + represents TUN-treated cells at IC₅₀ for 24 h, whereas – are untreated group. Molecular weights are indicated on the left. Data correspond to a representative experiment out of three replicates with similar findings. Membranes were further probed with actin antibody to confirm equal protein loading in each lane. (B) Inhibition of PrP^C glycosylation by TUN promotes cell death. Cell viability was determined by MTT assay following treatment with TUN at IC₅₀ (TUN IC50) in HSC-2 and LS 174T cells. The LS 174T cells stably-overexpressing PrP^C is annotated as sT-LS 174T-pcDNA 3.1/PrP while mock vector-transfected cells – sT-LS 174T-pcDNA 3.1. Data of cell viability was expressed in% and representing the mean ± SEM of three independent experiments as compared to the untreated control cells. Mean values were compared by using ANOVA followed by LSD's post hoc test for comparison of the means, using the SPSS software. **p* < 0.05 in treated sT-LS 174T-pcDNA 3.1/PrP vs. treated sT-LS 174T-pcDNA 3.1.

sylation-inhibited PrP^C using TUN is via apoptosis as shown by Annexin V-FITC binding. As shown in Fig. 3A, the percentages of viable cells in LL quadrant correlate to the MTT assay in Fig. 2B where there were significantly higher proportions of unlabeled viable cells in untreated PrP^C-expressing group compared to the untreated non-PrP^C expressing group. However, upon TUN treatment, proportions of unlabeled viable cells were significantly lower in PrP^C-expressing group compared to the untreated non-PrP^C expressing group. There were also significantly lower proportions of Annexin V-FITC-labeled cells in TUN-treated HSC-shRNA1 compared to the treated PrP^C expressing groups – HSC-pLKO.1 vector and HSC-pLKO.1 Scram. No significant difference was detected between the treated mock-transfected and PrP^C-expressing LS 174T cells. However, in the untreated group, the mock-transfected cells showed significantly higher percentage of cells in early apoptosis compared to the PrP^C-expressing LS 174T cells – suggesting that in the presence of PrP^C, cells were more likely to endure basal apoptotic stress. Due to this reason, the percentages of apoptotic cell population difference between the untreated and TUN-treated group were compared. The TUN-treated LS 174T cells expressing PrP^C had almost 2-fold increment of apoptotic cell death compared to the mock-transfected cells (14.3% vs. 7.3%). As a whole, these findings suggest that induction of apoptosis in PrP^C expressing cells upon TUN treatment was due to the formation of unglycosylated PrP through inhibition of N-linked glycosylation.

3.3. Blocking of PrP^C glycosylation impedes its ROS scavenging activity

This study has also intended to further examine the effect of glycosylation inhibition of PrP^C towards H₂O₂-induced reactive oxygen species (ROS) scavenging activity. The involvement of PrP^C in exerting its protective effect towards oxidative stress-induced cell death was first investigated by subjecting cells to H₂O₂ treatment at 0.2 mM for 24 h (Fig. 4A and B). There was an overall significant increment on cell viability in the PrP^C-expressing cells. PrP^C-depleted HSC-shRNA1 cells showed an estimated of 30% reduction in cell viability compared to the untransfected, HSC-pLKO.1 vector and HSC-pLKO.1 Scram. In parallel, the percentage of cell death in LS 174T cells stably transfected with PrP^C was significantly lower than the untransfected and mock-transfected cells. Both PrP^C-expressing and PrP^C-negative HSC-2 and LS 174T cells were also subjected to TUN treatment for 24 h at IC₅₀ (6 μg/ml and 2 μg/ml, respectively), as it has the ability to inhibit N-linked glycosylation as efficient as IC₅₀, while minimizing cell death. It was then followed by H₂O₂ treatment at 3 mM for 30 min to generate exogenous ROS which triggered oxidative stress within a short period of time. Fig. 4C and D shows that upon glycosylation inhibition of PrP^C prior to induction of oxidative stress, the cell viability in both HSC-2 and LS 174T PrP^C-expressing groups dropped at least 20% – but not significantly different – compared to the non-PrP^C expressing group. Upon treatment with H₂O₂, the glycosylation-inhibited PrP^C-

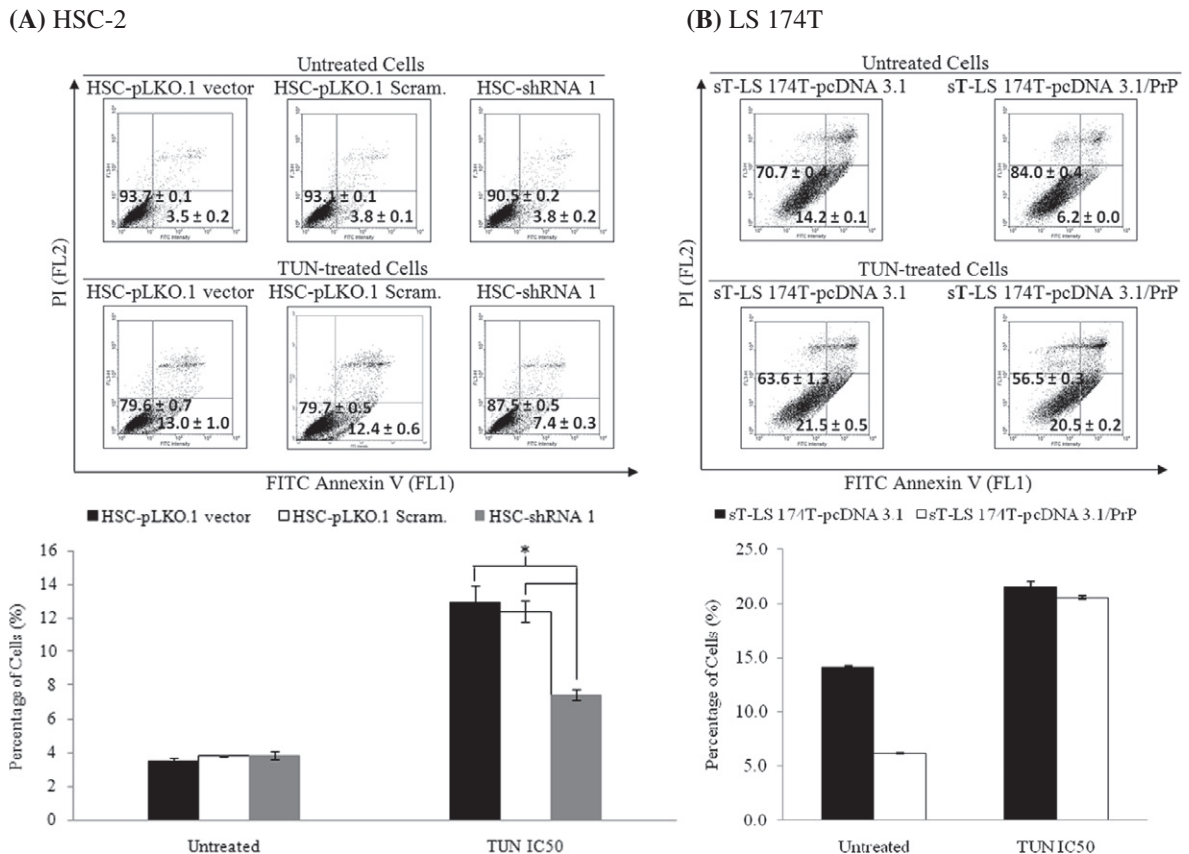


Fig. 3. Apoptosis induction in PrP^C expressing (A) HSC-2 and (B) LS 174T cells treated with TUN. Cells were treated with TUN at IC₅₀ for 24 h prior to flow cytometry analysis Annexin V-FITC/PI dual staining. The LS 174T cells stably-overexpressing PrP^C is annotated as sT-LS 174T-pcDNA 3.1/PrP while mock vector-transfected cells – sT-LS 174T-pcDNA 3.1. X-axis indicates the number of Annexin V-FITC-labeled cells. Y-axis indicates the number of PI-labeled cells. Unlabeled cells in the lower left (LL) quadrant represent viable cells while Annexin V-FITC-labeled cells in the lower right (LR) quadrant are the apoptotic population. Upper right (UR) quadrant represents Annexin V-FITC/PI-dual labeled cells, indicative of membrane permeability and late apoptosis. Data of each statistical graph of Annexin V-FITC/PI dual staining is expressed in % of cells in the LL or LR quadrant and represent the mean ± SEM of three independent experiments. The bar charts at the bottom of the flow cytometry scatterplots represent the % of cells undergoing apoptosis in the LR quadrant. Mean values were compared by using ANOVA followed by LSD's post hoc test for comparison of the means, using the SPSS software. **p* < 0.05 in treated HSC-shRNA 1 vs. treated HSC-pLKO.1 vector and HSC-pLKO.1 Scram., or in untreated sT-LS 174T-pcDNA 3.1/PrP vs. untreated sT-LS 174T-pcDNA 3.1.

expressing LS 174T cells showed a significantly lower percentage of cell viability compared to either untransfected or mock-transfected cells. As well as for HSC-2 cells, although not statistically significant, exposure of the glycosylation-inhibited PrP^C-expressing group (untransfected, pLKO.1 vector and pLKO.1 Scram.) to 3 mM H₂O₂ resulted in a decrease in cell viability compared to the PrP^C-depleted shRNA1 cells. These MTT results imply that unglycosylated PrP^C induces a rapid loss of cellular metabolic activity during H₂O₂-induced oxidative stress. Besides, in the absence of H₂O₂, the viabilities of both PrP^C-expressing and non-PrP^C expressing cells remained unchanged. These results implicate a profound role of PrP^C in attenuating H₂O₂-induced cell death in cultured cells.

Subsequently, the ability of both wild type PrP^C and the glycosylation-inhibited PrP^C to scavenge ROS production upon TUN IC₂₀ treatment was investigated. PrP^C-expressing cells were treated with TUN at IC₂₀ for 24 h to block glycosylation prior to flow cytometry analysis. Fig. 5A and B show the flow cytometric fluorescence distribution of HSC-2 and LS 174T cells, respectively. The glycosylation-inhibited PrP^C-expressing group of HSC-2 cells (untransfected, pLKO.1 vector and pLKO.1 Scram.) had significantly higher ROS levels upon exposure to 3 mM of H₂O₂ for 30 min, compared to the PrP^C-depleted shRNA1 cells. However, without glycosylation inhibition, it was the other way around. A comparable trend was also observed in the LS 174T cells, where the overexpression of PrP^C significantly decreased ROS production compared to the untransfected or mock-transfected cells (Fig. 5B). But once glycosylation was inhibited in PrP^C-expressing LS 174T cells, ROS generation was significantly increased.

Thus, these results demonstrate that upon glycosylation inhibition with TUN, the unglycosylated PrP^C isoform has significantly lower ROS scavenging capability.

4. Discussion

PrP^C is expressed most abundantly in the brain, but has also been detected in other non-neuronal tissues as diverse as lymphoid cells, lung, heart, kidney, gastrointestinal tract, muscle, and mammary glands [15]. Most studies have focused on the role of PrP^C in neurodegenerative prion diseases since its discovery. However, several captivating lines of evidence have emerged signifying that it plays an essential role in cancer biology (reviewed in [15]). In the present study, MTT, Annexin V-FITC/PI and DCFH-DA flow cytometric assays revealed that cancer cells expressing glycosylated PrP^C exhibit significantly higher viability, reduced apoptosis and reduced oxidative stress compared to the unglycosylated cells. However, the anti-apoptotic property seems to differ from one cell line to an-

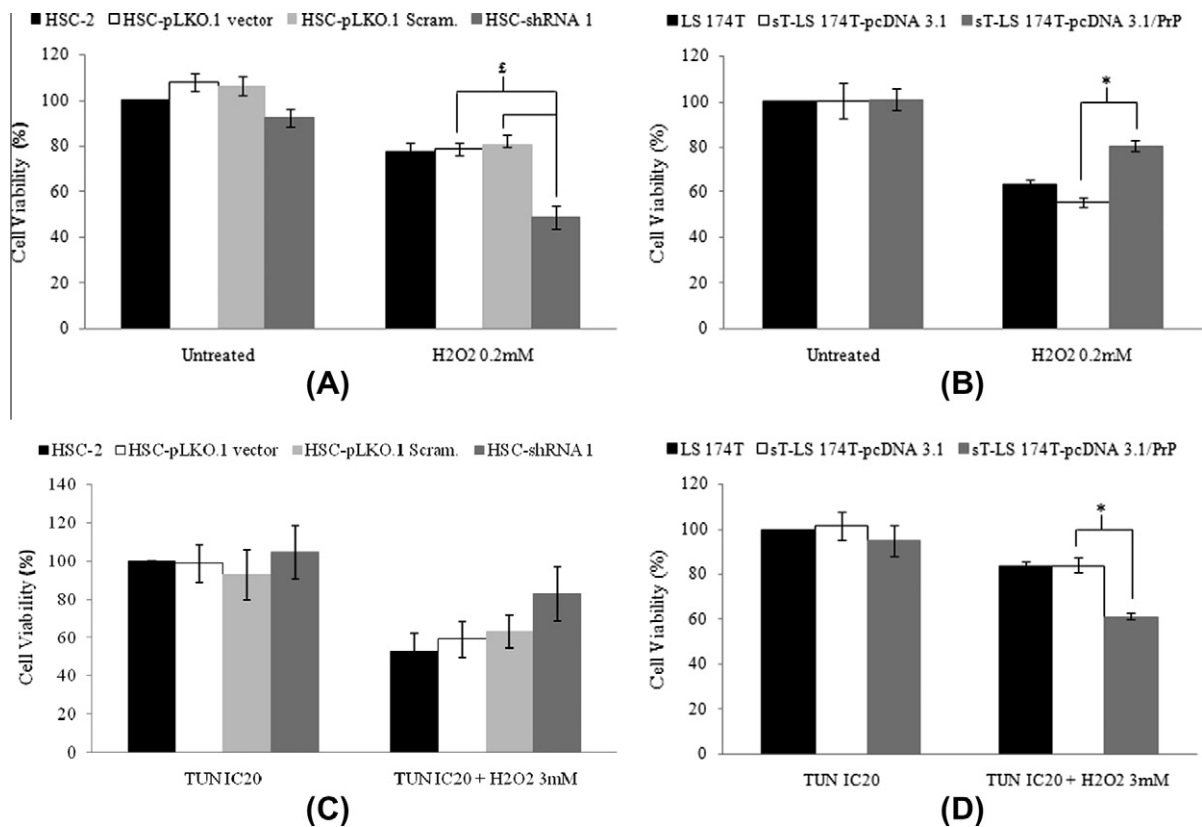


Fig. 4. PrP^C exerts its protective effect towards oxidative stress-induced cell death in cultured cancer cells. Cell viability was determined by MTT assay following treatment with or without 0.2 mM H₂O₂ (H₂O₂ 0.2 mM) for 24 h in (A) HSC-2 and (B) LS 174T cells, or following treatment with or without 3 mM H₂O₂ (H₂O₂ 3 mM) for 30 min in (C) HSC-2 and (D) LS 174T cells which have been glycosylation-inhibited by TUN IC₂₀ (TUN IC20) for 24 h. The LS 174T cells stably-overexpressing PrP^C is annotated as sT-LS 174T-pcDNA 3.1/PrP while mock vector-transfected cells – sT-LS 174T-pcDNA 3.1. Data of cell viability was expressed in % and representing the mean ± SEM of three independent experiments as compared to the untreated control cells. Mean values were compared by using ANOVA followed by LSD's post hoc test for comparison of the means, using the SPSS software. [£]*p* < 0.05 in treated HSC-shRNA 1 vs. treated HSC-pLKO.1 vector and HSC-pLKO.1 Scram. **p* < 0.05 in treated sT-LS 174T-pcDNA 3.1/PrP vs. treated sT-LS 174T-pcDNA 3.1.

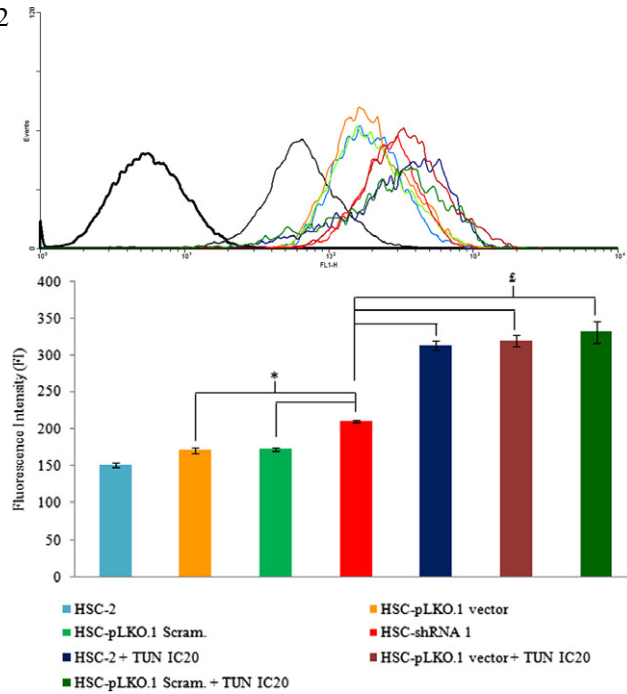
other, with less profound apoptosis in PrP^C-depleted and glycosylation-inhibited oral squamous cell carcinoma HSC-2 cells, and more profound general cell death (less profound proliferative effect) in PrP^C-overexpressing and glycosylation-inhibited colon adenocarcinoma LS 174T cells in our study.

Of note, a 19–22 kDa species was generated in the presence of TUN, possibly the C-terminal fragment C2 that has the 3F4 epitope intact, resulting from the β-cleavage of PrP^C [16]. ROS has been shown to be responsible for the β-cleavage that takes place within the unstructured region of the molecule, near or within the octarepeat region of PrP^C [17,18]. Thus, these studies offer a supportive explanation to the occurrence of p19–22, since TUN is as well able to induce oxidative stress regulated by protein degradation [19]. β-cleavage has been shown to be protective against oxidative stress [18,20]. Hence, aberrant or compromised PrP^C processing could instigate an event of oxidative damage and further cellular injury that may be implicated in neurodegeneration as observed in prion diseases, or possibly influences susceptibility to prion infection by facilitating the conversion of PrP^C to PrP^{Sc} [20].

The association between TUN and apoptosis is attributed to the unfolded protein response (UPR). UPR is acti-

vated upon endoplasmic reticulum (ER) stress induction in TUN-treated PrP^C-expressing HeLa transfectants, and the translocation of the misfolded PrP^C into ER involves multifaceted interaction between oxidative folding, glycosylation, and calcium homeostasis [21]. In accord, the connection between ER stress and oxidative stress has been proposed in a review by Malhotra and Kaufman [22], which stated that generation of ROS as a byproduct of protein oxidation during protein misfolding in the ER is a coupled event that causes the activation of UPR and subsequent cell death. Malhotra et al. [23] further testified the protective role of antioxidant during ER stress, by showing an increase of coagulation factor VIII (FVIII) secretion, both *in vitro* and *in vivo* in mice, along with marked reduction in UPR activation and oxidative stress-mediated apoptosis upon subjection to antioxidant. However, the exact mechanism on how oxidative stress affects protein misfolding and *vice versa* is still a question mark. Owing to the relation between ROS and ER stress, the ROS level in PrP^C-expressing cells upon TUN treatment was measured using DCFH-DA assay. The ROS scavenging activity of PrP^C was suppressed upon ER stress induction in cells. There was almost a 2-fold increment of ROS level in the unglycosylated PrP^C-expressing HSC-2 and LS 174T cells

(A) HSC-2



(B) LS 174T

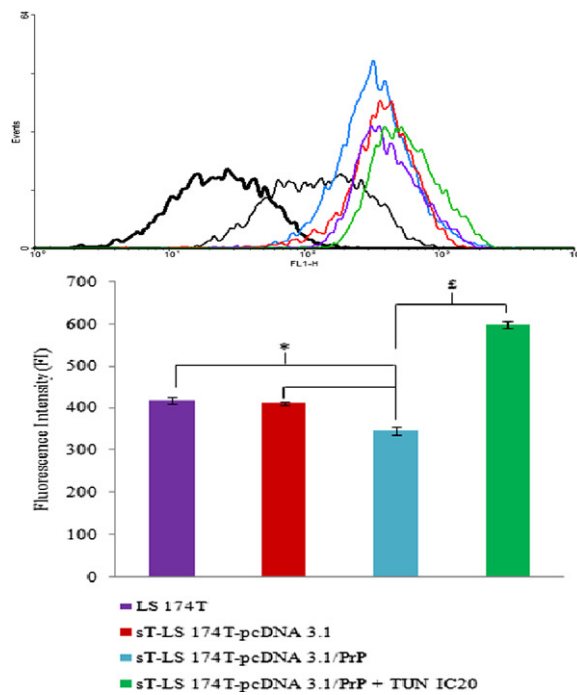


Fig. 5. PrP^C modulates H₂O₂-induced burst of ROS in (A) HSC-2 and (B) LS 174T cells. Reactive oxygen species (ROS) generated within cells was detected using fluorescent probe DCFH-DA upon treatment with 3 mM of H₂O₂ for 30 min. Data of graphical representation of flow cytometric analysis are represented as mean Fluorescence Intensity (FI) ± SEM of triplicate from three independent experiments. Results are expressed in FI unit which is proportional to the amount of ROS generated, particularly H₂O₂. Baseline fluorescence and negative control (DCFH-DA alone, without H₂O₂) are represented with broad and fine black lines, respectively. Each sample was depicted according to the color legend shown. The LS 174T cells stably-overexpressing PrP^C is annotated as sT-LS 174T-pcDNA 3.1/PrP while mock vector-transfected cells – sT-LS 174T-pcDNA 3.1. Mean values were compared by using ANOVA followed by LSD's post hoc test for comparison of the means, using the SPSS software. **p* < 0.05 in HSC-shRNA 1 vs. HSC-pLKO.1 vector and HSC-pLKO.1 Scram., as well as sT-LS 174T-pcDNA 3.1/PrP vs. sT-LS 174T-pcDNA 3.1. §*p* < 0.05 in unglycosylated PrP expressing group of cells vs. HSC-shRNA 1 and unglycosylated sT-LS 174T-pcDNA 3.1/PrP vs. sT-LS 174T-pcDNA 3.1.

compared to the glycosylated PrP^C-expressing cells. Taken together, the present study has demonstrated that upon induction of ER stress, apoptosis is aggravated in the presence of unglycosylated variant of PrP^C, which does not exhibit the antioxidant activity as shown in the fully glycosylated PrP^C.

Due to the participation of ROS elevation during ER stress-induced apoptosis as shown in the current study, it is likely that the underlying mechanism behind the induction of apoptosis in unglycosylated PrP^C is highly allied to the mitochondria-mediated signal transduction pathway. In fact, Yang et al. [12] have shown that upon apoptosis instigation in the HeLa cells transiently expressing PRNP glycosylation mutants – N181Q N197Q and T183A T199A, pro-apoptotic trends were observed, such as cell growth retardation, reduction in mitochondrial membrane potential, elevated ROS generation, along with lower levels of apoptosis-related Bcl-xL and cleaved Caspase-9 was activated. The involvement of Bcl-2 family proteins and mitochondrial membrane potential diminution during apoptosis in transiently-expressing unglycosylated PrP^C mutants – N181Q/N197Q and T183A/T199A in human astrocytoma SF-126 cells further supported the observations [24]. The experimental settings above using mutant PrP^C devoid of the glycosylation sites could be extended as our future studies, whereby these mutants could be stably transfected into HSC-2 cells with a knock-downed endogenous PrP^C background, and further subjecting the cells to apoptotic and oxidative stress insults. This could directly answer the role of PrP^C glycosylation in the survival of cancer cells besides HeLa and SF-126 cells, like our current HSC-2 and LS 174T cells.

The aggravation of apoptosis and induction of oxidative stress in cancer cells expressing the unglycosylated variant of PrP^C implicates the potential role of TUN as an anticancer agent or a potent enhancer during cancer therapy, especially in cancer cells overexpressing PrP^C. Since it has been shown in this study that PrP^C is responsible for ROS scavenging (mainly H₂O₂), the suppression of this antioxidant activity upon glycosylation inhibition – probably by down-regulating Superoxide Dismutase (SOD) – may further lead to a severe accumulation of ROS and ultimately oxidative stress-induced apoptosis via superoxide- and mitochondria-dependent pathways in cancer cells. Hence, glycosylation inhibition of PrP^C via TUN may provide a novel approach for the selective killing of cancer cells. To support this notion, an earlier study by Noda et al. [25] suggests that the glycosylation modification by TUN in human head-and-neck carcinoma cells might be a constructive therapeutic approach for successful chemotherapy using cisplatin both *in vivo* and *in vitro*. The pharmacomodulatory effects of TUN are intervened by global inhibition of protein and glycoprotein synthesis, via N-glycosylation suppression and synergistic interaction with anticancer drugs [26]. Interestingly, the interaction between PrP^C and P-glycoprotein (P-gp) has been documented in a recent study by Li et al. [27] in multi-drug resistant (MDR) breast cancer cells treated with paclitaxel, a P-gp substrate. Induction of paclitaxel-mediated invasion upon up-regulation of P-gp activity or PrP^C expression further facilitated the formation of P-gp/PrP^C complex, which is important

in initiating the anti-apoptotic activity of adriamycin-resistant MCF7/Adr cells. Up-regulation of PrP^C and its significance in MDR gastric carcinoma cell line SGC7901/ADR has also been reported by Du et al. [28]. Their study demonstrated that the expression of the classical MDR-related molecule P-gp was significantly up-regulated by PrP^C, where the protein itself is resistant to both P-gp-related and P-gp-nonrelated drugs in SGC7901 cells. Besides, PrP^C was shown to inhibit adriamycin-induced apoptosis by modulating the expression of Bcl-2 and Bax, which might be the other pathway contributing to PrP^C-related MDR. Noteworthy, upon inhibition of PrP^C expression, the MDR phenotype of SGC7901/ADR was partially reversed. Once again, PrP^C shows promise as a potential therapeutic target not only in prion diseases, but as well as in PrP^C-related carcinoma treatment.

In conclusion, overexpression of PrP^C in HSC-2 and LS 174T cancer cell lines exhibits antioxidant activity during H₂O₂-induced oxidative stress. On the contrary, such protective effect of PrP^C is diminished upon TUN-induced ER stress. The aggravation of apoptosis and induction of oxidative stress in cancer cells expressing the unglycosylated variant of PrP^C implicates the potential role of TUN as an anticancer agent or a potent enhancer during cancer therapy, especially in cancer cells overexpressing PrP^C. Thus, targeting PrP^C might be an attractive strategy in the treatment of human oral squamous cell and colon carcinomas, and this calls for more research on the role of PrP^C in cancer biology.

Conflict of interest

None declared.

Role of funding source

None declared.

Acknowledgements

This work was supported by Malaysian Ministry of Science, Technology and Innovation e-Science Grant 02-02-11-SF0068. We would like to thank Dr. Yang-Mooi Lim (Faculty of Medicine and Health Sciences, UTAR) for providing us with the cancer cell lines.

References

- [1] S.B. Prusiner, Prions, Proc. Natl. Acad. Sci. USA 95 (1998) 13363–13383.
- [2] B. Caughey, D.A. Kocisko, G.J. Raymond, P.T.Jr. Lansbury, Aggregates of scrapie-associated prion protein induce the cell-free conversion of protease-sensitive prion protein to the protease-resistant state, Chem. Biol. 2 (1995) 807–817.
- [3] D. A Harris, Cellular biology of prion diseases, Clin. Microbiol. Rev. 12 (1999) 429–444.
- [4] S. Lehmann, O. Milhavet, A. Mangé, Trafficking of the cellular isoform of the prion protein, Biomed. Pharmacother. 53 (1999) 39–46.
- [5] H. C Joao, R.A. Dwek, Effects of glycosylation on protein structure and dynamics in ribonuclease B and some of its individual glycoforms, Eur. J. Biochem. 218 (1993) 239–244.
- [6] A. Taraboulos, M. Rogers, D.R. Borchelt, M.P. McKinley, M. Scott, D. Serban, S.B. Prusiner, Acquisition of protease resistance by prion

- proteins in scrapie-infected cells does not require asparagine-linked glycosylation, *Proc. Natl. Acad. Sci. USA* 87 (1990) 8262–8266.
- [7] C. Korth, K. Kaneko, S.B. Prusiner, Expression of unglycosylated mutated prion protein facilitates PrP(Sc) formation in neuroblastoma cells infected with different prion strains, *J. Gen. Virol.* 81 (2000) 2555–2563.
- [8] S. Lehmann, D.A. Harris, Blockade of glycosylation promotes acquisition of scrapie-like properties by the prion protein in cultured cells, *J. Biol. Chem.* 272 (1997) 21479–21487.
- [9] V.A. Lawson, S.J. Collins, C.L. Masters, A.F. Hill, Prion protein glycosylation, *J. Neurochem.* 93 (2005) 793–801.
- [10] A. Dricu, M. Carlberg, M. Wang, O. Larsson, Inhibition of N-linked glycosylation using tunicamycin causes cell death in malignant cells: role of down-regulation of the insulin-like growth factor 1 receptor in induction of apoptosis, *Cancer Res.* 57 (1997) 543–548.
- [11] M. Carlberg, A. Dricu, H. Blegen, G.E.N. Kass, S. Orrenius, O. Larsson, Short exposures to tunicamycin induce apoptosis in SV40-transformed but not in normal human fibroblasts, *Carcinogenesis* 17 (1996) 2589–2596.
- [12] Y. Yang, L. Chen, H.Z. Pan, Y. Kou, C.M. Xu, Glycosylation modification of human prion protein provokes apoptosis in HeLa cells *in vitro*, *BMB Rep.* 42 (2009) 331–337.
- [13] B. Yuan, R. Latek, M. Hossbach, T. Tuschl, F. Lewitter, siRNA selection server: an automated siRNA oligonucleotide prediction server, *Nucl. Acids. Res.* 32 (2004) W130–W134.
- [14] J. Moffat, D.A. Grueneberg, X. Yang, S.Y. Kim, A.M. Kloepper, G. Hinkle, B. Piqani, T.M. Eisenhaure, B. Luo, J.K. Grenier, A.E. Carpenter, S.Y. Foo, S.A. Stewart, B.R. Stockwell, N. Hacohen, W.C. Hahn, E.S. Lander, D.M. Sabatini, D.E. Root, A lentiviral RNAi library for human and mouse genes applied to an arrayed viral high-content screen, *Cell* 124 (2006) 1283–1298.
- [15] M. Mehrpour, P. Codogno, Prion protein: From physiology to cancer biology, *Cancer Lett.* 290 (2010) 1–23.
- [16] A. Mangé, F. Béranger, K. Peoc'h, T. Onodera, Y. Frobert, S. Lehmann, Alpha- and beta-cleavages of the amino-terminus of the cellular prion protein, *Biol. Cell* 96 (2004) 125–132.
- [17] H.E. McMahon, A. Mangé, N. Nishida, C. Créminon, D. Casanova, S. Lehmann, Cleavage of the amino terminus of the prion protein by reactive oxygen species, *J. Biol. Chem.* 276 (2001) 2286–2291.
- [18] N.T. Watt, D.R. Taylor, A. Gillott, D.A. Thomas, W.S. Perera, N.M. Hooper, Reactive oxygen species-mediated beta-cleavage of the prion protein in the cellular response to oxidative stress, *J. Biol. Chem.* 280 (2005) 35914–35921.
- [19] Y.H. Hsieh, I.J. Su, H.Y. Lei, M.D. Lai, W.W. Chang, W. Huang, Differential endoplasmic reticulum stress signaling pathways mediated by iNOS, *Biochem. Biophys. Res. Commun.* 359 (2007) 643–648.
- [20] V. Lewis, S.J. Collins, Analysis of endogenous PrP^C processing in neuronal and non-neuronal cell lines, *Methods Mol. Biol.* 459 (2008) 229–239.
- [21] A. Orsi, L. Fioriti, R. Chiesa, R. Sitia, Conditions of endoplasmic reticulum stress favor the accumulation of cytosolic prion protein, *J. Biol. Chem.* 281 (2006) 30431–30438.
- [22] J.D. Malhotra, R.J. Kaufman, Endoplasmic reticulum stress and oxidative stress: a vicious cycle or a double-edged sword?, *Antioxid Redox Signal.* 9 (2007) 2277–2293.
- [23] J.D. Malhotra, H. Miao, K. Zhang, A. Wolfson, S. Pennathur, S.W. Pipe, et al., Antioxidants reduce endoplasmic reticulum stress and improve protein secretion, *Proc. Natl. Acad. Sci. USA* 105 (2008) 18525–18530.
- [24] L. Chen, Y. Yang, J. Han, B.Y. Zhang, L. Zhao, K. Nie, X.F. Wang, F. Li, C. Gao, X.P. Dong, C.M. Xu, Removal of the glycosylation of prion protein provokes apoptosis in SF126, *J. Biochem. Mol. Biol.* 40 (2007) 662–669.
- [25] I. Noda, S. Fujieda, M. Seki, N. Tanaka, H. Sunaga, T. Ohtsubo, H. Tsuzuki, G.-K. Fan, H. Saito, Inhibition of N-linked glycosylation by tunicamycin enhances sensitivity to cisplatin in human head-and-neck carcinoma cells, *Int. J. Cancer* 80 (1999) 279–284.
- [26] D.C. Hiss, G.A. Gabriels, P.I. Folb, Combination of tunicamycin with anticancer drugs synergistically enhances their toxicity in multidrug-resistant human ovarian cystadenocarcinoma cells, *Cancer Cell Int.* 7 (2007) 5.
- [27] Q.Q. Li, X.X. Cao, J.D. Xu, Q. Chen, W.J. Wang, F. Tang, Z.Q. Chen, X.P. Liu, Z.D. Xu, The role of P-glycoprotein/cellular prion protein interaction in multidrug-resistant breast cancer cells treated with paclitaxel, *Cell Mol. Life Sci.* 66 (2009) 504–515.
- [28] J. Du, Y. Pan, Y. Shi, C. Guo, X. Jin, L. Sun, N. Liu, T. Qiao, D. Fan, Overexpression and significance of prion protein in gastric cancer and multidrug-resistant gastric carcinoma cell line SGC7901/ADR, *Int. J. Cancer* 113 (2005) 213–220.